Toshikazu Hirao *Editor*

Functionalized Redox Systems

Synthetic Reactions and Design of π- and Bio-Conjugates

Springer

Functionalized Redox Systems

Toshikazu Hirao
Editor

Functionalized Redox Systems

Synthetic Reactions and Design of π- and Bio-Conjugates

Springer

Editor
Toshikazu Hirao
Department of Applied Chemistry
Graduate School of Engineering
Osaka University, Yamada-oka, Suita
Osaka, Japan

Printed on acid-free paper

Preface

Oxidation and reduction reactions play important roles in biological systems, as exemplified by photosynthesis or metabolism. An efficient electron transfer mechanism operates in these redox processes. From these points of view, bio-inspired chemistry permits the construction of conceptually new artificial molecular catalysts and electrical materials for electron transfer, the function of which might be beyond the biological systems. A variety of strategies have been investigated for this purpose. A promising approach depends on how to develop synthetic reactions through electron transfer, how to construct functionalized redox systems, or how to design chirality-organized redox spaces. A combination of these approaches is allowed to provide efficient artificial systems for redox reactions. Our focus in this book is mainly on such redox systems. The book consists of three parts, depending on the research done in our group, which cover various pioneering fields in synthetic organic chemistry, materials synthetic chemistry, and bioorganometallic chemistry.

For future investigation, their reactions, systems, and spaces should be more beautiful. I hope that this book will deepen the readers' background and widen the scope of science, so that they will find a new approach in bio-inspired chemistry.

This work was done by postdoctoral researchers and students in our laboratory, whose names are cited in the references.

Osaka, Japan   Toshikazu Hirao

Contents

Chapter 1
Introduction

Toshikazu Hirao

Abstract The concept of this book is described in the introduction. Fuctionalized redox systems are essential in efficient redox reactions and materials. From this point of view, redox reactions via electron transfer, π-, d, π-, and d, nonplanar π-conjugated systems, and chirality-organized spaces are developed. A combination of them will permit novel bio-inspired chemistry.

Oxidative and reductive transformations are mostly induced by transition metals or organic compounds like coenzymes with various oxidation states. Chemoselective reactions are mostly controlled by their redox potentials. Since the coordination interaction between transition metals and ligands participates in the redox processes, ligand design is important in attaining their utility. A great deal of progress has been made in designing coordinated complexes to induce organic reactions via electron transfer.

Versatile synthetic methods for oxidative or reductive transformations depending on the redox properties of metals or heteroatoms are described in Chap. 2. The tautomerism of dialkyl phosphonate between P(III) and P(V) species can be used in a variety of synthetic transformations.

Through one-electron oxidation with transition metals involving either inner- or outer sphere electron transfer can generate radical species. This reaction proceeds through a radical cation intermediate. Likewise, a radical anion can be generated through one-electron reduction. The complementary nature of these processes could be profitably exploited for organic synthesis, but little work has been reported in these selective catalytic transformations. Efficient regulation of the electron-transfer process allows the catalytic generation of radical species under redox potential control.

There is an increasing demand for catalytic reduction reactions involving low-valent transition metals, and this has led to investigations into the redox chemistry of species such as titanium(II or III), vanadium(II) and samarium(II). Low-valent vanadiums and titaniums contribute to reductive transformations as observed in nitrogenase. In addition to the catalytic reduction of organic halides, the construction of efficient catalytic systems for synthetically important catalytic pinacol

T. Hirao (✉)
Department of Applied Chemistry, Graduate School of Engineering,
Osaka University, Yamada-oka, Suita, Osaka 565-0871, Japan
e-mail: hirao@chem.eng.osaka-u.ac.jp

coupling reaction is achieved. Samarium(II) compounds can be also used for reduction reactions.

A higher oxidation state of transition metals and their oxides is able to induce oxidative transformations. Furthermore, metal peroxides obtained from the reaction of metal oxides with hydrogen peroxide or alkyl peroxides serve as versatile oxidants in selective reactions. Using Lewis acidity with one-electron oxidation capability of oxovanadium(V) compounds, oxidative transformations of carbonyl compounds are performed. Organic substituents of main-group organometallic compounds are coupled by treatment with oxovanadium(V) compounds to give ligand coupling products. Such oxidative cross-coupling of organometallic nucleophiles is considered to be a complementary method for the conventional nucleophile-electrophile coupling. Bio-inspired (haloperoxidase-like) and environmentally harmonic vanadium-catalyzed halogenation is attained under molecular oxygen to give halogenated compounds, the function of which is beyond the enzyme.

In Chap. 3, redox-active π-conjugated systems allow us to construct a variety of potential redox catalysts and electronic materials. A coenzyme PQQ possessing the π-conjugated pyrroloquinoline quinone function, serves as a catalyst or mediator in redox reactions under molecular oxygen.

To extend the quinone chemistry, polyanilines and quinonediimines as π-conjugated polymers or molecules are studied to serve as organic catalysts for proton-conjugated electron transfer. Dimension of π-conjugated systems is controlled by use of a porphyrin or its zinc complex as a molecular scaffold to permit photorefractive electron transfer.

To widen their scopes in coordination chemistry, the hybrid d,π-conjugated systems composed of redox-active π-conjugated compounds and transition metals are constructed, affording the potential field reflected by both redox properties. The design of the conjugated complexes with π-conjugated polyanilines and quinonediimines as a redox-active ligand is described here, where the redox-active ligands contribute to the redox reactions. Chirality induction of the π-conjugated chain is attained by chiral complexation or hydrogen bonding.

The d,π-conjugated complex is reduced to small and well-dispersed nanoparticles. In oxidative reaction induced by a hybrid system of transition metal nanoparticles and polyanilines, the latters are found to serve as a redox-active mediator.

Another strategy depends on the introduction of π-conjugated group to imidovanadium moiety. In such a sense, imidovanadium compounds bearing the π-conjugated substituents at the *N*-position are synthesized and characterized.

Fullerenes and carbon nanotubes are typical nonplanar π-conjugated compounds, which provide unique π- and d,π-conjugated systems. Bowl-shaped π-conjugated "sumanene", which possesses a partial C_{3v} symmetric structure of fullerene, is synthesized for the first time. X-ray single crystal structural analysis reveals its columnar stacking. n-Type electron transportation ability comparable to C_{60} is exhibited. Bowl-to-bowl inversion behavior is mentioned as a sumanene function. Short synthesis of more highly-strained π-extended π bowls with hemifullerene skeletons is achieved utilizing bowl-shaped sumanene.

The unique π-conjugated moieties are permitted to be coordinated to metals, to give d, nonplanar π-conjugated systems. The concave or convex π-bent surface is demonstrated to serve as a ligand to give the corresponding d,π-conjugated bowl complex. Chiral complexation and the bowl-to-bowl inversion dynamics of such a complex are investigated.

Bioorganometallic chemistry, which is focused on in Chap. 4, is considered to be a new research field, allowing the development of medicinary chemistry, probe chemistry, and bio-inspired chemistry. Ferrocene-peptide bioconjugates provide a variety of secondary structures in peptide-like systems. 1,1′-Disubstituted ferrocene-dipeptide bioconjugates are designed to obtain peptidomimetic basis for protein folding through interchain hydrogen bonding and to construct the chirality-organized structures. This architectural control of the dimensional structures utilizing minimum-sized peptide chains with chiral centers and hydrogen bonding sites provides a versatile approach to artificial highly ordered systems. Crystal engineering in bioorganometallic chemistry is also discussed. The monosubstituted ferrocene-dipeptide bioconjugates form highly ordered molecular assemblies in solid states.

Chirality organization of amino acid and dipeptide bearing the organic scaffolds, 2,6-pyridinedicarboxamide and urea scaffold, respectively, and polypeptide is also described here.

The redox-active ferrocene bearing a long alkylene chain is aggregated along the backbone of double helical DNA to afford the redox-active (outer) and hydrophobic (inner) spheres. Nucleobases are used to organize a variety of bioorganometallic compounds. The controlled molecular arrangement of organometallic moieties through programming self-assembly of nucleobases is attained.

A description of the focus of the book consists of functionalized redox systems. Rationale for organization of the book is presented since efficient redox reactions, redox systems, and organized redox spaces are essential to realize the enzyme-like artificial redox systems.

Chapter 2
Synthetic Methods for Redox Reactions Using Phosphorus, Vanadium and Samarium Compounds

Toshikazu Hirao, Toshiyuki Moriuchi, Toru Amaya, Akiya Ogawa, and Akihiro Nomoto

Abstract The tautomerism of dialkyl phosphonate between P(III) and P(V) species is applied to a variety of synthetic transformations, including reductive dehalogenation and palladium-catalyzed phophonation. Low-valent vanadiums contribute to reductive transformations as observed in catalytic reduction of organic halides. Catalytic pinacol coupling reaction is induced by vanadiums or titaniums in the presence of a chlorosilane and a co-reductant zinc. Use of the heterobimetallic catalyst permits the selective cross-coupling. Samarium(II) compounds are also used for the reduction reactions. Using Lewis acidity with one-electron oxidation capability of oxovanadium(V) compounds, oxidative transformations of carbonyl compounds are developed. Silyl enol ethers and boron enolates undergo selective oxidative coupling. Organic substituents of main-group organometallic compounds are coupled by oxidation with oxovanadium(V) compounds to give ligand coupling products. Bio-inspired and environmentally harmonic vanadium-catalyzed halogenation is attained in the presence of halide anion and Lewis or Brønsted acid under molecular oxygen to give halogenated compounds.

Keywords Aryl phosphonate • Ate complex • Boron enolate • Brønsted acid • Carbon–phosphorus bond formation • Cross coupling • Dehalogenation • Dinuclear complex • Electron transfer • Hirao reaction • Hirao reduction • Lewis acid • Ligand coupling • Main-group organometallics • Molecular oxygen • One-electron oxidation • Organotin • Organozirconium • Oxidative bromination • Palladium catalyst

T. Hirao (✉) • T. Moriuchi • T. Amaya
Department of Applied Chemistry, Graduate School of Engineering, Osaka University, Yamada-oka, Suita, Osaka 565-0871, Japan
e-mail: hirao@chem.eng.osaka-u.ac.jp; moriuchi@chem.eng.osaka-u.ac.jp; amaya@chem.eng.osaka-u.ac.jp

A. Ogawa • A. Nomoto
Department of Applied Chemistry, Graduate School of Engineering, Osaka Prefecture University, 1-1 Gakuen-cho, Naka-ku, Sakai, Osaka 599-8531, Japan
e-mail: ogawa@chem.osakafu-u.ac.jp; nomoto@chem.osakafu-u.ac.jp

• Phophonate • Pinacol coupling • Reductive deconjugation • Ring-opening oxidation
• Silyl enol ether • Silyl ketene acetal • Tautomerism • Vanadium bromoperoxidase
• Vanadium catalyst • Vinyl phosphonate

Abbreviations

acac	Acetylacetonate
2-BPEPA	*N,N′*-Bis[2-(2-pyridyl)ethyl]-2,6-pyridinedicarboxamide
BIPA	*N,N′*-Bis[2-(4-imidazolyl)ethyl]-2.6-pyridinedicarboxamide
CAN	Cerium(IV) ammonium nitrate
DIPHOS	1,2-Bis(diphenylphosphino)ethane
DME	1,2-Dimethoxyethane
Et	Ethyl
HMPA	Hexamethylphosphoramide
L	Liter(s)
Me	Methyl
MeCN	Acetonitrile
mol	Mole(s)
Ph	Phenyl
PTS•H$_2$O	*p*-Toluenesulfonic acid monohydrate
TBS	*tert*-Butyldimethylsilyl
TFA	Trifluoroacetic acid
THF	Tetrahydrofuran
VBrPO	Vanadium bromoperoxidase

2.1 Reductive Transformations of Organic Halides with Phosphonate

Toshikazu Hirao

Dialkyl phosphonate (**1**) is known to be present in tautomerism with dialkyl phosphite (**2**). Although the phosphonate form mainly exists under neutral conditions, the equilibrium to phosphite is observed under basic conditions. The interconversion between P(V) and P(III) species shown in Scheme 2.1 is considered to contribute to the redox processes. In this section, the dehalogenation reaction depending on the tautomerism is described.
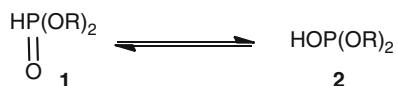
Scheme 2.1 Tautomerism of dialkyl phosphonate

The transformations of *gem*-dihalocyclopropanes are synthetically useful because the cyclopropanes are readily prepared by the addition of dihalocarbene to olefins. In most of dehalogenation reactions to monohalocyclopropanes, the reagents are limited to metallic reductants such as organotin hydride, lithium aluminum hydride, sodium borohydride, Grignard reagent, and zinc-copper couple [1–9]. A versatile method for the reduction of *gem*-dibromocyclopropanes **3** with an organic reductant is achieved by use of diethyl phosphonate (commercially named diethyl phosphite) and triethylamine to give the monobromocyclopropanes **4** (Scheme 2.2) [10].
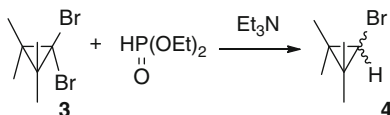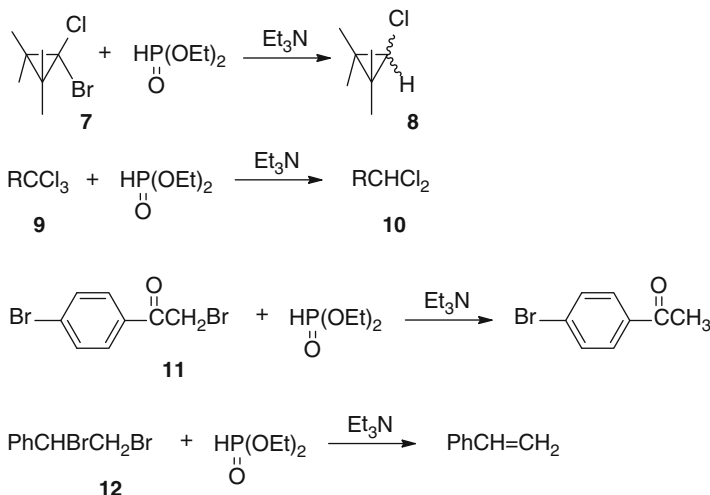

Scheme 2.2 Reductive debromination of *gem*-dibromocyclopropanes **3**

This reduction method can be extended to the reductive conversion of *gem*-dibromoalkenes **4** into monobromoalkenes **5** (Hirao reduction [11–13]) as shown in Scheme 2.3, which makes this method more synthetically useful.
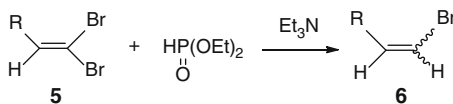
Scheme 2.3 Reductive debromination of *gem*-dibromoalkenes **5**

Starting from *gem*-bromochlorocyclopropanes **7**, the corresponding chlorocyclopropanes **8** are prepared without formation of bromocyclopropanes (Scheme 2.4) [14]. One of the chlorine atoms of the trichloromethane derivatives **9** is reduced to give the dichloromethane ones **10**. Furthermore, methyl α-bromocinnamate is

Scheme 2.4 Reductive debromination of various halides

allowed to be reduced into methyl cinnamate, which is in contrast with Michael addition of diethyl phosphonate to methyl cinnamate. α-Bromo ketone **11** also undergoes the debromination. (1,2-Dibromoethyl)benzene (**12**) is reduced to styrene. The attack of diethyl phosphonate or its anion on the bromine or chlorine atom is considered to be an initial step in these reduction reactions.

The reaction of α-bromo-α,β-unsaturated ketones with diethyl phosphonate and triethylamine affords β,γ-unsaturated ketones selectively (Scheme 2.5) [15]. This process comprises reduction of the bromide and deconjugation of an olefinic moiety. α-Bromo-α,β-unsaturated carbonyl compounds are readily prepared by treatment of l,l-dibromo-2-siloxycyclopropanes with diethyl phosphonate. This finding makes it possible to prepare β,γ-unsaturated ketones from l,l-dibromo-2-siloxycyclopropanes in one pot. As one of the plausible reaction paths, the α-bromo-β,γ-unsaturated ketone, arising from the intervention of the dienol, is subjected to debromination with diethyl phosphonate and triethylamine to give the β,γ-unsaturated ketone.
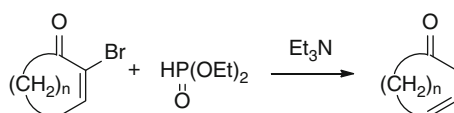
**Scheme 2.5** Reductive deconjugation of α-bromo-α,β-unsaturated ketones

The highly stereoselective synthesis of β,γ-unsaturated esters or lactones, being accompanied by one-carbon homologation of starting saturated esters or lactones, is also permitted (Scheme 2.6) [16]. The α-bromo-α,β-unsaturated ester **14**, easily prepared by the addition of dibromocarbene to the silyl ketene acetal **13**, is treated with dialkyl phosphonate and triethylamine to afford the β,γ-unsaturated ester **15**. A variety of α-bromo-α,β-unsaturated esters are allowed to undergo reductive deconjugation. Another interesting feature is the high stereoselectivity of the present transformation; for example, a mixture of ethyl (*E*)- and (*Z*)-2-bromo-2-hexenoates is consumed in the same rate, giving ethyl (*E*)-3-hexenoate exclusively.

The present process provides a synthetically useful route for the stereoselective introduction of a carbon–carbon double bond β,γ to the carbonyl group together with
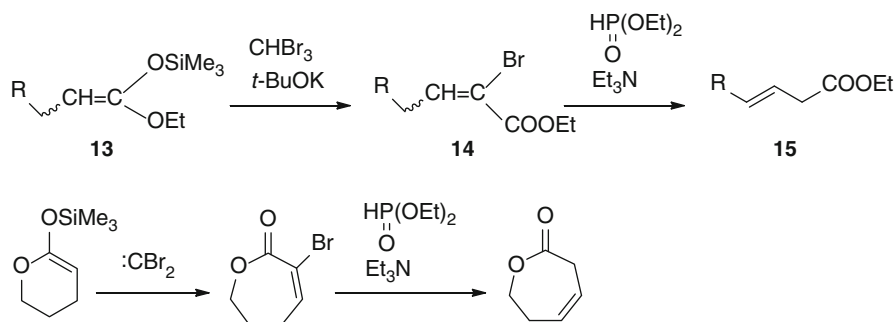
Scheme 2.6 Reductive deconjugation of α-bromo-α,β-unsaturated esters and lactones

one-carbon homologation. A synthetic route to (±)-11-hydroxy-*trans*-8-dodecenoic acid, a precursor of (±)-recifeiolide [17], from the commercially available 10-undecenoic acid is achieved by using the present methodology as a key step (Scheme 2.7). This process is also applied to the synthesis of (±)-pyrenophorin (Scheme 2.8) [16].
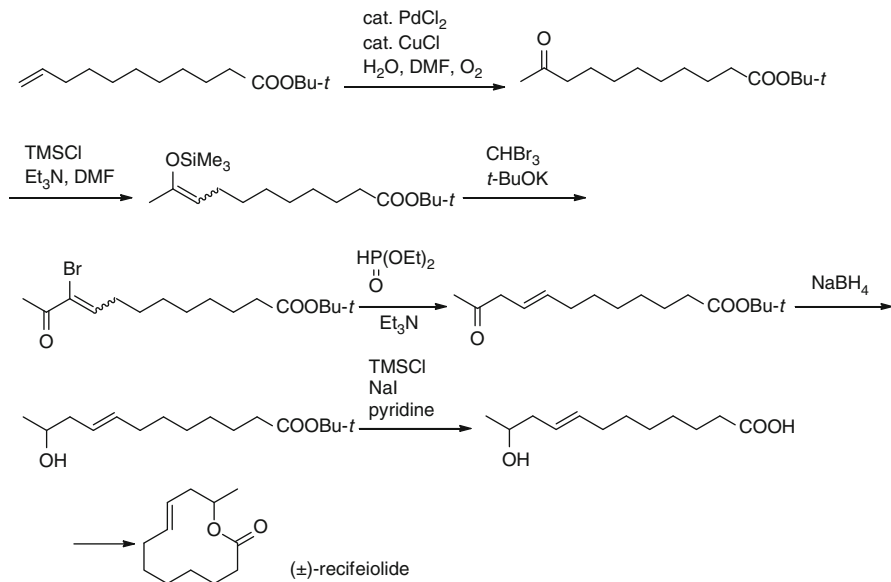
Scheme 2.7 Synthesis of recifeiolide
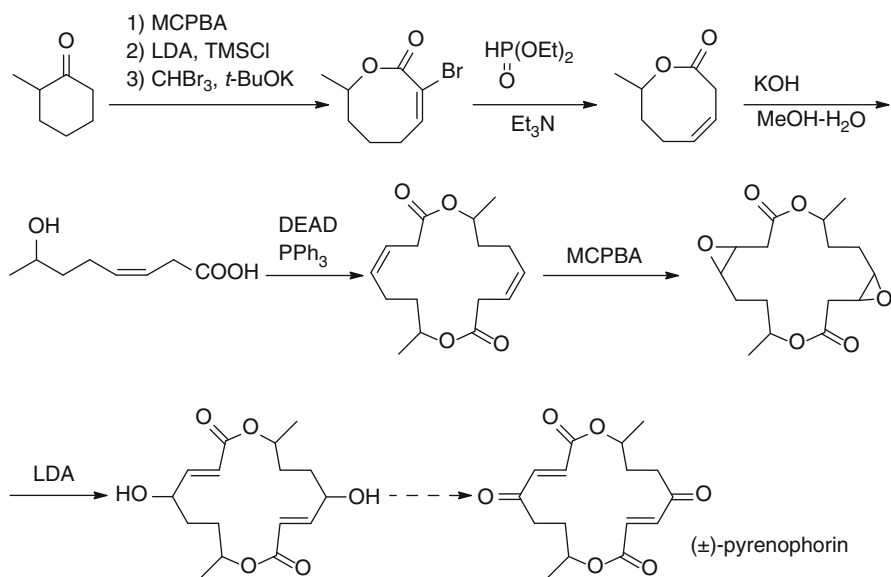
Scheme 2.8 Synthesis of pyrenophorin

2.2   Carbon–Phosphorus Bond Formation

Toshikazu Hirao

Cyclopropylphosphonates are known as another class of less readily obtainable compounds due to the difficulty of nucleophilic displacement on a cyclopropane ring. A novel reductive phosphonation of *gem*-dibromocyclopropanes **16** is achieved by treatment with triethyl phosphite and water or diethyl phosphonate as shown in Scheme 2.9, giving the corresponding diethyl cyclopropylphosphonates **17** [18].
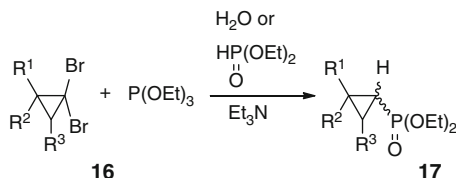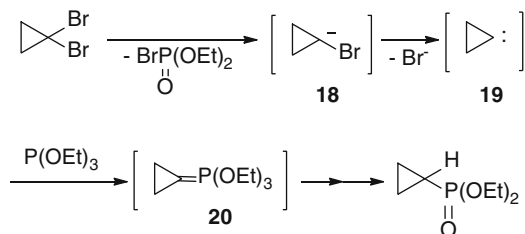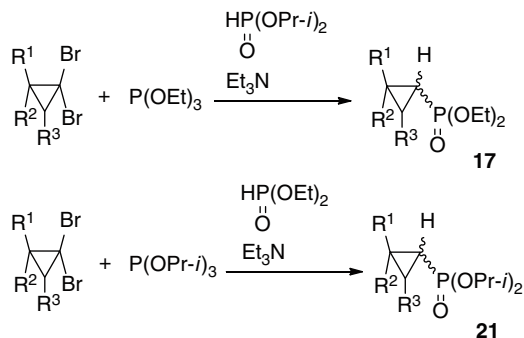

Scheme 2.9 Synthesis of cyclopropylphosphonates **17**

The reaction path to the cyclopropylphosphonate might be postulated as depicted in Scheme 2.10 [19]. The *gem*-dibromocyclopropane undergoes debromination with diethyl phosphonate and triethylamine, giving the carbanion **18**. Protonation with diethyl phosphonate or water leads to the monobromocyclopropane, which is consistent with reduction with diethyl phosphonate and triethylamine [10]. Elimination of Br⁻ from results in the generation of the cyclopropylidene **19**. Prior to ring cleavage into the allene, is assumed to interact with triethyl phosphite to afford the ylide **20**. It is conceivable that the degradation completes the route to the cyclopropylphosphonate **17**.

Scheme 2.10 A reaction route to cyclorpopylphosphonate

Treatment of the *gem*-dibromocyclopropane with triethyl phosphite, diisopropyl phosphonate, and triethylamine results in the formation of the diethyl cyclopropylphosphonate **17** exclusively (Scheme 2.11). The formation of the diisopropyl cyclopropylphosphonate is not detected. The reverse combination of triisopropyl phosphite and diethyl phosphonate leads to the exclusive formation of the diisopropyl cyclopropylphosphonate **21**. Thus-obtained cyclopropylphosphonates undergo addition reaction with aldehydes [20].

Scheme 2.11 Cross reaction for the synthesis of cyclopropylphosphonates **17** and **21**

Arbuzov and Michaelis-Becker reactions provide facile and versatile procedures for the formation of carbon–phosphorus bonds. These methods, however, are not applicable to the formation of sp^2 hybridized carbon–phosphorus bonds. Only few methods have been reported for the syntheses of arylphosphonates and vinylphosphonates. Direct reaction of aryl or vinyl halides with trialkyl phosphite in the presence of nickel halide requires severe reaction conditions [21, 22], and the stereochemistry of vinylphosphonates has not been clarified. Synthesis of dialkyl arylphosphonates **22** [23, 24] is achieved by the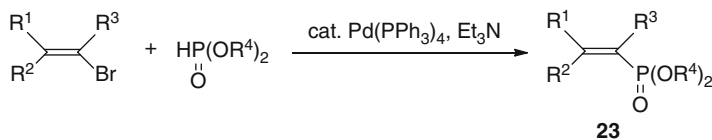 palladium-catalyzed reaction (Scheme 2.12), which is called by "Hirao reaction". The stereoselective synthesis of dialkyl vinylphosphonates **23** [24–26] is similarly accomplished by this method (Scheme 2.13). A variety of modified procedures have been developed recently [27–37].
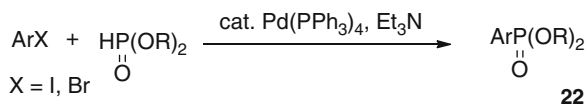
Scheme 2.12 Palladium-catalyzed synthesis of arylphosphonates **22**

Scheme 2.13 Palladium-catalyzed synthesis of vinylphosphonates **23**

A plausible formation path for dialkyl arylphosphonates is as follows. Palladium(0) species undergoes oxidative addition with aryl bromide to give the arylpalladium species, which reacts with dialkyl phosphite or phosphonate to give dialkyl arylphosphonate.

In addition to the above-mentioned carbon–phosphorus bond formation, the reaction of dienes with nucleophiles is also catalyzed by a palladium complex.

Isoprene is treated with diethyl phosphonate in the presence of a catalytic amount of tetrakis(triphenylphosphine)palladium and 1,2-bis(diphenylphosphino) ethane (DIPHOS) to give diethyl 3-methyl-2-butenylphosphonate (**24**) selectively (Scheme 2.14) [24]. This protocol is used in various carbon–phosphorus bond forming reactions [38–42].
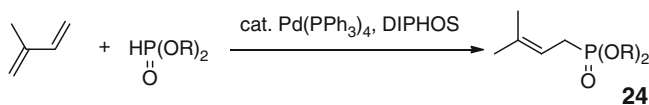
Scheme 2.14 Palladium-catalyzed phosphonation of isoprene

2.3 Vanadium-Induced Reductive Transformations

Toshikazu Hirao

Vanadium can exist in various oxidation states ranging from −3 to +5 and generally converts between states via one-electron redox processes. These properties permit the development of a wide range of organic reactions by controlling the redox potentials of vanadium compounds [43]. This control can be achieved by selecting the substituents or ligands on vanadium compounds and solvent. In general, more positive potentials are obtained through electron-withdrawing interactions with the vanadium while electron-donating interactions lead to more negative potentials. Furthermore, the redox cycles should be constructed to be reversible and/or catalytic. Thus far, only a few catalytic homogeneous processes have been reported.

This section primarily surveys reduction reactions with synthetic potential, which utilize vanadium compounds in low oxidation states to serve as versatile one-electron reductants for the generation of radical intermediates, but their synthetic utility in this respect has been limited. The efficiency of the one-electron transfer system depends on the redox potential of both the vanadium compounds and radicophiles.

A low-valent vanadium species with diethyl phosphonate or triethyl phosphite is effective for the stereoselective reduction of *gem*-dibromocyclopropanes to the corresponding monobromocyclopropanes (Scheme 2.15) [44, 45]. The less hindered bromine atom is reduced almost exclusively. The catalytic reaction proceeds with a higher stereoselectivity in the presence of zinc as a stoichiometric co-reductant. The presence of diethyl phosphonate or triethyl phosphite as a hydrogen source is
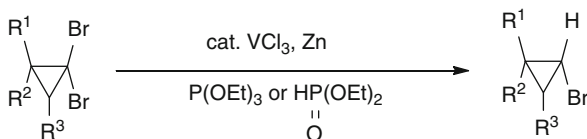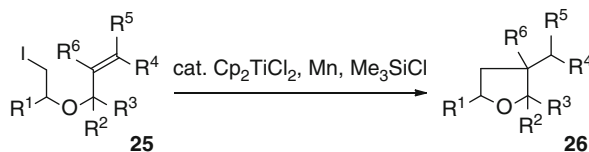
Scheme 2.15 Vanadium-catalyzed debromination of *gem*-dibromocyclopropanes

also essential to the reduction reaction. CpV(CO)$_4$ gives the higher stereoselectivity. A reversible redox cycle involving a low-valent vanadium species formed in situ operates with zinc. An ionic mechanism does not probably work in this case because triethyl phosphite produces the vanadium-containing reductant system with equal ease. The radical formed via one-electron reduction is considered to be converted to the monobromocyclopropane. The requirement for diethyl phosphonate or triethyl phosphite as a key component of the reductant system suggests that the coordination of the phosphorus raises the reduction capability. The complexation appears to increase the steric bulkiness of the reductant, which is thus compelled to attack the less-hindered bromine atom selectively. Furthermore, diethyl phosphonate is assumed to serve as a hydrogen source, possibly within the coordination sphere.

Diethyl phosphonate/low-valent vanadium and diethyl phosphonate/triethylamine [10] are two complementary reducing agents that operate probably by one-electron reduction and ionic mechanisms, respectively.

Reductive transformations are also achieved by using other low-valent metals, which permits the functionalization of *gem*-dihalocyclopropanes. For example, use of Ni(CO)$_4$ as a reductant leads to reductive cabonylation of *gem*-dibromocyclopropanes via nickel enolates [46–50].

A catalytic reductive cyclization of olefinic iodoethers **25** is performed by use of cat. Cp$_2$TiCl$_2$ in the presence of Mn and Me$_3$SiCl (Scheme 2.16). This protocol provides a selective method for the synthesis of multi-substituted tetrahydrofurans **26** [51].

Scheme 2.16 Vanadium-catalyzed reductive cyclization of olefinic iodoethers **25**

Vanadium(II) chloride catalyzes the radical-chain addition of bromotrichloromethane to terminal olefins such as allyl acetate, allyl phenyl ether, and vinyl acetate, to regioselectively form the corresponding adduct **27** [52]. Hydroxy olefins undergo the addition and subsequent cyclization to give oxacycloalkanes **28** (Scheme 2.17).
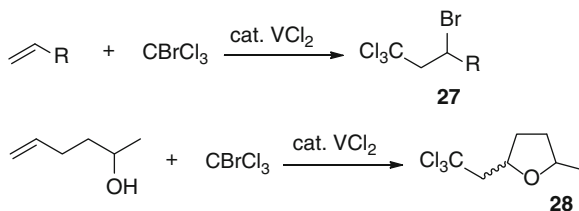
Scheme 2.17 Vanadium-catalyzed radical-chain addition reaction

2.4 Vanadium-Catalyzed Reductive Coupling

Toshikazu Hirao and Toru Amaya

The reductive dimerization of carbonyl compounds is a useful synthetic method for forming vicinally functionalized carbon–carbon bonds. One-electron transfer from a metal to a carbonyl group generates the corresponding anion radical, which can dimerize to give 1,2-diol. For the stoichiometric reductive dimerization, low-valent metals such as aluminum amalgam, zinc, titanium, vanadium, and samarium have been employed conveniently. For example, the pinacol coupling reaction using $TiCl_3/Zn$-Cu or $[V_2Cl_3(THF)_6]_2[Zn_2Cl_6]$ has been developed successfully for the synthesis of paclitaxel or C_2-symmetrical HIV protease inhibitors, respectively [53, 54]. To synthesize such compounds, the stereochemistry should be controlled [55–58]. Furthermore, a catalytic system is to be constructed. The ternary system consisting of a vanadium catalyst, a chlorosilane, and a stoichiometric co-reductant provides a catalytic protocol for the pinacol coupling. A vanadium catalyst is essential although the combination of Zn and Me_3SiCl allows the reductive dimerization of aldehydes. The low-valent vanadium species mediating the electron transfer is generated in situ, and a reversible redox cycle is formed in the presence of Zn as a stoichiometric co-reductant and a chlorosilane as an additive (Scheme 2.18).
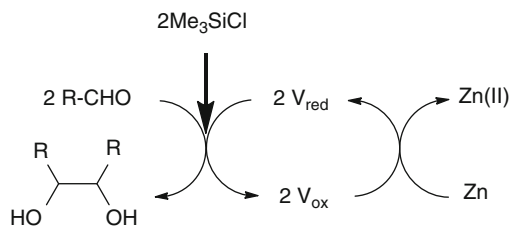
Scheme 2.18 A catalytic cycle for the vansdium-catalyzed pinacol coupling reaction

Cp_2VCl_2-catalyzed reaction of secondary aliphatic aldehydes in THF leads to the highly diastereoselective formation of the *dl*-1,2-diols **29** (Scheme 2.19) [59, 60]. The diastereoselectivity also depends on chlorosilanes: $PhMe_2SiCl$ is superior to Me_3SiCl. Cp_2TiCl_2 can be similarly employed as a catalyst [61]. The reaction in DME gives the 1,3-dioxolanes **30** via the pinacol coupling and acetalization (Scheme 2.20) [62]. A catalytic $VOCl_3/Me_3SiCl/Al$ system works well in the *dl*-selective pinacol coupling of benzaldehydes [63]. Fürstner has independently developed a similar catalytic method for the McMurry coupling of the oxoamide to the indoles in the presence of a catalytic amount of $TiCl_3$, Zn, and a chlorosilane [64].
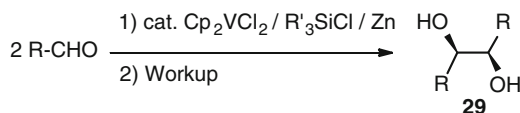
Scheme 2.19 Vanadium-catalyzed diatereoselective pinacol coupling reaction

$$3 \text{ R-CHO} \xrightarrow{\text{cat. Cp}_2\text{VCl}_2 / \text{R'}_3\text{SiCl} / \text{Zn}}$$
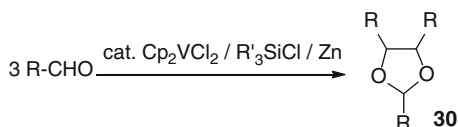
Scheme 2.20 Vanadium-catalyzed synthesis of dioxolanes **30**

In the absence of a chlorosilane, a catalytic reaction does not proceed. Silylation is assumed to liberate the catalyst from the alkoxide intermediate. The Lewis-acidic-like interaction of a chlorosilane with a carbonyl oxygen is suggested to facilitate the electron transfer to the carbonyl group, generating the stabilized silyloxyalkyl radical for dimerization. The diastereoselectivity depends on the substituent of chlorosilanes, which implies its steric effect in the coupling step. Based on these observations, a variety of modified catalytic systems have been investigated for the diastereoselective carbon–carbon bond formation [45]. A catalytic system for the enantioselective pinacol coupling is also achieved by a titanium or chromium catalyst with a chiral ligand [65–69].

This method is applied to the selective intramolecular coupling reaction of the 1,5-diketone **31** (Scheme 2.21) [59].

$$\xrightarrow{\text{cat. Cp}_2\text{VCl}_2 / \text{Me}_3\text{SiCl} / \text{Zn}}$$

syn : anti = 91 : 9
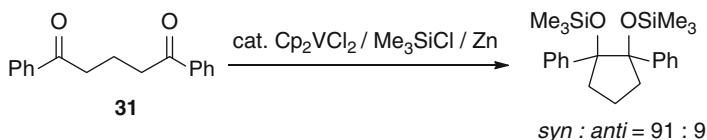
Scheme 2.21 Vanadium-catalyzed intramolecular pinacol coupling reaction of **31**

Ac$_2$O or AcCl can be utilized instead of a chlorosilane in the VOCl$_3$-catalyzed pinacol coupling reaction of aromatic aldehyde to give the diacetate **32** (Scheme 2.22) [70]. As mentioned above, a low-valent vanadium catalyst appears to be generated in situ.

$$\text{PhCHO} \xrightarrow{\text{cat. VOCl}_3 / \text{Ac}_2\text{O} / \text{Zn}}$$

dl : meso = 80 : 20
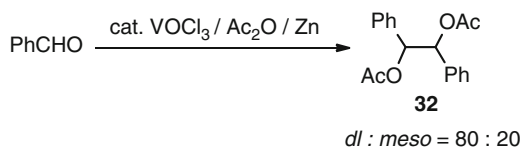
Scheme 2.22 Vanadium-catalyzed pinacol coupling reaction in the presence of Ac$_2$O

It should be noted that the reaction in water does not require the coexistence of a chlorosilane as an additive, probably since a proton source is available in this catalytic system (Scheme 2.23) [71].

$$\text{ArCHO} \xrightarrow[\text{3 equiv Zn or Al,H}_2\text{O}]{\text{0.2-0.33 equiv VCl}_3}$$
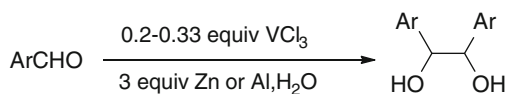
Scheme 2.23 Vanadium-catalyzed pinacol coupling reaction in water

The Cp$_2$VCl$_2$/R$_3$SiCl/Zn catalytic system can be also applicable to the reductive coupling of aldimine (Scheme 2.24) [72]. *meso*-Diamine **33** is obtained as a major product. The diastereoselectivity depends on the substituents on both the nitrogen and silane atoms. The allyl or benzyl group on the nitrogen atom is advantageous for *meso* selection.

Scheme 2.24 Vanadium-catalyzed pinacol coupling reaction of aldimines

The above-mentioned catalytic system is of synthetic potential. The reaction of the δ,ε-unsaturated aldehyde **34** with cat. Cp$_2$VCl$_2$/Me$_3$SiCl/Zn is conducted in THF to afford the cyclic alcohol **35** with excellent diastereoselectivity (Scheme 2.25) [59], probably through 5-*exo*-cyclization of the radical anion intermediate, followed by chlorination.

Scheme 2.25 Vanadium-catalyzed cyclization reaction of unsaturated aldehyde **34**

Arylidene malononitrile **36** undergoes diastereoselective catalytic cyclodimerization to **37** in the presence of chlorotrimethylsilane as shown in Scheme 2.26 [73].

Scheme 2.26 Vanadium-catalyzed cyclodimerization reaction of **36**

This method is extended to the Cp$_2$TiCl$_2$-catalyzed reductive cyclization of the ketonitrile **38**, giving the 2-amino-3-cyano-2-cyclopenten-1-ol (**39**) with high *trans* selectivity (up to 94 % *trans*) (Scheme 2.27) [74].

Scheme 2.27 Titanium-catalyzed reductive cyclization reaction of **38**

TiCl$_4$-Zn is found to induce reductive acylation of ketones with acylsilanes **40** although a stoichiometric amount of low-valent titanium species is required (Scheme 2.28) [75].

**Scheme 2.28** Titanium-induced redutive acylation reaction

For a cross-pinacol coupling, the three-dimensionally arranged bis-biphenol ligand **41** on a hexaarylbenzene scaffold for a dinuclear complex is designed and synthesized. The titanium-induced stoichiometric cross-pinacol coupling reaction is conducted using this ligand with Zn as a co-reductant to give the corresponding 1,2-diol (Scheme 2.29), where the effect of dinuclear catalyst on the cross-selectivity is clearly exhibited by comparing to the control experiment using 2,2′-biphenol instead of the bis-biphenol ligand **41** [76].
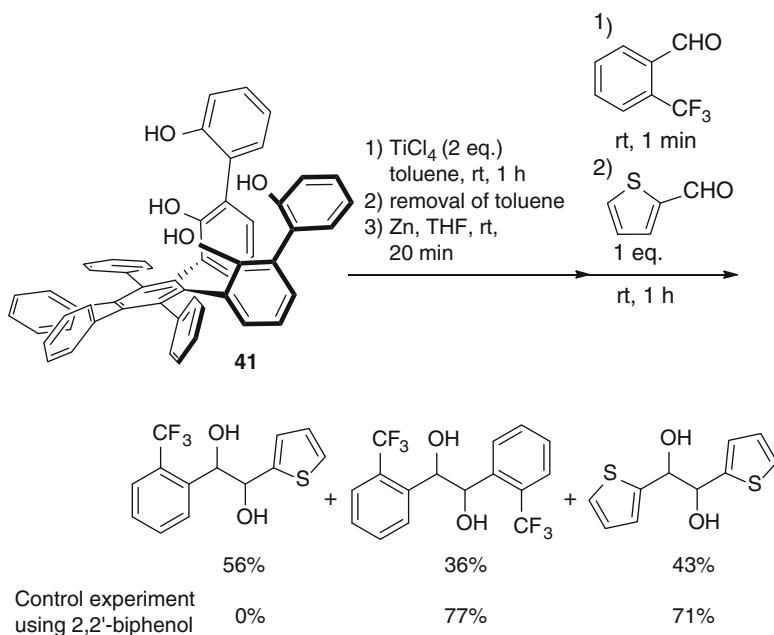
Scheme 2.29 Titanium-catalyzed cross-pinacol coupling reaction in the presence of the bis-biphenol ligand **41**

As an advanced version of the three-dimensionally arranged bis-biphenol ligand, the dinuclear dihemisalen complex **42** on the hexaarylbenzene scaffold is designed and synthesized [77, 78]. Model study for homo-pinacol coupling using mononuclear catalyst indicates the clear difference in the reactivity on aliphatic aldehyde between Ti(IV)- and V(V)-hemisalen complexes. Ti(IV)-hemisalen complex catalyzes the pinacol coupling reaction of aliphatic aldehydes, but V(V)-hemisalen complex does not. The hetero dinuclear dihemisalen complex with V(V) and Ti(IV) induces the catalytic intermolecular cross-pinacol coupling reaction between aliphatic and aromatic aldehydes in the presence of Me₃SiCl and Zn (Scheme 2.30) [78]. This is accounted for by the individual activation of two aldehydes by vanadium and titanium species, which are placed through a suitable space on the rigid scaffold.
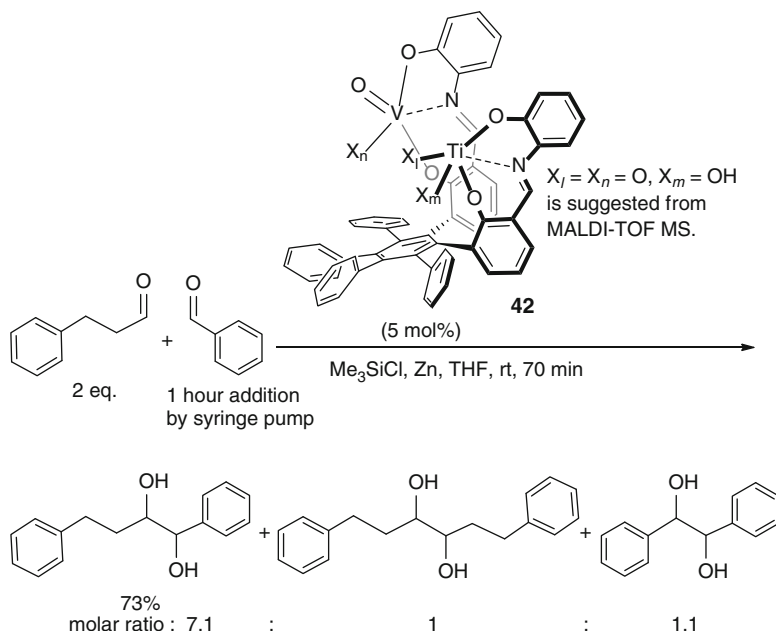
Scheme 2.30 Cross-pinacol coupling reaction catalyzed by the hetero dinuclear dihemisalen complex **42**

2.5 Samarium-Induced Reductive Transformations

Akiya Ogawa and Akihiro Nomoto

Samarium has various oxidation states: divalent species act as reducing agents, whereas trivalent species act as Lewis acids. In particular, SmI_2 as a representative divalent rare earth species is well-known to be a mild one-electron reducing reagent, which is soluble in organic solvents such as tetrahydrofuran (THF). It has been widely employed in organic synthesis, since Kagan developed a convenient preparation method of SmI_2 from samarium metal and 1,2-diiodoethane (Scheme 2.31) [79, 80]. The redox potential of SmI_2 is as follows: $(Sm^{3+}/Sm^{2+}) = -1.55$ V in water [81], $(SmI_2^+/SmI_2) = -1.41$ V in THF [82, 83]. SmI_2 itself can reduce several functional groups [80] such as aldehydes, ketones, alkyl bromides, alkyl iodides, α,β-unsaturated carbonyl compounds, epoxides, and sulfoxides. However, the co-presence of additives such as hexamethylphosphoramide (HMPA) [84], acid [85, 86], base [87], water [88, 89], and other metals [90, 91] dramatically

$$Sm + ICH_2CH_2I \xrightarrow{\quad THF \quad} SmI_2 + CH_2=CH_2$$

**Scheme 2.31** Preparation method of SmI_2 from samarium metal and 1,2-diiodoethane

enhances the reducing ability of SmI_2. Recently, we have developed two activation methods of SmI_2: one is photoirradiated activation and the other is activation by the combination with Sm metal. This section describes the synthetic advance using these SmI_2-$h\nu$ and SmI_2-Sm systems.

The wavelengths of maximum absorption of SmI_2 in THF are observed at 565 and 617 nm based on transitions from $4f^6$ to $4f^5 5d^1$ [92]. Therefore, visible light-irradiation to the THF solution of SmI_2 is a promising approach to enhance the reducing ability of SmI_2. In fact, irradiation with the light of wavelength over 500 nm or between 560 and 800 nm promotes reduction of dodecyl chloride to give dodecane efficiently. In contrast, the reduction does not take place upon irradiation with near UV light (300–420 nm) or the light of wavelength greater than 700 nm. The reduction of organic chlorides with SmI_2 alone is difficult in the dark (Scheme 2.32) [93, 94]. These results clearly indicate that irradiation with the light of wavelength between 560 and 700 nm activates SmI_2 and enhances the reducing ability of SmI_2 without addition of any additives.

| $h\nu$	300-420 nm	trace
	> 500 nm	91%
	560-800 nm	66%
	> 700 nm	trace
	dark	0
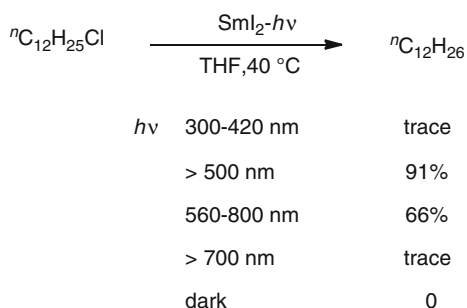
Scheme 2.32 Reducing ability of SmI_2 upon visible light-irradiation

SmI_2-induced Barbier reaction also takes place upon photoirradiation (Scheme 2.33) [93]. When o-chlorophenyl allyl ether (**43**) is reduced in the presence of diethyl ketone with SmI_2 upon photoirradiation, a cyclic ether is produced in 72 % yield. Most probably, the cyclic ether is formed by 5-exo cyclization of the aryl radical followed by reduction with SmI_2 and the subsequent addition of alkylsamarium species to diethyl ketone.
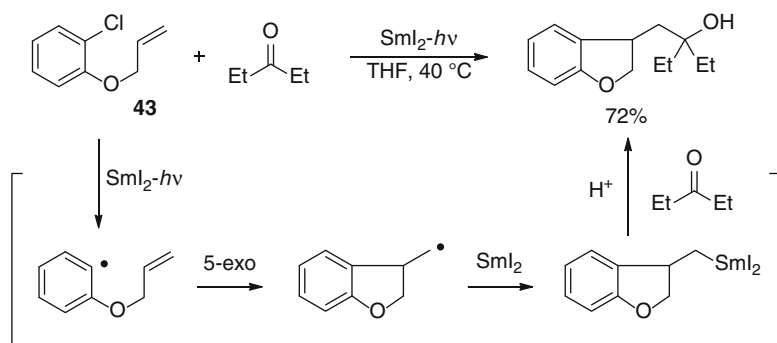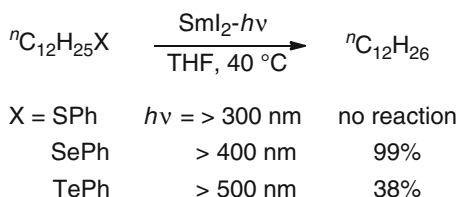

Scheme 2.33 SmI_2-induced Barbier reaction upon photoirradiation

This procedure is expected to be applied to a novel carbonylation by reduction of alkyl chlorides with SmI_2 in the presence of carbon monoxide [93]. Primary alkyl halides are allowed to react with SmI_2 upon photoirradiation under an atmosphere of CO to produce the corresponding unsymmetrical ketones in moderate yields (Scheme 2.34). In contrast, no reductive carbonylation takes place at all in the dark.
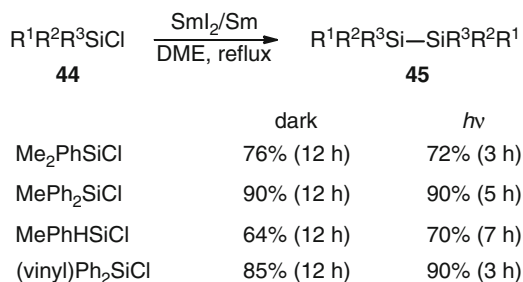
$$RCl \ + \ CO \quad \xrightarrow{SmI_2\text{-}h\nu} \quad \underset{R}{\overset{O}{\|}} \diagdown R$$
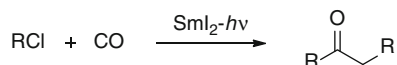
Scheme 2.34 Reaction of primary alkyl halides with CO

Not only alkyl halides but also group 16 heteroatom compounds are reduced with SmI_2 upon photoirradiation. This SmI_2-$h\nu$ system is extremely effective for the reduction of organic selenides. On the other hand, the photoinduced reduction of sulfides with SmI_2 does not proceed at all, while dodecane is obtained in 38 % yield by the photoinduced reduction of dodecyl phenyl telluride with SmI_2 (Scheme 2.35) [95].

$$^nC_{12}H_{25}X \quad \xrightarrow[\text{THF, 40 °C}]{SmI_2\text{-}h\nu} \quad ^nC_{12}H_{26}$$

X = SPh	$h\nu$ = > 300 nm	no reaction
SePh	> 400 nm	99%
TePh	> 500 nm	38%

Scheme 2.35 Photoinduced reduction of group 16 heteroatom compounds

Since SmI_2-induced reduction systems are found to be useful for the C–Cl bond reduction as mentioned above, the reduction of Si–Cl bond by using the SmI_2 systems is studied. In general, the most frequently used method for the reductive coupling of organochlorosilanes is Wurtz-type coupling with alkali metals which have ignition quality and explosibility. SmI_2-induced reductive coupling of organochlorosilanes takes place under mild conditions with safety, and successfully leads to Si–Si bond formation under mild conditions [96, 97]. Substituted aromatic chlorosilanes **44** undergo reductive dimerization to give the corresponding disilanes **45** in good to excellent yields using a SmI_2/Sm system in refluxing DME (84 °C) for 12–14 h in the dark. On the other hand, photoinduced reductive coupling of them with SmI_2/Sm in refluxing DME also affords the corresponding disilanes in high yields in a shorter time (3–7 h) (Scheme 2.36). It is remarkable that the vinyl group is unaffected under these reaction conditions.
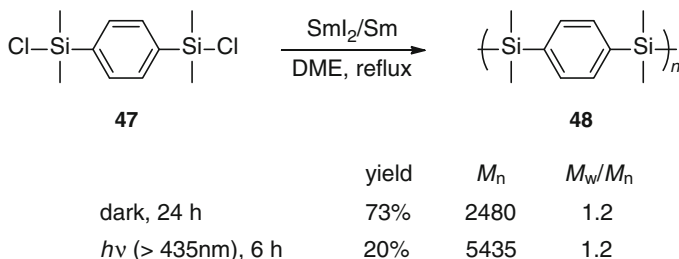
$$\underset{\mathbf{44}}{R^1R^2R^3SiCl} \quad \xrightarrow[\text{DME, reflux}]{SmI_2/Sm} \quad \underset{\mathbf{45}}{R^1R^2R^3Si-SiR^3R^2R^1}$$

	dark	$h\nu$
$Me_2PhSiCl$	76% (12 h)	72% (3 h)
$MePh_2SiCl$	90% (12 h)	90% (5 h)
MePhHSiCl	64% (12 h)	70% (7 h)
$(vinyl)Ph_2SiCl$	85% (12 h)	90% (3 h)

Scheme 2.36 SmI_2-induced reductive coupling of organochlorosilanes

These reductive coupling methods are applied to the synthesis of Si-polymers such as poly(phenylmethyl)silane and poly(*p*-disilanylenephenylene). When the reductive polymerization of dichloromethylphenylsilane with SmI$_2$/Sm is performed in the dark, the poly(methylphenyl)silane **46** is obtained in moderate yield. The molecular weight of the obtained polymer is 1,450, and the molecular weight distribution is 2.6. Reductive polymerization of the chlorosilane also takes place using SmI$_2$/Sm upon photoirradiation. Compared with the polymer synthesized in the dark, the molecular weight of the polymer synthesized under photoirradiation is higher and the molecular distribution is narrower (Scheme 2.37). 1,4-Bis(dimetylchlorosilyl)benzene (**47**) undergoes reductive coupling to give the corresponding σ-π conjugated disilane polymer **48** both in the dark and upon photoirradiation (Scheme 2.38).

|	yield	M_n	M_w/M_n
dark	42%	1450	2.6
$h\nu$ (> 435 nm)	11%	3682	1.7
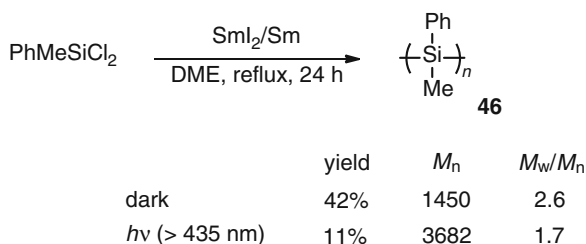
Scheme 2.37 Synthesis of Si-polymers

	yield	M_n	M_w/M_n
dark, 24 h	73%	2480	1.2
$h\nu$ (> 435nm), 6 h	20%	5435	1.2

**Scheme 2.38** Synthesis of σ-π conjugated polymer

In the Sect. 2.4, the vanadium-catalyzed reductive coupling of carbonyl compounds is described. This section also deals with the pinacol coupling using Sm reagent and chlorosilane.

Sm metal-induced reductive coupling of acetophenone in THF with sonication in the presence of Me$_3$SiCl leads to the corresponding *vic*-diol **49** in a high yield with moderate diastereoselectivity (Scheme 2.39). The yield of the *vic*-diol is lower without sonication. In the absence of Me$_3$SiCl, both yield and diastereoselectivity decrease dramatically [98].


75% (*dl*/meso = 75/25)
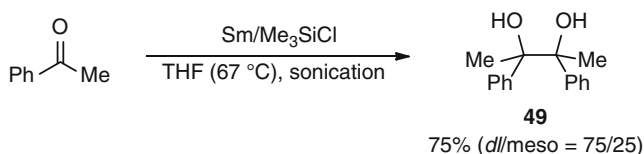
Scheme 2.39 Sm metal-induced reductive coupling of acetophenone in the presence of Me$_3$SiCl

To expand the versatility of the pinacol coupling using Sm reagents, the pinacol coupling using the SmI_2/Sm system is next studied (A. Yoshimura, A. Nomoto, T. Saeki, A. Ogawa, unpublished results). The reductive coupling of a number of carbonyl compounds such as both aromatic and aliphatic ones takes place using SmI_2/Sm system in the presence of Me_3SiCl. For example, the coupling of benzaldehyde proceeds to give the corresponding *vic*-diol **50** in a high yield using the SmI_2/Sm system in the presence of Me_3SiCl for 10 min at room temperature (Scheme 2.40). Moreover, $SmI_2/Sm/Me_3SiCl$ works well in the reductive coupling of aliphatic carbonyl compounds such as cyclohexanecarboxaldehyde, providing *dl*-selective coupling product **51** selectively (Scheme 2.41).
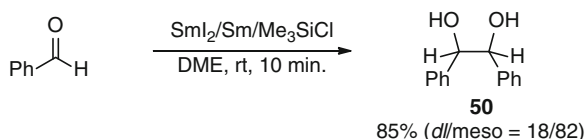
Scheme 2.40 Reductive coupling of benzaldehyde
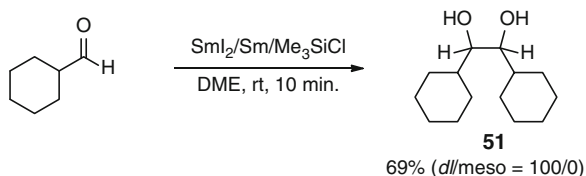
Scheme 2.41 Reductive coupling of aliphatic carbonyl compound

2.6 Oxovanadium(V)-Induced Oxidative Transformations of Olefinic and Carbonyl Compounds

Toshikazu Hirao

The synthetic scope of oxidation reactions can be broadened by exploiting the versatility of vanadium compounds as an oxidant. Vanadium compounds in high oxidation states are capable of inducing oxidative transformations. Pentavalent vanadium compounds are generally considered to be one-electron oxidants depending on the V(V)-V(IV) couple. The redox potential of this couple increases with acidity, so the reactions are usually carried out in acidic aqueous media. One-electron oxidation is also possible with the V(IV)-V(III) couple (E_0, 0.38 V), but the V(V)-V(III) couple (E_0, 0.68 V) is less useful for organic oxidation. The oxo functionality of oxovanadium compounds participates in a number of oxo-transfer reactions. Vanadium peroxides can cause either oxygenation or epoxidation. Vanadium compounds can also activate molecular oxygen for oxygenation reactions. A variety of oxidative transformations with vanadium oxidants have been developed in organic solvent. Especially, oxidation of alcohols, phenols and halide ions, epoxidation, and oxygenation of sulfides, hydrocarbons and arenes have been investigated to provide useful synthetic tools.

The VO(OEt)Cl$_2$-catalyzed reaction of styrenes with molecular oxygen in the presence of a co-reductant such as PhSiH$_3$ results in oxidation–reduction and oxidative bond cleavage of styrenes (Scheme 2.42) [99]. Coordination of the *N*-heterocyclic multidentate ligand, the 2,6-pyridinedicarboxamide of histamine (BIPA), increases the relative yield of the latter product. The Mn(OAc)$_2$-catalyzed oxidation of α-methylstyrene in the presence of BIPA under molecular oxygen selectively leads to 2-phenyl-2-propanol via oxidation-reduction. BIPA is also useful as a ligand in the Mn(OAc)$_2$-catalyzed epoxidation of α-methylstyrene with PhIO.
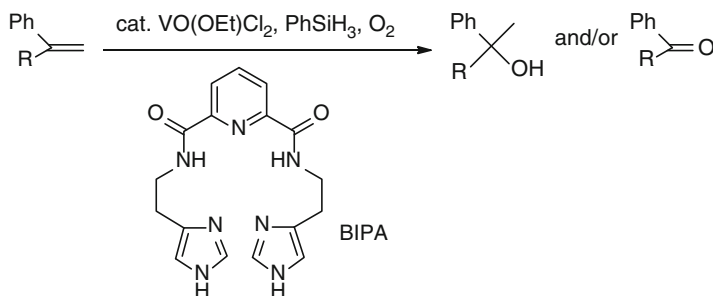
Scheme 2.42 Oxovanadium-catalyzed oxidation with molecular oxygen in the presence BIPA

Efficiency of the oxygenation catalysts largely depends on the coordination interaction with the *N*-heterocyclic moieties of podand ligands [100–102]. The catalytic epoxidation reaction of olefins with molecular oxygen is achieved by the utilization of FeCl$_2$ and BIPA. The pyridyl substituted podand ligand, 2-BPEPA shown in Scheme 2.43 is useful in the Co(OAc)$_2$-catalyzed oxygenation of phenols to the corresponding *p*- and *o*-quinones under molecular oxygen. Two 2-BPEPA is linked by the flexible spacer to lead the formation of the bimetallic nickel complex [103].
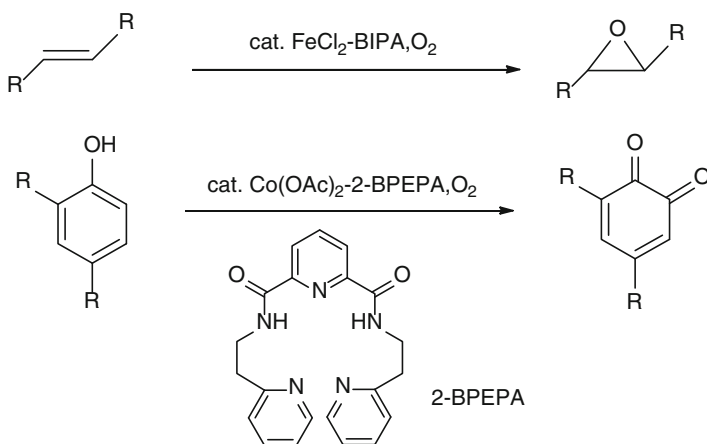

Scheme 2.43 Iron- or cobalt-catalyzed oxidation with molecular oxygen in the presence of BIPA or 2-BPEPA

VO(OR)Cl$_2$ is a Lewis acid which is capable of performing one-electron oxidation, permitting oxidative transformation of carbonyl compounds. Cyclic ketone undergoes catalytic ring-opening oxygenation in the presence of an alkanol under molecular oxygen to give the keto ester **52** or diester **53**, depending on the α-substituent (Scheme 2.44) [104]. Oxygenation accompanies the introduction of an alkoxy group. The regioselective bond cleavage is observed between the more substituted α-carbon and the carbonyl carbon.
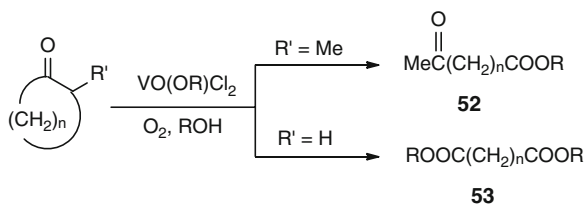
Scheme 2.44 Oxovanadium-catalyzed ring-opening oxygenation reaction

This oxygenation reaction proceeds under milder conditions as compared to conventional methods. Despite the lower reactivities, VO(OR)$_3$ and VO(acac)$_2$ can be employed as an oxidant, although a stoichiometric amount is required in each case. Use of α,β-unsaturated ketones leads the different reaction routes. 2-Cyclohexen-1-ones **54** undergo dehydrogenative aromatization to give the aryl alkyl ethers **55** [105]. More than 2 equiv. of VO(OR)Cl$_2$ are required to complete the reaction, since the oxovanadium(V) compound is a one-electron oxidant. Isophorone is also oxidatively aromatized to the aryl ether **56** with the migration of the methyl group (Scheme 2.45).
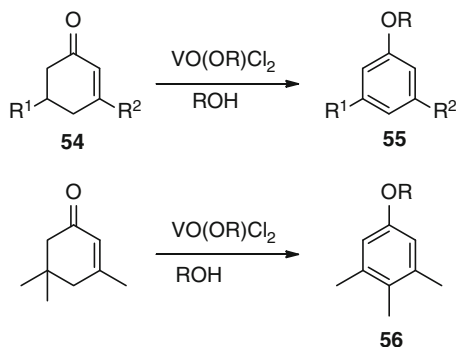
Scheme 2.45 Oxovanadium-induced oxidaion of 2-cyclohexenones

An oxovanadium species generated from VO(OR)Cl$_2$ and AgOTf or Me$_3$SiOTf induces the aromatization more effectively under the milder conditions than VO(OR)Cl$_2$ alone [106], probably due to the in situ generation of an oxovanadium triflate species.

An oxo or alkoxy group is introduced at the allylic position of 2-cyclopentenones depending on their substitution pattern, as shown in Scheme 2.46 [107]. Similarly, 1-acetyl-1-cyclohexene undergoes allylic oxidation to give 1-acetyl-3-ethoxy-1-
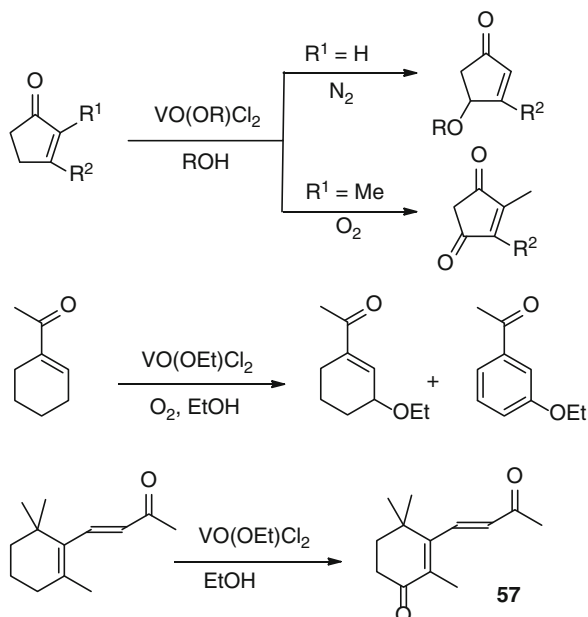
Scheme 2.46 Oxovanadium-induced allylic oxidation of α,β-unasaturated ketones

cyclohexene and 3-ethoxyacetophenone. The latter reaction is accompanied by dehydrogenative aromatization. β-Ionone is also oxygenated at the allylic position to give the dione **57**. One-electron oxidation of the dienolate intermediate is assumed to be a key step in these transformations.

The treatment of cyclobutanone with VO(OR)Cl$_2$, in the presence of an olefin bearing an electron-withdrawing group, results in tandem oxidative ring opening and addition to an olefin to give the corresponding coupled adduct **58** [108]. This reaction is facilitated by the addition of CuCl$_2$ as a co-catalyst. In the absence of an olefin, cyclobutanone undergoes chlorination to the alkyl 4-chlorobutyrate, while the addition of bromotrichloromethane leads to 4-bromobutyrate (Scheme 2.47). These reactions might proceed through the radical intermediate **60**, which is generated by ring-opening and one-electron oxidation of the alkoxide adduct **59**.
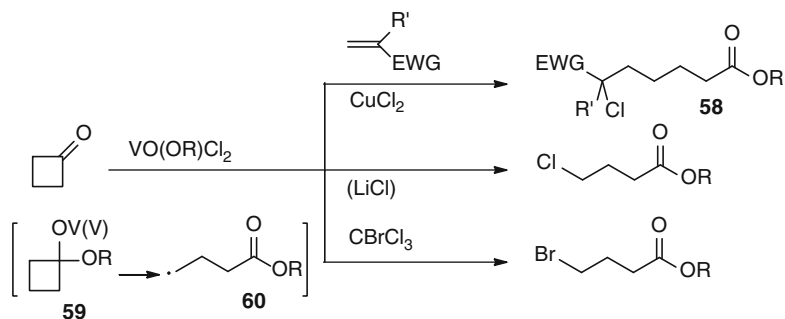
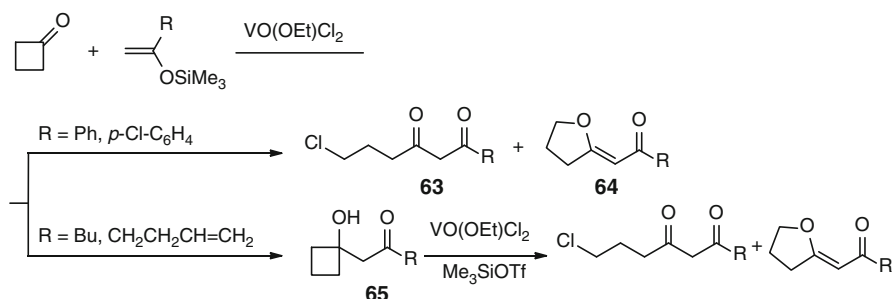**Scheme 2.47** Oxovanadium-induced ring-opening oxidation of cyclobutanone

The treatment of cyclobutanone with alkyllithium followed by VO(OEt)Cl$_2$ leads to the alkoxide intermediate, which undergo oxidative ring opening to the γ-chloro ketone **61** or the olefinic ketone **62**. Additional one-electron oxidation of the radical intermediate affords a cationic species, which is then deprotonated to give **62** (Scheme 2.48).
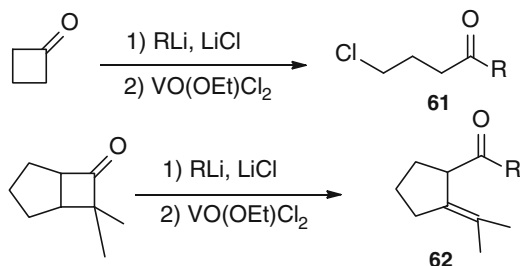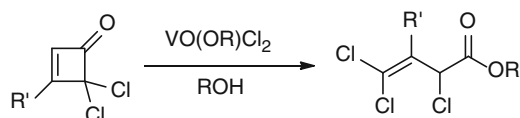

Scheme 2.48 Oxovanadium-induced ring-opening oxidation via nucleophilic addition of RLi to cyclobutanones

The nucleophilic addition of cyclobutanone with silyl enol ether is facilitated by Lewis acidic VO(OEt)Cl$_2$. The following ring-opening oxidation leads to the 6-chloro-1,3-diketone **63** and 2-tetrahydrofurylidene ketone **64** [109]. Adding lithium chloride facilitates the formation of the former product. Use of alkyl-substituted silyl enol ether leads to the cyclobutanol **65**. This product is not oxidized only with VO(OEt)Cl$_2$ under the reaction conditions, but undergoes ring-opening oxidation by treatment with VO(OEt)Cl$_2$ and Me$_3$SiOTf (Scheme 2.49).
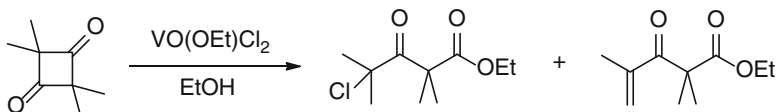

Scheme 2.49 Vanadium-induced ring-opening oxidation via nucleophilic addition of silyl enol ether to cyclobutanone

2,2-Dichloro-3-cyclobuten-1-ones are similarly oxidized with VO(OR)Cl$_2$ to give alkyl 2,4,4-trichloro-3-butenoates, regioselectively (Scheme 2.50) [110].
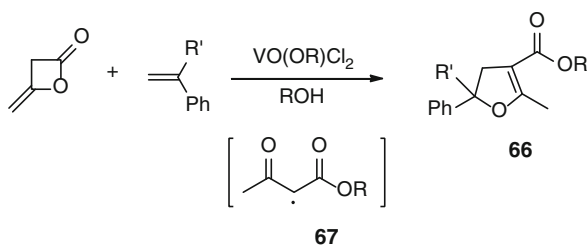

Scheme 2.50 Oxovanadium-induced ring-opening oxidation of 2,2-dichloro-3-cyclobuten-1-ones

VO(OEt)Cl$_2$-induced oxidative ring cleavage of 1,1,3,3-tetramethylcyclobutane-2, 4-dione affords 4-chloro-3-oxo-2,2,4-trimethylpentanoate and 3-oxo-2,2,4-trimethyl-4-pentenoate (Scheme 2.51) [111]


Scheme 2.51 Oxovanadium-induced ring-opening oxidation of 1,1,3,3-tetramethyl cyclobutan-2,4-dione

The VO(OR)Cl$_2$-induced ring-opening cycloaddition of diketene with styrenes leads to the 4,5-dihydofurans **66** [112]. The oxidation of diketene with VO(OR)Cl$_2$ generates a radical intermediate **67**, which then adds to olefin, followed by one-electron oxidation to the corresponding cation, to give the dihydrofuran **66** (Scheme 2.52). A similar transformation was reported in the metal-induced radical cyclization of ethyl acetoacetate [113–115].


Scheme 2.52 Oxovanadium-induced ring-opening oxidation of diketene

The oxidative mono- or diallylation of 1,3-dicarbonyl compounds by allylic silanes proceeds in the presence of VO(OEt)Cl$_2$ as shown in Scheme 2.53 [116]. The 1,3-dicarbonyl compounds formally act as electrophiles in this oxidative carbon–carbon bond forming reaction.
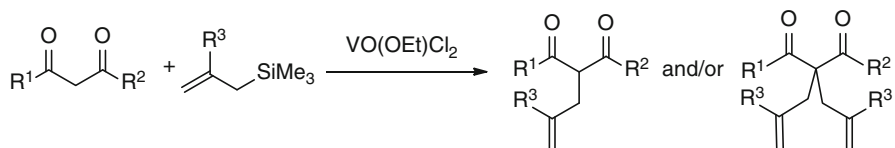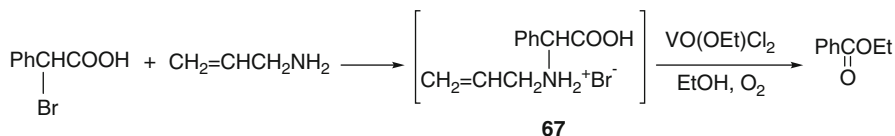

Scheme 2.53 Oxovanadium-induced oxidative mono- and diallylation reaction of 1,3-dicarbonyl compounds

The oxidative decarboxylation of amino acids is performed by VO(OEt)Cl$_2$ [117]. For example, 2-phenylglycine undergoes decarboxylative dehydrogenation, followed by oxidative esterification, to give ethyl benzoate as a major product (Scheme 2.54).

$$\text{PhCHCOOR}^1 \xrightarrow[\text{O}_2,\ \text{EtOH}]{\text{VO(OEt)Cl}_2} \text{PhCOEt} + \text{PhCCOEt}$$
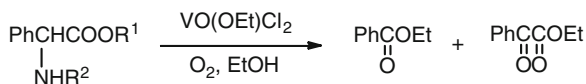
Scheme 2.54 Oxovanadium-induced oxidarion of 2-phenylglysine

This protocol is also applied to the oxidation of 2-bromo-2-phenylacetic acid via the formation of the corresponding ammonium salt **67** with allylamine as shown in Scheme 2.55.

$$\text{PhCHCOOH} + \text{CH}_2=\text{CHCH}_2\text{NH}_2 \longrightarrow \left[\begin{array}{c} \text{PhCHCOOH} \\ \text{CH}_2=\text{CHCH}_2\text{NH}_2{}^+\text{Br}^- \end{array} \right] \xrightarrow[\text{EtOH, O}_2]{\text{VO(OEt)Cl}_2} \text{PhCOEt}$$

67

Scheme 2.55 Oxovanadium-induced oxidation of 2-bromo-2-phenylacetic acid via ammonium formation

Organovanadium compounds exhibit unique reactivities based on the redox characteristics of vanadium. The organovanadium compounds generated in situ couple chemoselectively with acid chlorides or allyl halides [118]. The reaction with aldehydes gives coupled ketones possibly through oxidative nucleophilic addition (Scheme 2.56) [119, 120].

$$\text{R}^1\text{-Li} \xrightarrow{\text{VCl}_3 \qquad \text{R}^2\text{CHO}} \text{R}^1\text{COR}^2$$
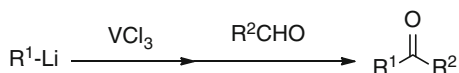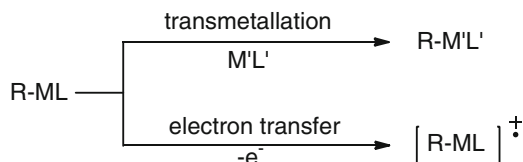
Scheme 2.56 Oxidative nucleophilic addition reaction of organovanadiums

2.7 Oxovanadium(V)-Induced or -Catalyzed Oxidative Transformations of Main-Group Organometallic Compounds

Toshikazu Hirao and Toru Amaya

Reaction of main-group organometallic compounds with a metallic oxidant is considered to proceed via transmetallation. Another reaction path lies in the redox interaction between them, affording the radical species (Scheme 2.57). These reactions are considered to provide a new route to reactive intermediates in oxidative transformations.

$$\text{R-ML} \begin{array}{c} \xrightarrow[\text{M'L'}]{\text{transmetallation}} \text{R-M'L'} \\ \\ \xrightarrow[\text{-e}^-]{\text{electron transfer}} \left[\text{R-ML} \right]^{+\cdot} \end{array}$$

Scheme 2.57 Plausible paths in the reaction of main-group organometallic compounds with a metallic oxidant

Oxidative Transformation of Organosilicon Compounds

Silyl enol ethers as electron-rich olefins are susceptible to one-electron oxidation by metallic oxidants [121–123]. The chemoselectivity in the oxidative transformations is controlled by the redox potentials of the reactants. $VO(OEt)Cl_2$ induces chemoselective homo- or cross-coupling of silyl enol ethers as shown in Scheme 2.58 to give the 1,4-diketones via regioselective carbon–carbon bond formation [124]. The more highly substituted the silyl enol ethers **68** are, the more readily they are oxidized. The silyl ketene acetals **73** are also readily oxidized and undergo cross-coupling with silyl enol ethers **69** to give the γ-keto esters **74** (Scheme 2.59).
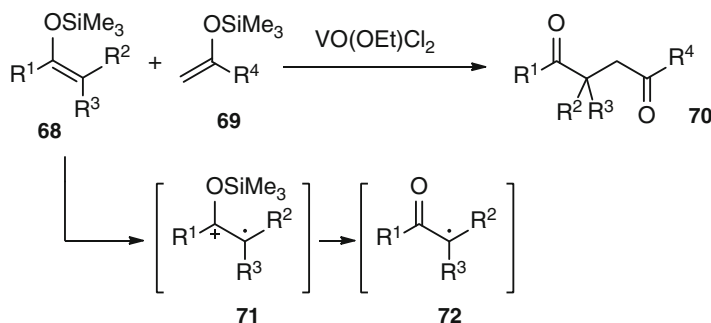
Scheme 2.58 Oxovanadium-induced oxidative cross-coupling reaction of silyl enol ethers **68** and **69**
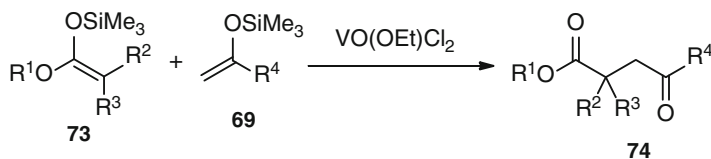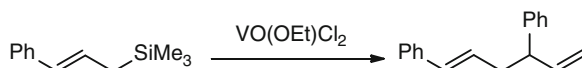

Scheme 2.59 Oxovanadium-induced oxidative cross-coupling reaction of silyl enol ethers **69** with silyl ketene acetals **73**
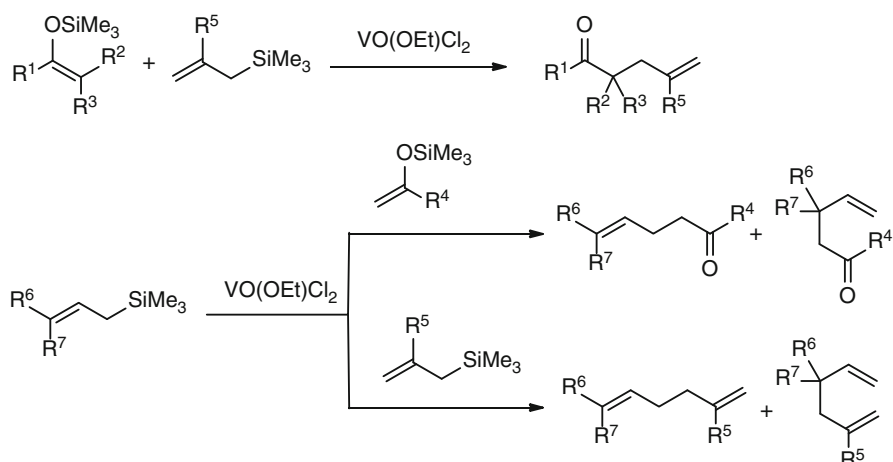
One-electron oxidation of the silyl enol ether **68** with oxovanadium(V) species affords the radical cation **71**, which is then desilylated to the radical **72**. The radical **72** intermolecularly adds to another equivalent of the silyl enol ether **69**, giving the addition adduct, which is again oxidized by the oxovanadium(V) species to form the cation. Then, this cation undergoes desilylation to give the 1,4-diketone **70**.

The selective carbon–silicon bond cleavage is of synthetic potential. Oxidative carbon–silicon bond cleavage is similarly achieved through oxovanadium(V)-induced one-electron oxidation. The carbon–silicon bond of the dihydrofuran, which is obtained by the $VO(OR)Cl_2$-induced cyclization of diketene with α-trimethylsilylstyrene is oxidatively cleaved by using $VO(OEt)Cl_2$-Me_3SiOTf, to give the furan [125].

Desilylative coupling of cinnamyltrimethylsilane results in 3,6-diphenyl-1,5-hexadiene as shown in Scheme 2.60. The cross-coupling reaction of silyl enol ethers and allylic silanes proceeds chemoselectively to give γ,δ-unsaturated ketones, in which the oxovanadium(V) oxidatively desilylate the more readily oxidizable organosilicon compound [126]. Their redox potentials determine whether they will act as a radical generator or acceptor. These redox potentials can be predicted from calculated ionization potentials. $VO(OR)Cl_2$ is a versatile oxidant, which can induce chemoselective coupling via the oxidative desilylation of a variety of organosilicon compounds under controlled conditions, as shown in Scheme 2.61.
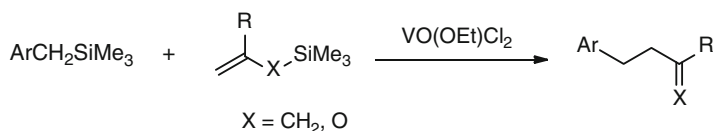

Scheme 2.60 Oxovanadium-induced oxidative coupling reaction of cinnamyltrimethylsilane
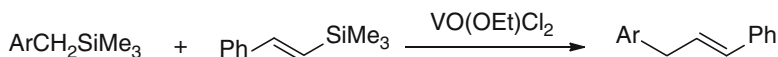

Scheme 2.61 Oxovanadium-induced oxidative cross-coupling reaction of silyl enol ethers and allylic silanes

Benzylic silane bearing an electron-donating group at the *ortho*- or *para*-position similarly undergo the oxidative desilylation. The electron-donating group lowers the ionization potential, thus activating it for desilylation. The desilylation reaction is applied to intermolecular regioselective coupling between substituted benzylic silane and allylic silane or silyl enol ether (Scheme 2.62) [127].

$$X = CH_2, O$$

Scheme 2.62 Oxovanadium-induced oxidation of benzylic silanes with allylic silanes or silyl enol ethers

The β-stabilizing effect of the trimethylsilyl group is a key factor in controlling the regiochemistry of the carbon–carbon bond formation. Benzyltrimethylsilanes react with β-trimethylsilylstyrene, but not with α-trimethylsilylstyrene (Scheme 2.63).

$$ArCH_2SiMe_3 \quad + \quad Ph\diagup\diagdown SiMe_3 \xrightarrow{\text{VO(OEt)Cl}_2} Ar\diagdown\diagup Ph$$

Scheme 2.63 Oxovanadium-induced oxidative cross-coupling reaction of benzylic silanes with β-trimethylsilylstyrene

These oxidative desilylation reactions mentioned here provide a versatile method for intermolecular carbon–carbon bond formation, in which the organosilicon compounds formally act as an electrophile (umpolung).
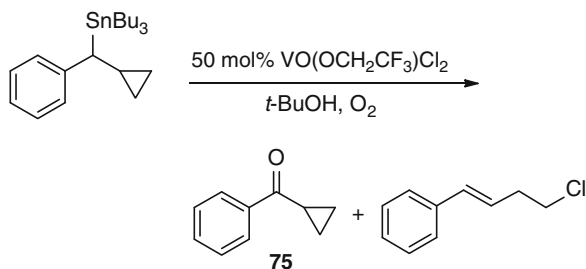
Oxidative Transformation of Organotin Compounds

Allylic and benzylic tins are known to undergo more facile oxidation than the corresponding silicon compounds, and are converted to the alcohols or their derivatives by a metallic oxidant such as Mn(IV), Ce(IV), Tl(III), or Fe(III) [128–132]. The reaction of benzyltributyltins with $VO(OCH_2CF_3)Cl_2$ in t-BuOH under molecular oxygen leads to the aldehydes (ketones) and the carboxylic acids (Scheme 2.64) [133, 134]. The susceptibility to the oxidation depends on the substituent on the arene ring. $VO(OCH_2CF_3)Cl_2$ and $VO(OPr$-$i)_2Cl$ are superior to a weaker oxidant such as $VO(acac)_2$, $VO(OPr$-$i)_3$, or $VO(OEt)_3$. Furthermore, the catalytic reaction proceeds with $VO(OCH_2CF_3)Cl_2$.
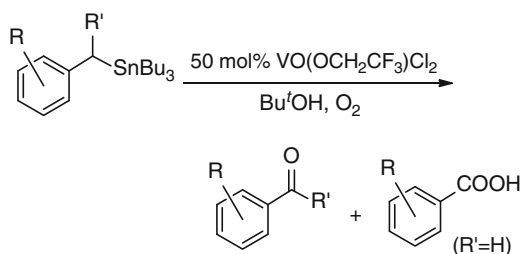
Scheme 2.64 Oxovanadium-induced oxidation of benzylic tins

Cyclopropyl-1-phenylmethyltributyltin is oxidized to the cyclopropyl ketone **75** as a major product (Scheme 2.65). As for ring-opened compounds, neither the aldehyde nor the carboxylic acid is detected, although only a small amount of the chloride is obtained, suggesting that the electron-transfer mechanism is not involved. Although benzyltins undergo more facile oxidation than benzylsilanes, the cyclopropyl ketone may be derived by transmetallation [134].
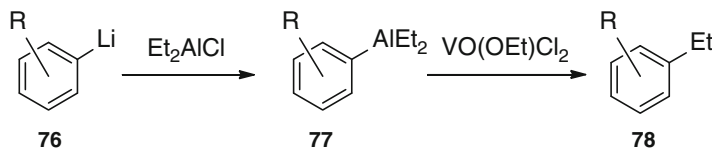
Scheme 2.65 Oxovanadium-induced oxidation of cyclopropyl-1-phenylmethyltributyltin

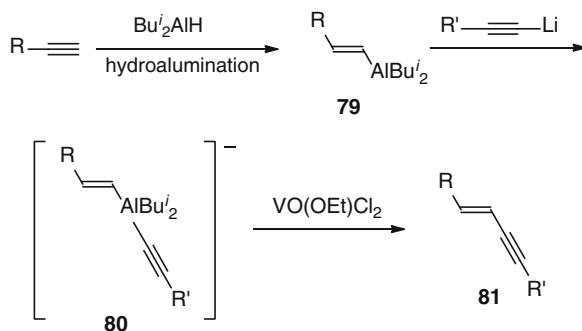## Oxidative Transformation of Organoaluminum Compounds

The transition-metal-catalyzed cross-coupling reactions of main-group organometallic compounds with organic halides provide versatile synthetic tools in organic synthesis. The reaction pattern lies in the coupling between an electrophile and a nucleophile. As mentioned above, the transmetallation and/or electronic interaction can widen the reactivities of main-group organometallic compounds. One-electron oxidation of d^o-transition metal compounds such as titanocene, zirconocene, and platinum compound with a metallic oxidant permits synthetically versatile transformations via organometallic cation radical species as key intermediates. In these reactions, selective coupling is achieved between two ligands on the transition metal, providing a useful method for carbon–carbon bond formation. From this point of view, the usage of main-group organometallics is limited due to their restricted redox properties. Oxidation of organoaluminum compounds usually affords alcohols, but the selective carbon–carbon bond formation of organic substituents on aluminum has not been investigated.

Treatment of the aryldiethylaluminums, obtained from aryllithiums **76** and diethylaluminum chloride, with VO(OEt)Cl$_2$ results in ethylation to give ethylarenes **78** (Scheme 2.66) [135]. This method is applied to a wide variety of arylaluminums **77** bearing an electron-donating group, permitting the selective ligand coupling of the organic substituents on aluminum.
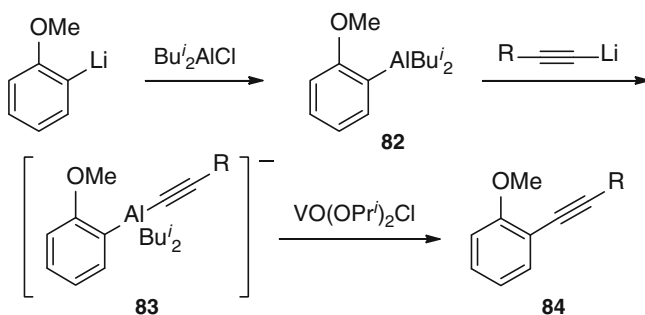

Scheme 2.66 Oxovanadium-induced oxidative ligand coupling reaction of organoaluminums **77**

The ate complexes **80** can be similarly employed in the coupling of organic substituents on aluminum. The addition of 1-alkynyllithium to the 1-alkenylaluminum **79**, followed by treatment with VO(OEt)Cl$_2$, leads to the *trans*-enyne **81** via chemoselective and stereoselective bond formation between *sp* and *sp*^{2} carbons (Scheme 2.67) [136].

Scheme 2.67 Oxovanadium-induced oxidative ligand coupling reaction of organoaluminum ate complexes **80** (between alkenyl and alkynyl carbons)

The ate complex **83** derived from the aryl-substituted aluminum **82** and 1-alkynyllithium also undergoes the selective ligand coupling to give the aryl-1-alkynyl coupling product **84** (Scheme 2.68).
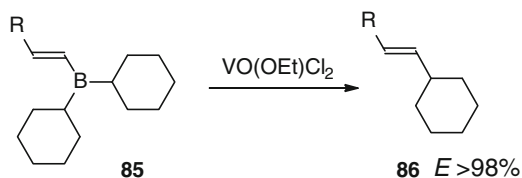

Scheme 2.68 Oxovanadium-induced oxidative ligand coupling reaction of organoaluminum ate complexes **83** (between aryl and alkynyl carbons)

Although the reaction mechanism is ambiguous, coordination of oxovanadium(V) species to organoaluminums is considered to promote electron transfer or transmetallation for the oxidative ligand coupling. This transformation is the first example for the formal reductive elimination on aluminum.
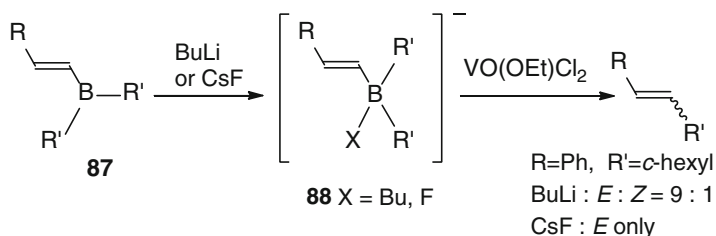
Oxidative Transformation of Organoboron Compounds

The organoboron compound **85**, prepared from dicyclohexylborane and phenylacetylene or acetylenecarboxylic ester, is oxidized with VO(OEt)Cl$_2$ to give the (*E*)-ethenylcyclohexane **86** chemoselectively without the formation of dicyclohexyl and 1,4-butadiene derivative (Scheme 2.69) [137]. A cross-over reaction indicates that the coupling reaction occurs mostly in an intramolecular fashion.

Scheme 2.69 Oxovanadium-induced oxidative ligand coupling reaction of organoborons **85**

The ate complexes **88** of the organoborons **87** shown in Scheme 2.70 undergo more facile oxidation with VO(OEt)Cl$_2$, as observed in the aluminum ate complexes. The organic groups are differentiated in the coupling reaction. Although small amounts of the *Z* isomer is obtained in the case of the BuLi-derived ate complex, use of the organoborate derived from CsF improves the stereoselectivity, giving the *E* isomer exclusively.
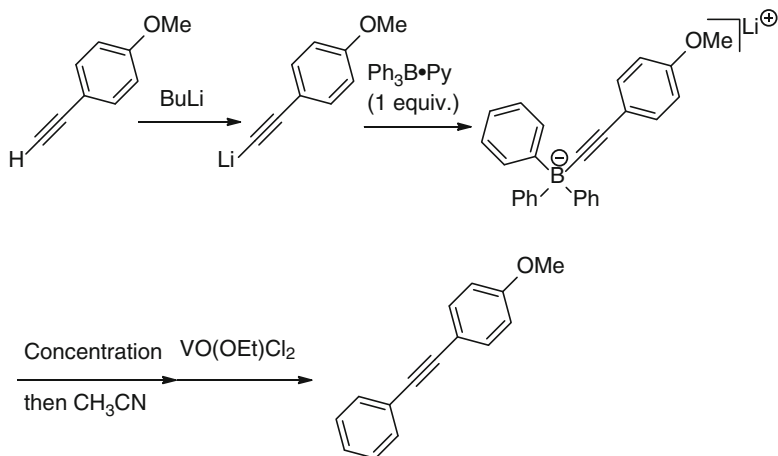

Scheme 2.70 Oxovanadium-induced oxidative ligand coupling reaction of organoborates **88**

Alkenyltrialkylborates are known to be oxidized to alkylated alkenes with I$_2$ or BrCN [138]. Biaryl formation also occurs by photochemical, electrochemical, and chemical oxidation, for example with Ir(IV), of tetraarylborates [139–141]. The oxovanadium(V)-induced ligand coupling provides another promising method for the carbon–carbon bond formation on boron.

Catalytic oxidative ligand coupling of the organoborates is achieved by VO(OEt)Cl$_2$ under molecular oxygen, affording a versatile method for the chemoselective synthesis of symmetrical or unsymmetrical biaryls (Scheme 2.71) [142]. The reduced oxovanadium species is reoxidized in situ under molecular oxygen. This intramolecular oxidative ligand coupling is extended to the selective aryl-alkynyl coupling (Scheme 2.72) [143].
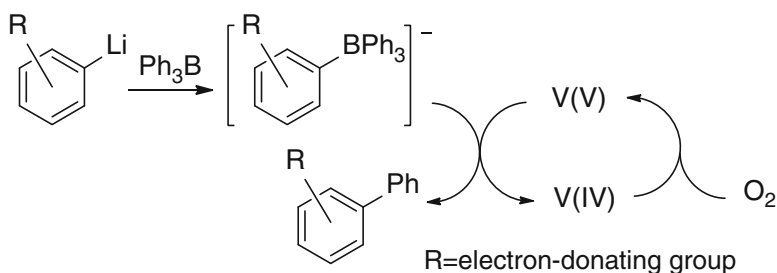

Scheme 2.71 A catlytic cycle for the ligand coupling reaction of aryltriphenylborates

Scheme 2.72 Oxovanadium-induced oxidative ligand coupling reaction of organoborates (between aryl and alkynyl carbons)

Oxovanadium(V)-induced oxidative coupling of boron enolates **89** provides the corresponding 2,3-disubstituted 1,4-diketone **90** in a good yield (Scheme 2.73) [144]. High *dl*-selectivity is attained when the reaction is performed with (*Z*)-boron enolates and VO(OPr-*i*)$_2$Cl at −30 °C.
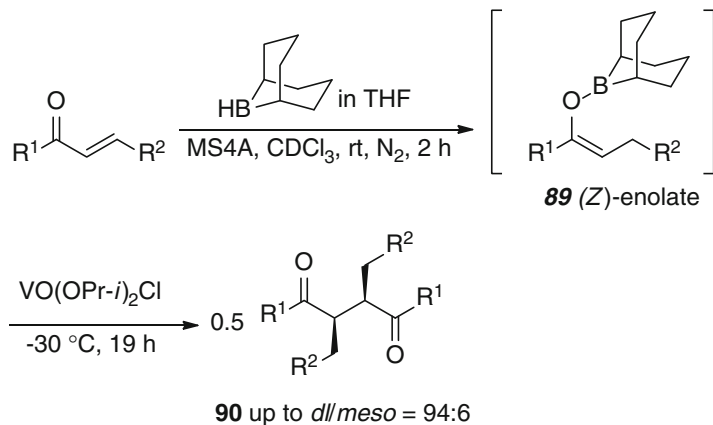

Scheme 2.73 Oxovanadium-induced oxidative coupling reaction of boron enolates **89**

Oxidative Transformation of Organozinc Compounds

Organozinc compounds tolerate a broad range of functional groups. Cross-coupling reactions between organozinc reagents and electrophiles such as organic halides are catalyzed by transition metal complexes. However, examples for the selective

cross-coupling of two ligands of organozinc compounds are limited to a few cases, which include 1,2-migration of zincate carbenoids and intramolecular coupling of organozinc compounds by organocopper reagents [145–147].

The organozinc compound **91**, prepared in situ by transmetallation of methylzinc chloride with the aryllithium, is oxidized with Cp_2FePF_6, to give the homo-coupled biaryl selectively (Scheme 2.74). $AgBF_4$ serves as an oxidant to give the desired cross-coupling product, probably via one-electron oxidation process. Using $VO(OEt)Cl_2$ instead of $AgBF_4$, the cross-coupling reaction proceeds in preference to the homo-coupling reaction [148]. The higher selectivity for the cross-coupling is observed with $VO(OEt)Cl_2$ than with $VO(OPr-i)Cl_2$ or $VO(OPr-i)_2Cl$.
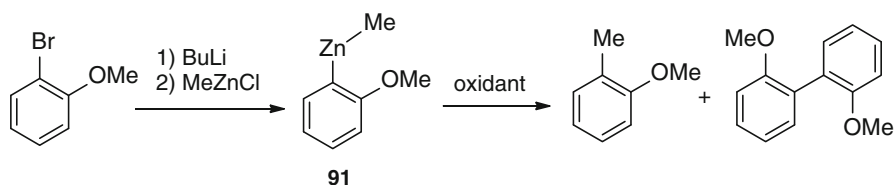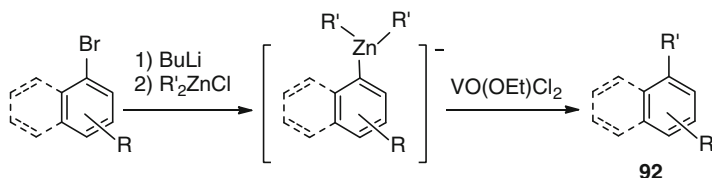

Scheme 2.74 Oxidative ligand coupling reaction of organozinc **91**

The coupling reaction of organozinc compounds bearing an *o*-methoxy, *o*-phenyl, or *o*-methylthio group on the arene ring proceeds smoothly. The alkyl(*o*-cyano substituted aryl)zinc exhibits a lower reactivity, although organoaluminum compounds bearing an electron-withdrawing substituent do not undergo oxidative coupling under the similar conditions. Alkyl and 1-alkynyl groups can couple with the aryl group (Scheme 2.75).
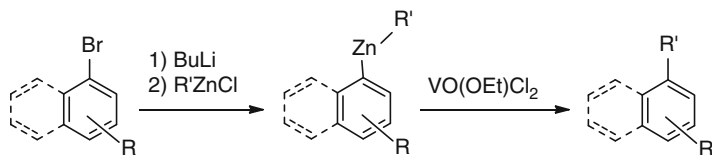
Scheme 2.75 Oxovanadium-induced oxidative ligand coupling reaction of organozincs

Triorganozincates are oxidized with $VO(OEt)Cl_2$ more smoothly to give the cross-coupling compounds **92** as shown in Scheme 2.76 [148].

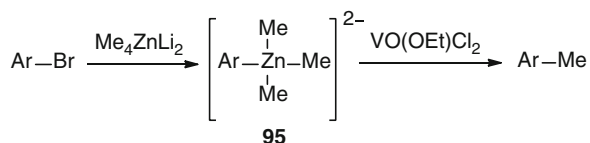**Scheme 2.76** Oxovanadium-induced oxidative ligand coupling reaction of organozincates

When the conversion to the zinc ate complex is not complete, the homo-coupling product derived from the oxovanadium(V)-induced oxidation of aryllithium is accompanied

[136]. Such a reaction is avoided by the preparation of the ate complex through iodine-zinc exchange. Arylzincate **93**, obtained from R$_3$ZnL [149] and aryl iodide, is oxidized to give the cross-coupling product **94** exclusively (Scheme 2.77) [148].
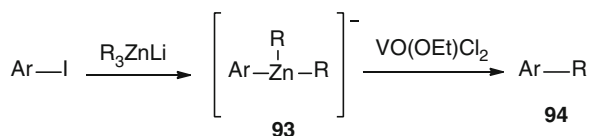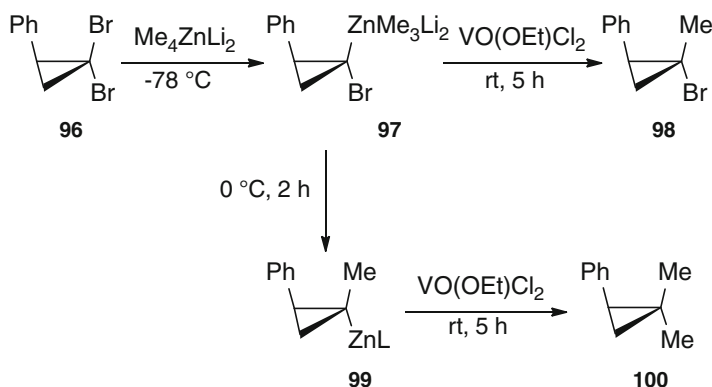

Scheme 2.77 Oxovanadium-induced oxidative ligand coupling reaction of organozincates **93** generated from aryl iodides and R$_3$ZnLi

The organozincates, prepared from Me$_4$ZnLi$_2$ and various bromoarenes [149], undergo similar oxidative coupling with VO(OEt)Cl$_2$ to give the methylarene (Scheme 2.78) [150]. Thus, the coupling between sp^2 carbon (aryl group) and sp^3 carbon (methyl group) of aryltrimethylzincates is achieved chemoselectively.

Scheme 2.78 Oxovanadium-induced oxidative ligand coupling reaction of organozincates **95** generated from aryl bromides and R$_4$ZnLi

The above-mentioned method is applied to the selective carbon–carbon bond formation between sp^3 carbons [150]. A bromine-zinc exchange reaction of the *gem*-dibromocyclopropane **96** selectively occurs at the position *cis* to the phenyl group by treatment with Me$_4$ZnLi$_2$ [151]. The reaction of the thus-obtained zincate **97** with VO(OEt)Cl$_2$ leads to the stereoselective formation of 1-bromo-1-methyl-2-phenylcyclopropane (**98**). On the other hand, when the reaction mixture is warmed up to 0 °C, followed by treatment with VO(OEt)Cl$_2$, dimethylation at the *gem*-positions takes place to give the dimethylcyclopropane (**100**) via the organozinc **99** as shown in Scheme 2.79)


Scheme 2.79 Oxovanadium-induced oxidative ligand coupling reaction of organozincates derived from **96**

Dialkylzinc reagents (R_2Zn) are known as a mild nucleophile in the presence of an additional promoter such as a Lewis acid. The properties of oxovanadium(V) compounds as a Lewis acid and one-electron oxidant permit vicinal dialkylation at both the α and β positions of cyclic α,β-unsaturated carbonyl compounds with dialkylzinc reagents via conjugate addition and ligand coupling (Scheme 2.80) [152]. For example, the reaction of 2-cyclohexenone with dimethylzinc in the presence of VO(OEt)Cl$_2$ affords 2,3-dimethylcyclohexanone (Scheme 2.81). Use of a stronger Lewis acid, VO(OEt)Cl$_2$ > VO(OPr-i)Cl$_2$ > VO(OPr-i)$_2$Cl, gives a better result.
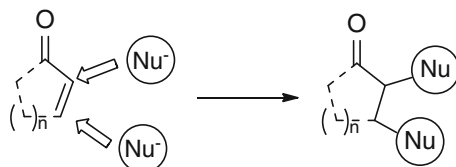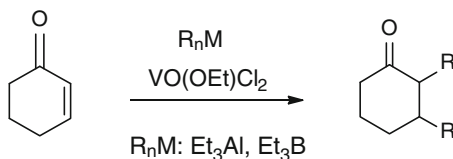

Scheme 2.80 Vicinal dialkylation via conjugate addition and ligand coupling
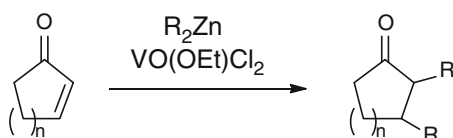
Scheme 2.81 Oxovanadium-induced vicinal dialkylation of cyclic α,β-unsaturated carbonyl compounds with dialkylzincs

This method is applied to vicinal alkylation with triethylaluminum or triethylborane as shown in Scheme 2.82 [152], but the similar oxidative dialkylation is not observed with organocuprate reagents.

Scheme 2.82 Oxovanadium-induced vicinal dialkylation of 2-cyclohexenone with triethylaluminum or triethylborane

Contrary to dialkylzincs, lithium trialkylzincates (R_3ZnLi) is nucleophilic enough for conjugate addition without the aid of a Lewis acid. The conjugate addition adduct with $R_2R'ZnLi$ is then treated with VO(OEt)Cl$_2$, leading to vicinal dialkylation as shown in Scheme 2.83. It is noteworthy that introduction of alkyl groups is differentiated regioselectively. For example, use of BuMe$_2$ZnLi leads to regioselective formation of 3-butyl-2-methylcycloalkanone.

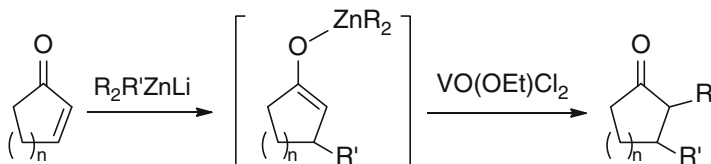**Scheme 2.83** Oxovanadium-induced vicinal dialkylation of cyclic α,β-unsaturated carbonyl compounds with R$_3$ZnLi

Oxidative Transformation of Organozirconium Compounds

The oxidation reaction of (*E*)-1-alkenylchlorozirconocenes **101** with VO(OPr-*i*)$_2$Cl results in the stereoselective homo-coupling product, the (*E,E*)-diene **102** (Scheme 2.84) [153]. (*E*)-1-Alkenyl-1-alkynylzirconocenes **103** undergo the oxovanadium(V)-induced ligand coupling of the organic substituents on zirconium to give the (*E*)-enynes **104** stereoselectively.
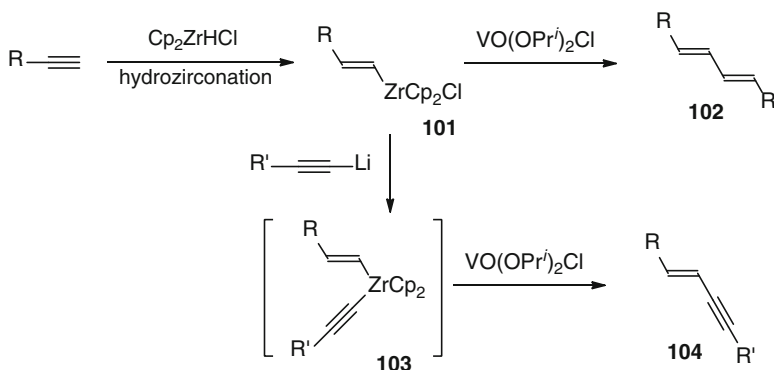
Scheme 2.84 Vanadium-induced oxidative coupling reaction of organozirconocenes **101** and **103**

As mentioned above, the ligand coupling reaction of main-group organometallic compounds provides a versatile method foe carbon–carbon bond formation of nucleophiles, which is a complementary strategy of nucleophile–electrophile coupling reaction.

2.8 Oxovanadium(V)-Catalyzed Halogenation

Toshikazu Hirao and Toshiyuki Moriuchi

The bromination reaction of organic compounds is regarded as one of the most fundamental reactions in organic synthesis, providing important precursors for various transformations. Conventional bromination reaction requires toxic and hazardous elemental bromine. An alternative environmentally friendly method is to be developed. Considerable efforts have been focused on developing a practical bromination method by using a bromide ion as a bromide source instead of bromine [154, 155]. In these methods, the bromination reaction proceeds by utilizing generation of a bromonium-like species which is generated by two-electron oxidation of a bromide ion. Hydrogen peroxide [156], oxone® [157], cerium(IV) ammonium nitrate (CAN) [158], sodium periiodate [159], lead tetraacetate [160], and Selectfluor® [161]

have been demonstrated to serve as an oxidant, inducing oxidative bromination of alkenes and alkynes in the presence of bromide salts such as alkali metal bromide or Bu$_4$NBr (Scheme 2.85a).
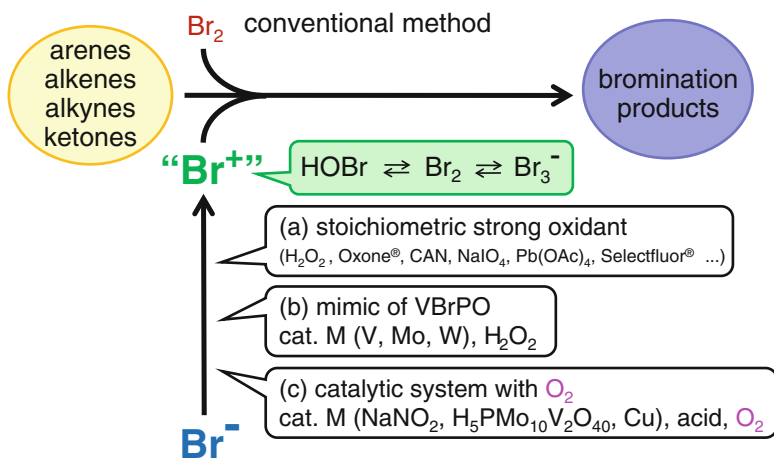
Scheme 2.85 Development of practical methods for bromination

Vanadium bromoperoxidase (VBrPO) [162–165], which is a naturally occurring enzyme found in marine algae, catalyzes two-electron oxidation of the bromide ion in the presence of H$_2$O$_2$, affording a bromonium cation-like species. The catalytic bromination of organic compounds has been demonstrated by using VBrPO [164–168]. Much attention has been paid to the oxidative bromination reaction induced by mimicking of the catalytic activity of VBrPO (Scheme 2.85b) [167, 169–182]. An environmentally friendly catalytic oxidative bromination of arenes, alkenes, and alkynes in aqueous media is demonstrated under relatively mild conditions by using a commercially available inexpensive NH$_4$VO$_3$ catalyst combined with H$_2$O$_2$, HBr, and KBr (Scheme 2.86) [183]. Dodecyltrimethylammonium bromide serves as an efficient surfactant to facilitate the NH$_4$VO$_3$-catalyzed oxidative bromination in aqueous media.
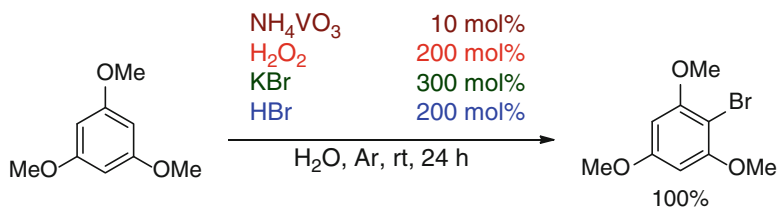
Scheme 2.86 Oxidative bromination reaction of 1,3,5-trimethoxybenzene with hydrogen peroxide

From an environmental point of view, molecular oxygen is regarded as the best candidate for oxidants. Some oxidative bromination reactions with molecular oxygen as a terminal oxidant in place of a strong oxidant have been reported, providing the more advanced catalytic systems rather than the enzyme (Scheme 2.85c) [184, 185]. The combination of the redox properties of a vanadium catalyst and molecular oxygen is performed to provide an environmentally benign catalytic system in oxidative bromination. The oxidative bromination reaction of 1,3,5-trimethoxybenzene with 5 mol% of NH_4VO_3, 300 mol% of Bu_4NBr, and 300 mol% of trifluoroacetic acid (TFA) in 1,4-dioxane with molecular oxygen at 80 °C proceeds to give the formation of the monobromination product in 80 % isolated yield (Scheme 2.87) [186]. The use of p-toluenesulfonic acid monohydrate ($PTS \cdot H_2O$) in place of TFA results in the lower yield of the monobromination product (62 % NMR yield). The similar catalytic activity is observed with $NaVO_3$ as compared with the ammonium counterpart. V_2O_5 is found to be less effective than NH_4VO_3. $VO(acac)_2$ and $VOSO_4$ work similarly as observed with NH_4VO_3. WO_3, which is known to catalyze the oxidative bromination with H_2O_2 [44], does not serve as a catalyst. No promising results are observed with the oxo metal complexes including $TiO(acac)_2$, $MoO_2(acac)_2$, and MnO_2. Acetonitrile, dimethylformamide, acetic acid, and dimethoxyethane are less effective than 1,4-dioxane. The oxidative bromination reaction of 1,3,5-trimethoxybenzene proceeds well, even under air, in the presence of 600 mol% of Bu_4NBr and TFA to give the bromination compound in 70 % yield. The catalytic activity depends on the amounts of the bromide source and acid. The oxidative bromination reaction in the presence of 900 mol% of the bromide source and acid leads to the dibromide with the concomitant monobromo compound (Scheme 2.88). The presence of acid and molecular oxygen is essential for an efficient catalytic oxidative bromination reaction.
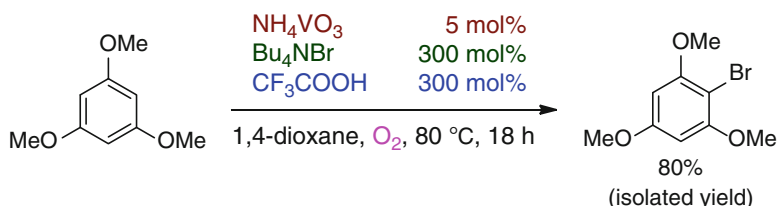
Scheme 2.87 Oxidative bromination reaction of 1,3,5-trimethoxybenzene with molecular oxygen
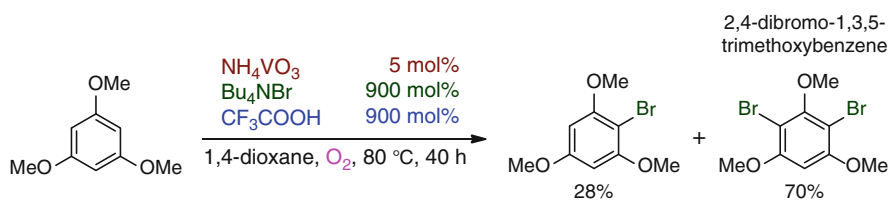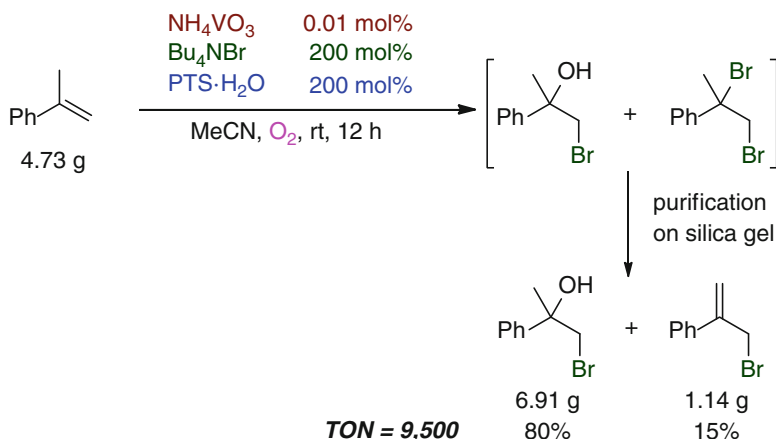

Scheme 2.88 Oxidative bromination reaction of 1,3,5-trimethoxybenzene in the presence of 900 mol% of the bromide source and acid

This catalytic system can be applied to the oxidative bromination reaction of a variety of arenes, alkenes, and alkynes [186]. The oxidative bromination reaction of the phenol derivatives, such as 2,6-xylenol and resorcinol, leads to the monobrominated compounds regioselectively. The oxidative bromination reaction of α-methylstyrene in the presence of 5 mol% NH_4VO_3, 900 mol% Bu_4NBr, and 900 mol% TFA in 1,4-dioxane at 80 °C affords only the bromohydrin in 60 % yield. On the other hand, the dibromide (33 %) and the bromohydrin (62 %) are obtained in the case of α-methylstyrene by using 1 mol% of NH_4VO_3 and 200 mol% of $PTS \cdot H_2O$ and Bu_4NBr in acetonitrile. The oxidative bromination reaction of *trans*-β-methylstyrene affords the *erythro*-dibromide (59 %) and 2-bromo-1-phenylpropan-1-ol (18 %), wherein 2-bromo-1-phenylpropan-1-one (15 %) is also obtained. In the case of *cis*-β-methylstyrene, the *threo*-dibromide (51 %) together with small amounts of the *erythro* isomer (9 %), 2-bromo-1-phenylpropan-1-ol (17 %), and 2-bromo-1-phenylpropan-1-one (11 %) are produced. The oxidative bromination reaction of allylbenzene and 1-decene proceeds well to give the dibromides in 94 % and 97 % yields, respectively (5 mol% NH_4VO_3, 900 mol% Bu_4NBr, and 900 mol% TFA in 1,4-dioxane at 80 °C). Starting from 5-hexene-1-ol, the dibromide is obtained in a 94 % yield, with the hydroxy group intact under the similar reaction conditions. The oxidative bromination reaction of 1-phenylpropyne and 1,4-dimethoxy-2-butyne affords only the *trans*-1,2-dibromoalkenes in 98 % and 77 % yields, respectively.

The catalyst loading can be successfully reduced to 0.01 mol% in the gram-scale reaction of α-methylstyrene as shown in Scheme 2.89, indicating an extremely high efficiency of the catalyst [186].

Scheme 2.89 Gram-scale catalytic oxidative bromination reaction of α-methylstyrene

Use of a Lewis acid in place of a Brønsted acid is expected to provide the more practical bromination reaction system as follows: (1) Expanding of the substrate adaptability. (2) Improvement of efficiency by controlling the Lewis acidity. (3) Enantioselective bromination induced by a chiral Lewis acid. The catalytic bromination reaction of 1,3,5-trimethoxybenzene in the presence of 5 mol% of NH_4VO_3, 120 mol% of Bu_4NBr, and 120 mol% of $AlCl_3$ as a Lewis acid in 1,4-dioxane at 80 °C for 18 h with molecular oxygen proceeds well to afford the monobromide (Scheme 2.90) [187, 188]. $FeCl_3$, $CoCl_2$, and $ZnCl_2$ are less or not effective as a Lewis acid. When $CuCl_2$ or $BF_3 \cdot OEt_2$ is employed instead of $AlCl_3$, the bromination product is obtained in a lower yield. In the presence of 300 mol% of Bu_4NBr and 300 mol% of $AlCl_3$, the dibromination product, 2,4-dibromo-1,3,5-trimethoxybenzene, is obtained in a quantitative yield. Use of 300 mol% of TFA in place of $AlCl_3$ leads to the formation of only 80 % of the monobromide, indicating that $AlCl_3$ exhibits the higher efficiency than TFA.
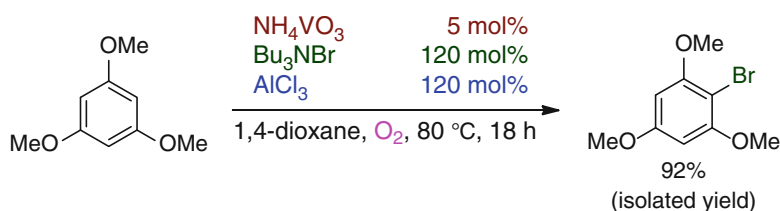
Scheme 2.90 Oxidative bromination reaction of 1,3,5-trimethoxybenzene in the presence of 120 mol% of Bu4NBr, and 120 mol% of $AlCl_3$

The catalytic bromination reaction of 2,6-dimethylphenol in the presence of 5 mol% of NH_4VO_3, 120 mol% of Bu_4NBr, and 120 mol% of $AlCl_3$ as a Lewis acid in 1,4-dioxane at 80 °C for 18 h proceeds to give 4-bromo-2,6-dimethylphenol in 95 % yield without the formation of the benzyl bromide. Starting from 3-hydroxyphenol, monobromination product, 4-bromo-3-hydroxyphenol, or dibromination product, 4,6-dibromo-3-hydroxyphenol, are obtained in a high yield in the presence of 120 or 300 mol% of $AlCl_3$ and Bu_4NBr, respectively. 1-Decene and allylbenzene are converted to the corresponding dibromide. Both aromatic and aliphatic alkynes undergo the selective *vic*-dibromination to afford the corresponding *trans*-dibromides, suggesting the involvement of a bromonium cation-like species as an intermediate for *anti*-bromination.

$AlBr_3$ is expected to serve as both a bromide source and a Lewis acid. Actually, the oxidative bromination reaction of 1,3,5-trimethoxybenzene with 5 mol% of NH_4VO_3 and 120 mol% of $AlBr_3$ with molecular oxygen leads to the quantitative formation of the dibromide (Scheme 2.91) [188]. Furthermore, the monobromide is selectively obtained in a high yield by using 50 mol% amount of $AlBr_3$. These results indicate that two bromides of $AlBr_3$ are employed as a bromide source. The high reactivity is observed in ether even at room temperature although 1,4-dioxane
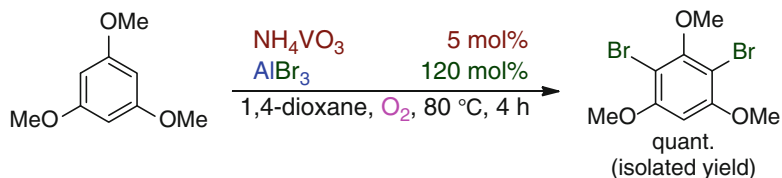
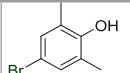**Scheme 2.91** Oxidative bromination reaction of 1,3,5-trimethoxybenzene in the presence of 120 mol% of AlBr₃

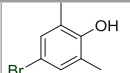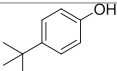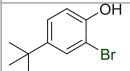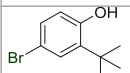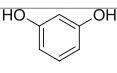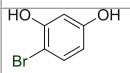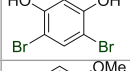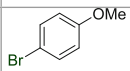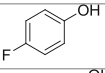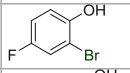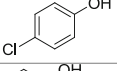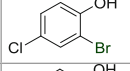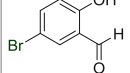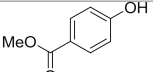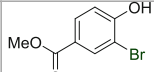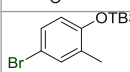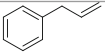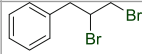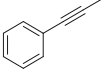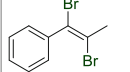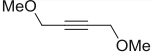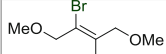requires heating for the bromination reaction. The vanadium catalyst and molecular oxygen are essential for the oxidative bromination.

The results of the bromination reaction by using NH_4VO_3 catalyst and $AlBr_3$ with molecular oxygen either in 1,4-dioxane at 80 °C (method A) or in ether at room temperature (method B) are shown in Table 2.1 [188]. In both conditions, the oxidative bromination of phenol derivative proceeds well to afford the mono- or dibromide in a high yield by selecting appropriate conditions (entries 1–6). A simple aromatic compound like anisole is converted to the monobromide (entry 7). Starting from 4-halophenols, the corresponding bromination products are obtained (entries 8–9). The oxidative bromination of phenol derivatives with the formyl or methoxycarbonyl group leads to the formation of the corresponding monobromide, wherein the further oxidation of the aldehyde moiety or decomposition of the ester moiety is not observed (entries 10–11). In the bromination reaction of TBS-protected *o*-cresol, the TBS group is survived to give only the brominated product (entry 12). The oxidative bromination reaction of alkenes and alkynes affords the corresponding dibromides by using NH_4VO_3 catalyst together with $AlBr_3$ (method C), although the presence of 120 mol% Bu₄NBr is required. The bromination reaction of 1-decene proceeds well to give the dibromide quantitatively (entry 13). The selective *vic*-dibromination of allylbenzene is observed to give 1,2-dibromo-3-phenylpropane, without formation of the benzylbromide (entry 14). The aromatic and aliphatic alkynes such as 1-phenylpropyne and 1,4-dimethoxy-2-butyne undergo the selective *anti*-dibromination by using method C to give the corresponding *trans*-dibromides in high yields (entries 15–16).

Moreover, this catalytic oxidative bromination using cat. $NH_4VO_3/AlBr_3/O_2$ system can be applied to the α-bromination of ketones (Table 2.2) [188]. The bromination reaction of β-keto esters such as ethyl benzoylacetate occurs to give mono- or dibromination products depending on the amount of $AlBr_3$ (entries 1 and 2). Substitution at α-position leads to the formation of the monobromination product (entry 3). 4′-Methoxyacetophenone is converted to the monobromide together with the dibromide. Bromination reaction of 4′-chloroacetophenone affords the monobromide as a major product (entry 4). The trihalo compound is obtained from 3-chloro-4′-fluoropropiophenone (entry 5).
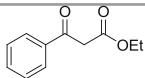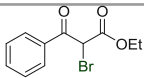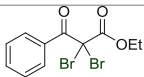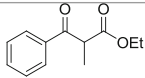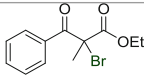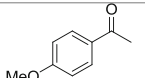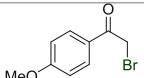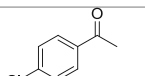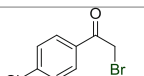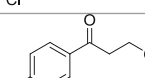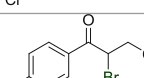
Moreover, a gram-scale practical reaction is successfully performed to give the bromination product in a high yield, as exemplified by the monobromination of 4-*t*-butylphenol to the monobromide in 94 % isolated yield (Scheme 2.92) [188].

Table 2.1 Oxidative bromination of arenes, alkenes, and alkynes by using cat. $NH_4VO_3/AlBr_3/O_2$ system

Entry	Substrate	Condition[a,b]	Product, isolated yield (%)	
1	2-methylphenol (with OH)	A, 60, 8	4-bromo-2-methylphenol	94
2		B, 60, 18		95
3	4-tert-butylphenol	A, 60, 8	2-bromo-4-tert-butylphenol	98
4	2-tert-butylphenol	B, 110, 18	4-bromo-2-tert-butylphenol	99
5	resorcinol (HO, OH)	A, 40, 8	bromoresorcinol	80
6		A, 80, 8	dibromoresorcinol	66
7	anisole (OMe)	A, 120, 8	4-bromoanisole	96
8	4-fluorophenol (F, OH)	A, 120, 8	2-bromo-4-fluorophenol	95
9	4-chlorophenol (Cl, OH)	B, 110, 18	2-bromo-4-chlorophenol	97
10	salicylaldehyde (OH, CHO)	A, 60, 8	5-bromosalicylaldehyde	86[c]
11	methyl 4-hydroxybenzoate (MeO–C(O)–, OH)	A, 110, 18	methyl 3-bromo-4-hydroxybenzoate	Quant.
12	2-methylphenyl OTBS	B, 120, 18	bromo-2-methylphenyl OTBS	Quant.
13	terminal alkene (chain, 7)	C, 120, 18	dibromide (Br, Br)	99[d,e]
14	allylbenzene	C, 120, 18	dibromide (Br, Br)	93[d,e]
15	phenylacetylene derivative (alkyne)	C, 120, 18	dibromoalkene (Br, Br)	98[d]
16	MeO–alkyne–OMe	C, 120, 18	MeO, Br, Br, OMe dibromoalkene	97[d]

[a]Method, amount of $AlBr_3$ (mol%), time (h)

[b]Method A: 0.50 mmol of substrate, 5 mol% NH_4VO_3, $AlBr_3$, 1.5 mL of 1,4-dioxane, under atmospheric oxygen, 80 °C. Method B: 0.50 mmol of substrate, 5 mol% NH_4VO_3, $AlBr_3$, 1.5 mL of ether, under atmospheric oxygen, rt. Method C: 0.50 mmol of substrate, 5 mol% NH_4VO_3, 120 mol% $AlBr_3$, 1.5 mL of MeCN, under atmospheric oxygen, 80 °C

[c]Together with 3-bromosalicylaldehde (11 %)

[d]120 mol% Bu_4NBr was used as an additive

[e]Reaction was conducted at 50 °C

Table 2.2 Oxidative bromination of ketones by using cat. NH$_4$VO$_3$/AlBr$_3$/O$_2$ system[a]

Entry	Substrate	AlBr$_3$ (mol%)	Product, yield (%)	
1		55		95
2		110		98
3		55		96
4		55		52[b,c]
5		55		70[b,d]
6		55		72[b]

[a]Condition: 0.5 mmol of substrate, 5 mol% NH$_4$VO$_3$, AlBr$_3$, 1.5 mL of MeCN, under atmospheric oxygen, 80 °C, 18 h
[b]NMR yield
[c]Together with dibromide (45 %)
[d]Together with dibromide (27 %)
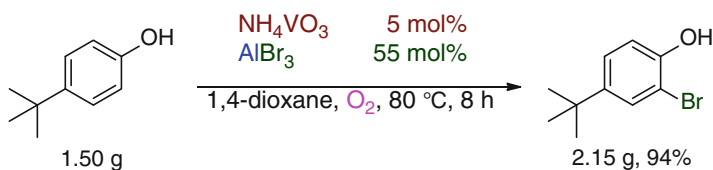
Scheme 2.92 Oxidative bromination reaction of 4-*tert*-butylphenol

References

1. D. Seyferth, H. Yamazaki, D.L. Alleston, J. Org. Chem. **28**, 70S (1968)
2. C.W. Jeffoid, D. Kirkpatrick, F. Delav, J. Am. Chem. Soc. **94**, 8905 (1972)
3. J.T. Groves, K.W. Ma, J. Am. Chem. Soc. **96**, 6627 (1974)
4. D. Seyferth, B. Prokai, J. Org. Chem. **31**, 1702 (1966)
5. R.M. Blankenship, K.A. Burdett, J.S. Swenton, J. Org. Chem. **39**, 2300 (1974)
6. H. Nosaki, T. Aratani, R. Noyori, Tetrahedron **23**, 3845 (1967)
7. J. Moreau, P. Caubare, J. Org. Chem. **27**, 5741 (1971)
8. T. Ando, H. Hosaka, W. Funasaka, H. Yamaiiaka, Bull. Chem. Soc. Jpn. **46**, 3513 (1973)
9. R.J. Kinney, W.D. Jones, R.G. Bergman, J. Am. Chem. Soc. **100**, 635 (1978)
10. T. Hirao, T. Masunaga, Y. Ohshiro, T. Agawa, J. Org. Chem. **46**, 3745 (1981)

11. S. Abbas, C.J. Hayes, S. Worden, Tetrahedron Lett. **41**, 3215 (2000)
12. C. Kuang, H. Senboku, M. Tokuda, Tetrahedron **58**, 1491 (2002)
13. Y. Wang, J. Gan, L. Liu, H. Yuan, Y. Gao, Y. Liu, Y. Zhao, J. Org. Chem. **79**, 3678 (2014)
14. T. Hirao, S. Kohno, Y. Ohshiro, T. Agawa, Bull. Chem. Soc. Jpn. **56**, 1881 (1983)
15. T. Hirao, T. Masunaga, K.-i. Hayashi, Y. Ohshiro, T. Agawa, Tetrahedron Lett. **24**, 399 (1983)
16. T. Hirao, Y. Fujihara, K. Kurokawa, Y. Ohshiro, T. Agawa, J. Org. Chem. **51**, 2830 (1986)
17. T. Hirao, K.-i. Hayashi, Y. Fujihara, Y. Ohshiro, T. Agawa, J. Org. Chem. **50**, 279 (1985)
18. T. Hirao, M. Hagihara, Y. Ohshiro, T. Agawa, Synthesis, 60 (1984)
19. T. Hirao, M. Hagihara, T. Agawa, Bull. Chem. Soc. Jpn. **58**, 3104 (1985)
20. T. Hirao, T. Nakamura, M. Hagihara, T. Agawa, J. Org. Chem. **50**, 5860 (1985)
21. P. Tavs, Chem. Ber. **103**, 2428 (1970)
22. P. Tavs, H. Weitkamp, Tetrahedron **26**, 5529 (1970)
23. T. Hirao, T. Masunaga, Y. Ohshiro, T. Agawa, Synthesis, 56 (1981)
24. T. Hirao, T. Masunaga, N. Yamada, Y. Ohshiro, T. Agawa, Bull. Chem. Soc. Jpn. **55**, 909 (1982)
25. T. Hirao, T. Masunaga, Y. Ohshiro, T. Agawa, Tetrahedron Lett. **21**, 3595 (1980)
26. T. Hirao, Y. Ohshiro, K. Kurokawa, T. Agawa, Yukagaku **32**, 274 (1983)
27. A.L. Schwan, Chem. Soc. Rev. **33**, 218 (2004)
28. B.R. Aluri, M.K. Kindermann, P.G. Jones, I. Dix, J. Heinicke, Inorg. Chem. **47**, 6900 (2008)
29. M.S.S. Adam, O. Kühl, M.K. Kindermann, J.W. Heinicke, P.G. Jones, Tetrahedron **64**, 7960 (2008)
30. Y. Belabassi, S. Alzhari, J.-L. Montchamp, J. Organomet. Chem. **693**, 3171 (2008)
31. M. Kalek, A. Ziadi, J. Stawinski, Org. Lett. **10**, 4637 (2008)
32. M. Kalek, J. Stawinski, Tetrahedron **65**, 10406 (2009)
33. M.C. Kohler, J.G. Sokol, R.A. Stockland Jr., Tetrahedron Lett. **50**, 457 (2009)
34. A. Bessmertnykh, C.M. Douaihy, S. Muniappan, R. Guilard, Synthesis, 1575 (2008)
35. A. Bessmertnykh, C.M. Douaihy, R. Guilard, Chem. Lett. **38**, 738 (2009)
36. E. Deal, C. Petit, J.-L. Montchamp, Org. Lett. **13**, 3270 (2011)
37. C.-G. Feng, M. Ye, K.-J. Xiao, S. Li, J.-Q. Yu, J. Am. Chem. Soc. **135**, 9322 (2013)
38. S.K. Nune, M. Tanaka, Chem. Commun. 2858 (2007)
39. K. Bravo-Altamirano, J.L. Montchamp, Tetrahedron Lett. **48**, 5755 (2007)
40. Y. Gao, G. Wang, L. Chen, P. Xu, Y. Zhao, Y. Zhou, L.B. Han, J. Am. Chem. Soc. **131**, 7956 (2009)
41. V.P. Ananikov, L.L. Khemchyan, I.P. Beletskaya, Synlett, 2375 (2009)
42. Y. Belabassi, K. Bravo-Altamirano, J.-L. Montchamp, J. Organomet. Chem. **696**, 106 (2011)
43. T. Hirao, Chem. Rev. **97**, 2707 (1997)
44. T. Hirao, K. Hirano, T. Hasegawa, I. Ikeda, Y. Ohshiro, J. Org. Chem. **58**, 6529 (1993)
45. T. Hirao, Synlett, 175 (1999)
46. T. Hirao, Y. Harano, Y. Yamana, Y. Ohshiro, T. Agawa, Tetrahedron Lett. **24**, 1255 (1983)
47. T. Hirao, S. Nagata, Y. Yamana, T. Agawa, Tetrahedron Lett. **26**, 5061 (1985)
48. T. Hirao, S. Nagata, T. Agawa, Tetrahedron Lett. **26**, 5795 (1985)
49. T. Hirao, S. Nagata, T. Agawa, Chem. Lett. 1625 (1985)
50. T. Hirao, Y. Harano, Y. Yamana, Y. Hamada, S. Nagata, T. Agawa, Bull. Chem. Soc. Jpn. **59**, 1341 (1986)
51. L. Zhou, T. Hirao, J. Org. Chem. **68**, 1633 (2003)
52. T. Hirao, Y. Ohshiro, Synlett, 217 (1990)
53. K.C. Nicolaou, J.-J. Liu, Z. Yang, H. Ueno, R.K. Guy, E.J. Sorensen, C.F. Claiborne, C.-K. Hwang, M. Nakada, P.G. Nantermet, J. Am. Chem. Soc. **117**, 634 (1995)
54. B. Kammermeier, G. Beck, D. Jacobi, H. Jendralla, Angew. Chem. Int. Ed. Engl. **33**, 685 (1994)
55. J.H. Freudenberger, A.W. Konradi, S.F. Pedersen, J. Am. Chem. Soc. **111**, 8014 (1989)
56. J. Park, S.F. Pedersen, J. Org. Chem. **55**, 5924 (1990)
57. A.W. Konradi, S.F. Pedersen, J. Org. Chem. **57**, 28 (1992)
58. A.W. Konradi, S.J. Kemp, S.F. Pedersen, J. Am. Chem. Soc. **116**, 1316 (1994)
59. T. Hirao, M. Asahara, Y. Muguruma, A. Ogawa, J. Org. Chem. **62**, 4566 (1998)

60. T. Hirao, A. Ogawa, M. Asahara, Y. Muguruma, H. Sakurai, Org. Synth. **81**, 26 (2005)
61. T. Hirao, B. Hatano, M. Asahara, Y. Muguruma, A. Ogawa, Tetrahedron Lett. **39**, 5247 (1998)
62. T. Hirao, T. Hasegawa, M. Muguruma, I. Ikeda, J. Org. Chem. **61**, 366 (1996)
63. T. Hirao, B. Hatano, Y. Imamoto, A. Ogawa, J. Org. Chem. **64**, 7665 (1999)
64. A. Fürstner, A. Hupperts, J. Am. Chem. Soc. **117**, 4468 (1995)
65. R.L. Halterman, C. Zhu, Z. Chen, M.S. Dunlap, M.A. Khan, K.M. Nicholas, Organometallics **19**, 3824 (2000)
66. A. Bensari, J.-L. Renaud, O. Riant, Org. Lett. **3**, 3863 (2001)
67. A. Chatterjee, T.H. Bennur, N.N. Joshi, J. Org. Chem. **68**, 5668 (2003)
68. N. Takenaka, G. Xia, H. Yamamoto, J. Am. Chem. Soc. **126**, 13198 (2004)
69. Y.-G. Li, Q.-S. Tian, J. Zhao, Y. Feng, M.-J. Li, T.-P. You, Tetrahedron Asymmetry **15**, 1707 (2004)
70. T. Hirao, H. Takeuchi, A. Ogawa, H. Sakurai, Synlett, 1658 (2000)
71. X. Xu, T. Hirao, J. Org. Chem. **70**, 8594 (2005)
72. B. Hatano, A. Ogawa, T. Hirao, J. Org. Chem. **63**, 9421 (1998)
73. L. Zhou, T. Hirao, Tetrahedron Lett. **41**, 8517 (2000)
74. L. Zhou, T. Hirao, Tetrahedron **57**, 6927 (2001)
75. H. Sakurai, Y. Imamoto, T. Hirao, Chem. Lett. **44** (2002)
76. T. Amaya, A. Miyasaka, T. Hirao, Tetrahedron Lett. **52**, 4567 (2011)
77. A. Miyasaka, T. Amaya, T. Hirao, Tetrahedron Lett. **53**, 5589 (2012)
78. A. Miyasaka, T. Amaya, T. Hirao, Chem. Eur. J. **20**, 1615 (2014)
79. J.-L. Namy, P. Girard, H.B. Kagan, Nouv. J. Chim. **1**, 5 (1977)
80. P. Girard, J.-L. Namy, H.B. Kagan, J. Am. Chem. Soc. **102**, 2693 (1980)
81. D.A. Johnson, J. Chem. Soc. Dalton Trans., 1671 (1974)
82. M. Shabangi, R.A. Flowers II, Tetrahedron Lett. **38**, 1137 (1997)
83. R.J. Enemaerke, K. Daasbjerg, T. Skrydstrup, Chem. Commun. 343 (1999)
84. J. Inanaga, M. Ishikawa, M. Yamaguchi, Chem. Lett. 1485 (1987)
85. Y. Kamochi, T. Kudo, Tetrahedron **48**, 4301 (1992)
86. A. Studer, D.P. Curran, Synlett **3**, 255 (1996)
87. Y. Kamochi, T. Kudo, Chem. Lett. 893 (1991)
88. E. Hasegawa, D.P. Curran, J. Org. Chem. **58**, 5008 (1993)
89. A. Dahlén, G. Hilmersson, J. Inorg. Chem. 3393 (2004)
90. A. Ogawa, N. Takami, M. Sekiguchi, I. Ryu, N. Kambe, N. Sonoda, J. Am. Chem. Soc. **114**, 8729 (1992)
91. R. Nomura, T. Matsuno, T. Endo, J. Am. Chem. Soc. **118**, 11666 (1996)
92. Y. Okaue, T. Isobe, Inorg. Chim. Acta **114**, 143 (1988)
93. A. Ogawa, Y. Sumino, T. Nanke, S. Ohya, N. Sonoda, T. Hirao, J. Am. Chem. Soc. **119**, 2745 (1997)
94. A. Ogawa, S. Ohya, T. Hirao, Chem. Lett. **275** (1997)
95. A. Ogawa, S. Ohya, M. Doi, Y. Sumino, N. Sonoda, T. Hirao, Tetrahedron Lett. **39**, 6341 (1998)
96. Z. Li, K. Iida, Y. Tomisaka, A. Yoshimura, T. Hirao, A. Nomoto, A. Ogawa, Organometallics **26**, 1212 (2007)
97. A. Yoshimura, Y. Tomisaka, Z. Li, A. Nomoto, A. Ogawa, Heteroatom Chem. **25**, 684 (2014)
98. A. Ogawa, H. Takeuchi, T. Hirao, Tetrahedron Lett. **40**, 7113 (1999)
99. T. Hirao, S. Mikami, Y. Ohshiro, Synlett, 541 (1990)
100. T. Hirao, T. Moriuchi, S. Mikami, Y. Ohshiro, I. Ikeda, Tetrahedron Lett. **34**, 1031 (1993)
101. T. Moriuchi, T. Hirao, Y. Ohshiro, I. Ikeda, Chem. Lett. 915 (1994)
102. T. Hirao, T. Moriuchi, T. Ishikawa, K. Nishimura, S. Mikami, Y. Ohshiro, I. Ikeda, J. Mol. Catal. A: Chem. **113**, 117 (1996)
103. T. Moriuchi, I. Nakayama, K. Nishimura, M. Nishiyama, E. Mochizuki, Y. Kai, T. Hirao, Chem. Lett. 1328 (2001)
104. T. Hirao, M. Mori, Y. Ohshiro, Bull. Chem. Soc. Jpn. **62**, 2399 (1989)
105. T. Hirao, M. Mori, Y. Ohshiro, J. Org. Chem. **55**, 358 (1990)
106. T. Hirao, M. Mori, Y. Ohshiro, Chem. Lett. 783 (1991)

107. T. Hirao, S. Mikami, M. Mori, Y. Ohshiro, Tetrahedron Lett. **32**, 1741 (1991)
108. T. Hirao, T. Fujii, S.-i. Miyata, Y. Ohshiro, J. Org. Chem. **56**, 2264 (1991)
109. T. Hirao, T. Fujii, T. Tanaka, Y. Ohshiro, Synlett, 845 (1994)
110. T. Hirao, T. Fujii, T. Tanaka, Y. Ohshiro, J. Chem. Soc. Perkin Trans. **1**, 3 (1994)
111. T. Hirao, T. Fujii, T. Tanaka, Y. Ohshiro, I. Ikeda, J. Synth. Org. Chem. Jpn. **52**, 197 (1994)
112. T. Hirao, T. Fujii, T. Tanaka, Y. Ohshiro, Y.J. Organometal, J. Organomet. Chem. **407**, C1 (1991)
113. K. Ichikawa, S. Uemura, T. Sugita, Tetrahedron **22**, 407 (1966)
114. E.I. Heiba, R.M. Dessau, J. Org. Chem. **39**, 3456 (1974)
115. B.B. Snider, J.J. Patricia, S.A. Kates, J. Org. Chem. **53**, 541 (1988)
116. T. Hirao, M. Sakaguchi, T. Ishikawa, I. Ikeda, Synth. Commun. **25**, 845 (1995)
117. T. Hirao, Y. Ohshiro, Tetrahedron Lett. **31**, 3917 (1990)
118. T. Hirao, D. Misu, K. Yao, T. Agawa, Tetrahedron Lett. **27**, 929 (1986)
119. T. Hirao, D. Misu, T. Agawa, J. Am. Chem. Soc. **107**, 7179 (1985)
120. T. Hirao, D. Misu, T. Agawa, Tetrahedron Lett. **27**, 933 (1986)
121. Y. Ito, T. Konoike, T. Saegusa, J. Am. Chem. Soc. **97**, 649 (1975)
122. Y. Kobayashi, T. Taguchi, T. Morikawa, E. Tokuno, S. Sekiguchi, Chem. Pharm. Bull. **28**, 262 (1980)
123. E. Baciocchi, A. Casu, R. Ruzziconi, Synlett, 679 (1990)
124. T. Fujii, T. Hirao, Y. Ohshiro, Tetrahedron Lett. **33**, 5823 (1992)
125. T. Fujii, T. Hirao, Y. Ohshiro, Tetrahedron Lett. **34**, 5601 (1993)
126. T. Hirao, T. Fujii, Y. Ohshiro, Tetrahedron **50**, 10207 (1994)
127. T. Hirao, T. Fujii, Y. Ohshiro, Tetrahedron **35**, 8005 (1994)
128. E. Baciocchi, T. Del Giacco, C. Rol, G.V. Sebastiani, Tetrahedron Lett. **30**, 3573 (1989)
129. W.C. Still, J. Am. Chem. Soc. **99**, 4186 (1977)
130. M. Ochiai, E. Fujita, M. Arimoto, H. Yamaguchi, Chem. Pharm. Bull. **32**, 887 (1984)
131. M. Ochiai, E. Fujita, M. Arimoto, H. Yamaguchi, Chem. Pharm. Bull. **32**, 5027 (1984)
132. E.J. Corey, J.C. Walker, J. Am. Chem. Soc. **109**, 8108 (1987)
133. T. Hirao, C. Morimoto, T. Takada, H. Sakurai, Tetrahedron Lett. **42**, 1961 (2001)
134. T. Hirao, C. Morimoto, T. Takada, H. Sakurai, Tetrahedron **57**, 5073 (2001)
135. T. Ishikawa, A. Ogawa, T. Hirao, J. Am. Chem. Soc. **120**, 5124 (1998)
136. T. Ishikawa, A. Ogawa, T. Hirao, Organometallics **17**, 5713 (1998)
137. T. Ishikawa, S. Nonaka, A. Ogawa, T. Hirao, Chem. Commun. 1209 (1998)
138. A. Pelter, K. Smith, H.C. Brown, *Borane Reagents* (Academic, London, 1988)
139. D.H. Geske, J. Phys. Chem. **63**, 1062 (1959); **66**, 1743 (1962)
140. A. Pelter, R. Pardasani, P. Pardasani, Tetrahedron **56**, 7339 (2000)
141. P. Abley, J. Halpern, J. Chem. Soc. Chem. Commun., 1238 (1971)
142. H. Mizuno, H. Sakurai, T. Amaya, T. Hirao, Chem. Commun. 5042 (2006)
143. T. Amaya, Y. Tsukamura, T. Hirao, Adv. Synth. Catal. **351**, 1025 (2009)
144. T. Amaya, T. Masuda, Y. Maegawa, T. Hirao, Chem. Commun. **50**, 2279 (2014)
145. M. Iyoda, S.M.H. Kabir, A. Vorasingha, Y. Kuwatani, M. Yosihda, Tetrahedron Lett. **39**, 5393 (1998)
146. T. Harada, K. Iwazaki, D. Hara, K. Hattori, A. Oku, J. Org. Chem. **62**, 8966 (1997)
147. T. Harada, T. Katsuhira, K. Takeshi, O. Atusshi, I. Katsuhiro, M. Keiji, A. Oku, J. Am. Chem. Soc. **118**, 11377 (1996)
148. T. Hirao, T. Takada, A. Ogawa, J. Org. Chem. **65**, 1511 (2000)
149. M. Uchiyama, M. Kameda, O. Mishima, N. Yokoyama, M. Koike, Y. Kondo, T. Sakamoto, J. Am. Chem. Soc. **120**, 4934 (1998)
150. T. Takada, H. Sakurai, T. Hirao, J. Org. Chem. **66**, 300 (2001)
151. T. Harada, T. Katsuhira, K. Hattori, A. Oku, J. Org. Chem. **58**, 2958 (1993)
152. T. Hirao, T. Takada, H. Sakurai, Org. Lett. **2**, 3659 (2000)
153. T. Ishikawa, A. Ogawa, T. Hirao, J. Organomet. Chem. **575**, 76 (1999)
154. M. Eissen, D. Lenoir, Chem. Eur. J. **14**, 9830 (2008)
155. A. Podgoršek, M. Zupan, J. Iskra, Angew. Chem. Int. Ed. **48**, 8424 (2009)
156. T.-L. Ho, B.G.B. Gupta, G.A. Olah, Synthesis, 676 (1977)

157. R.K. Dieter, L.E. Nice, S.E. Velu, Tetrahedron Lett. **37**, 2377 (1996)
158. V. Nair, S.B. Panicker, A. Augstine, T.G. George, S. Thomas, M. Vairamani, Tetrahedron **57**, 7417 (2001)
159. K.G. Dewkar, V.S. Narina, A. Sudalai, Org. Lett. **5**, 4501 (2003)
160. H.A. Muathen, Synth. Commun. **34**, 3545 (2004)
161. C. Ye, M.J. Shreeve, J. Org. Chem. **69**, 8561 (2004)
162. A. Butler, A.H. Baldwin, Struct. Bond. **89**, 109 (1997)
163. J. Littlechild, E. Garcia-Rodrguez, Coord. Chem. Rev. **237**, 65 (2003)
164. A. Butler, J.N. Carter-Franklin, Nat. Prod. Rep. **21**, 180 (2004)
165. J. Hartung, Y. Dumont, M. Greb, D. Hach, F. Köhler, H. Schulz, M. Časný, D. Rehder, H. Vilter, Pure Appl. Chem. **81**, 1251 (2009)
166. A. Butler, J.V. Walker, Chem. Rev. **93**, 1937 (1993)
167. J.S. Martinez, G.L. Carroll, R.A. Tschirret-Guth, G. Altenhoff, R.D. Little, A. Butler, J. Am. Chem. Soc. **123**, 3289 (2001)
168. J.N. Carter-Franklin, J.D. Parrish, R.A. Tschirret-Guth, R.D. Little, A. Butler, J. Am. Chem. Soc. **125**, 3688 (2003)
169. R.I. de la Rosa, M.J. Clague, A. Butler, J. Am. Chem. Soc. **114**, 760 (1992)
170. V. Conte, F. Di Furia, S. Moro, S. Rabbolini, J. Mol. Catal. A: Chem. **113**, 175 (1996)
171. G.J. Colaps, B.J. Hamstra, J.W. Kampf, V.L. Pecoraro, J. Am. Chem. Soc. **118**, 3469 (1996)
172. S. Nica, A. Pohlmann, W. Plass, Eur. J. Inorg. Chem. 2032 (2005)
173. M. Bhattacharjee, Polyhedron **11**, 2817 (1992)
174. V. Conte, F. Di Furia, S. Moro, Tetrahedron Lett. **35**, 7429 (1994)
175. C.U. Dinesh, R. Kumar, B. Pandey, P. Kumar, J. Chem. Soc. Chem. Commun. 611 (1995)
176. H.B. ten Brink, A. Tuynman, H.L. Dekker, W. Hemrika, Y. Izumi, T. Oshiro, H.E. Schoemaker, R. Wever, Inorg. Chem. **37**, 6780 (1998)
177. U. Bora, G. Bose, M.K. Chaudhuri, S.S. Dhar, R. Gopinath, A.T. Khan, B.K. Patel, Org. Lett. **2**, 247 (2000)
178. G. Rothenberg, J.H. Clark, Org. Process. Res. Dev. **4**, 270 (2000)
179. M.R. Maurya, H. Saklani, S. Agarwal, Catal. Commun. **5**, 563 (2004)
180. M. Greb, J. Hartung, F. Köhler, K. Ŝpehar, R. Kluge, R. Csuk, Eur. J. Org. Chem. 3799 (2004)
181. A.T. Khan, P. Goswami, L.H. Choudhury, Tetrahedron Lett. **47**, 2751 (2006)
182. T. Moriuchi, M. Nishiyama, T. Beppu, T. Hirao, D. Rehder, Bull. Chem. Soc. Jpn. **80**, 957 (2007)
183. T. Moriuchi, M. Yamaguchi, K. Kikushima, T. Hirao, Tetrahedron Lett. **48**, 2667 (2007)
184. G. Zhang, R. Liu, Q. Xu, L. Ma, X. Liang, Adv. Synth. Catal. **348**, 862 (2006)
185. A. Podgoršek, M. Eissen, J. Fleckenstein, S. Stavber, M. Zupan, J. Iskra, Green Chem. **11**, 120 (2009)
186. K. Kikushima, T. Moriuchi, T. Hirao, Chem. Asian. J. **4**, 1213 (2009)
187. K. Kikushima, T. Moriuchi, T. Hirao, Tetrahedron Lett. **51**, 340 (2010)
188. K. Kikushima, T. Moriuchi, T. Hirao, Tetrahedron **66**, 6906 (2010)

Chapter 3
π-Conjugated Systems with Coenzyme PQQ, Polyanilines or Quinonediimines, and Sumanene

Toshikazu Hirao, Toshiyuki Moriuchi, and Toru Amaya

Abstract Coenzyme PQQ serves as a catalyst or mediator in redox reactions under molecular oxygen. Polyanilines and quinonediimines are found to serve as redox-active organo catalysts for proton-conjugated electron transfer. The hybrid d,π-conjugated systems composed of transition metals and π-conjugated compounds as redox-active ligands are constructed and applied to the catalytic oxidation reaction. Chirality induction of the π-conjugated chain is attained through chiral complexation. The d,π-conjugated complex is reduced to small and well-dispersed nanoparticles. Oxidative reactions are induced by transition metal nanoparticles and polyanilines as a redox-active mediator. Imidovanadium compounds bearing the π-conjugated substituents at the *N*-position are characterized.

Bowl-shaped π-conjugated "sumanene" is synthesized for the first time. X-ray single crystal structural and conductivity analyses reveal its columnar stacking with n-type electron transportation ability. Bowl-to-bowl inversion behavior and generation of benzylic anions are studied. Short synthesis of extended π bowls is achieved utilizing bowl-shaped sumanene. The concave or convex π-bent surface is demonstrated to serve as a ligand to give the corresponding d,π-conjugated bowl complex selectively.

T. Hirao (✉) • T. Moriuchi • T. Amaya
Department of Applied Chemistry, Graduate School of Engineering,
Osaka University, Yamada-oka, Suita, Osaka 565-0871, Japan
e-mail: hirao@chem.eng.osaka-u.ac.jp; moriuchi@chem.eng.osaka-u.ac.jp;
amaya@chem.eng.osaka-u.ac.jp

organocatalyst • Redox-switching • Self-assembly • Sumanene • Sumanenyl anion • Three-dimensionally oriented π-electronic system • Vanadium(V) hydrazido complex • V–N Multiple bond • Zirconocene • π Bowl • π Conjugation • π-Bowl complex • π-Conjugated ligand

Abbreviations

AFM	Atomic force microscope
BN	Binaphthyl
bpy	2,2′-Bipyridine
BuLi	Butyllithium
CD	Circular dichroism
Cp	Cyclopentadienyl
Cp*	1,2,3,4,5-Pentamethylcyclopentadienyl
CTAB	Cetyltrimethylammonium bromide
DA	Diamine
DABCO	1,4-Diazabicyclo[2.2.2]octane
DDQ	2,3-Dichloro-5,6-dicyano-p-benzoquinone
DMH	N,N-dimethylhydrazine
en	Ethylenediamine
EXSY	Exchange spectroscopy
Fc	Ferrocene
ICD	Induced circular dichroism
^{i}Pr	Isopropyl
K_{c}	Equilibrium constant
Me	Methyl
MeCN	Acetonitrile
NGCs	Nitrogen-doped graphitic carbons
NMR	Nuclear magnetic resonance
NOE	Nuclear Overhauser effect
OAc	Acetate
OEt	Ethoxide
O^{i}Pr	Isopropoxide
PD	Phenylenediamine
Ph	Phenyl
PMAS	Poly(2-methoxyaniline-5-sulfonic acid)
POT	Poly(o-toluidine)
ppm	Parts per million
PQQ	Pyrroloquinoline quinone
PQQTME	Trimethyl 4,5-dihydro-4,5-dioxo-lH-pyrrolo[2,3-f]quinoline-2,7, 9-tricarboxylate
QD	Quinonediimine
SQ	Semiquinonediimine radical anion
TEA	Triethanolamine

THF	Tetrahydrofuran
TPP	Tetraphenylporphyrin
tpy	2,2′:6′,2″-Terpyridine
TRMC	Time-resolved microwave conductivity
UV–vis	Ultraviolet–visible

3.1   Redox Systems with Coenzyme PQQ

Toshikazu Hirao

PQQ (Fig. 3.1) is a coenzyme of alcohol dehydrogenase, methanol dehydrogenase, aldehyde dehydrogenase, glucose dehydrogenase, amine oxidase, etc [1, 2]. A model catalytic system for PQQ-containing enzymes is disclosed in a micelle-enhanced dehydrogenation reaction of amines and amino acids in the presence of CTAB under molecular oxygen (Scheme 3.1) [3, 4]. A quinone function of PQQ appears to play an important role as a redox-active organocatalyst.
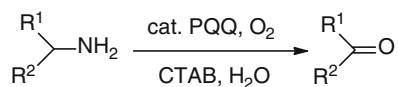
Scheme 3.1 Dehydrogenative oxidation with PQQ under molecular oxygen

A combination of PQQ derivatives with transition metals leads to form the efficient redox systems. Dropwise addition of terminal olefin to the solution of PdCl$_2$ (0.1 molar equiv.), trimethyl ester of PQQ, (PQQTME, 0.1 molar equiv.) and H$_2$O in DMF under molecular oxygen results in the formation of 2-alkanone (Scheme 3.2). It should be noted that PQQTME constitutes a catalytic redox cycle. The orthoquinone function appears to reoxidize the reduced palladium species generated in situ. Use of 1,7- or 1,10-phenanthrolinequinone gives a poor result maybe due to the coordination of palladium(II) species towards the pyridine moiety opposite to the quinone group [5]. Mediation of p-benzoquinone in the palladium-catalyzed oxidation reactions has been reported to require electrochemical or cobalt porphyrin catalyzed oxidation of the quinol [6–8]. The above-mentioned results provide an example for efficient redox systems of coenzyme derivatives with transition metals, which is demonstrated to be synthetically useful.
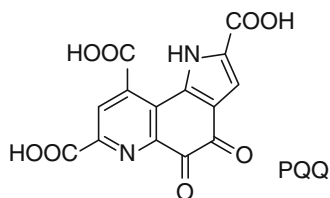
Fig. 3.1 Chemical structure of PQQ
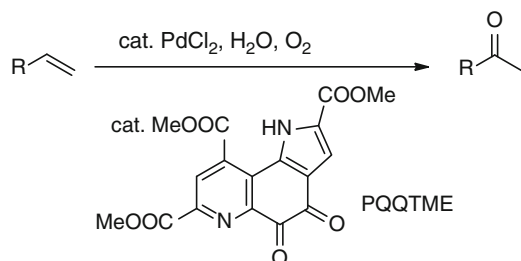
Scheme 3.2 The Wacker reaction mediated by PQQTME

This kind of the redox system is applied to the palladium(II)-induced regioselective ring-opening oxidation reaction of the α,β-epoxysilane **1** (Scheme 3.3) [9].
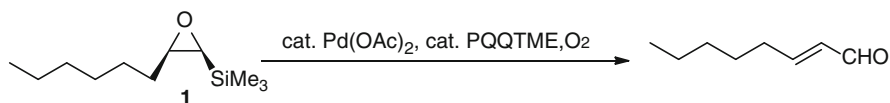
Scheme 3.3 Palladium-catalyzed oxidation of **1** in the presence of PQQTME

Furthermore, the reversible redox interconversion of PQQTME is performed by using two different oxidation states of vanadium compounds, VCl_2 and $VO(OEt)_3$, the processes of which are monitored by UV–vis spectroscopy (Scheme 3.4) [9].
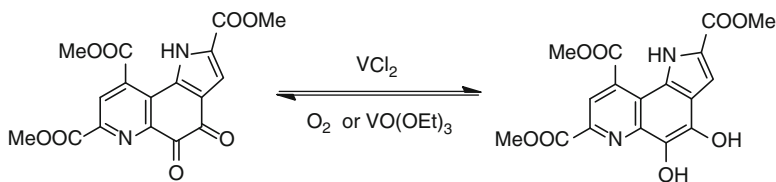
Scheme 3.4 Reversible redox interconversion

In this sense, quinone oxygen-coordinated palladium complexes **2** and **3** with anthraquinone ligands bearing *N*-heterocyclic coordination sites are synthesized and characterized (Fig. 3.2) [10].
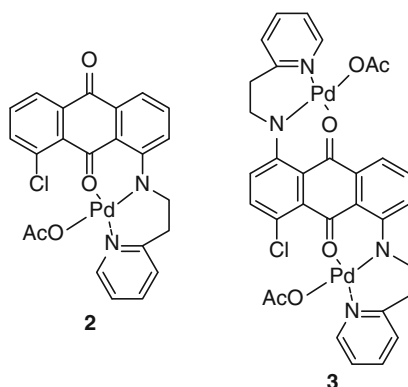
Fig. 3.2 Chemical structures of quinone oxygen-coordinated palladium complexes **2** and **3** with anthraquinone ligands bearing *N*-heterocyclic coordination sites

A variety of model systems for P-450 have been developed to elucidate the mechanism and provide a useful method for oxygenation reactions. Oxygen sources are molecular oxygen, hydrogen peroxide, *t*-butyl hydroperoxide, iodosylbenzene, sodium hypochlorite and so on, depending on the systems. Orthoquinones effectively mediate the MnTPPCl-catalyzed epoxidation reaction of olefins with hydrogen peroxide (Scheme 3.5) [11]. This might be due to the addition-adduct formation of the orthoquinone moiety with hydrogen peroxide. Under the conditions, orthoquinones are protected against their self-oxidation, and are considered to work as a redox mediator to generate an efficient oxidant.
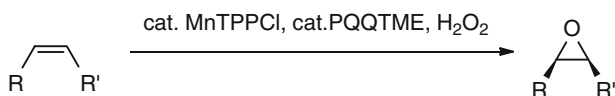
Scheme 3.5 MnTPPCl-catalyzed epoxidation with H_2O_2 in the presence of PQQTME

3.2 Redox Function of Polyanilines or Quinonediimines

Toshikazu Hirao and Toru Amaya

Synthetic Catalytic System

π-Conjugated polymers and oligomers have attracted much attention in the application to electronic materials depending on their electronic properties [12–16]. Polyaniline is one of the promising conducting π-conjugated polymers with redox properties and chemical stability. Polyanilines have been extensively studied because of their unique redox properties as well as numerous potential use in a wide range of applications in a variety of fields. Polyanilines are present in three different redox forms, which include a fully reduced leucoemeraldine base form, a semioxidized emeraldine one, and a fully oxidized pernigraniline one as shown in Scheme 3.6. The redox processes between them depend on protonic acid doping because the reduction of emeraldine base requires proton-coupled electron transfer to stabilize a reduced anionic species. The leucoemeraldine base is oxidizable with molecular oxygen [17].

These properties are envisaged to permit the construction of a catalytic system for oxidation reaction. Actually, polyanilines are demonstrated to serve as synthetic metal catalysts under molecular oxygen in the dehydrogenative oxidation of benzylamines, 2-phenylglycine, and 2,6-di-*t*-butylphenol (Scheme 3.7) [18–20]. Similar organo catalysis is also achieved with polypyrroles and the quinonediimine oligomer derivatives [21]. The activity of these catalysts depends on protonic acid doping.
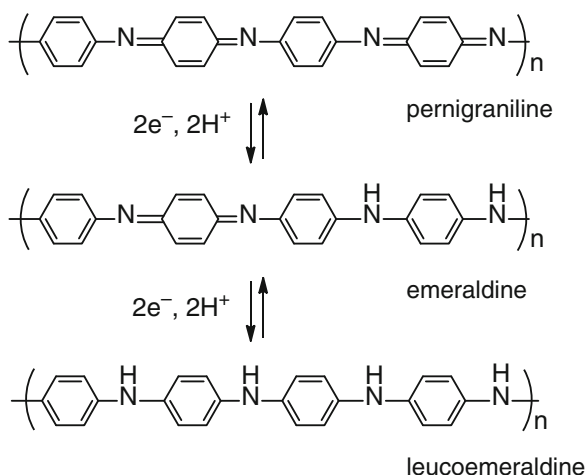
Scheme 3.6 Three representative oxidation states of polyaniline
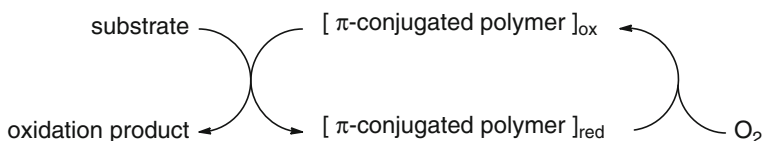
Scheme 3.7 Aerobic oxidation reaction mediated by redox-active π-conjugated polymer

p-Benzoquinonediimine compounds can accept two electrons. *N*,*N*′-Diphenyl-*p*-benzoquinonediimine efficiently induces the oxidative homo-coupling of various aryl- and vinylmagnesium reagents, where the expected side reactions such as 1,2- or 1,4-addition reaction are suppressed (Scheme 3.8) [22]. *N*,*N*′-Diphenyl-*p*-benzoquinone-diimine is transformed to the reduced benzenoid form after the reaction.
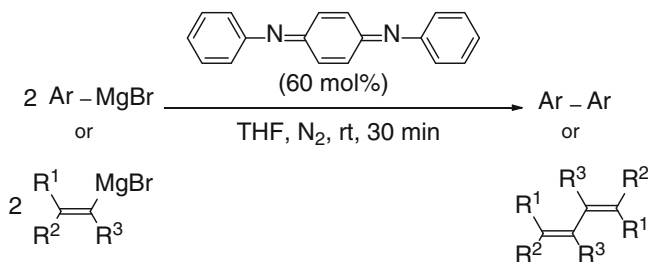
Scheme 3.8 *N*,*N*′-Diphenyl-*p*-benzoquinonediimine-induced oxidative coupling of aryl- and vinyl-magnesium reagents

Synthetic Metal-Transition Metal Catalytic System

Efficient redox processes of transition metals are essential to develop functionalized materials and catalysts. Coordination interaction with ligands is able to control the redox processes, If ligands are redox-active, a combination of both redox properties is considered to provide a multi-redox system as exemplified by Scheme 3.9. The redox interaction between transition metals and redox sites of ligands appears to operate through coordination. If the redox site is not coordinated directly, the redox interaction is also permitted through bond or space. An efficient redox function is likely to be realized in both cases. π-Conjugated polymers and molecules, which possess redox-active properties and coordination sites, are allowed to serve as redox-active ligands to afford the d,π-conjugated complexes.
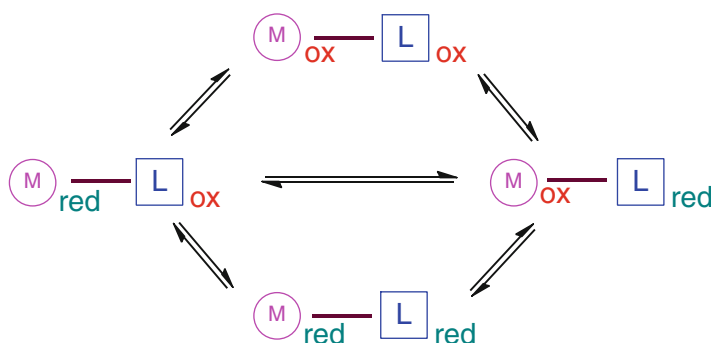
Scheme 3.9 Multi-redox system consisting of redox-active transition metal and redox-active ligand

The copper(II) complex with polyaniline exhibits a higher catalytic capability for the dehydrogenation of cinnamyl alcohol into cinnamaldehyde [18, 20]. The cooperative catalysis of both components is achieved. Iron(III) chloride is similarly employed instead of copper(II) chloride. The catalytic system is applicable to the decarboxylative dehydrogenation of mandelic acid to benzaldehyde. In these oxidation reactions, a complex catalyst consisting of polyaniline and metal salt forms a reversible redox cycle under molecular oxygen (Scheme 3.10). The copper salt appears to play a role as a metallic dopant, which is monitored spectroscopically.

substrate — [π-conjugated polymer – metal]$_{ox}$

oxidation product — [π-conjugated polymer – metal]$_{red}$ — O_2

metal = Cu(II), Fe(III)
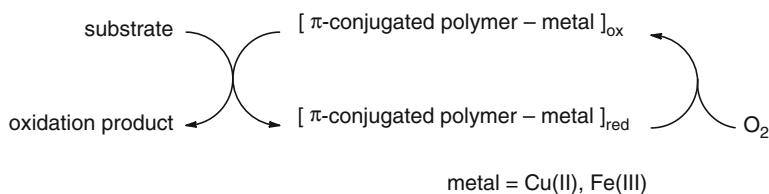
Scheme 3.10 The cooperative catalysis with π-conjugated polymer and transition metal for aerobic oxidation reaction

Redox-Active Ligand in Metal-Catalyzed Reaction

The redox interaction between metals and redox-active ligands is considered to contribute to a smooth redox process of transition-metal-catalyzed oxidation reactions. The Wacker oxidation reaction of a terminal olefin proceeds catalytically only in the presence of a catalytic amount of polyaniline derivative as a co-catalyst in acetonitrile-water under molecular oxygen as shown in Scheme 3.11 [23]. Polypyrroles can be employed similarly [24]. The catalysis is not observed in the absence of the π-conjugated polymer, indicating that the π-conjugated polymer mediates in the catalytic cycle. The redox processes of the π-conjugated polymer are monitored by UV–vis spectra, supporting that π-conjugated polymers behave as a redox-active ligand in the palladium(II)-catalyzed oxidation reaction under molecular oxygen [25].

redox-active ligand = polyanilines, polypyrroles
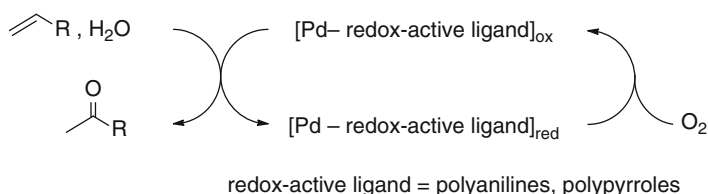
Scheme 3.11 The Wacker oxidation reaction using palladium(II)-redox-active ligand hybrid catalyst

Functionalization of Polyanilines and Oligoanilines

The strategy to control redox properties depends on design of aniline unit and self-doping. The reduced phenylenediamine **4**, which is synthesized by the palladium-catalyzed amination, is oxidized to the quinonediimine **5** [26, 27]. An alternating sequence of the donor-acceptor units of **4** permits low band-gap. Bidentate complexation is likely to be allowed with the quinonediimine **5** bearing a thiadiazole unit (Scheme 3.12), both of which serve as coordination sites [28].
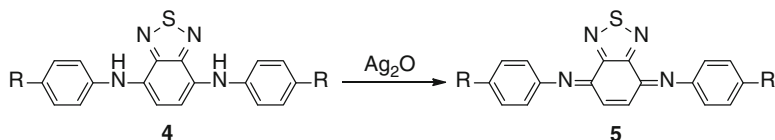
Scheme 3.12 Oxidation of phenylenediamine **4** bearing a thiadiazole unit to the quinonediimine **5**

A covalently attached acid moiety to the polyaniline backbone can dope itself without an external dopant. A self-doped conducting polyaniline bearing phosphonic acid, poly(2-methoxyaniline-5-phosphonic acid) (PMAP) is designed and

synthesized (Scheme 3.13) [29]. The phosphonate moiety is introduced via a Pd-catalysed coupling, as mentioned in Sect. 2.2. The monomer, 2-methoxyaniline-5-phosphonic acid, is oxidatively polymerized to provide PMAP. The practical synthetic procedure is developed [30]. The pyridinium salt of the thus-obtained PMAP is water-soluble and its film exhibits conductivity. Monoethyl ester derivative of PMAP is also synthesized [31].
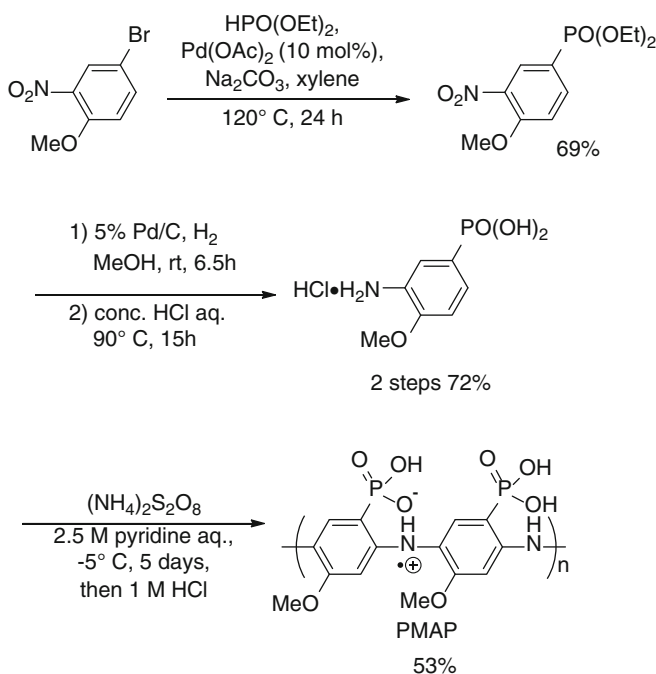
Scheme 3.13 Synthesis of a self-doped conducting polyaniline, PMAP

Three-Dimensional π-Electronic System

Regulated orientation of π-conjugated molecular chains is a challenging issue. Use of a molecular scaffold is considered to permit the design of such a system. The perpendicularly regulated orientation of π-conjugated molecular chains are allowed to provide three-dimensionally oriented π-electronic system **6** (Fig. 3.3).

This kind of orientation is achieved with the *p-t*-butylcalix[4]arene **7** bearing four redox-active phenylenediamine pendant groups on the lower rim [32]. The reversible redox transformation of the pendant group is observed chemically (Scheme 3.14).
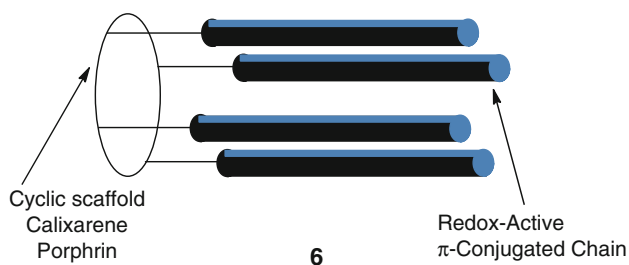
Fig. 3.3 The design of three-dimensionally oriented π-electronic system **6**
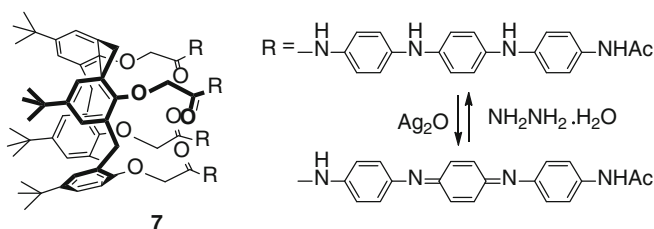
Scheme 3.14 The reversible redox transformation of the phenylenediamine pendant group on *p-t*-butylcalix[4]arene

The π-conjugated compounds **8** (αααα: **8a** and αβαβ: **8b**) are constructed by the introduction of four phenylenediamine pendant strands to the *meso*-positions of the atropisomeric porphyrin scaffolds (Fig. 3.4) [33]. In the fluorescence emission spectra, the emission from the porphyrin moiety is almost completely quenched in both atropisomers. This process is more efficient than that of the porphyrin bearing one pendant group, suggesting the interchain interaction of **8** [34].

8a: αααα isomer   **8b**: αβαβ isomer
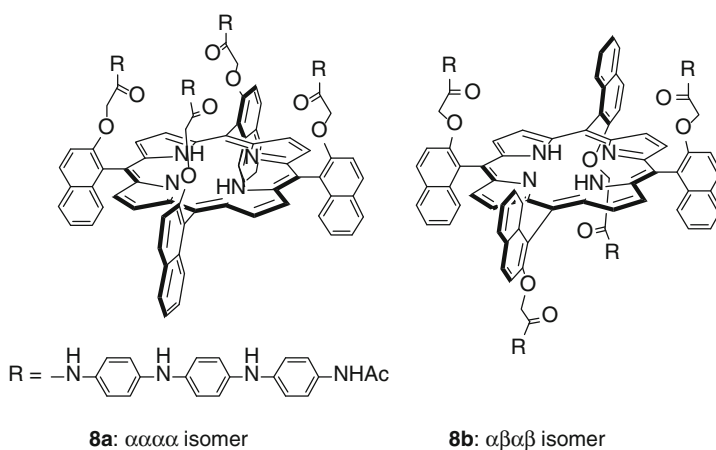
Fig. 3.4 Structures of compounds **8a** and **8b**

The zinc complex of **8c** and **8d** is treated with a bidentate ligand, DABCO, to form the sandwich dimer complex **9** (Scheme 3.15). Thus-obtained complex **9** is considered to be a unique redox system, which is composed of the electron acceptor moiety surrounded by the donor π-conjugated pendant groups [35].
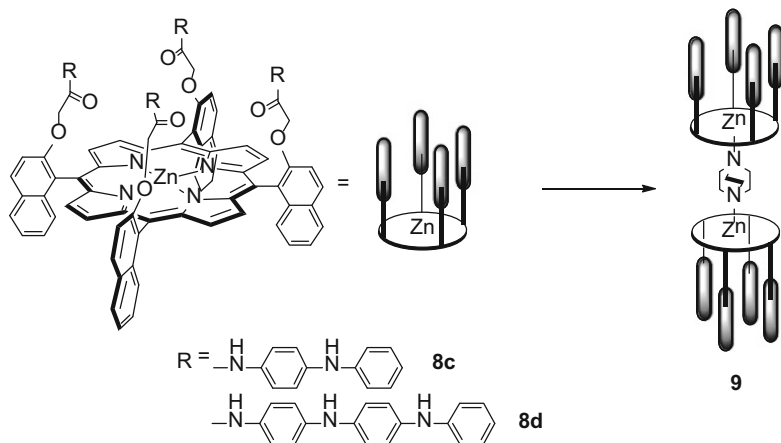
Scheme 3.15 Sandwich dimer complex **9** formed by coordination directed assembly of **8c** and **8d**

The porphyrins bearing three-dimensionally oriented terthiophene pendant strands **10a–c** are also designed and synthesized (Fig. 3.5) [36]. The significant quenching is again observed in their fluorescence emission spectroscopy.

Hybrids **11a** and **11b** consisting of zinc porphyrin and oligoaniline with a pyridine moiety at the terminal of the chain are designed (Fig. 3.6). This design allows the Zn(II)-directed self-assembly, giving polymeric, and/or oligomeric nanowire structures [37]. Their emission intensity is smaller than that of zinc tetraphenylporphyrin. The assembly on the Au nanoparticles' (NPs') surface is also demonstrated.

The porphyrins **11c** and **11d** bearing two three-dimensionally regulated oligoaniline chains with terminal pyridyl groups are also designed and synthesized. The self-assembled branched polymer complexes by introducing Zn(II) to the porphyrins are formed in solution, which undergo drop casting on the surface of mica to result in dome-like nanostructures (Fig. 3.6) [38]. The similar significant quenching as mentioned above is observed in the fluorescence emission spectroscopy.

Redox Interaction between Polyanilines and Transition Metals

To develop the redox catalyst system in water, a redox mediator is investigated using a water soluble polyaniline, poly(2-methoxyaniline-5-sulfonic acid) (PMAS). The redox interaction between PMAS (half ox) and V(IV) readily occurs to produce
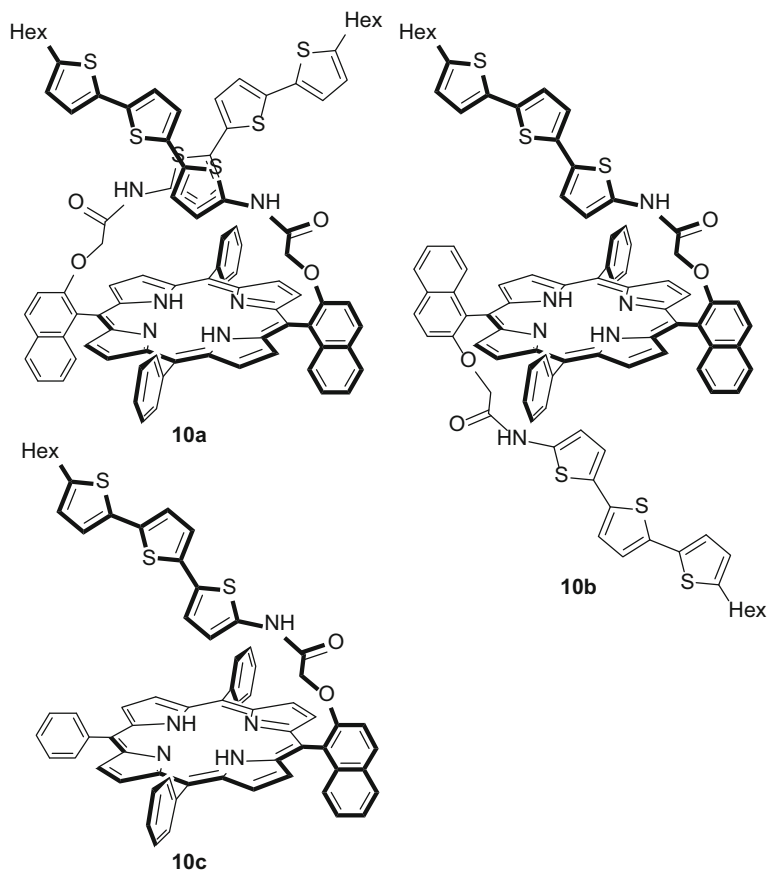
Fig. 3.5 Porphyrins bearing terthiophene pendant strands **10a–c**

the PMAS(red) and V(V) species in an aqueous solution. Notably, molecular oxygen reoxidizes PMAS(red) to form the catalytic redox cycle (Scheme 3.16) [39]. Graph in Scheme 3.16 shows increasing of V(V) with time in the presence of PMAS (10 mol%) under air (molecular oxygen). This redox interaction is effectively observed in basic conditions rather than in acidic ones.

Polyaniline (emeraldine salt) is known to possess mainly two conformations. One is an extended coil conformation and another is a compact coil conformation. Generally, the former shows the higher conductivity than the latter. The conformational change of PMAS (half ox) from extended coil to compact coil conformation
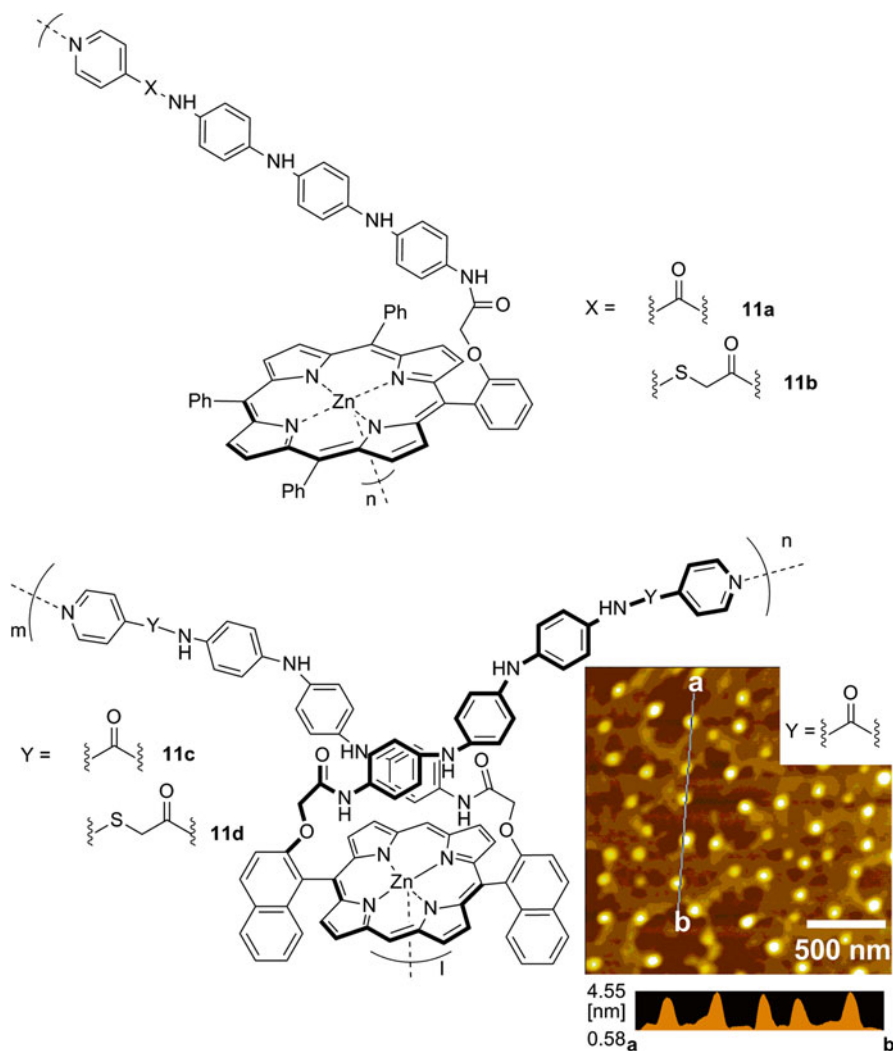
Fig. 3.6 Zinc porphyrins bearing oligoaniline with a pyridine moiety at the terminal of the chain. AFM image of the self-assembled branched polymer complex

is induced by a catalytic amount of Cu(II) under air (Scheme 3.17) [40]. This conformational change is likely to depend on the partial scission of π conjugation of the main chain due to partial oxidation by Cu(II). Reverse conformational change is performed by the addition of reductant $N_2H_4 \cdot H_2O$ under air (Scheme 3.17) [40].
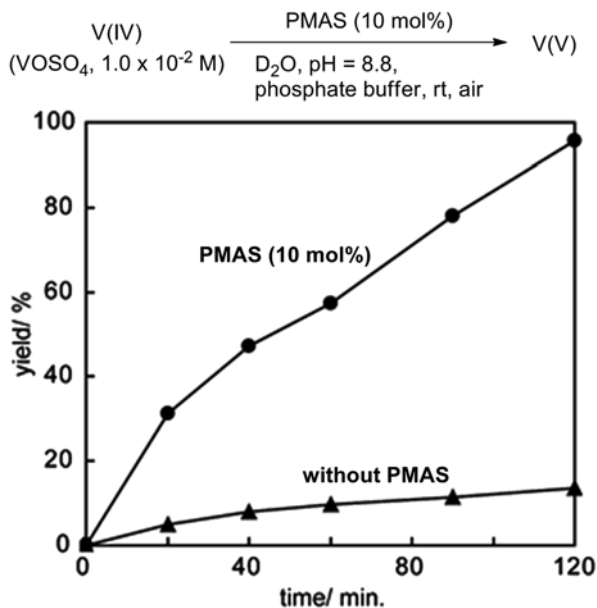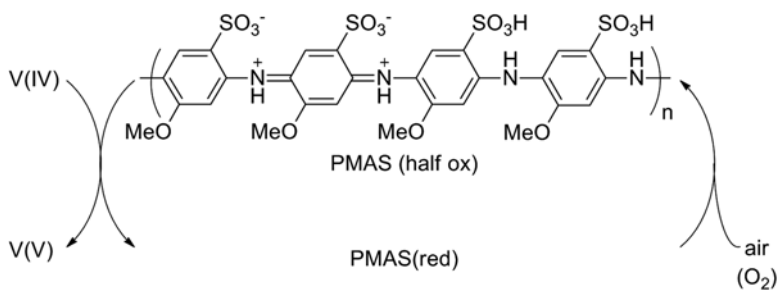
Scheme 3.16 Aerobic oxidation of V(IV) mediated by PMAS
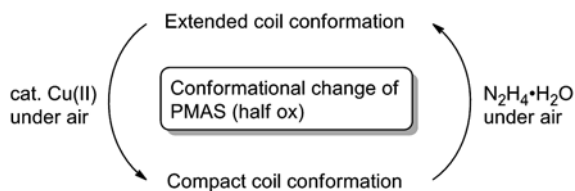
Scheme 3.17 Conformational change of PMAS (half ox)

3.3 Hybrid Systems Consisting of Polyanilines or Quinonediimines and Transition Metals

Toshikazu Hirao and Toshiyuki Moriuchi

The neutral emeraldine base of polyaniline is composed of the phenylenediamine (PD) moiety as a reduced form and the quinonediimine (QD) moiety as an oxidized form. Polyanilines has coordination properties of two nitrogen atoms of the QD moiety. The functional properties of π-conjugated polymers are envisioned to be modified dramatically by incorporation of metal centers into the polymers [41–49]. π-Conjugated polymers and molecules, which have redox-active and coordination properties, are allowed to serve as redox-active ligands to give the d,π-conjugated complexes. Depending on the number and geometry of the coordination sites, the systems with a variety of regulated structures can be constructed as shown in Fig. 3.7. The multi-nuclear complexes are obtained by multi-coordination of the π-conjugated polymers. In the case of both metals and ligands having two coordination sites, these components array alternatively to give the corresponding polymer complexes. Depending on their coordination geometries, a cyclic skeleton structure is also allowed to be formed. In this section, the conjugated complexes with redox-active π-conjugated polyanilines and 1,4-benzoquinonediimines.

The complexation of the emeraldine base form of poly(*o*-toluidine) (POT) with palladium(II) compounds is performed in an organic solvent to give the conjugated polymer complexes. Two nitrogen atoms of the QD moiety of the emeraldine base form of POT are capable of participating in the complexation with the palladium(II) complex [**L¹Pd(MeCN)**] [50, 51] bearing one interchangeable coordination site, which is obtained by treatment of the *N*-heterocyclic tridentate ligand, *N*,*N*′-bis(2-phenylethyl)-2,6-pyridinedicarboxamide (**L¹H₂**) [52, 53] with Pd(OAc)₂, to afford the single-strand conjugated complex **12** (Scheme 3.18). In contrast, the complexation
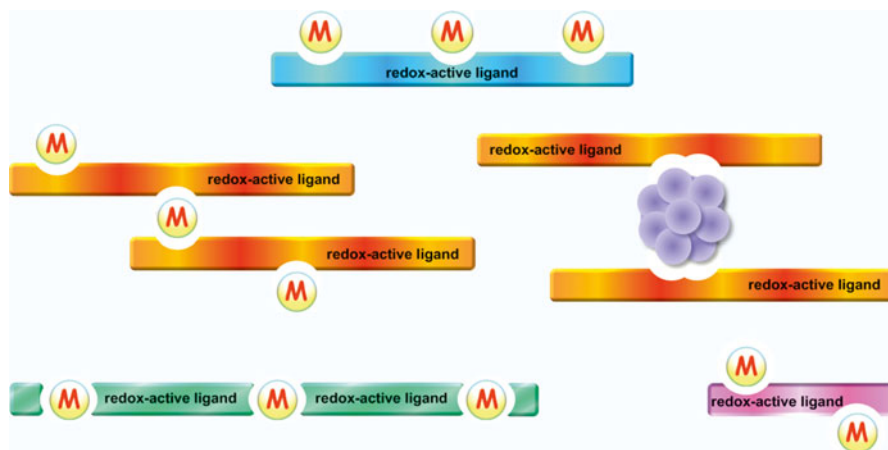
Fig. 3.7 Controlled design of the conjugated complexes with redox-active π-conjugated ligands
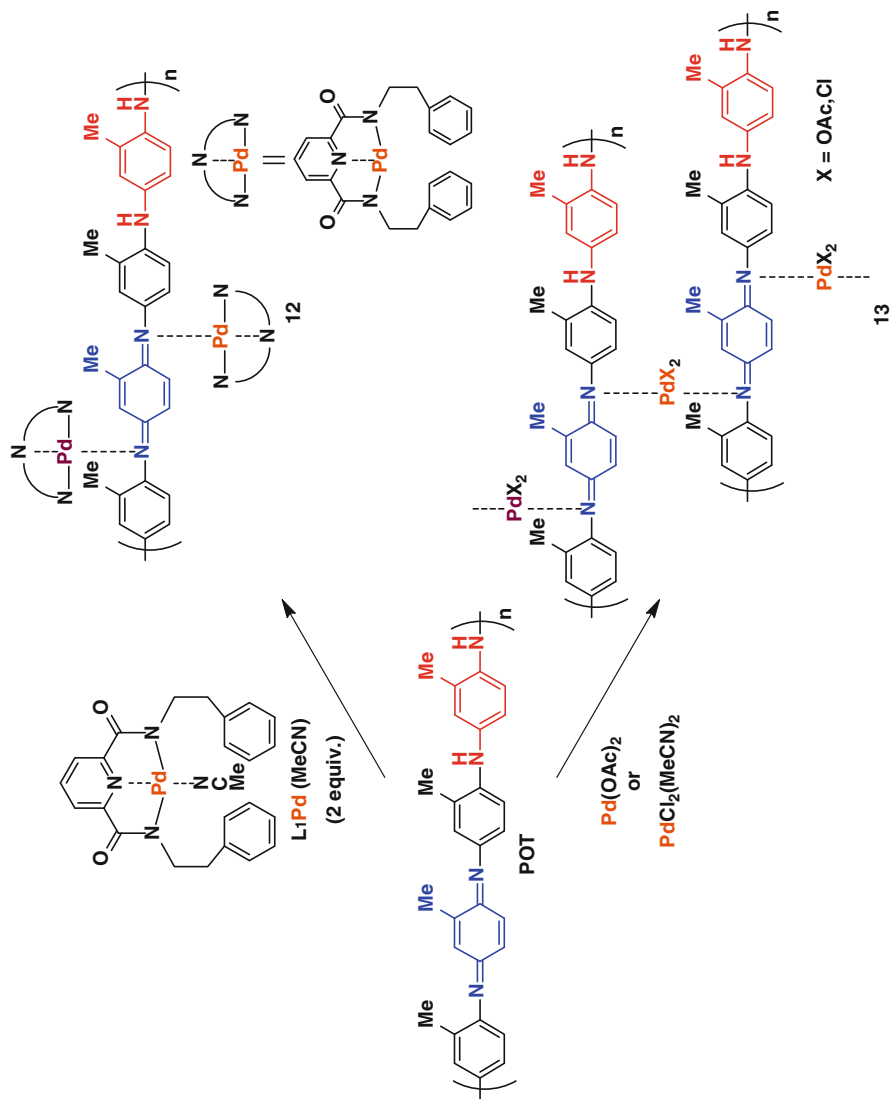
Scheme 3.18 Control formation of the single-strand conjugated complex **12** and the cross-linked conjugated complexes **13**

with Pd(OAc)$_2$ or PdCl$_2$(MeCN)$_2$, which have two coordination sites, leads to the formation of the cross-linked conjugated complex **13** (Scheme 3.18) [54]. Poly(3-heptylpyrrole) is demonstrated to serve as an efficient π-conjugated polymer ligand to afford the similar conjugated complex with PdCl$_2$(MeCN)$_2$. An organic light emitting diode device with the thus-obtained conjugated complex film as a hole injection layer exhibits the higher efficiency than a device with the conventional copper phthalocyanine hole injection layer [55].

The conjugated polymer complexes composed of polyanilines or polypyrroles are performed to afford the redox systems depending on their structures and redox properties. As mentioned in the Sect. 3.2, the complexation with copper salts can affect the redox properties of polyanilines to form the reversible redox cycle [17]. The conjugated polymer complex can serve as an oxidation catalyst [18, 20, 23, 24], wherein the coordination of the QD moiety might play an important role in a reversible redox processes of the complexes. Polyanilines or polypyrroles are effectively employed as a redox-active ligand in the Wacker reaction as mentioned in Sect. 3.2.

The complexation behavior of the redox-active π-conjugated molecule, *N,N′*-bis(4′-dimethylaminophenyl)-1,4-benzoquinonediimine (L^2) [56], as a model molecule of polyanilines gives the further insight into the coordination and redox properties of the QD moieties. The complexation of L^2 with two equimolar amounts of the palladium(II) complex [**L^{1}Pd(MeCN)**] affords the 1:2 conjugated homobimetallic palladium(II) complex [(L^1)Pd(L^2)Pd(L^1)] (**14**) as shown in Scheme 3.19 [57]. Variable temperature ^{1}H NMR studies of the conjugated complex **14** show that the
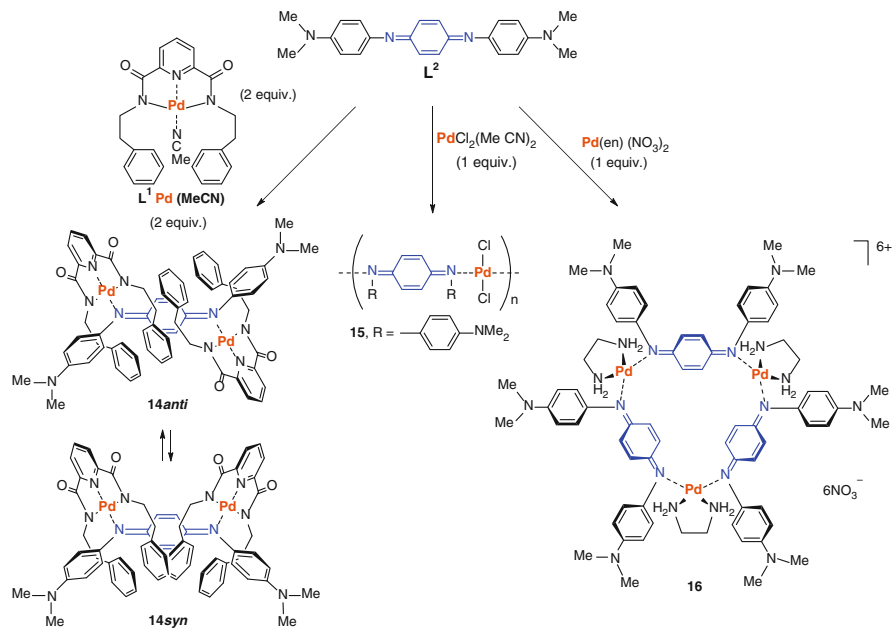
Scheme 3.19   Controlled formation of **14**, **15**, or **16** with L^2
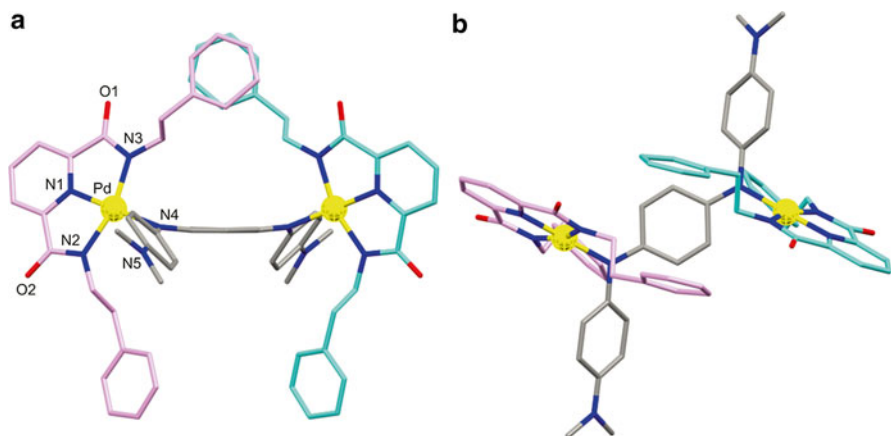
Fig. 3.8 (**a**) A *top view* and (**b**) a *side view* of the crystal structure of **14anti** (hydrogen atoms are omitted for clarity)

syn configuration is enthalpically more favorable than the *anti* configuration in CD_2Cl_2, but entropically less favorable. The crystal structure of **14anti** reveals that the two [L^1Pd] units are bridged by the QD moiety of L^2 in *anti* configuration (Fig. 3.8). The redox properties of the QD moiety are modulated by complexation with the palladium(II) complex [**$L^1Pd(MeCN)$**]. The conjugated complex **14** in dichloromethane shows the successive one-electron reduction of the QD moiety to afford the corresponding reduced species. On the contrary, L^2 shows an irreversible reduction wave. Compared with the uncomplexed QD, the complexed QD might be stabilized as an electron sink.

The conjugated polymeric complex **15**, in which palladium centers are incorporated in the main chain, is obtained by the complexation of L^2 with [$PdCl_2(MeCN)_2$] having two interchangeable coordination sites in acetonitrile (Scheme 3.19) [58].

A metal-directed assembly to regulate the coordination mode of the QD moiety is a convenient approach to the construction of metallomacrocycle. The conjugated trinuclear macrocycle [{$Pd(en)(L^2)$}$_3$](NO_3)$_6$ (**16**) is formed quantitatively by the reaction of L^2 with an equimolar amount of [$Pd(NO_3)_2(en)$], which has *cis* binding sites as a "metal clip" (Scheme 3.19) [58]. The crystal structure of **16** confirms a trimetallic macrocyclic skelton and the coordination of both QD nitrogen atoms to the palladium centers in the *syn* configuration as depicted in Fig. 3.9. The interesting structural feature is the orientation of the phenylene rings of L^2 in a face-to-face arrangement with a distance of about 3.5 Å at each corner of the triangle, which indicates a π–π interaction. The conjugated trinuclear macrocycle **16** forms an open cavity possessing different faces with the cone conformation, resulting in the accommodation of two methanol molecules at the top and bottom of the cavity. A preliminary experiment on guest binding in D_2O reveals that the association constant for 1,2-dimethoxybenzene is calculated as $4.0 \times 10^3\ M^{-1}$ from ^1H NMR spectroscopy.

Chirality induction into polyanilines and oligomers have drawn much attention due to their potential use in diverse areas such as surface modified electrodes, molecular recognition, and chiral separation [59]. The complexation of the emeraldine
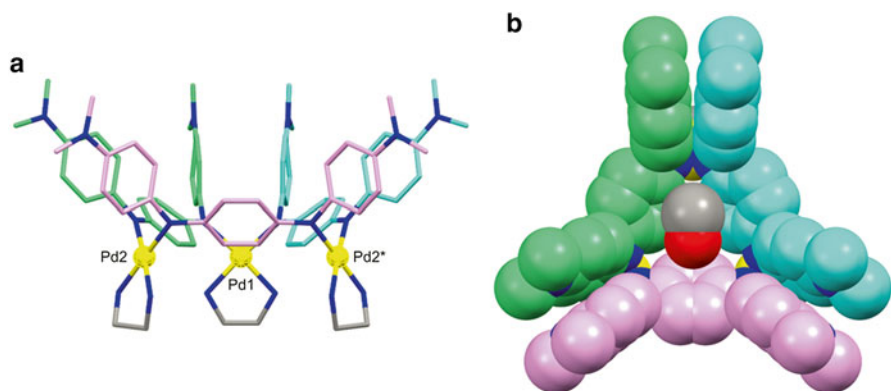
Fig. 3.9 (**a**) The crystal structure of **16** (hydrogen atoms and NO_3^- ions are omitted for clarity). (**b**) Space-filling representation of the molecular structure of **16** (hydrogen atoms and NO_3^- ions are omitted for clarity). Two methanol molecules are located at the *top* and *bottom* of the cavity

base form of POT with the chiral palladium(II) complex [(*S,S*)-L³Pd(MeCN)] induces chirality into a π-conjugated backbone of POT, affording the corresponding optically active conjugated polymer complex (***S,S***)**-17** (Scheme 3.20) [60, 61]. The CD spectrum of (***S,S***)**-17** exhibits an induced circular dichroism (ICD) at the
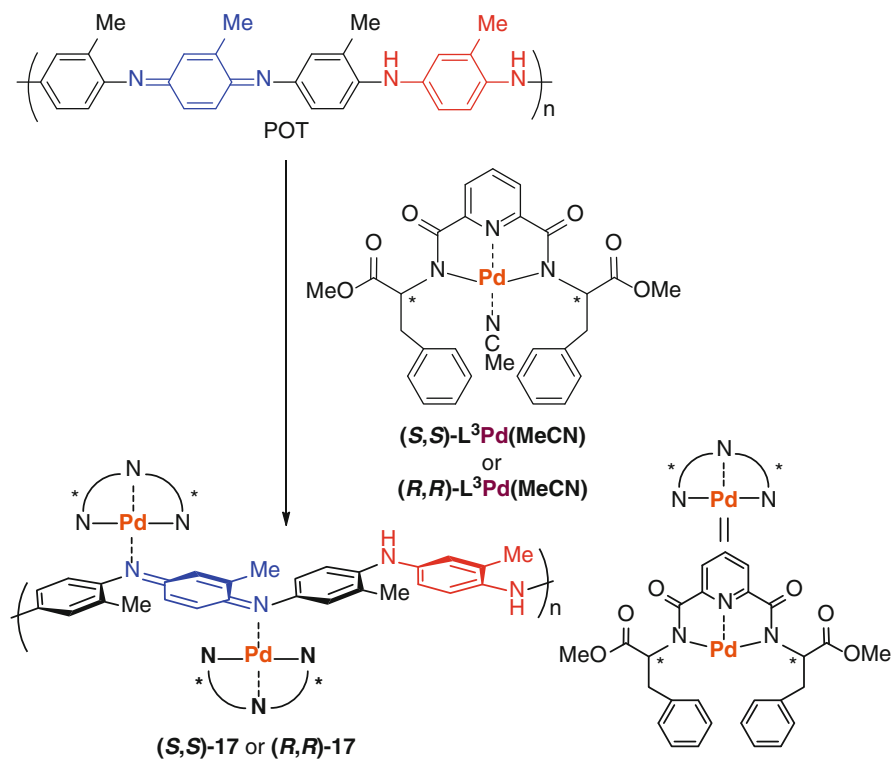
Scheme 3.20 Formation of optically active conjugated polymer complexes
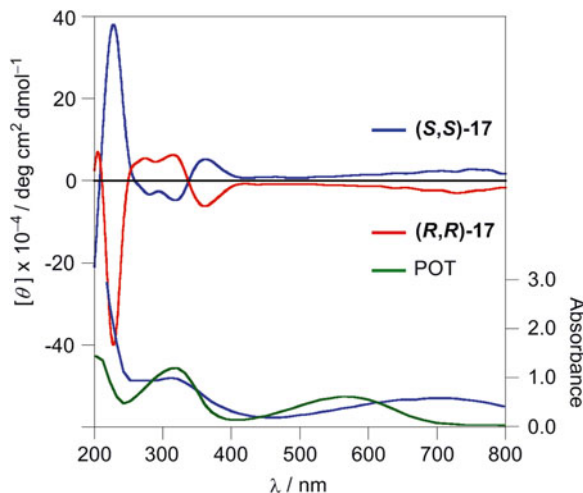
Fig. 3.10 CD spectra (*top*) of (*S,S*)-**17** and (*R,R*)-**17**, and UV–vis spectra (*bottom*) of (*S,S*)-**17** and POT in THF (1.3×10^{-3} M)

absorbance region of the π-conjugated moiety at around 500–800 nm (Fig. 3.10). The mirror imaged ICD signal at around 500–800 nm is observed in the CD spectrum of the conjugated polymer complex (*R,R*)-**17** (Fig. 3.10), supporting the chirality induction into a π-conjugated backbone of POT. The helical conformation with a predominant screw sense might be formed through chirality-induced complexation.

The chiral complexation behavior of L^2 affords further insights into the chirality induction of π-conjugated backbones. The treatment of L^2 with two equimolar amounts of chiral palladium(II) complex [(*S,S*)-L^3Pd(MeCN)] or [(*R,R*)-L^3Pd(MeCN)] affords the chiral 1:2 conjugated homobimetallic palladium(II) complex (*S,S*)-**18** or (*R,R*)-**18**, respectively (Scheme 3.21) [60, 61]. The mirror image relationship of the CD signals at around a low-energy charge-transfer transition with significant contribution from palladium (600–900 nm) of the QD moiety is obtained between (*S,S*)-**18** and (*R,R*)-**18**, suggesting the chirality induction into the π-conjugated backbone of the QD moiety through chirality-induced complexation. The crystal structure of (*R,R*)-**18***syn* shows that the two [(L³)Pd] units are bridged by the QD moiety of L^2 as shown in Fig. 3.11. Each phenylene ring of L^2 has an opposite dihedral angle with respect to the QD plane, resulting in a propeller twist between the planes of the two phenylene rings. The chirality of the podand moieties of [(L³)Pd] is likely to induce a propeller twist of the π-conjugated molecular chain.

In principle, a conjugated complex containing an [M^{n+}(QD)M^{n+}] unit might be converted to two other valence isomers, [$M^{(n+1)+}$(SQ)M^{n+}] (SQ = semiquinonediimine radical anion) or [$M^{(n+1)+}$(PD)$M^{(n+1)+}$], which differ only in the electron distribution between the QD moiety and metals. This valence isomerization depends on the redox properties of both components. Vanadium compounds can exist in a variety of oxidation states and generally convert between the redox states via a one-electron
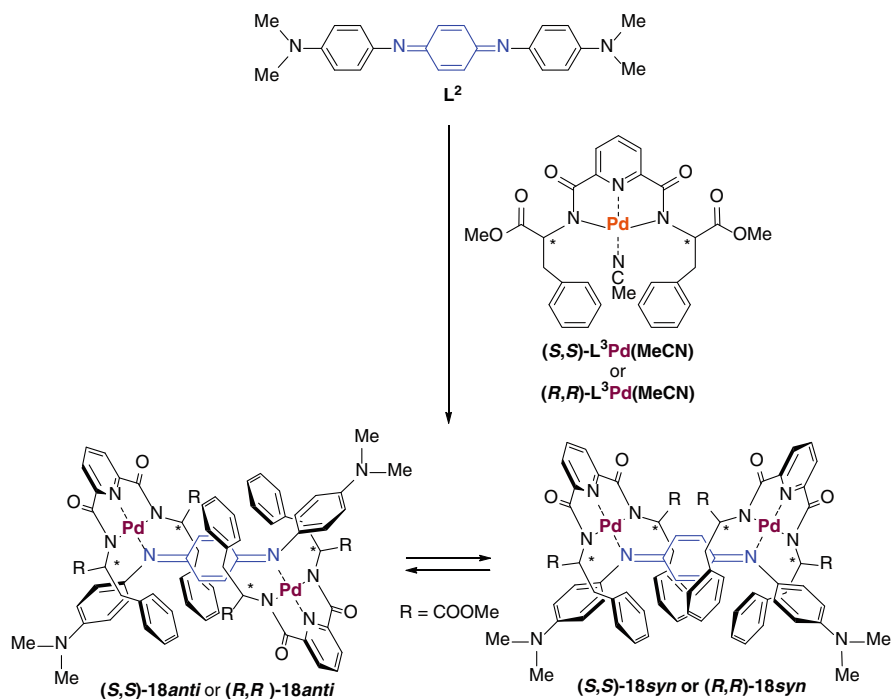
Scheme 3.21 Formation of optically active conjugated complexes
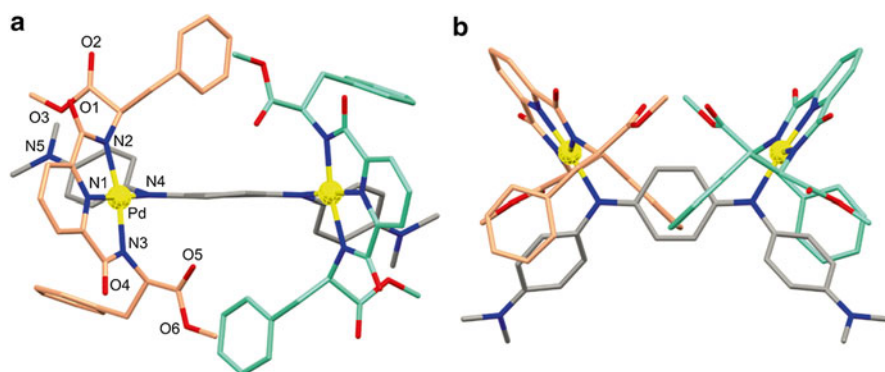
Fig. 3.11 (**a**) A *top view* and (**b**) a *side view* of the molecular structure of **(R,R)-18syn** (hydrogen atoms are omitted for clarity)

redox process [62]. The complexation of π-conjugated molecule L^2 or POT with VCl$_3$ proceeds together with redox reaction, affording the conjugated complexes **19** or **20**, respectively, wherein reduction of the QD moiety occurs with oxidation of V(III) to V(IV). The vanadium species is considered to play an important role in both complexation and reduction processes (Scheme 3.22) [63].
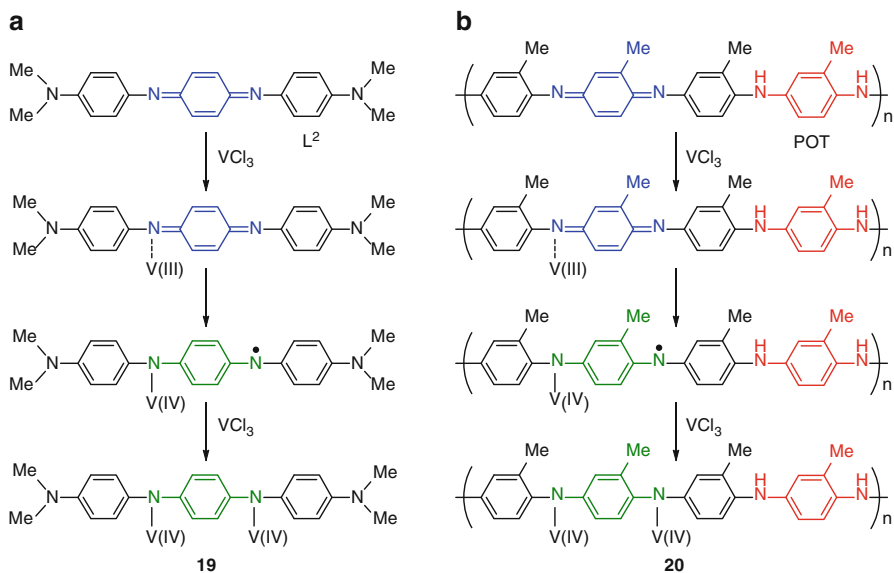
Scheme 3.22 Complexation behavior of (**a**) L^2 and (**b**) POT with VCl_3
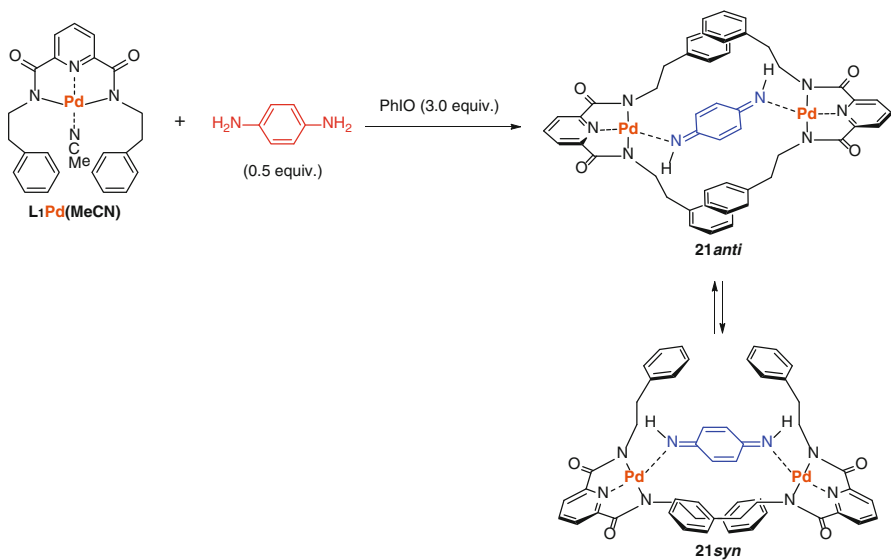
Scheme 3.23 Oxidative complexation of PD with **L¹Pd(MeCN)** to form **21**

The in-situ oxidative complexation of PD with the palladium(II) complex **L¹Pd(MeCN)** lead to the formation of the 1:2 conjugated homobimetallic palladium(II) complex **21** (Scheme 3.23) [51]. The cyclic voltammogram of **21** shows two separate redox waves assignable to the successive one-electron reduction of the QD moiety. The crystal structure of **21anti** shows that the two [(L¹)Pd] units are bridged by the QD spacer as depicted in Fig. 3.12.
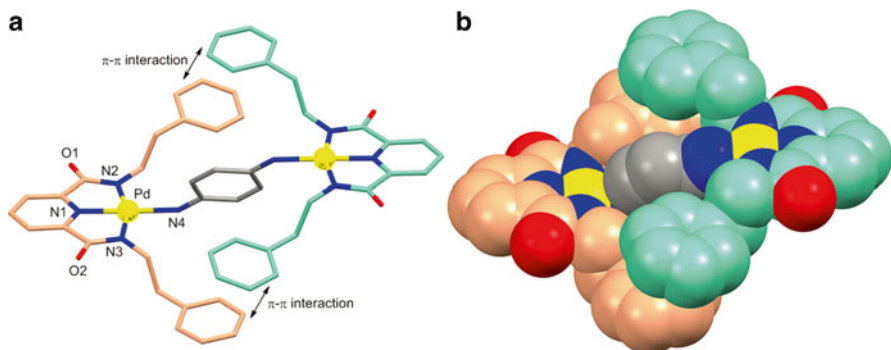
Fig. 3.12 (**a**) The molecular structure of **21*anti*** (hydrogen atoms are omitted for clarity). (**b**) Space-filling representation of the molecular structure of **21*anti*** (hydrogen atoms are omitted for clarity)

Bimetallic complexes composed of π-conjugated bridging spacers have gained growing interest as functional materials, in which electronic communication through a π-conjugated spacer is focused on [41–44]. Regulation of functional properties depending on the redox states for such transition metals have been investigated in only few cases [64–66]. The redox-active PD derivative L^3_{red} is synthesized by the introduction of the terminal redox-active ferrocenyl groups into PD bridging spacer (Scheme 3.24) [67, 68]. The crystal structure of L^3_{red} shows a twist conformation of the PD moiety as depicted in Fig. 3.13. The QD derivative L^3_{ox} as *syn* and *anti* (1:1 ratio) QD isomers is readily obtained by the oxidation of the PD derivative L^3_{red} with PhIO (Scheme 3.24). The oxidized forms L^3_{ox} can be reduced again to L^3_{red} with hydrazine monohydrate. The regulation of the electronic communication is performed by changing the redox states of the bridging spacer. The redox-active PD derivative L^3_{red} exhibits the successive one-electron oxidation processes of the ferrocene moieties, suggesting the electronic communication between the terminal ferrocenyl moieties
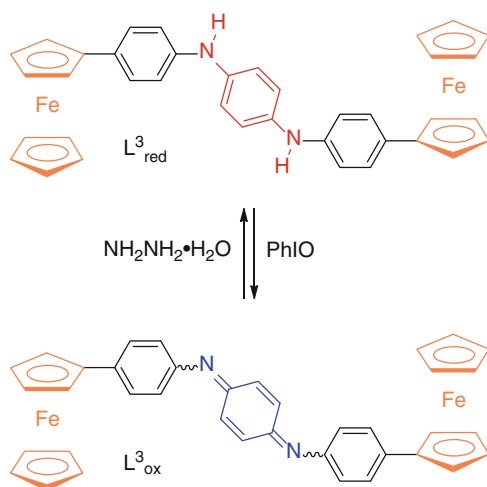
Scheme 3.24 Redox interconversion between L^3_{red} and L^3_{ox}
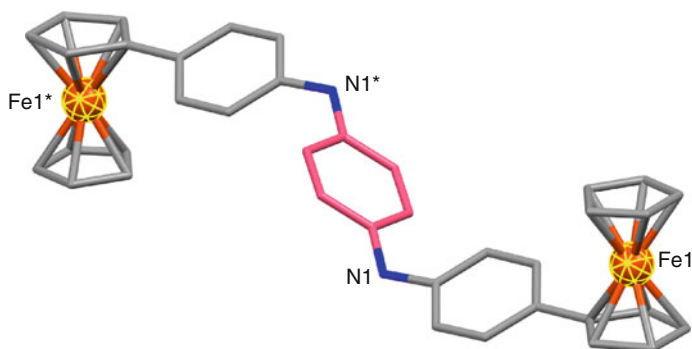
Fig. 3.13 The crystal structure of L^3_{red} (hydrogen atoms are omitted for clarity)
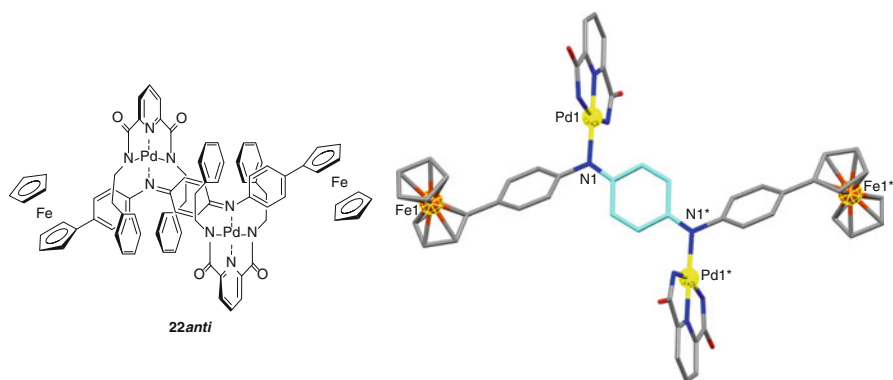
Fig. 3.14 The crystal structure of **22anti** (phenylethyl moieties and hydrogen atoms are omitted for clarity)

through the PD bridging spacer. The corresponding equilibrium constant (K_c) for the comproportionation reaction ([Fc–Fc] + [Fc$^+$–Fc$^+$] = 2[Fc$^+$–Fc]) is calculated as 49. Such electronic communication between the terminal ferrocenyl moieties is not observed in the case of the oxidized form L^3_{ox}.

Complexation of L^3_{ox} with the palladium(II) complex [**L^{1}Pd(MeCN)**] affords the 1:2 conjugated homobimetallic palladium(II) complex [(L^1)Pd(L$^3_{ox}$)Pd(L^1)] (**22**) [67]. The crystal structure of **22anti** reveals that the two [(L^1)Pd] units are bridged by the QD spacer to form the 1:2 complex in *anti* configuration (Fig. 3.14).

The photo active ruthenium complex is used as a redox catalyst [69]. The redox interconversion between the ruthenium(II) complex **23$_{red}$** bearing PD moieties and **23$_{ox}$** bearing QD moieties is demonstrated as shown in Scheme 3.25 [70]. In the emission spectrum of **23$_{red}$**, almost complete quenching is observed. An efficient photoinduced electron transfer is likely to be operated in **23$_{red}$**, wherein the PD moieties serve an electron donor. The oxidized form **23$_{ox}$** also showed a quenched spectrum probably due to the electron transfer in a direction opposite to that of **23$_{red}$** or energy transfer. As observed in the ruthenium complex **23**, Almost complete quenching is also observed in both bimetallic ruthenium(II) complexes **24$_{red}$** and **24$_{ox}$** composed of PD or QD bridging spacer, respectively (Scheme 3.26) [71].
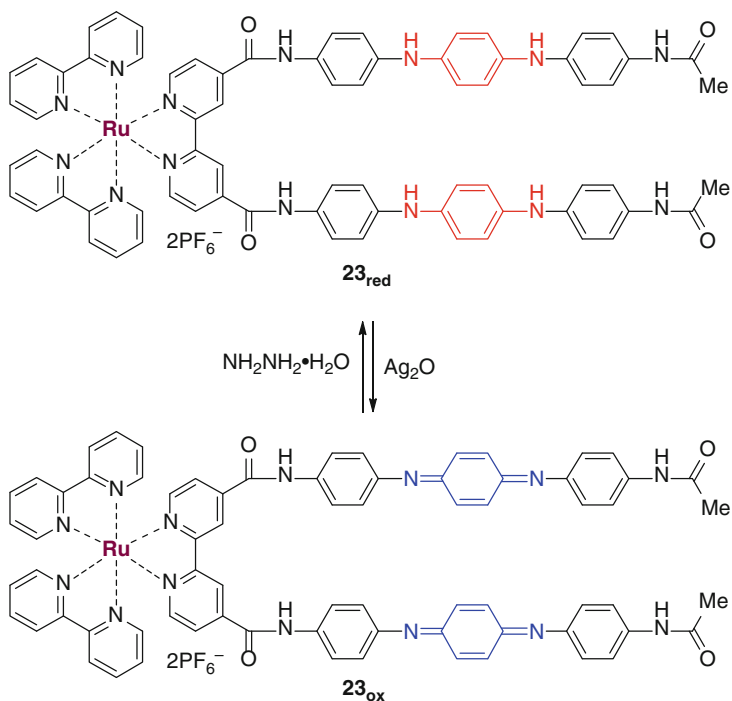
Scheme 3.25 Redox interconversion between **23_red** and **23_ox**
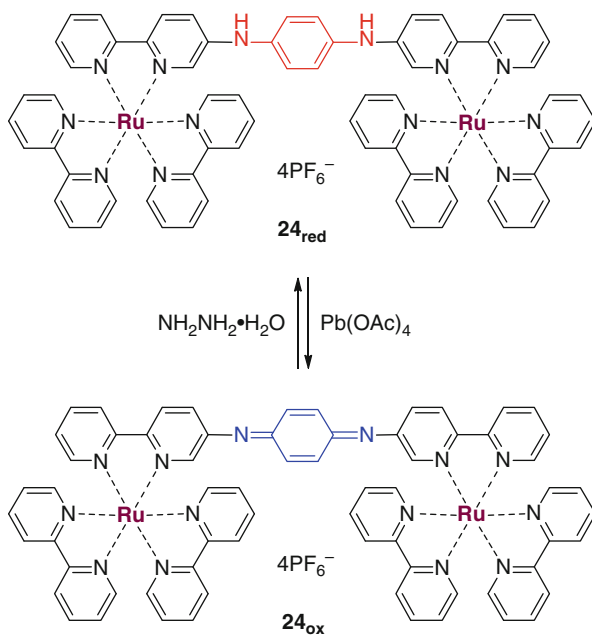
Scheme 3.26 Redox interconversion between **24_red** and **24_ox**

Photo irradiation of (acetonitrile)(2,2′-bipyridine)(2,2′:6′,2″-terpyridine)ruthenium (II) hexafluorophosphate, [Ru(tpy)(bpy)(CH₃CN)](PF₆)₂, in the presence of PD leads to the formation of the conjugated ruthenium(II) complex **25$_{red}$** in a one-pot reaction (Scheme 3.27) [72]. The crystal structure of **25$_{red}$** confirms that the two [(tpy)(bpy)Ru] units are bridged by the PD spacer to form the C_2-symmetrical 1:2 complex in *anti* configuration as shown in Fig. 3.15. The redox interconversion between the reduced form **25$_{red}$** and the oxidized form **25$_{ox}$** is possible (Scheme 3.27). Changing the redox states of the redox-active π-conjugated spacer permits the
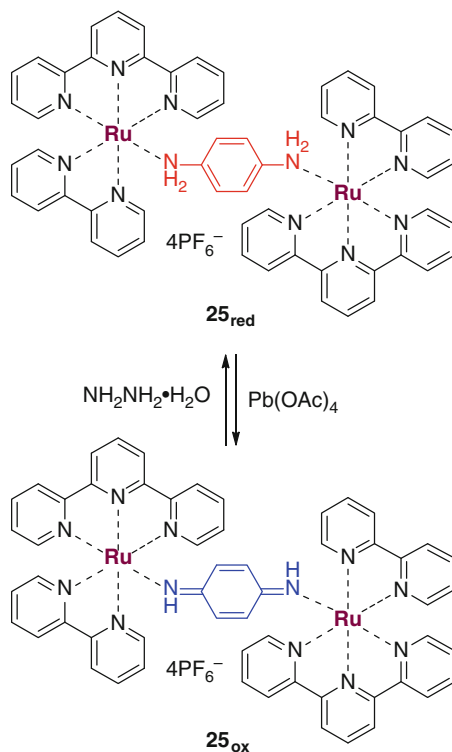
Scheme 3.27 Redox interconversion between **25$_{red}$** and **25$_{ox}$**
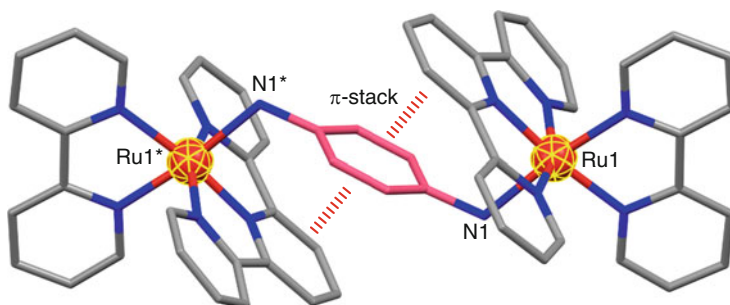
Fig. 3.15 The crystal structure of **25$_{red}$** (hydrogen atoms are omitted for clarity)

modulation of the emission properties of **25**. The reduced form **25$_{red}$** exhibits the emission at 605 nm in acetonitrile. On the contrary, almost complete quenching is observed in the emission spectrum of the oxidized form **25$_{ox}$**.

3.4 Hybrid Systems Consisting of Polyanilines or Quinonediimines and Transition Metal Nanoparticles

Toshikazu Hirao and Toru Amaya

As described in the Sect. 3.3, transition metals are conjugated with π-conjugated polymer like polyanilines. The transition metals can be extended to the transition metal nanoparticles (NPs). The resulting hybrids of metal NPs and polyanilines are expected to be of their potential applicability as electronic devices, chemical sensors, and catalysts. The NPs with small size and high surface-to-bulk ratio exhibit advantages compared with the bulk materials in the catalytic applications [73]. Therefore, the smaller and well-dispersed NPs are desired.

Pd NPs are known to catalyze various reactions [74]. Furthermore, their catalytic activity is often superior to that of mononuclear Pd complexes [74]. Polyaniline/Pd NPs are investigated in this context. They are prepared by simple reduction of Pd(II) in the presence of polyaniline (Scheme 3.28). [75] As a result of optimization for reductants such as hydroquinone, EtOH, ascorbic acid, or NaBH$_4$, the procedure using NaBH$_4$ in the presence of PdCl$_2$ and polyaniline (emeraldine base) with 1/10 ratio is revealed to provide well-dispersed and small Pd particles (2–6 nm, average diameter = 3.4 nm, see TEM image in Scheme 3.28) [75].
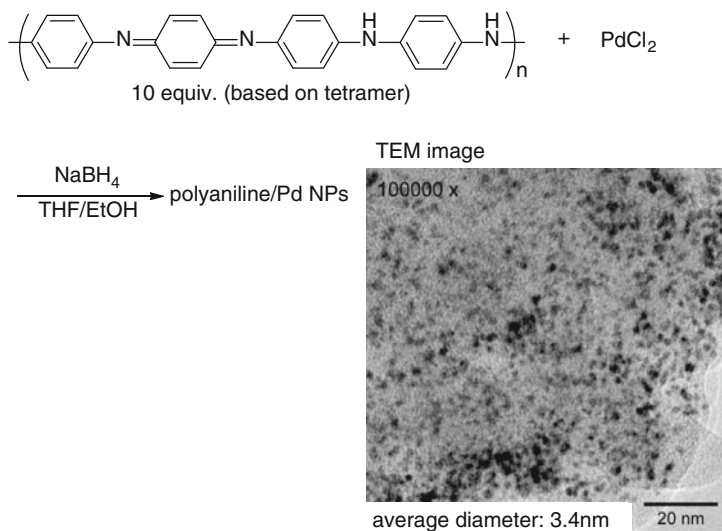
Scheme 3.28 Synthesis of polyaniline/Pd NPs by reduction with NaBH$_4$

To prepare the smaller particles, Pd(II) is preorganized on polyaniline, and reduced with NaBH$_4$. The preorganized Pd(II) complexes are already described in the Sect. 3.3. Preparation of the smaller Pd NPs is achieved by this procedure (average diameter = 2.4 nm, see TEM image in Scheme 3.29), where each particle is independent despite the high Pd density (16 wt %) [76]. The thus-obtained polyaniline/Pd NPs catalyze the oxidative dimerization of 2,6-di-*t*-butylphenol under molecular oxygen to give the corresponding diphenoquinone in a good yield (Scheme 3.30) [76].
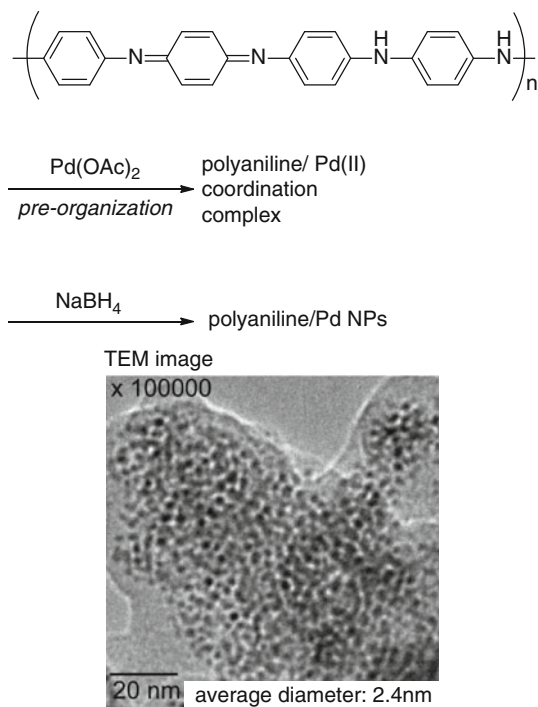
Scheme 3.29 Synthesis of polyaniline/Pd NPs by reduction of polyaniline/Pd(II) complex with NaBH$_4$
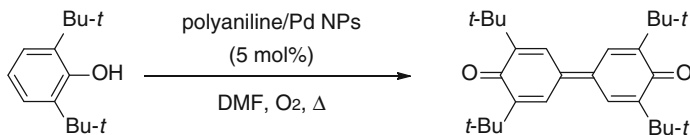
Scheme 3.30 Oxidative coupling of 2,6-di-*t*-butylphenol using polyaniline/Pd NPs under molecular oxygen

The preparation method using reductant causes partial or complete reduction of redox-active polyaniline, whose redox state significantly contributes to the electronic, coordinating, and catalytic properties. Ligand exchange approach as a reductant-less method is investigated to preserve the redox-state of polyaniline.

The small and well-dispersed starch/Pd NPs (average diameter = 2.3 nm) are first prepared by reduction of $Pd(OAc)_2$ with $NaBH_4$ in the presence of starch, followed by neutralization with 1 M HCl (Scheme 3.31) [77]. The ligand (here, it is starch) of the Pd NPs is exchanged for polyaniline by simple mixing in THF/H_2O. Starch is removed by washing with H_2O. The redox state of the polyaniline (emeraldine base) is maintained before and after the reaction. The size of the thus-obtained polyaniline/Pd NPs is distributed in a range of diameter 2–7 nm (average diameter = 3.0 nm), showing a little growth of the particles during the ligand exchange reaction (Scheme 3.31) [77]. Thus-developed ligand exchange procedure is applied to the preparation of polyaniline/Pt NPs [78].

Hybrid of iron oxide NPs and polyaniline are also prepared by the thermal reaction of $Fe(acac)_3$ in the presence of polyaniline (Scheme 3.32) [79]. The particle size

average diameter: 2.3 nm   average diameter: 3.0 nm
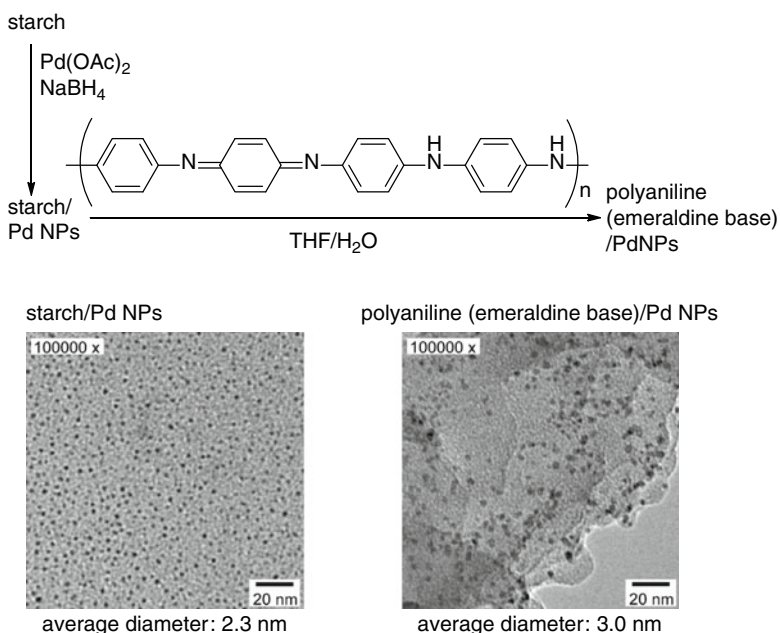
Scheme 3.31 Synthesis of polyaniline/Pd NPs via ligand exchange

average diameter: 5.6 nm
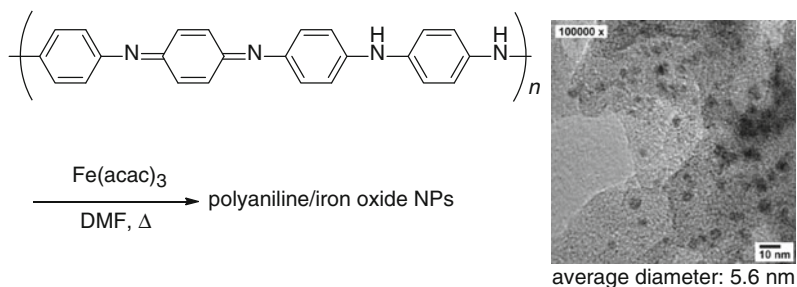
Scheme 3.32 Synthesis of polyaniline/iron oxide NPs

is distributed in a range of diameter 3–9 nm as shown in the TEM image (Scheme 3.32). The hybrid catalyzes the oxidative dimerization of 2,6-di-*t*-butylphenol under molecular oxygen to give the corresponding diphenoquinone.

In the catalytic reaction using metal NPs, polymer works as a stabilizer of metal NPs to avoid aggregation. Given the function of redox activity to the polymer, it is considered to mediate the transfer of electrons and/or protons in a metal-NPs catalyzed redox reaction system. PMAS/Au NPs are such a catalyst for aerobic oxidation. PMAS/Au NPs are prepared according to Scheme 3.33. PMAS is treated with $N_2H_4 \cdot H_2O$, then $NaAuCl_4$ is added to the reaction mixture to give PMAS (half ox)/ Au NPs (average diameter = 7.9 nm) [80]. The thus-obtained PMAS/Au NPs efficiently catalyze the oxidation of alcohol in pH 9.0 aqueous buffer solution under molecular oxygen (Scheme 3.34) [80]. Following the reaction using by UV–vis–NIR spectroscopy reveals the redox mediating effect of PMAS. Proposed catalytic cycles are shown in Scheme 3.34. Recycle use of this catalyst up to four times is demonstrated without loss of the activity. Concerning the scope of the substrate, secondary alcohols are transformed to the corresponding ketones in good yields. Primary alcohols are less reactive, but over oxidation to the corresponding carboxylic acid or ester is observed. The reaction under basic conditions improves the conversion.

PMAS (half ox)/Au NPs also catalyze the dehydrogenative oxidation of cyclic secondary amines such as 2-substituted indoline derivatives in aqueous solution under molecular oxygen (Scheme 3.35), where the redox mediating effect is demonstrated by
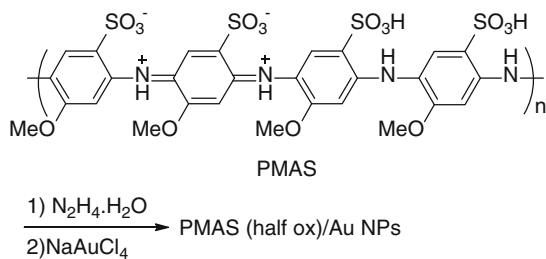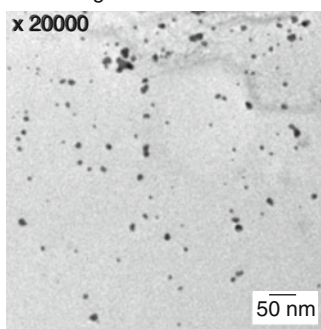
Scheme 3.33 Synthesis of PMAS/Au NPs
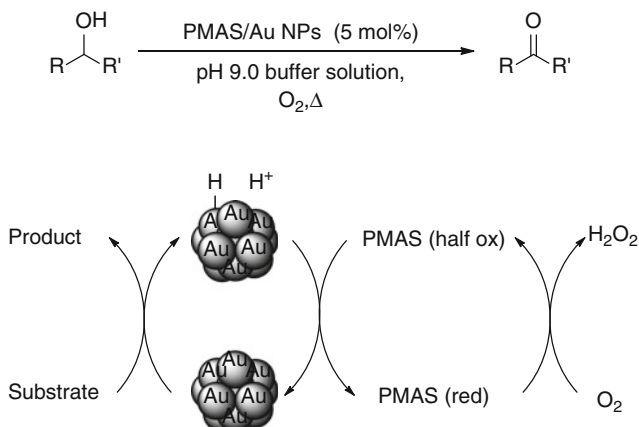
Scheme 3.34 Aerobic oxidation of alcohols using PMAS/Au NPs

Nu-H = dimethyl malonate, ethyl aceto acetate, CH_3NO_2
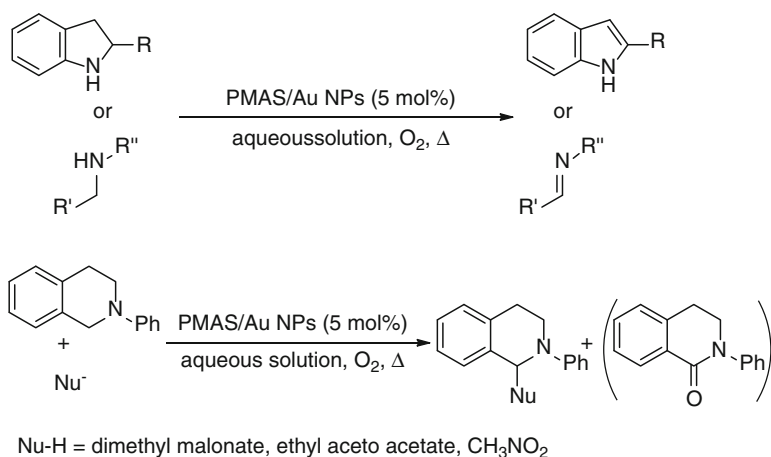
Scheme 3.35 Aerobic oxidation of nitrogen-including compounds using PMAS/Au NPs

monitoring UV–vis–NIR spectra of the reaction mixture [81]. The dehydrogenative aerobic oxidation of acyclic secondary amines takes place to give the corresponding imines. Notably, hydrolysis of the imines is almost inhibited even though the reaction is conducted in the complete aqueous solution (Scheme 3.35) [82]. Oxidation of tertiary amines in the presence of carbon nucleophiles induces the cross-dehydrogenative coupling via the iminium cations. However, the difficulty of this cross-dehydrogenative coupling is much raised if the reaction is conducted in the presence of water, because water can attack to the iminium cationic intermediate and the further oxidation leads to the lactam. PMAS (half ox)/Au NPs catalytic system allows the selective cross-dehydrogenative coupling of *N*-phenyltetrahydroisoquinoline with carbon nucleophiles such as dimethyl malonate, ethyl acetoacetate, and nitromethane in complete aqueous solution under molecular oxygen (Scheme 3.35) [83].

3.5 Chemistry of π-Conjugated Imidovanadiums

Toshikazu Hirao and Toshiyuki Moriuchi

The imido ligand coordinates to metals through a metal-nitrogen multiple bond [84], wherein the imido ligand can serve as an ancillary or supporting ligand. The imido ligand is a particularly suitable ligand for stabilization of transition metal complexes in high oxidation states through extensive ligand-to-metal π donation [85, 86]. The (imido)vanadium(V) complexes have gained growing interest because of their potential application as catalysts ([87, 88], and references therein). Introduction of a substituent onto the imido ligands is expected to influence the structural and electronic properties of a vanadium center through π conjugation. From these points of view, the design of the imido ligands is considered to be one of key factors in the development of efficient catalysts. The substituent effect of the aryl moiety of the imido ligands has been reported only spectroscopically and theoretically [89]. The control of the structurally defined molecular arrangements in a solid state is an area of current interest as crystal engineering [90, 91]. Architectural design of molecular self-organization is of importance for the development of functional materials [92, 93]. The utilization of the metal-directed assembly is regarded as a convenient strategy to construct the organized nanostructures [94–100]. This section describes the structural tuning and the self-assembling properties of (arylimido)vanadium(V) compounds.

The (arylimido)vanadium(V) triisopropoxides $[(p\text{-}RC_6H_4N)V(O^iPr)_3]$ (**26a**: R = NMe$_2$, **27a**: R = OMe, **28a**: R = H, **29a**: R = Br, **30a**: R = CN) are prepared by the reaction of VO(O^{i}Pr)$_3$ with the corresponding *para*-substituted aryl isocyanates (Fig. 3.16).

The crystal structure of **26a** bearing the electron-donating dimethylamino group reveals the μ-isopropoxido-bridged dimeric structure with the V(1)-N(1) distance of 1.678(3) Å and the nearly linear V(1)-N(1)-C(1) angle of 174.3(3)°, suggesting the greater participation of an *sp*-hybridized character in the nitrogen of the imido bond (Fig. 3.17a) [101]. Each vanadium atom is coordinated in a trigonal-bipyramidal geometry ($\tau_5 = 0.95$) [102] with the imido and bridging isopropoxido ligands in the apical positions. The crystal structures of **27a** bearing the electron-donating methoxy group and the non-substituted complex **28a** are also characterized by the μ-isopropoxido-bridged dimeric structures (Fig. 3.17b, c). The (arylimido)

26a: R = NMe$_2$ **27a**: R = OMe
28a: R = H   **29a**: R = Br
30a: R = CN

29b

31: R = H   **32**: R = Br
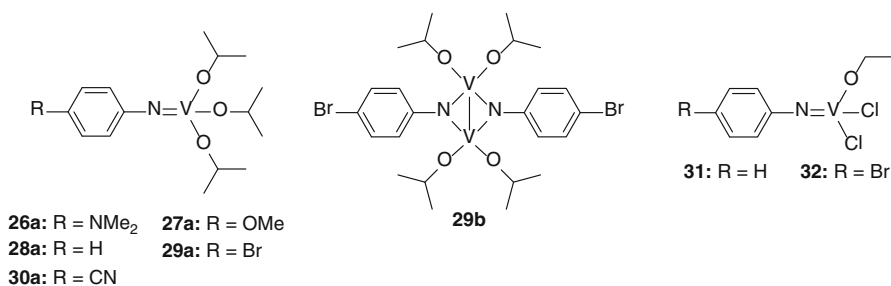
Fig. 3.16 Chemical structures of the (arylimido)vanadium(V) triisopropoxides **26a–30a**, **29b**, and **31–32**
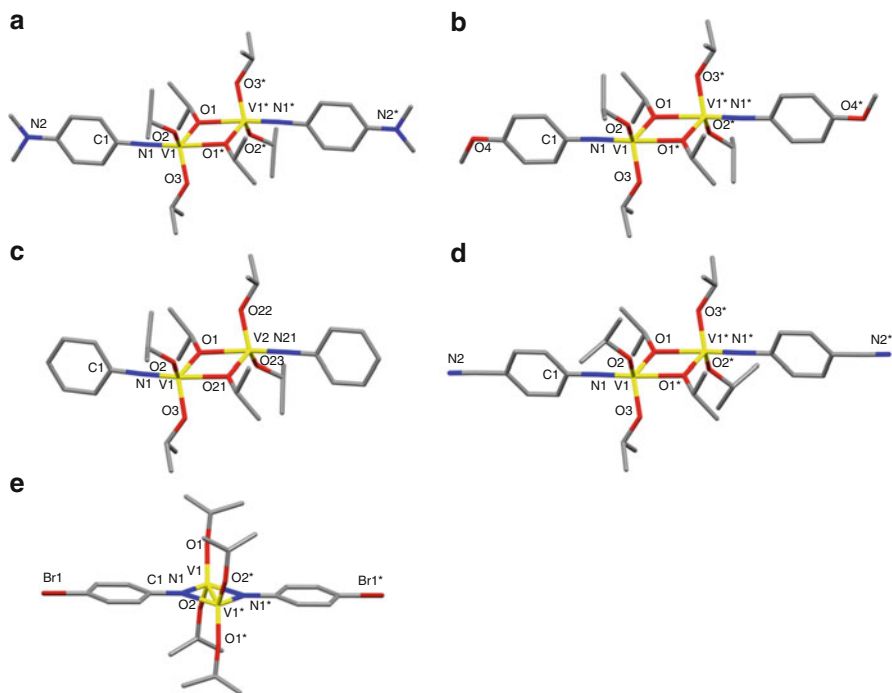
Fig. 3.17 μ-Isopropoxido-bridged dimeric structures of (**a**) **26a**, (**b**) **27a**, (**c**) **28a**, (**d**) **30a**, and (**e**) μ-arylimido-bridged dinuclear structure of **29b**

vanadium(V) triisopropoxide **30a** bearing the electron-withdrawing cyano group shows the μ-isopropoxido-bridged dimeric structure with the V(1)-N(1) distance of 1.674(2) Å and the nearly linear V(1)-N(1)-C(1) angle of 178.6(2)° (Fig. 3.17d). Linearity of the imido angle increases as compared with **26a**, probably due to the contribution of π-conjugation.

The self-association depends on the characteristics of the V–N imido bond, which is controlled by the difference in π conjugation of the *p*-substituent on the benzene ring. The recrystallization of the (arylimido)vanadium(V) complex [(*p*-BrC₆H₄N)V(O*i*Pr)₃] (**29a**), which is initially formed by the reaction of 4-bromophenylisocyanate with VO(O*i*Pr)₃, leads to the formation of the μ-imido-brigded dinuclear vanadium(IV) complex [V(μ-N-*p*-C₆H₄Br)(O*i*Pr)₂]₂ (**29b**). The lone pair on the nitrogen atom is likely to coordinate to the vanadium center to afford the cyclodivanadazene **29b**. The single-crystal X-ray structure determination of **29b** reveals a dinuclear structure with two imido ligands bridging two V(O*i*Pr)₂ moieties as depicted in Fig. 3.17e [101]. The geometry at the vanadium center is coordinated in a distorted tetrahedral geometry.

As observed in the (arylimido)vanadium(V) triisopropoxides, the crystal structure of the (phenylimido)vanadium(V) ethoxydichloride [(C₆H₅N)V(OEt)Cl₂] (**31**) reveals the μ-ethoxido-bridged dimeric structure with the V(1)-N(1) distance of 1.6554(14) Å and the nearly linear C(1)-N(1)-V(1) angle of 173.46(13)°, in which each vanadium atom is coordinated in a trigonal-bipyramidal geometry by bridging
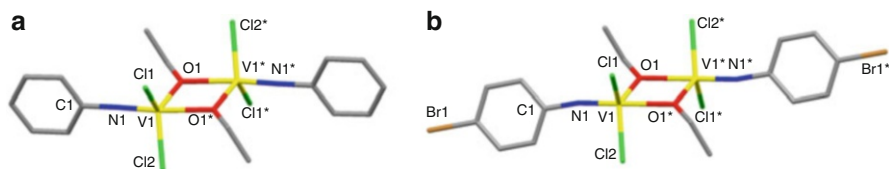
Fig. 3.18 μ-Ethoxido-bridged dimeric structures of (**a**) **31** and (**b**) **32**
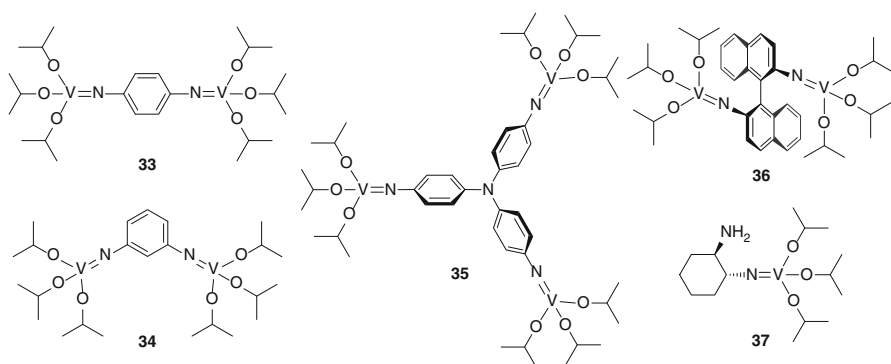
Fig. 3.19 Chemical structures of the (imido)vanadium(V) triisopropoxides **33–37**

the ethoxido group in an apical position as shown in Fig. 3.18a [103]. The μ-ethoxido-bridged dimeric structure with the V(1)-N(1) distance of 1.661(3) Å and the nearly linear V(1)-N(1)-C(1) angle of 169.5(2)° is also observed in the crystal structure of [(*p*-BrC$_6$H$_4$N)V(OEt)Cl$_2$] (**32**) bearing the bromo group on the benzene ring (Fig. 3.18b) [22]. The imido angle is almost 4° bent as compared with **31**, indicating the less contribution of the *sp*-hybridized character with the imido nitrogen of **32**. The bromo group might weaken the *sp*-hybridized character probably due to the conjugation of the electron-withdrawing group.

Generally, (imido)vanadium(V) complexes have been prepared by the reaction of (oxido)vanadium(V) complexes with the corresponding isocyanates. However, there are some limitations preventing the preparation of functional (imido) vanadium(V) complexes because the isocyanates are not necessarily available through an easily accessible synthetic method. (Arylimido)vanadium(V) triisopropoxides can be prepared in one-pot from aniline derivatives by using NaH as a base [104]. This one-pot synthesis permits the use of a wide range of commercial available aromatic amines in the straightforward synthesis of a variety of (arylimido) vanadium(V) triisopropoxides. For example, the binuclear (arylimido)vanadium(V) triisopropoxide [(*i*PrO)$_3$V(N-*p*-Ph-N)V(O*i*Pr)$_3$] (**33**) is obtained by the reaction of 1,4-phenylenediamine with VO(O*i*Pr)$_3$ (2.4 equiv.) in the presence of NaH (2.4 equiv.) (Fig. 3.19). The crystal structure of **33** reveals that the V-N-Ph-N-V core is almost linear with the V(1)-N(1) distance of 1.678(2) Å and the V(1)-N(1)-C(1) angle of 177.8(1)° probably due to the conjugation. As expected, the μ-isopropoxido-bridging permits the one-dimensional linear polymeric structure in the crystal packing as shown in Fig. 3.20a [101]. The bimetallic complex [(*i*PrO)$_3$V(N-*m*-C$_6$H$_4$N)
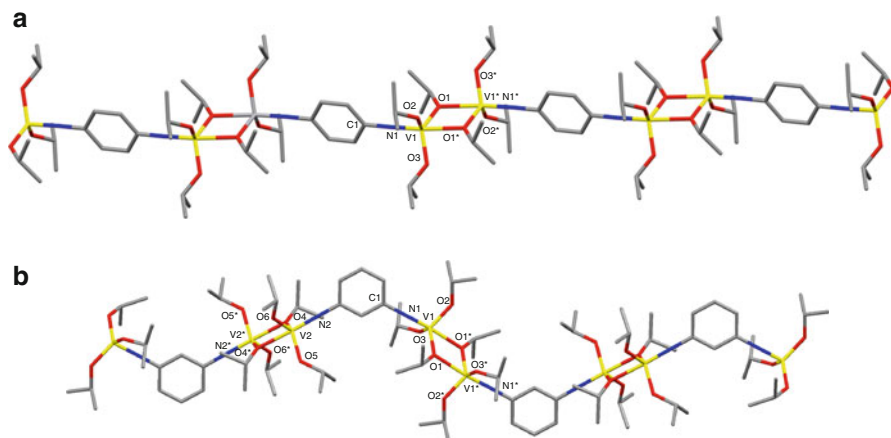
Fig. 3.20 A portion of a layer containing the one-dimensional linear polymeric structure of (**a**) **33** and (**b**) the one-dimensional zigzag polymeric structure of **34** through μ-isopropoxido-bridging in the crystal packings
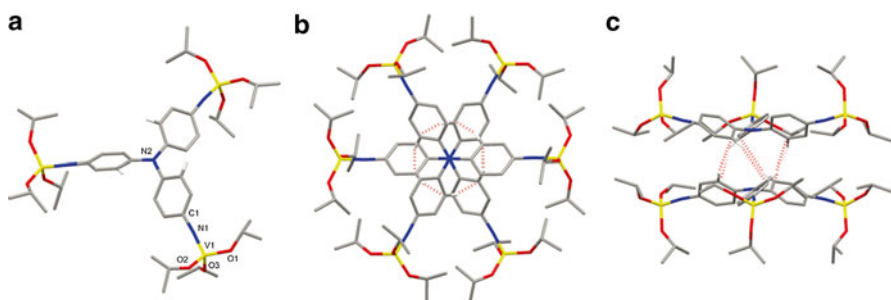
Fig. 3.21 (**a**) Crystal structure of **35**, (**b**) a *top view*, and (**c**) a *side view* of a "gear pair" like dimeric structure of **35** through six intermolecular CH-**π** interactions

V(O^{i}Pr)$_3$] (**34**) exhibits the one-dimensional zigzag polymeric structure through μ-isopropoxido-bridging (Fig. 3.20b) [101].

The crystal structure of the trinuclear (arylimido)vanadium(V) triisopropoxide [N[(-*p*-Ph-N)V(O^{i}Pr)$_3$]$_3$] (**35**), which is prepared by one-pot synthesis from tris(4-aminophenyl)amine, is characterized by a tridendritic centrosymmetric structural motif with a distorted pyramidal geometry at the central nitrogen as shown in Fig. 3.21a [104]. The imido structure with the V(1)-N(1) distance of 1.657(3) Å and the nearly linear V(1)-N(1)-C(1) angle of 173.3(2)° based on the higher participation of an *sp*-hybridized character in the nitrogen of the imido bond. Two mirror imaged molecules exist in the asymmetric unit, in which the triphenylamine moieties of these molecules adopt a mirror imaged propeller twist conformation. These molecules pack in a face-to-face manner to form a "gear pair"-like dimeric structure through six intermolecular CH-π interactions between the aryl moieties in the crystal packing as depicted in Fig. 3.21b, c.
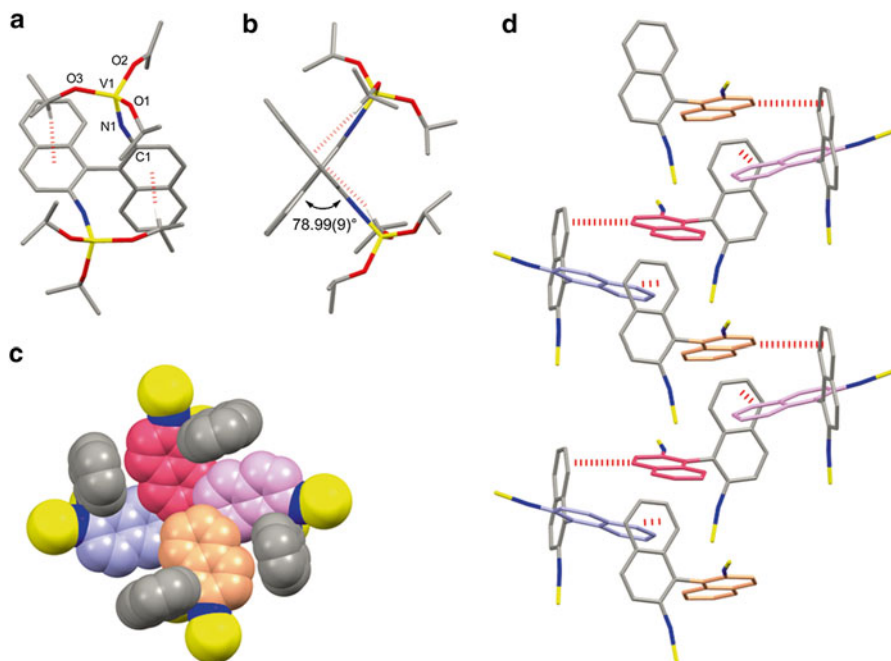
Fig. 3.22 (**a**) A *top view*, (**b**) a *side view* of the molecular structure of **36**, (**c**) space-filling representations of the *top view* of the crystal packing of **36** (isopropoxy groups are omitted for clarity), and (**d**) the *side view* of a portion of a layer containing the helically ordered molecular assembly through CH-π interaction in the crystal packing of **36** (isopropoxy groups are omitted for clarity)

The utilization of an axially chiral binaphthyl skeleton is expected to induce a helically ordered molecular assembly. The axially chiral binuclear (arylimido) vanadium(V) triisopropoxide [(^{i}PrO)$_3$V(N-(*R*)-1,1′-BN-N)V(O^{i}Pr)$_3$] (**36**) is prepared by the reaction of (*R*)-(+)-binaphthyl-2,2′-diamine with 250 mol% of VO(O^{i}Pr)$_3$ in the presence of 240 mol% of NaH [104]. As a result of the CH-π interaction between the hydrogen atom on the methine carbon atom and the π-electrons of the naphthalene ring, the binaphthyl moiety adopts in a conformation with a dihedral angle of 78.99(9)° between the naphthalene planes in the crystal structure of **36** (Fig. 3.22a, b). The bent imido structures with the V(1)-N(1)-C(1) angles of 161.7(3), 167.8(3), 167.0(4), and 168.0(4)° are observed probably due to the CH-π interaction and steric hindrance. A left-handed helically ordered molecular arrangement is created through the intermolecular CH-π interaction in the crystal packing of the axially chiral binuclear complex **36** as depicted in Fig. 3.22c, d. The positive Cotton effect at 326 and the negative Cotton effect at 421 nm around the absorbance region of the (imido)vanadium(V) triisopropoxide moieties supports the axially chiral structure in the circular dichroism spectrum of **36**.

(Alkylimido)vanadium(V) triisopropoxides are also synthesized by one-step method. The reaction of (1*R*,2*R*)-1,2-cyclohexanediamine with an equal amount of VO(O^{i}Pr)$_3$ affords the chiral mononuclear complex [(1*R*,2*R*)-(2-NH$_2$-*c*-C$_6$H$_{10}$N)

V(O^{i}Pr)$_3$] **37(R,R)** with an unreacted amino group [105]. The single-crystal X-ray structure determination of **37(R,R)** reveals that the cyclohexane moiety has a chair conformation with the chiral mononuclear structure, in which the amino group and imidovanadium moiety are in the equatorial positions as shown in Fig. 3.23a. A one-dimensional polymeric zigzag arrangement is created through intermolecular coordination interaction of the amino group to the vanadium metal center in a crystal packing (Fig. 3.23b). As observed in the dimerized structure of (arylimido) vanadium(V) alkoxides in a solid state, the geometry at the vanadium center is a trigonal-bipyramidal geometry ($\tau_5 = 0.96$) with the imido nitrogen N(1) and amino nitrogen N(2*) in the apical positions.

The use of *trans*-1,4-cyclohexanediamine (*trans*-c-C$_6$H$_{10}$DA) leads to the formation of the binuclear (alkylimido)vanadium(V) triisopropoxide **38** (Scheme 3.36) [105]. The single-crystal X-ray structure determination reveals that **38** has the vanadium metal centers in the equatorial positions of the cyclohexane ring as observed with **37(R,R)** (Fig. 3.24a). In the crystal packing, the dinuclear complex **38** shows a one-dimensional polymeric molecular arrangement through the μ-isopropoxido-bridging (Scheme 3.36 and Fig. 3.24b). In the presence of an equal amount of *trans*-c-C$_6$H$_{10}$DA, the dinuclear complex **38** forms the 1:1 complex **39** [105].

Fig. 3.23 (**a**) The repeat unit and (**b**) a portion of polymeric molecular arrangement of **37(R,R)**
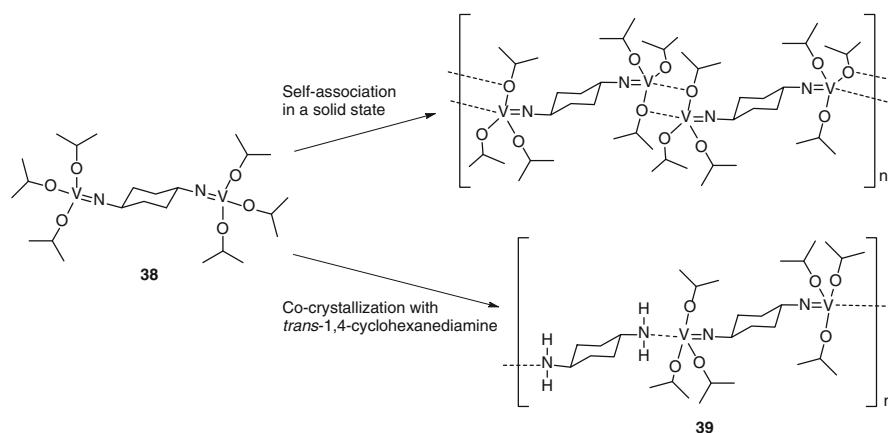
Scheme 3.36 Self-association of **38** and **39** to give a one-dimensional polymeric molecular arrangement
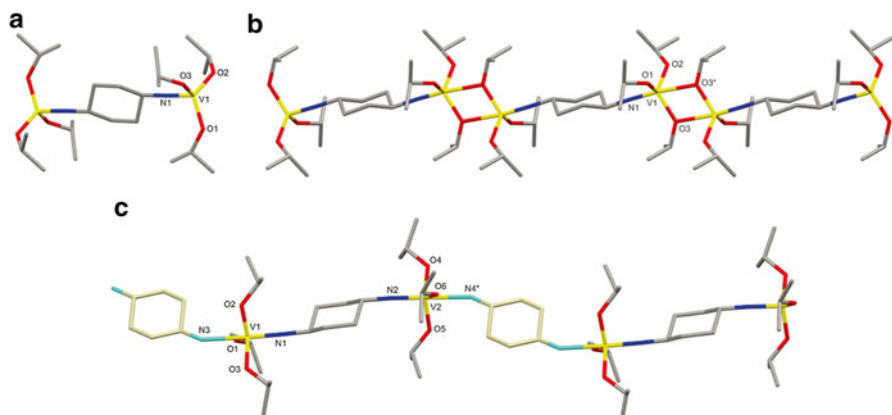
Fig. 3.24 (**a**) The repeat unit and (**b**) a portion of a one-dimensional polymeric molecular arrangement of **38**. (**c**) A portion of a one-dimensional polymeric molecular arrangement of **39**

26b: R = NMe$_2$ **27b:** R = OMe

28b: R = H   **29b:** R = Br

30b: R = CN
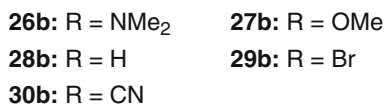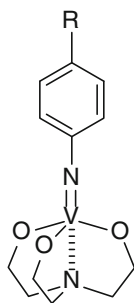
Fig. 3.25 Chemical structures of the (arylimido)vanadium(V) triethanolaminates **26b–30b**

The crystal structure of **39** confirms the coordination of *trans-c*-C$_6$H$_{10}$DA to the dinuclear complex **38**, affording a one-dimensional polymeric molecular arrangement as shown in Scheme 3.36 and Fig. 3.24c.

To clarify the substituent effect on the electronic environment of the vanadium centers, triethanolamine (TEA) is employed as a basal ligand to prevent the dimerization [106, 107]. The ligand exchange reaction of the (arylimido)vanadium(V) triisopropoxides [(*p*-RC$_6$H$_4$N)V(O^{i}Pr)$_3$] with TEA in CH$_2$Cl$_2$ at room temperature affords the corresponding (arylimido)vanadium(V) triethanolaminates [(*p*-RC$_6$H$_4$N) V(TEA)] (**26b**: R = NMe$_2$, **27b**: R = OMe, **28b**: R = H, **29b**: R = Br, **30b**: R = CN) (Fig. 3.25) [108]. [51]V NMR measurements are demonstrated to clarify the substituent effect on the electronic environment of the vanadium centers. The [51]V chemical
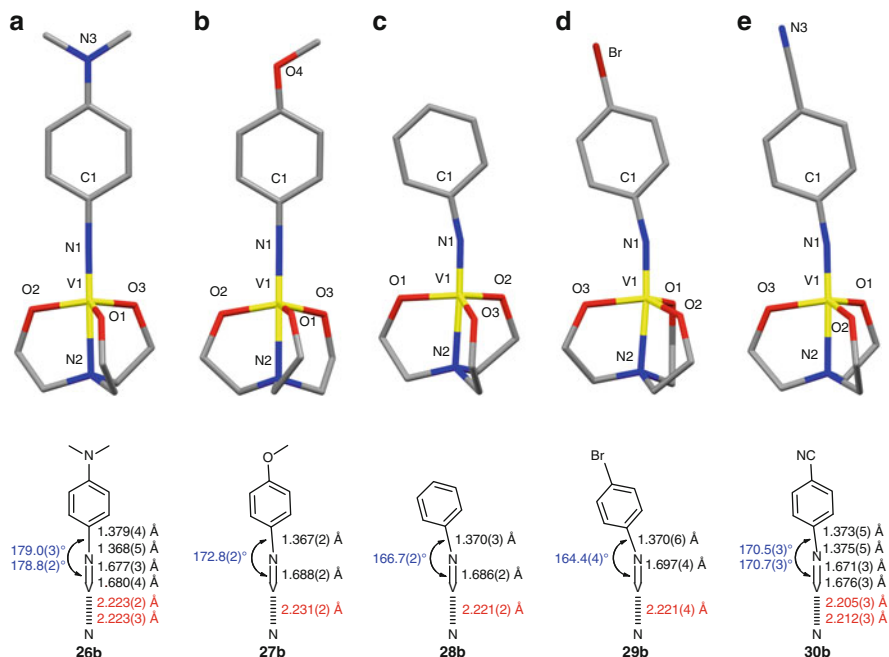
Fig. 3.26 Crystal structures and schematic representation of (**a**) **26b**, (**b**) **27b**, (**c**) **28b**, (**d**) **29b**, and (**e**) **30b**

shift of the non-substituted (phenylimido)vanadium(V) triethanolaminate **28b** is observed at −327 ppm. The ^{51}V chemical shifts are detected at the lower field with increase of the electron-donating capability of the *para*-substituents (**26b**: −224 ppm, **27b**: −292 ppm) in the ^{51}V NMR spectra of the (arylimido)vanadium(V) triethanol-aminates. On the contrary, the electron-withdrawing substituent, in which the nitrogen atom of the imido bond becomes more electronegative to increase ^{51}V nuclear shielding, induces the higher field shift (**29b**: −328 ppm, **30b**: −340 ppm). The vana-dium nuclei is known to become increasingly shielded as the electronegativity of the ligand attached to the coordination center increases in the ^{51}V NMR spectra of d^0 diamagnetic vanadium complexes [89].

The single-crystal X-ray structure determination of the (arylimido)vanadium(V) triethanolaminates elucidates the substituent effect on the imido structures [108]. The crystal structure of the non-substituted (phenylimido)vanadium(V) triethanol-aminate **28b** shows the imido structure with the V(1)-N(1) distance of 1.686(2) Å and the bent V(1)-N(1)-C(1) angle of 166.7(2)° (Fig. 3.26c). A monomeric structure with a pseudo-trigonal bipyramidal geometry at the metal center (τ = 0.99) is observed, wherein the vanadium atom is pulled out of the plane formed by triethanolaminate oxygen atoms in the direction of the imido nitrogen. Linearity of the imido angle is increased (V(1)-N(1)-C(1), 172.8(2)°) in the case of the (arylimido)vanadium(V) triethanolaminate **27b** with the electron-donating methoxy
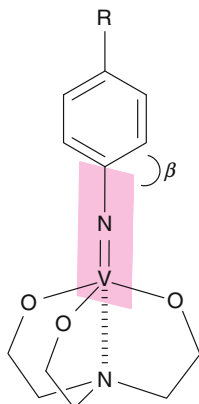
Fig. 3.27 The twist angle β defined as the angle between the least squares planes of the benzene ring and the C(*ipso*)-imido bond

group although the V(1)-N(1) distance of 1.688(2) Å is almost the same to the one observed with **28b** (Fig. 3.26b). Furthermore, the (arylimido)vanadium(V) trietha-nolaminate **26b** bearing the dimethylamino group, in which two independent molecules exist in the asymmetric unit, shows the more straightened imido angle with the V(1)-N(1)-C(1) angles (179.0(3) and 178.8(2)°) and the V(1)-N(1) distances (1.677(3) and 1.680(4) Å) (Fig. 3.26a). On the contrary, the use of the bromo substituent leads to the more bent imido bond (**29b**: V(1)-N(1)-C(1), 164.4(4)°; V(1)-N(1), 1.697(4) Å) as shown in Fig. 3.26d. The crystal structure of the (ary-limido) vanadium(V) complex **30b** with the cyano group, in which two independent molecules exist in the asymmetric unit, is characterized by the near-linear V(1)-N(1)-C(1) angles of 170.5(3) and 170.7(3)° with the V(1)-N(1) distances of 1.671(3) and 1.676(3) Å, probably due to the π-conjugation contribution (Fig. 3.26e).

The twist angle β defined as the angle between the least-squares planes of the benzene ring and the C(*ipso*)-imido bond (Fig. 3.27), which is considered to correlate to the properties of the imido bond, is affected by the *para* substituent of the aryl moiety [108]. The (arylimido)vanadium(V) triethanolaminates with the π-conjugative electron-donating substituent shows an almost perpendicular twist angle β (43.11(9)° and 101.82(9)° for **26b**; 95.92(5)° for **27b**). However, nearly parallel twist angles β are observed in other (arylimido)vanadium(V) triethanolami-nates (8.35(6)° for **28b**; 11.2(1)° for **29b**; 10.4(1)° for **30b**). The linear imido angle and the almost perpendicular twist angle β of the (arylimido)vanadium(V) trietha-nolaminate with the π-conjugating electron-donating substituent indicate the greater participation of *sp* hybrid character in the nitrogen of the imido bond, wherein the lone pair of electrons in a nitrogen *p* orbital is likely to interact with the metal π-acceptor orbitals and aryl π orbitals (Fig. 3.28). In contrast, the bent imido bond and the nearly parallel twist angle β in the case of the (arylimido)vanadium(V) tri-ethanolaminates bearing no π-conjugating electron-donating substituent might be due to the larger contribution of sp^2 hybrid character in the nitrogen of the imido bond, wherein the filled imido π orbital seems to interact with the aryl π orbitals.
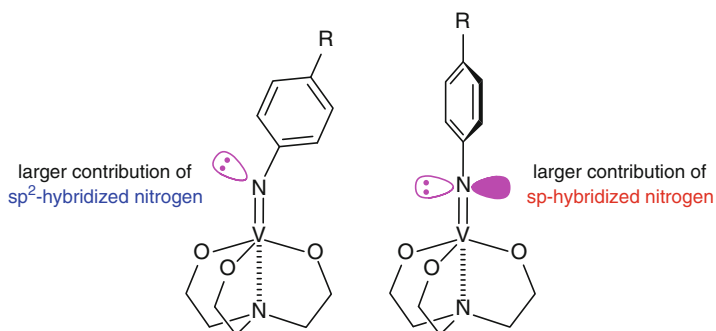
Fig. 3.28 Proposal valence bond structures for a vanadium bound imido ligand

40a: X = Me   **40b**: X = H   **41a**: X = Me   **41b**: X = H
40c: X = Br   **40d**: X = F   **41c**: X = Br   **41d**: X = F
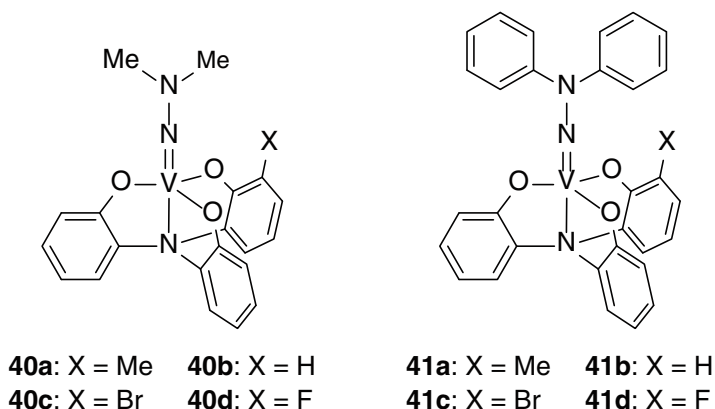
Fig. 3.29 Chemical structures of the vanadium(V) hydrazido complexes **40–41**

Metal hydrazido compounds are of potential due to their intermediacy in dinitrogen activation [109–113]. The vanadium(V) hydrazido complexes **40** and **41** with tris(2-hydroxyphenyl)amine ligands are designed to reveal the influence of the coordination of the apical nitrogen and the substituent of the tris(2-hydroxyphenyl) amine ligand on the vanadium center (Fig. 3.29) [114]. ^{51}V NMR measurement is a powerful tool to clarify the substituent effect on the electronic environment of the vanadium species. The ^{51}V NMR spectrum of the non-substituted vanadium(V) dimethylhydrazido complex **40b** shows the ^{51}V chemical shift at 335 ppm. The ^{51}V chemical shift of **40a** with the electron-donating substituent is observed at 328 ppm. On the contrary, the electron-withdrawing substituent causes the ^{51}V chemical shift to the lower field (**40c**: 381 ppm, **40d**: 378 ppm). These results indicate that the substituent at the 3-position of the tris(2-hydroxyphenyl)amine ligand influences the electron density of the vanadium center directly. The vanadium(V) diphenylhydrazido complexes **41** (**41a**: 164 ppm, **41b**: 178 ppm, **41c**: 206 ppm, **41d**: 209 ppm) show the similar substituent effect. ^{51}V chemical shifts of **41** are detected at the
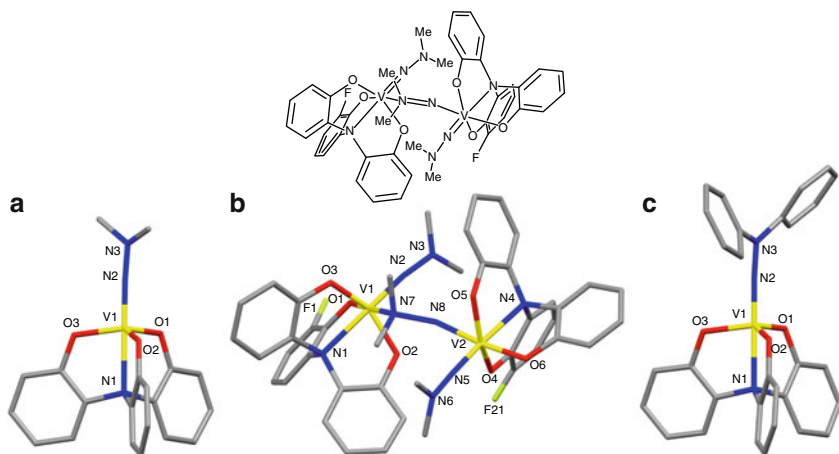
Fig. 3.30 Crystal structures of (**a**) **40b**, (**b**) **40d-DMH-40d**, and (**c**) **41b**

higher field compared to those of **40**. The electron-withdrawing diphenyl substituent, in which the nitrogen atom of the imido bond become more electronegative to increase ^{51}V nuclear shielding, is likely to cause the ^{51}V chemical shift to the higher field. These results are consistent with those of the (arylimido)vanadium(V) complexes reported [89].

The crystal structure of **40b**, in which two independent molecules exist in the asymmetric unit, reveals the near-linear V(1)-N(2)-N(3) angles of 176.60(17) and 173.11(16)° with the V(1)-N(2) distances of 1.6891(19) and 1.6837(19) Å, suggesting the high participation of an *sp*-hybridized character in the nitrogen of the V–N imido bond (Fig. 3.30a) [114]. The vanadium centers are distorted trigonal bipyramidal geometries with the phenolate oxygen atoms in equatorial positions, wherein the vanadium atom is pulled out of the plane formed by the phenolate oxygen atoms in the direction of the hydrazido nitrogen. The V(1)-N(2) distances of **40b** with the coordination from apical nitrogen is longer than that of the vanadium(V) dimethylhydrazido complex, [V(NNMe$_2$)(OC$_6$H$_3$^{i}Pr$_2$-2,6)$_3$], with tetrahedral geometry at vanadium center (V(1)-N(2), 1.653(3)) [115]. The electron donation from apical nitrogen N(2) to vanadium metal might be weaken to some extent.

Recrystallization of **40d** in the presence of *N,N*-dimethylhydrazine affords the *N,N*-dimethylhydrazine-bridged dinuclear vanadium(V) hydrazido complex **40d-DMH-40d**. The single-crystal X-ray structure determination of **40d-DMH-40d** confirms that two **40d** units are bridged by *N,N*-dimethylhydrazine to form the 2:1 complex in *anti*-configuration, wherein each vanadium center is a hexacoordinate geometry (Fig. 3.30b) [114]. This hydrazido complex **40d-DMH-40d** has the near-linear V(1)-N(2)-N(3) angles of 171.8(7) and 174.0(7)° with the V(1)-N(2) distances of 1.663(7) and 1.690(7) Å, respectively.

The structure of the vanadium(V) diphenylhydrazido complex **41b**, in which two independent molecules exist in the asymmetric unit, is also characterized by a distorted trigonal bipyramidal geometry with phenolate oxygen atoms in equatorial positions as depicted in Fig. 3.30c [114].

3.6 Synthesis and Structure of Molecular Bowl Sumanene

Toshikazu Hirao and Toru Amaya

Molecular bowl sumanene is a C_{3v} symmetric bowl-shaped π-conjugated molecule (the term "π bowls" is used for bowl-shaped π-conjugated molecules here, whereas they have been also called open geodesic polyarenes [116] or buckybowls [117].) [118–120], consisting of the alternating benzene rings and cyclopentadiene rings around the hub benzene ring (Scheme 3.37). The structure is one of the fragments for the structural motifs of fullerene C_{60} or an end-cap of carbon nanotubes. The name *sumanene* is given after "suman" which means flower in Hindi and Sanskrit due to its shape, with the ring edges on the rim resembling petals, is reminiscent of a flower [121]. The accounts of sumanene chemistry are reported in [122, 123].
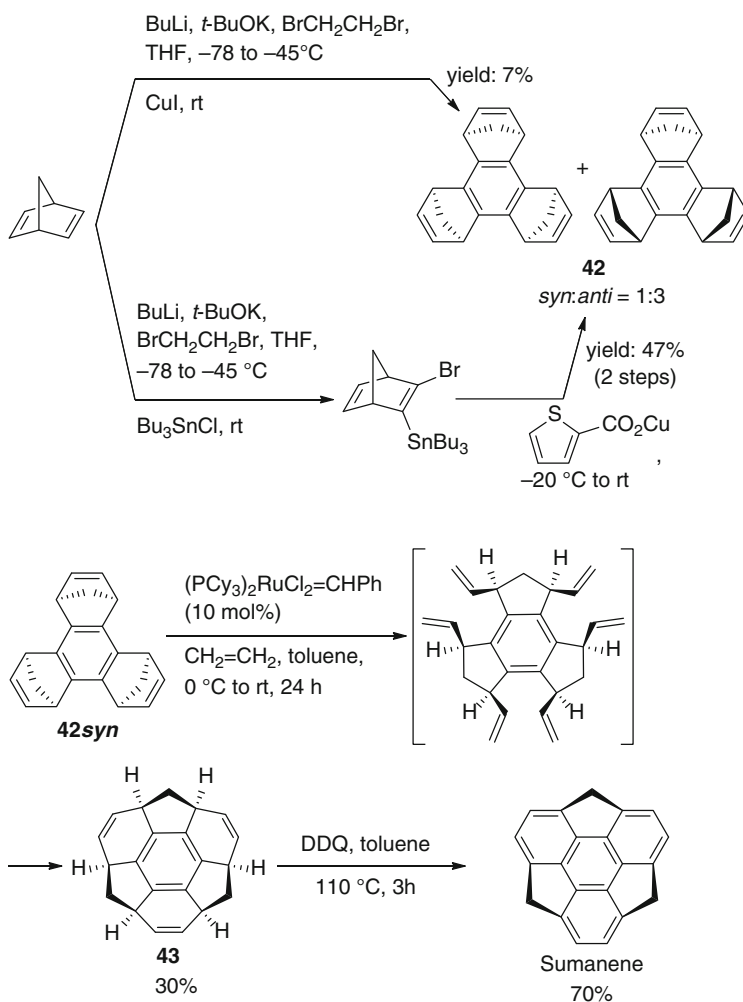
Scheme 3.37 Synthesis of sumanene
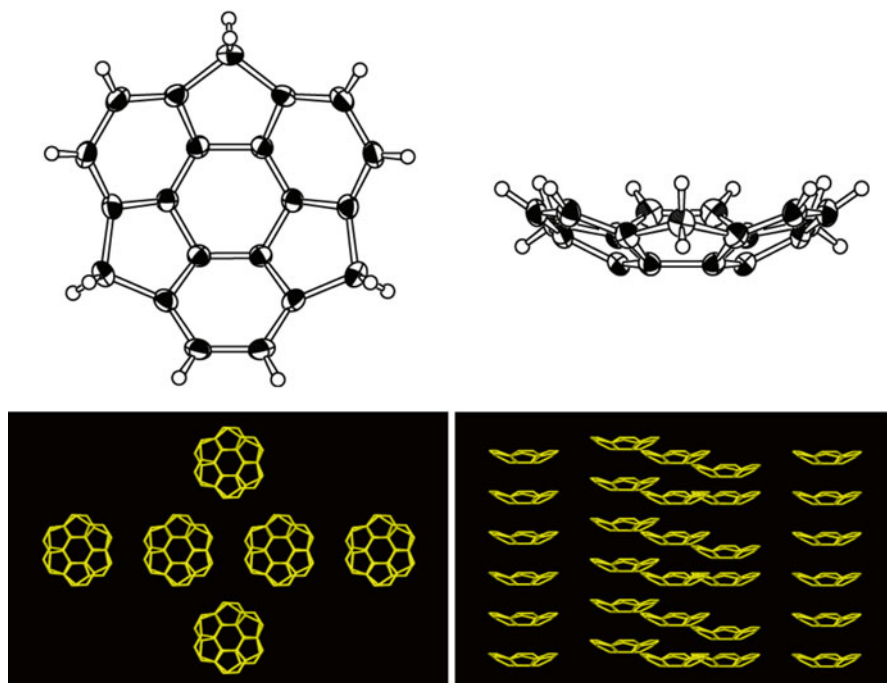
Fig. 3.31 X-ray crystal structure and packing of sumanene

Attempts for the synthesis of sumanene based on the approaches from planar aromatic compounds have been failed, which is considered to be due to the strain of sumanene [121]. Construction of a three-dimensional framework followed by oxidative aromatization provides a solution [124]. The aromatization energy compensates a disadvantage of the strain. Scheme 3.37 shows the synthetic scheme. The synthesis commences with the trimerization of 2,5-norbornadiene. The trimerization is conducted via the copper-mediated cyclization of (3-bromobicyclo[2.2.1] hepta-2,5-dien-2-yl)potassium (or lithium) species or (3-bromobicyclo[2.2.1]hepta-2,5-dien-2-yl)tributylstannane. The resulting trimer **42** includes *syn*- and *anti*-isomers. The double bonds in *syn*-isomer **42syn** are formally exchanged each other by Ru-catalyzed tandem ring-opening metathesis and ring-closing metathesis reactions under an atmospheric pressure of ethylene to give hexahydrosumanene **43**. Its oxidative aromatization with DDQ results in sumanene. This is the first report for the synthesis of sumanene [124].

X-ray crystal structure of sumanene clearly shows the bowl-shaped structure (Fig. 3.31). The bowl depth defined as a distance between a plane of a hub benzene ring and a rim aromatic carbon is 1.11 Å [125]. Sumanene favors a stacking structure in a concave–convex fashion. Each layer of the column is stapled in a staggered fashion. Every column is oriented in the same direction giving polar crystals (Fig. 3.31) [125]. Solid state NMR is also studied [126].

Anions can be stabilized at the benzylic positions. Treatment of sumanene with strong base generates the sumanenyl anions. Careful amount control of *t*-BuLi to sumanene leads to the corresponding benzylic mono-, di-, and trianions **44–46**, selectively (Scheme 3.38) [125]. The trapping of trianion with Me₃SiCl takes place from outside of the bowl (Scheme 3.38) [125].
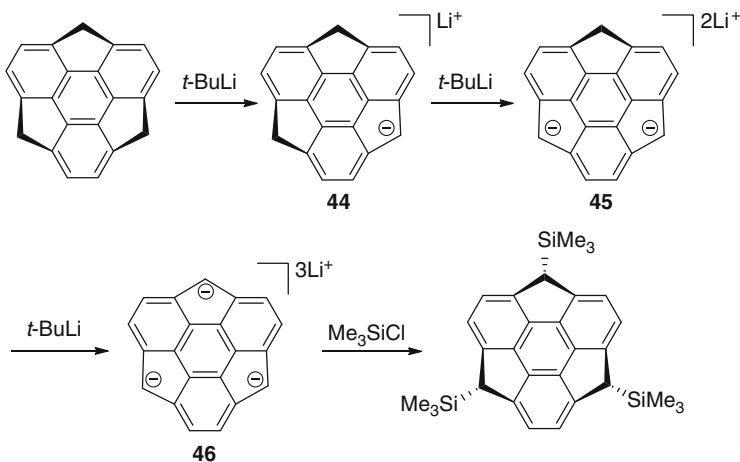
Scheme 3.38 Stepwise generation of benzylic anions of sumanene

Bowl-to-bowl inversion is one of the characteristic behaviors for some flexible π bowls [127]. Activation energy of sumanene for the bowl-to-bowl inversion is indicated to be approximately 20 kcal mol⁻¹ by variable temperature ¹H NMR experiments (Scheme 3.39) [124]. The 2D EXSY (exchange spectroscopy) experiments of trideuteriosumanene also suggest the similar value for the activation energy [128]. This value is consistent with the estimate one using theoretical calculation [129]. Sumanenyl mono- and dianion show a little larger activation barrier (21.8 and 21.5 kcal mol⁻¹ in THF-d_8, respectively) for the bowl-to-bowl inversion relative to that of sumanene [128].

$\Delta G^{\ddagger} = \sim 20 \text{kcal/mol}$
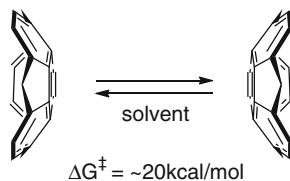
Scheme 3.39 Bowl-to-bowl inversion of sumanene

3.7 Function of Sumanene

Toshikazu Hirao and Toru Amaya

As described in the former section, the packing structure of sumanene crystal is columnar. Such stacking is considered to be effective for an anisotropic charge carrier transportation, which is investigated by the time-resolved microwave conductivity (TRMC) method [130]. This method allows one to evaluate the intrinsic intramolecular conductivity by minimizing the effect of impurity, defects, and interfaces i.e., as compared to conventional methods such as time-of-flight and field-effect transistor because the nanometer-scale mobility of charge carriers generated by laser pulse irradiation is quantified under oscillating microwave without electrodes. The charge carrier mobility of a needle-like crystal of sumanene along the stacking axis is larger than that along the perpendicular direction to the stacking axis. The anisotropic difference of conductivity reaches 9.2 times. The mobility along the stacking axis is estimated to be $>7.5 \times 10^{-1}$ cm^2 V^{-1} s^{-1} by TRMC method and photocurrent integration measurement, where the charge carrier is the electron (Fig. 3.32) [131].

Laser annealing of sumanene derivatives leads to carbon materials. The research on graphitic carbons is now one of the most active fields in materials chemistry [132]. Among graphitic carbons, nitrogen-doped graphitic carbons (NGCs) have attracted much interest due to their electrical and catalytic properties [133]. Laser annealing induces the transformation of sumanene derivatives **47** or **48** bearing the imine moiety into NGC (Scheme 3.40) [134, 135]. Notably, the nitrogen/carbon ratios are almost retained in the resulting NGCs although most nitrogen atoms are generally known to get lost during the carbonization process when it is conducted above 600–800 °C. The conductivity (up to 4 S cm^{-1}) of the NGCs is exhibited [134].
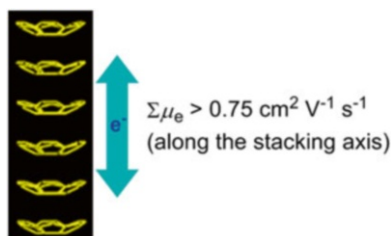
Fig. 3.32 Mobility of sumanene along stacking axis

47

or

48

laser

nitrogen-doped graphitic carbons(NGCs)
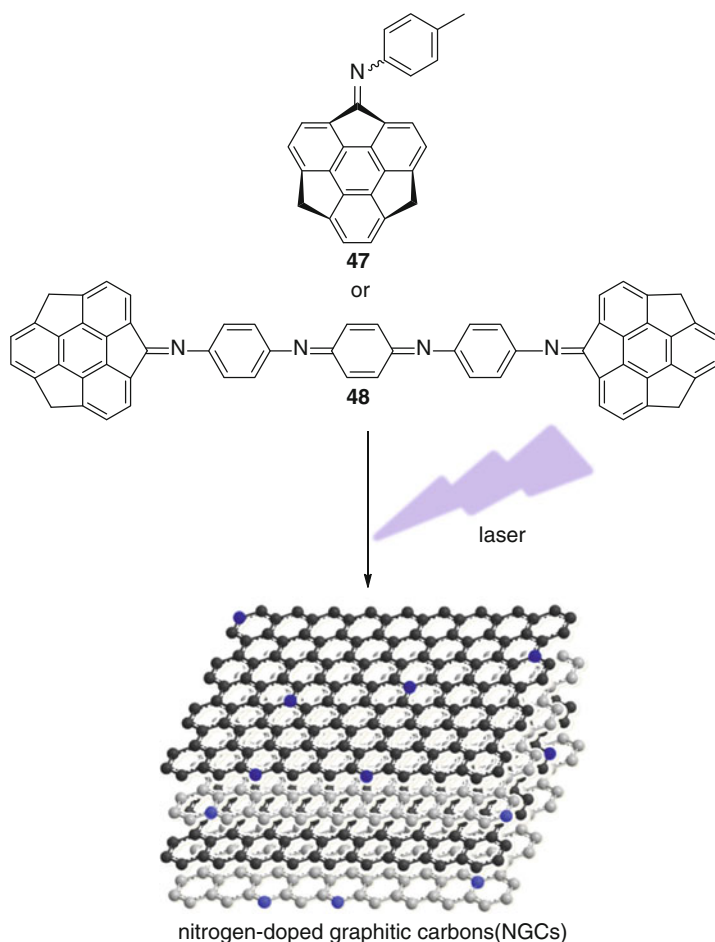
Scheme 3.40 Laser-induced formation of NGCs from sumanene derivatives **47** and **48**

3.8 Extended π-Conjugation of Sumanene

Toshikazu Hirao and Toru Amaya

Extension of the π conjugation at the benzylic position of sumanene is considered as the most efficient method to synthesize the π-conjugation extended sumanenes. As described above, benzylic anions are available for derivatization. Condensation of the benzylic anions of sumanene with various aldehydes affords the corresponding π-conjugation extended sumanenes **49** by using aqueous 30 % NaOH solution as a base (Scheme 3.41) [136]. The obtained products **49** have absorption in the longer wavelength region relative to sumanene.

R = Ph, 4-MeC$_6$H$_4$, 4-MeOC$_6$H$_4$, 4-ClC$_6$H$_4$, 4-CF$_3$C$_6$H$_4$,
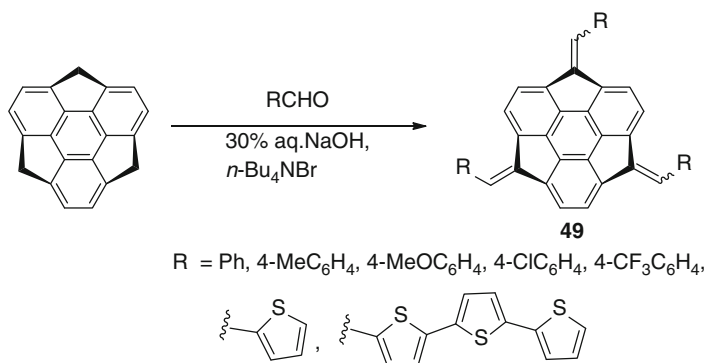
Scheme 3.41 Synthesis of π-conjugation extended sumanenes **49**

Naphthosumanenes **50–53**, having a more ring-fused structure, are synthesized. The synthetic scheme includes the following three steps: (1) bromination of the arene periphery, (2) introduction of 2-formylphenyl moiety by Suzuki-Miyaura coupling, and (3) intramolecular condensation in the presence of base. Mono-, di-, and tri-naphthosumanenes **50–53** are synthesized based on the strategy (Scheme 3.42) [137]. Bowl-to-bowl inversion of dideuteriomononaphthosumanene (32.2 kcal mol^{-1}) is much slower than sumanene. The structural optimization of naphthosumanenes shows the deeper bowl structures [129, 137].

The synthesis of mono- and trioxosumanenes **54–55** is performed by oxidation of benzylic positions of sumanene (Scheme 3.43) [138]. Oxosumanenes **54–55** have the extended π conjugation relative to sumanene. Imination of monooxo-sumanene **54** leads to further π extension [134, 135]. Crystal structure of mono-oxosumanene **54** shows the bowl-shaped structure and columnar packing (Fig. 3.33) [138]. In the reaction of trioxosumanene **55** with methylmagnesium bromide, it selectively attacks from outside of the bowl (Scheme 3.43).

Bisumanenyl **56**, the aryl-aryl coupled sumanene dimer, is synthesized via one-pot borylation and Suzuki-Miyaura coupling of bromosumanene (Scheme 3.44) [139]. Despite the inherent rich isomerism based on the relative bowl direction and bond rotation, the selective formation of one isomer is suggested by variable temperature NMR experiments. The extension of π conjugation is shown from the absorption and emission spectra.
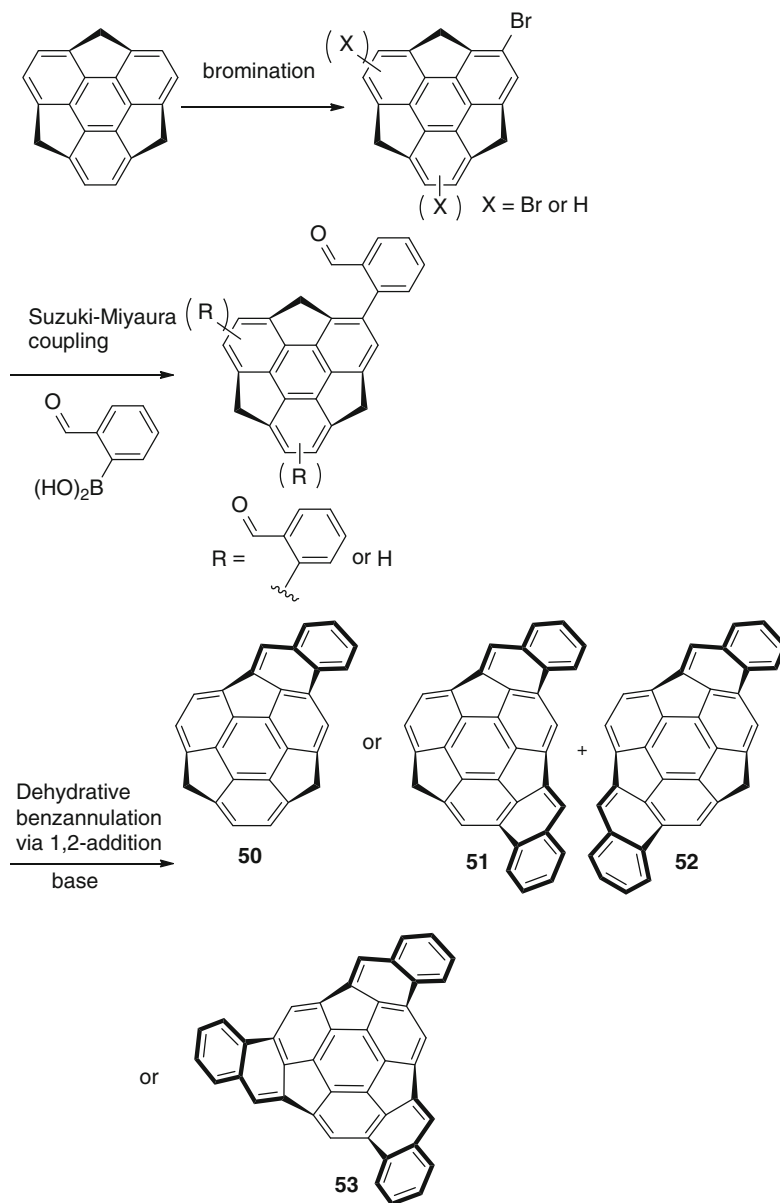
Scheme 3.42 Synthesis of naphthosumanenes **50–53**
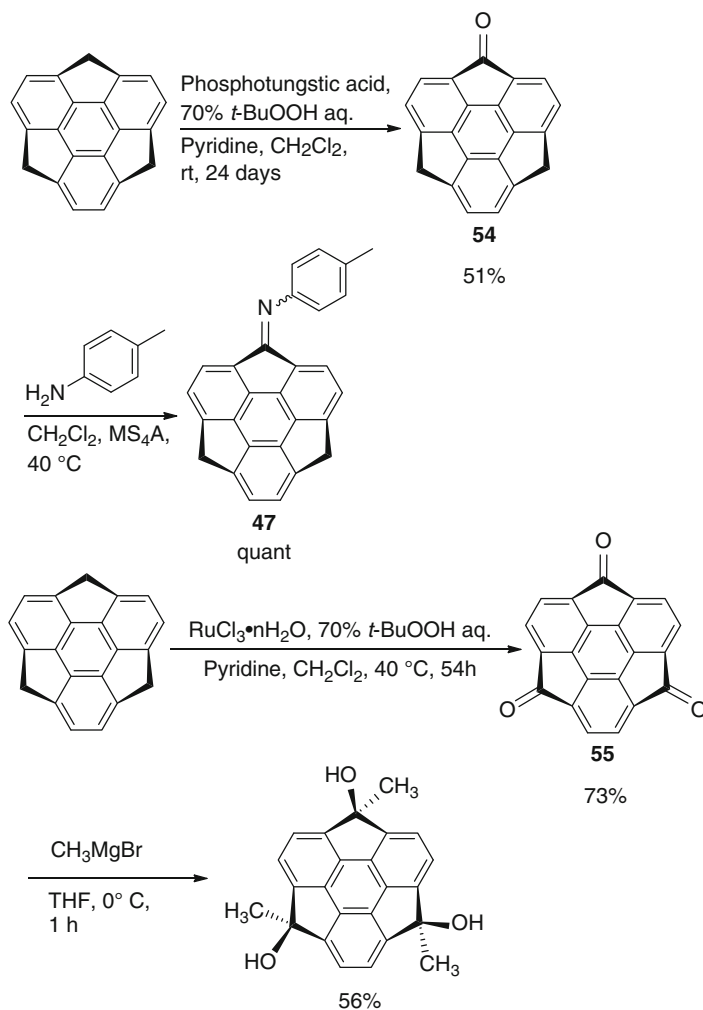
Scheme 3.43 Synthesis of oxosumanenes **54** and **55**, and their derivatization

Bisumanenylidene **57**, consisting of two sumanene components connected by a double bond, is synthesized by McMurry coupling of monooxosumanene **54** (Scheme 3.45) [140]. The calculation and low temperature ^{1}H NMR experiments suggest that bisumanenylidene is likely to be dominantly present as a C_{2h} symmetric
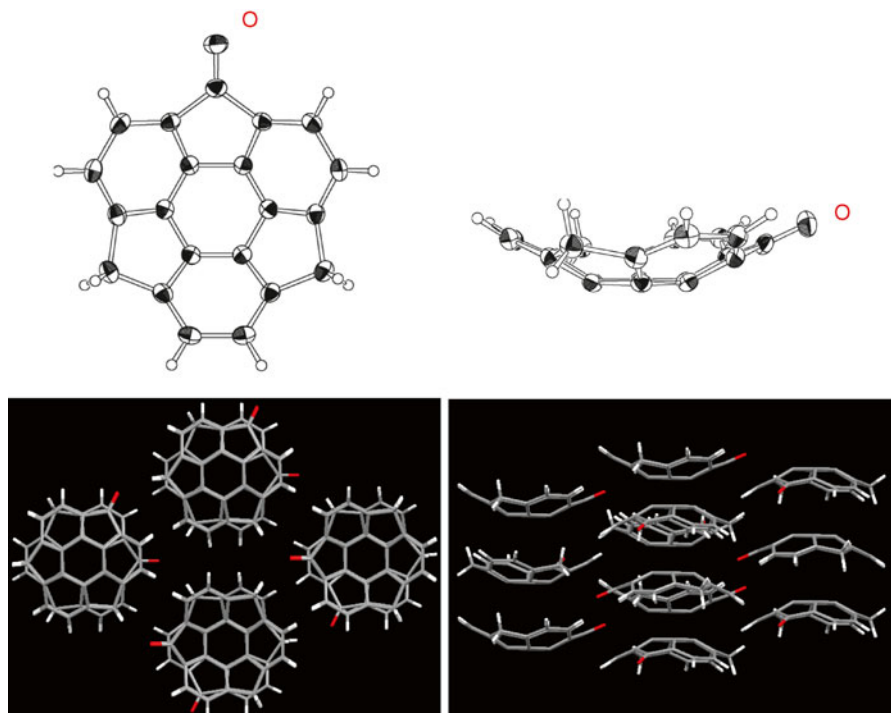
Fig. 3.33 X-ray crystal structure and packing of monooxosumanene **54**
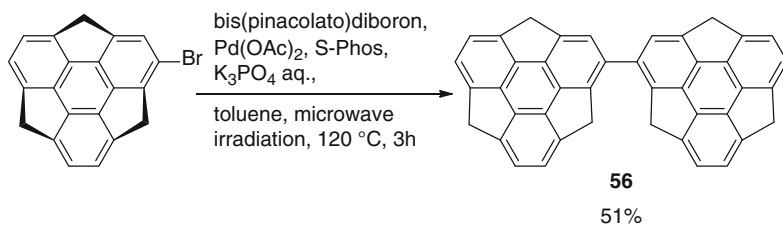
Scheme 3.44 Synthesis of bisumanenyl **56**

structure (the two bowls direct the opposite side each other) rather than a C_2 symmetric one (the two bowls direct the same side each other) (Scheme 3.45). The extension of π conjugation of bisumanenylidene is also shown from the absorption and emission spectra.

C_{2h} symmetry C_2 symmetry
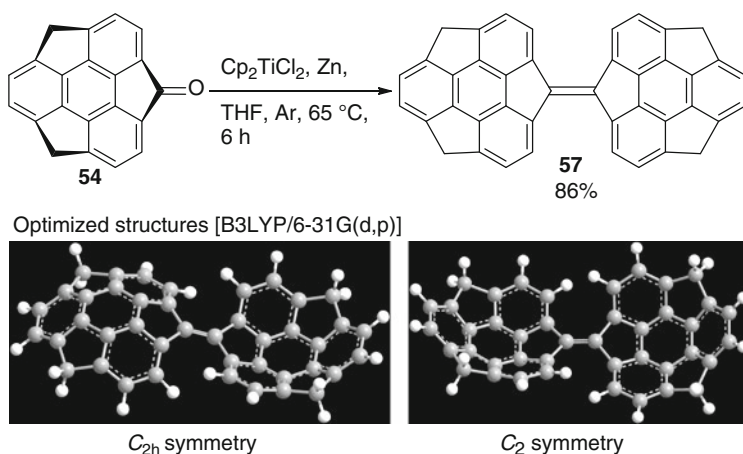
Scheme 3.45 Synthesis of bisumanenylidene **57**

3.9 Coordination Chemistry of Sumanene

Toshikazu Hirao and Toru Amaya

In the coordination chemistry of π bowls, there is an intriguing issue on the preference for metal binding to a concave surface versus a convex one. A convex binding has been found to be favorable so far, especially for corannulene [141–145].

The selective synthesis of the concave-bound complex [CpFe(sumanene)]PF$_6$ is achieved by ligand exchange of ferrocene with sumanene (Scheme 3.46) [146, 147]. The structure is confirmed in both solution and solid states. This is the first report for the selective synthesis of concave-bound π-bowl complexes (Fig. 3.34). The curved concave π surface serves as an η^6 ligand. The selectivity of the complexation is theoretically discussed [148]. The redox properties of the complex are investigated through electrochemical study. The complex exhibits the Fe(II)/Fe(I) reduction, which displays features of partial chemical reversibility, coupled to the fragmentation of the corresponding Fe(I) species to ferrocene [149].
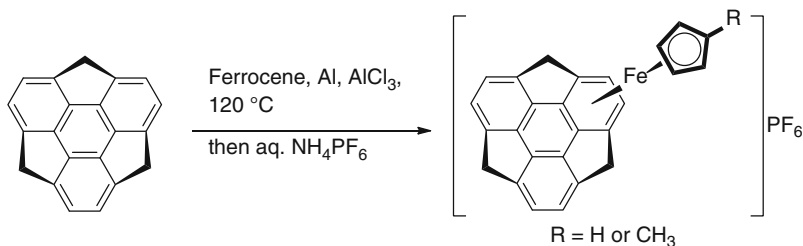
Scheme 3.46 Synthesis of [RCpFe(sumanene)]PF$_3$ (R = H or CH$_3$)
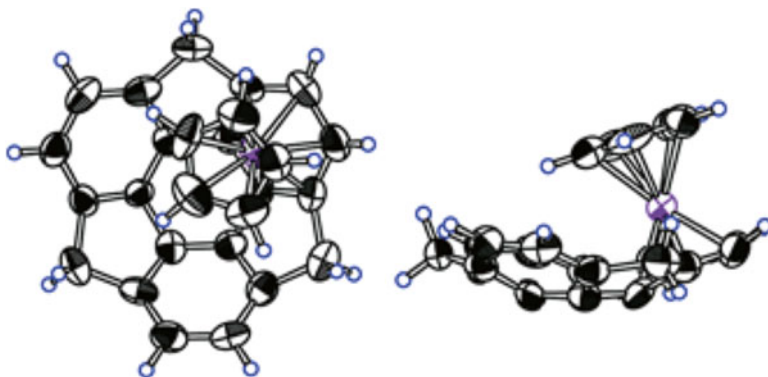
Fig. 3.34 Crystal structure of [CpFe(sumanene)]PF$_6$ (PF$_6$ ion is omitted for clarity)
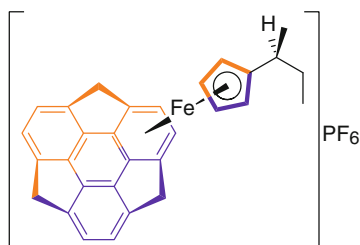
Fig. 3.35 Chiral π-bowl complex

The methyl-substituted complex [CH$_3$CpFe(sumanene)]PF$_6$ is also synthesized (Scheme 3.46) [150]. The complex shows the concave-binding of CH$_3$CpFe. The ^{1}H NMR experiments suggest that the methyl group is directed out of the bowl with a restricted rotation. Iron atom dynamics of CH$_3$CpFe ligated to a concave-face in sumanene is investigated using temperature-dependent Mössbauer effect spectroscopy [151]. CH$_3$CpFe in the sumanene complex is revealed to be bound more tightly than that in the corresponding fluorene complex.

Synthesis of an Fe(II) complex of sumanene having a Cp ligand with chiral *s*-butyl group attached is performed in a similar manner to the preparation of [CpFe(sumanene)]PF$_6$. The complex also shows a concave-face selective coordination in solution, in which the rotation of the Cp ring is restricted. Magnetic and optical desymmetrization in the sumanene ligand is found in the complex (Fig. 3.35) [150]. This is the first optical active complex with a π-bowl ligand.

[CpRu(sumanene)]PF$_6$ is synthesized in the similar manner [CpFe(sumanene)] PF$_6$. However, the resulting complex is a mixture of concave- and convex-binding of CpRu, where concave-binding is much preferable. The dynamic isomerization via bowl-to-bowl inversion between them is observed in solution (Scheme 3.47) [152]. The preference can be accounted for by the thermodynamic stability.
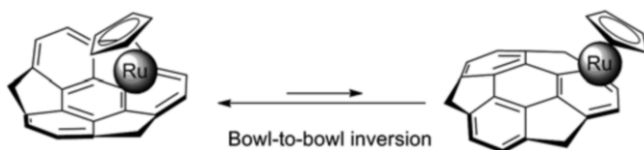
Scheme 3.47 Bowl-to-bowl inversion of [CpRu(sumanene)]PF$_6$

In π-bowl complexes, the metallocene-type complexes have been less studied so far despite their potential for catalyst application in addition to the unique structural properties. On the other hand, sumanenyl mono-, di- and trianions can be generated selectively by treatment with a strong base as shown in the Sect. 3.6 [125]. Such a cyclopentadienyl-like anion is considered to provide mono- and even multi-nuclear metallocene-type complexes. In this context, mono- and trinuclear sumanenyl zirconocene complexes Cp(sumanenyl)ZrCl$_2$, Cp*(sumanenyl)ZrCl$_2$, and (C$_{21}$H$_9$) [(Cp*)ZrCl$_2$]$_3$ are successfully synthesized (Scheme 3.48) [153]. In the mononuclear complexes, convex binding with disturbed η^5-bonding is confirmed in a solid state (Fig. 3.36) [153]. Figure 3.37 shows the DFT-optimized structure of the tri-convex η^5-binding complex (C, H, Cl: B3LYP/3-21G; Zr: B3LYP/LANL2DZ). As demonstrated in the trinuclear complex, the multi-benzylic anion of sumanenyl ligand offers a novel ligand for the multinuclear metallocenes.
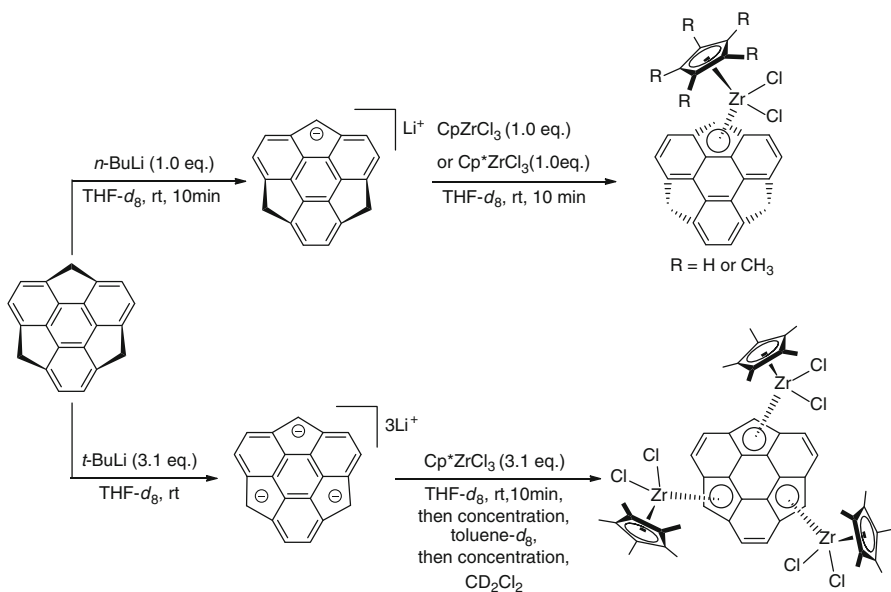
Scheme 3.48 Synthesis of mono- and trinuclear sumanenyl metallocenes
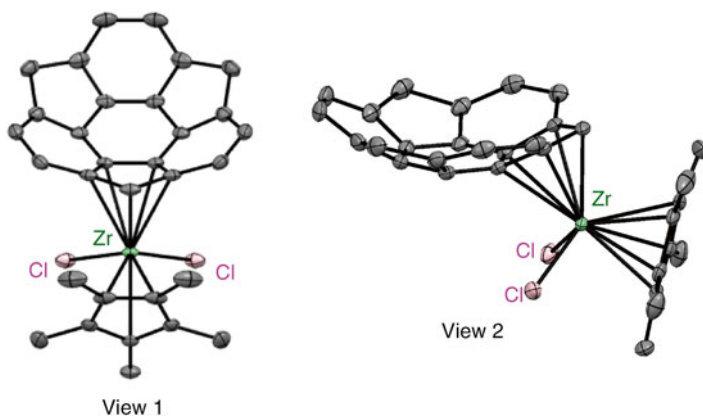
Fig. 3.36 Crystal structure of Cp*(sumanenyl)ZrCl$_2$
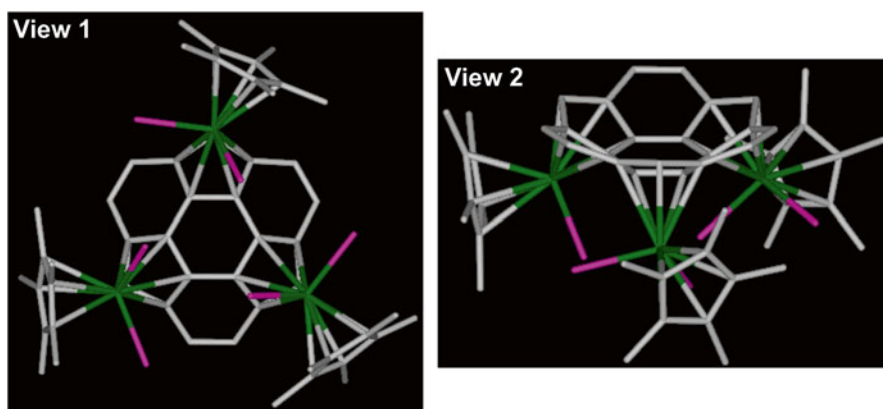
Fig. 3.37 DFT-optimized structure of the triconvex η^5-binding complex of (C$_{21}$H$_9$)[(Cp*)ZrCl$_2$]$_3$

References

1. M. Ameyama, M. Nonobe, E. Shinagawa, K. Matsushita, O. Adachi, Anal. Biochem. **151**, 263 (1985)
2. J.A. Duine, J. Frank, J.A. Jongejan, Adv. Enzymol. **59**, 169 (1987)
3. Y. Ohshiro, S. Itoh, K. Kurokawa, J. Kato, T. Hirao, T. Agawa, Tetrahedron Lett. **24**, 3465 (1983)
4. S. Itoh, N. Kato, Y. Ohshiro, T. Agawa, Tetrahedron Lett. **25**, 4753 (1984)
5. T. Hirao, T. Murakami, M. Ohno, Y. Ohshiro, Chem. Lett. 785 (1989)
6. J.E. Backvall, A. Gogoll, J. Chem. Soc. Chem. Commun., 1236 (1987)
7. J. Tsuji, M. Minato, Tetrahedron Lett. **28**, 3683 (1987)
8. J.E. Backvall, A.K. Awasthi, Z.D. Renko, J. Am. Chem. Soc. **109**, 4750 (1987)
9. T. Hirao, T. Murakami, M. Ohno, Y. Ohshiro, Chem. Lett. 299 (1991)
10. T. Moriuchi, T. Watanabe, I. Ikeda, A. Ogawa, T. Hirao, Eur. J. Inorg. Chem. 277 (2001)

11. T. Hirao, M. Ohno, Y. Ohshiro, Tetrahedron Lett. **31**, 6039 (1990)
12. L. Alcacer, *Conducting Polymers: Special Applications* (Reidel, Holland, 1987)
13. W.R. Salaneck, D.T. Clark, E.J. Samuelsen, *Science and Application of Conductive Polymers* (Adams Hilger, New York, 1990)
14. H. Shirakawa, Angew. Chem. Int. Ed. **40**, 2574 (2001)
15. A.G. MacDiarmid, Angew. Chem. Int. Ed. **40**, 2581 (2001)
16. A.J. Heeger, Angew. Chem. Int. Ed. **40**, 2591 (2001)
17. M. Higuchi, D. Imoda, T. Hirao, Macromolecules **29**, 8277 (1996)
18. T. Hirao, M. Higuchi, I. Ikeda, Y. Ohshiro, J. Chem. Soc. Chem. Commun., 194 (1993)
19. T. Hirao, M. Higuchi, Y. Ohshiro, I. Ikeda, Chem. Lett. 1889 (1993)
20. M. Higuchi, I. Ikeda, T. Hirao, J. Org. Chem. **62**, 1072 (1997)
21. T. Hirao, S. Fukuhara, J. Org. Chem. **63**, 7534 (1998)
22. T. Amaya, R. Suzuki, T. Hirao, Chem. Eur. J. **20**, 653 (2014)
23. T. Hirao, M. Higuchi, B. Hatano, I. Ikeda, Tetrahedron Lett. **36**, 5925 (1995)
24. M. Higuchi, S. Yamaguchi, T. Hirao, Synlett, 1213 (1996)
25. T. Hirao, M. Higuchi, S. Yamaguchi, Macromol. Symp. 131 (1998)
26. M.T.S. Ritonga, H. Sakurai, T. Hirao, Tetrahedron Lett. **43**, 9009 (2002)
27. H. Sakurai, M.T.S. Ritonga, H. Shibatani, T. Hirao, J. Org. Chem. **70**, 2754 (2005)
28. M.T.S. Ritonga, H. Shibatani, H. Sakurai, T. Moriuchi, T. Hirao, Heterocycles **68**, 829 (2006)
29. T. Amaya, Y. Abe, Y. Inada, T. Hirao, Tetrahedron Lett. **55**, 3976 (2014)
30. Y. Abe, T. Amaya, T. Hirao, Bull. Chem. Soc. Jpn. **87**, 1026 (2014)
31. T. Amaya, Y. Abe, Y. Inada, T. Hirao, Synth. Met. **195**, 137 (2014)
32. K. Saito, T. Hirao, Bull. Chem. Soc. Jpn. **75**, 1845 (2002)
33. T. Hirao, K. Saito, Tetrahedron Lett. **41**, 1413 (2000)
34. K. Saito, T. Hirao, Tetrahedron **58**, 7491 (2002)
35. T. Hirao, K. Saito, Synlett, 415 (2002)
36. T. Amaya, K. Mori, T. Hirao, Heterocycles **78**, 2729 (2009)
37. T. Amaya, Y. Shimizu, Y. Yakushi, Y. Nishina, T. Hirao, Tetrahedron Lett. **51**, 2416 (2010)
38. T. Amaya, T. Ueda, T. Hirao, Tetrahedron Lett. **51**, 3376 (2010)
39. T. Amaya, S. Koga, T. Hirao, Tetrahedron Lett. **50**, 1032 (2009)
40. T. Amaya, D. Saio, S. Koga, T. Hirao, Macromolecules **43**, 1175 (2010)
41. B.J. Holliday, T.M. Swager, Chem. Commun. **23** (2005)
42. M.O. Wolf, J. Inorg. Organomet. Polym. Mater. **16**, 189 (2006)
43. P. Nguyen, P. Gómez-Elipe, I. Manners, Chem. Rev. **99**, 1515 (1999)
44. W.-Y. Wong, C.-L. Ho, Coord. Chem. Rev. **250**, 2627 (2006)
45. T. Hirao, Coord. Chem. Rev. **226**, 81 (2002)
46. T. Hirao, Macromol. Symp. **186**, 75 (2002)
47. T. Hirao, *Redox Systems Under Nano-Space Control* (Springer, Heidelberg, 2006)
48. T. Amaya, T. Hirao, Synlett, 435 (2011)
49. T. Moriuchi, T. Hirao, Acc. Chem. Res. **45**, 347 (2012)
50. T. Moriuchi, S. Bandoh, Y. Miyaji, T. Hirao, J. Organomet. Chem. **599**, 135 (2000)
51. T. Moriuchi, M. Kamikawa, S. Bandoh, T. Hirao, Chem. Commun. 1476 (2002)
52. T. Hirao, T. Moriuchi, S. Mikami, I. Ikeda, Y. Ohshiro, Tetrahedron Lett. **34**, 1031 (1993)
53. T. Hirao, T. Moriuchi, T. Ishikawa, K. Nishimura, S. Mikami, Y. Ohshiro, I. Ikeda, J. Mol. Catal. A Chem. **113**, 117 (1996)
54. T. Hirao, S. Yamaguchi, S. Fukuhara, Tetrahedron Lett. **40**, 3009 (1999)
55. T. Hirao, Y. Otomaru, Y. Inoue, T. Moriuchi, T. Ogata, Y. Sato, Synth. Met. **156**, 1378 (2006)
56. Y. Wei, C. Yang, T. Ding, Tetrahedron Lett. **37**, 731 (1996)
57. T. Moriuchi, S. Bandoh, M. Miyaishi, T. Hirao, Eur. J. Inorg. Chem. 651 (2001)
58. T. Moriuchi, M. Miyaishi, T. Hirao, Angew. Chem. Int. Ed. **40**, 3042 (2001)
59. L.A.P. Kane-Maguire, G.G. Wallace, Chem. Soc. Rev. **39**, 2545 (2010)
60. X. Shen, T. Moriuchi, T. Hirao, Tetrahedron Lett. **45**, 4733 (2004)
61. T. Moriuchi, X. Shen, T. Hirao, Tetrahedron **62**, 12237 (2006)
62. T. Hirao, Chem. Rev. **97**, 2707 (1997)

63. T. Hirao, S. Fukuhara, Y. Otomaru, T. Moriuchi, Synth. Met. **123**, 373 (2001)
64. P.R. Auburn, A.B.P. Lever, Inorg. Chem. **29**, 2551 (1990)
65. L.F. Joulié, E. Schatz, M.D. Ward, F. Weber, L.J. Yellowlees, J. Chem. Soc. Dalton Trans., 799 (1994)
66. T.E. Keyes, R.J. Forster, P.M. Jayaweera, C.G. Coates, J.J. McGarvey, J.G. Vos, Inorg. Chem. **37**, 5925 (1998)
67. T. Moriuchi, Y. Takagi, T. Hirao, Eur. J. Inorg. Chem. 3877 (2008)
68. T. Moriuchi, X. Shen, K. Saito, S. Bandoh, T. Hirao, Bull. Chem. Soc. Jpn. **76**, 595 (2003)
69. T. Hirao, J. Shiori, N. Okahata, Bull. Chem. Soc. Jpn. **77**, 1763 (2004)
70. T. Hirao, K. Iida, Chem. Commun. 431 (2001)
71. X. Shen, T. Moriuchi, T. Hirao, Tetrahedron Lett. **44**, 7711 (2003)
72. T. Moriuchi, J. Shiori, T. Hirao, Tetrahedron Lett. **48**, 5970 (2007)
73. A. Fihri, M. Bouhrara, B. Nekoueishahraki, J.-M. Basset, V. Polshettiwar, Chem. Soc. Rev. **40**, 181 (2011)
74. A. Balanta, C. Godard, C. Claver, Chem. Soc. Rev. **40**, 4973 (2011)
75. T. Amaya, D. Saio, T. Hirao, Macromol. Symp. **270**, 88 (2008)
76. T. Amaya, D. Saio, T. Hirao, Tetrahedron Lett. **48**, 2729 (2007)
77. D. Saio, T. Amaya, T. Hirao, J. Inorg. Organomet. Polym. Mater. **19**, 79 (2009)
78. T. Isaji, T. Amaya, Y. Inada, M. Abe, T. Hirao, Bull. Chem. Soc. Jpn. **87**, 1130 (2014)
79. T. Amaya, Y. Nishina, D. Saio, T. Hirao, Chem. Lett. **37**, 68 (2008)
80. D. Saio, T. Amaya, T. Hirao, Adv. Synth. Catal. **352**, 2177 (2010)
81. T. Amaya, T. Ito, Y. Inada, D. Saio, T. Hirao, Tetrahedron Lett. **53**, 6144 (2012)
82. T. Amaya, T. Ito, T. Hirao, Tetrahedron Lett. **54**, 2409 (2013)
83. T. Amaya, T. Ito, T. Hirao, Heterocycles **86**, 927 (2012)
84. T.R. Cundari, Chem. Rev. **100**, 807 (2000)
85. D.E. Wigley, in *Progress in Inorganic Chemistry*, ed. by K.D. Karlin, vol. 42 (Wiley-Interscience, New York, 1994), pp. 239–482
86. W.A. Nugent, J.M. Mayer, *Metal-Ligand Multiple Bonds* (Wiley-Interscience, New York, 1998)
87. T. Moriuchi, T. Hirao, Pure Appl. Chem. **81**, 1187 (2009)
88. T. Moriuchi, T. Hirao, Coord. Chem. Rev. **255**, 2371 (2011)
89. D.D. Devore, J.D. Lichtenhan, F. Takusagawa, E.A. Maatta, J. Am. Chem. Soc. **109**, 7408 (1987)
90. C.V.K. Sharma, G.R. Desiraju, in *The Crystal as a Supramolecular Entity*, ed. by G.R. Desiraju. Perspectives in Supramolecular Chemistry (Wiley, Chichester, 1996)
91. D. Braga, F. Grepioni, G.R. Desiraju, Chem. Rev. **98**, 1375 (1998)
92. V. Balzani, A. Credi, F.M. Raymo, J.F. Stoddart, Angew. Chem. Int. Ed. **39**, 3348 (2000)
93. G.F. Swiegers, T.J. Malefetse, Chem. Rev. **100**, 3483 (2000)
94. S. Leininger, B. Olenyuk, P.J. Stang, Chem. Rev. **100**, 853 (2000)
95. R. Ziessel, Coord. Chem. Rev. **216–217**, 195 (2001)
96. W.-Y. Sun, M. Yoshizawa, T. Kusukawa, M. Fujita, Curr. Opin. Chem. Biol. **6**, 757 (2002)
97. Y. Kobuke, Eur. J. Inorg. Chem. 2333 (2006)
98. S. Tanase, J. Reedijk, Coord. Chem. Rev. **250**, 2501 (2006)
99. A.W. Kleij, J.N.H. Reek, Chem. Eur. J. **12**, 4218 (2006)
100. J. Cookson, P.D. Beer, Dalton Trans., 1459 (2007)
101. T. Moriuchi, K. Ishino, T. Beppu, M. Nishina, T. Hirao, Inorg. Chem. **47**, 7638 (2008)
102. A.W. Addison, T.N. Rao, J. Reedijk, J. van Rijn, G.C. Verschoor, J. Chem. Soc. Dalton Trans., 1349 (1984)
103. M. Nishina, T. Moriuchi, T. Hirao, Dalton Trans. **39**, 9936 (2010)
104. T. Moriuchi, M. Nishina, T. Hirao, Angew. Chem. Int. Ed. **49**, 83 (2010)
105. M. Nishina, T. Moriuchi, T. Hirao, Bull. Chem. Soc. Jpn. **85**, 606 (2012)
106. D.C. Crans, H. Chen, O.P. Anderson, M.M. Miller, J. Am. Chem. Soc. **115**, 6769 (1993)
107. T. Moriuchi, K. Ishino, T. Hirao, Chem. Lett. **36**, 1486 (2007)
108. T. Moriuchi, T. Beppu, K. Ishino, M. Nishina, T. Hirao, Eur. J. Inorg. Chem. 1969 (2008)
109. D. Sutton, Chem. Rev. **93**, 995 (1993)

110. M. Hidai, Y. Mizobe, Chem. Rev. **95**, 1115 (1995)
111. R.L. Richards, Coord. Chem. Rev. **154**, 83 (1996)
112. B.A. MacKay, M.D. Fryzuk, Chem. Rev. **104**, 385 (2004)
113. R.R. Schrock, Acc. Chem. Res. **38**, 955 (2005)
114. T. Moriuchi, K. Ikeuchi, T. Hirao, Dalton Trans. **42**, 11824 (2013)
115. R.A. Henderson, Z. Janas, L.B. Jerzykiewicz, R.L. Richards, P. Sobota, Inorg. Chim. Acta **285**, 178 (1999)
116. L.T. Scott, H.E. Bronstein, D.V. Preda, R.B.M. Ansems, M.S. Bratcher, S. Hagen, Pure Appl. Chem. **71**, 209 (1999)
117. P.W. Rabideau, A.H. Abdourazak, H.E. Folsom, Z. Marcinow, A. Sygula, R. Sygula, J. Am. Chem. Soc. **116**, 7891 (1994)
118. Y.-T. Wu, J.S. Siegel, Chem. Rev. **106**, 4843 (2006)
119. V.M. Tsefrikas, L.T. Scott, Chem. Rev. **106**, 4868 (2006)
120. S. Higashibayashi, H. Sakurai, Chem. Lett. **40**, 122 (2011)
121. G. Mehta, S.R. Shah, K. Ravikumar, J. Chem. Soc. Chem. Commun., 1006 (1993)
122. T. Amaya, T. Hirao, Chem. Commun. **47**, 10524 (2011)
123. T. Hirao, T. Amaya, in *Fragments of Fullerenes and Carbon Nanotubes: Designed Synthesis, Unusual Reactions, and Coordination Chemistry*, ed. by M.A. Petrukhina, L.T. Scott (Wiley, New Jersey, 2011), Chap. 7, pp. 187–203
124. H. Sakurai, T. Daiko, T. Hirao, Science **301**, 1878 (2003)
125. H. Sakurai, T. Daiko, H. Sakane, T. Amaya, T. Hirao, J. Am. Chem. Soc. **127**, 11580 (2005)
126. M.D. Halling, A.M. Orendt, M. Strohmeier, M.S. Solum, V.M. Tsefrikas, T. Hirao, L.T. Scott, R.J. Pugmire, D.M. Grant, Phys. Chem. Chem. Phys. **12**, 7934 (2010)
127. T. Amaya, T. Hirao, Pure Appl. Chem. **84**, 1089 (2012)
128. T. Amaya, H. Sakane, T. Muneishi, T. Hirao, Chem. Commun. 765 (2008)
129. T. Amaya, T. Nakata, H. Sakane, T. Hirao, Pure Appl. Chem. **82**, 969 (2010)
130. S. Seki, A. Saeki, T. Sakurai, D. Sakamaki, Phys. Chem. Chem. Phys. **16**, 11093 (2014)
131. T. Amaya, S. Seki, T. Moriuchi, K. Nakamoto, T. Nakata, H. Sakane, A. Saeki, S. Tagawa, T. Hirao, J. Am. Chem. Soc. **131**, 408 (2009)
132. J. Robertson, Mater. Sci. Eng. R **37**, 129 (2002)
133. H. Wang, T. Maiyalagan, X. Wang, ACS Catal. **2**, 781 (2012)
134. Y. Inada, T. Amaya, Y. Shimizu, A. Saeki, T. Otsuka, R. Tsuji, S. Seki, T. Hirao, Chem. Asian. J. **8**, 2569 (2013)
135. T. Amaya, Y. Inada, Y. Shimizu, A. Saeki, R. Tsuji, S. Seki, T. Hirao, Chem. Asian. J. **9**, 2568 (2014)
136. T. Amaya, K. Mori, H.L. Wu, S. Ishida, J. Nakamura, K. Murata, T. Hirao, Chem. Commun. 1902 (2007)
137. T. Amaya, T. Nakata, T. Hirao, J. Am. Chem. Soc. **131**, 10810 (2009)
138. T. Amaya, M. Hifumi, M. Okada, Y. Shimizu, T. Moriuchi, K. Segawa, Y. Ando, T. Hirao, J. Org. Chem. **76**, 8049 (2011)
139. T. Amaya, K. Kobayashi, T. Hirao, Asian J. Org. Chem. **2**, 642 (2013)
140. T. Amaya, T. Ito, T. Hirao, Eur. J. Org. Chem. 3531 (2014)
141. J.S. Siegel, K.K. Baldridge, A. Linden, R. Dorta, J. Am. Chem. Soc. **128**, 10644 (2006)
142. M.A. Petrukhina, Y. Sevryugina, A.Y. Rogachev, E.A. Jackson, L.T. Scott, Organometallics **25**, 5492 (2006)
143. M.A. Petrukhina, Y. Sevryugina, A.Y. Rogachev, E.A. Jackson, L.T. Scott, Angew. Chem. Int. Ed. **45**, 7208 (2006)
144. B. Zhu, A. Ellern, A. Sygula, R. Sygula, R.J. Angelici, Organometallics **26**, 1721 (2007)
145. M.A. Petrukhina, Coord. Chem. Rev. **251**, 1690 (2007)
146. T. Amaya, H. Sakane, T. Hirao, Angew. Chem. Int. Ed. **46**, 8376 (2007)
147. M.A. Petrukhina, Angew. Chem. Int. Ed. **47**, 1550 (2008)
148. M. Okumura, Y. Nakanishi, K. Kinoshita, S. Yamada, Y. Kitagawa, T. Kawakami, S. Yamanaka, T. Amaya, T. Hirao, Int. J. Quantum Chem. **113**, 437 (2013)

149. P. Zanello, S. Fedi, F.F. de Biani, G. Giorgi, T. Amaya, H. Sakane, T. Hirao, Dalton Trans., 9192 (2009)
150. H. Sakane, T. Amaya, T. Moriuchi, T. Hirao, Angew. Chem. Int. Ed. **48**, 1640 (2009)
151. T. Hirao, T. Amaya, T. Moriuchi, M. Hifumi, Y. Takahashi, I. Nowik, R.H. Herber, J. Organomet. Chem. **696**, 3895 (2011)
152. T. Amaya, W.-Z. Wang, H. Sakane, T. Moriuchi, T. Hirao, Angew. Chem. Int. Ed. **49**, 403 (2010)
153. T. Amaya, Y. Takahashi, T. Moriuchi, T. Hirao, J. Am. Chem. Soc. **136**, 12794 (2014)

Chapter 4
Bioconjugates to Induce Chirality Organization

Toshikazu Hirao, Toshiyuki Moriuchi, and Annika Groß

Abstract A variety of ferrocene-dipeptide conjugates as bioorganometallics are designed to induce chirality-organized structures of peptides, wherein the ferrocene serves as a reliable organometallic scaffold with a central reverse-turn unit. The introduction of histidyl groups into the 2,6-pyridinedicarboxamide scaffold allows induction of the chiral helicity, creating the left- or right-handed helical assembly through continuous intermolecular hydrogen bonds in a solid state. Symmetrical introduction of two dipeptide chains into a urea molecular scaffold is performed to induce the formation of the chiral hydrogen-bonded duplex, wherein each hydrogen-bonded duplex is connected by continuous intermolecular hydrogen bonds to form a double helix-like arrangement. The chirality organization of polyaniline-unit molecules is achieved by the introduction of the amino acid moiety through intramolecular hydrogen bonds, which play an important role in the stabilization of the chirality-organized redox species. The luminescent properties depend on the redox state of the π-conjugated moiety of the phenylenediamine derivatives. The control of the emission properties of emissive compounds is performed by using ionic interaction of polypeptide, poly-L-lysine and poly-L-glutamic acid, as a polymeric scaffold. A guanosine-based organometallic compounds serve as a reliable G-octamer scaffold via self-assembly, exhibiting a switchable emission based on metal-metal interaction.

T. Hirao (✉) • T. Moriuchi
Department of Applied Chemistry, Graduate School of Engineering, Osaka University, Yamada-oka, Suita, Osaka 565-0871, Japan
e-mail: hirao@chem.eng.osaka-u.ac.jp; moriuchi@chem.eng.osaka-u.ac.jp

A. Groß
Institute of Medicinal and Pharmaceutical Chemistry, Technische Universität Braunschweig, Beethovenstr. 55, 38106 Braunschweig, Germany
e-mail: Annika.Gross@tu-bs.de

recognition • Molecular scaffold • Nucleobase • Palladium complex • Phenylenediamine
• Pincer complex • Platinum complex • Polyaniline • Polypeptide • Pyrene • Pyridine
• Quinonediimine • Redox-switching • Ruthenium complex • Secondary structure
• Self-assembly • Urea • π-Conjugated molecule • π–π Interaction

Abbreviations

A	Adenine
Ala	Alanine
bpy	2,2′-Bipyridine
C	Cytosine
CD	Circular dichroism
Cp	Cyclopentadienyl
dba	Dibenzylideneacetone
DDA	Didodecyldimethylammonium
DNA	Deoxyribonucleic acid
ESR	Electron spin resonance
Et	Ethyl
ET	Energy transfer
Fc	Ferrocene
G	Guanine
Glu	Glutamic acid
His	Histamine
ICD	Induced circular dichroism
K_a	Association constant
LLCT	Ligand-to-ligand charge transfer
Lys	Lysine
Me	Methyl
MeCN	Acetonitrile
MLCT	Metal-to-ligand charge transfer
MMLCT	Metal-metal-to-ligand charge transfer
OTf	Trifluoromethanesulfonate
P(Glu)	Poly-L-glutamic acid
P(Lys)	Poly-L-lysine
PAA	Poly(allylamine hydrochloride)
Ph	Phenyl
ppy	2-Phenylpyridine
ppyFF	2-(2,4-Difluorophenyl)pyridine
Pro	Proline
Py	Pyridine
T	Thymine
tpy	2,2′:6′,2″-Terpyridine

4.1 1,1′-Disubstituted Ferrocene-Peptide Bioconjugates

Toshikazu Hirao, Toshiyuki Moriuchi, and Annika Groß

Control of molecular self-assembly is of importance for the development of functional materials [1–3]. Highly-organized molecular assemblies are created in proteins to fulfill unique functions as observed in enzymes, receptors, etc. Hydrogen bonding is a key factor in regulating the aggregated structures and function of biological systems. Secondary structures of proteins such as α-helices, β-sheets, and β- or γ-turns play an important role in protein folding, which is mostly stabilized by hydrogen bond and hydrophobic interaction of side chains [4, 5]. Considerable efforts have been devoted to design secondary structure mimics composed of short peptides for fundamental insight into the factors affecting the protein folding and stability, and for rational design of pharmacologically useful compounds. Specific patterns of complementary intra- and intermolecular hydrogen bonds are formed in such secondary structures. Regulation of hydrogen bonding [6] has attracted much attention in the design of molecular assemblies by virtue of its directionality and specificity [7–9]. The tunability and reversibility of hydrogen bond is also of fundamental importance in the physical properties of molecular assemblies. The utilization of self-assembling properties of peptides, which possess hydrogen bonding sites and chiral centers, is considered to be a convenient approach to highly-organized molecular assemblies.

The research field of bioorganometallic chemistry, which is a hybrid area between biology and organometallic chemistry, has gained growing interest. Conjugation of organometallic compounds with biomolecules such as amino acids, peptides, and nucleic acids is envisioned to provide novel systems depending on both properties. In these conjugates, the organometallic part can serve as a molecular scaffold, a chromophore, a sensitive probe, a biological marker, a redox-active site, a catalytic active site, etc. Considerable efforts have focused on designing bioorganometallic conjugates composed of organometallic compounds and biomolecules ([10–14], and references therein). Ferrocene (Fc), which is one of the most stable organometallic compounds and the most useful one among metallocenes, has attracted much attention in their application to materials due to a reversible redox couple and two rotatory coplanar cyclopentadienyl (Cp) rings [15]. The inter-ring spacing of about 3.3 Å is appropriate for hydrogen bonding interaction between introduced peptide strands on the two Cp rings as observed in β-sheets. The utilization of a ferrocene unit as an organometallic scaffold with a central reverse-turn unit is considered to be one strategy to study the hydrogen bonding ability of introduced peptide strands. As a subgroup of ferrocene compounds, ferrocene-peptides have a variety of applications in medicinal chemistry. Ferrocene itself is a well known component in bioorganometallic chemistry due to its unique properties such as its exceptional stability, lipophilicity, redox properties and ease to functionalize. Therefore, several commercially available drugs have been functionalized with ferrocene such as tamoxifen [16], chloroquine [17] and platensimycin [18]. Also ferrocene peptides have been tested for therapeutical applications mostly as

anticancer or anti-infective agents. To keep the peptides biological activity is also important for ferrocene functionalized antibacterial peptides. Multiresistant bacteria becoming more and more widespread [19], therefore new compounds with unusual mode of action or targets are necessary. Ferrocene peptides might be interesting candidates for this purpose, since ferrocene is envisioned to enhance and modify the specificity and activity of the peptides [20]. Another important field of ferrocene peptides is anticancer therapy. Ferrocene presents itself as an untoxic compound whereas its oxidized form ferrocifen showed already in the 1980th its antitumor activity [21]. Thereon, Neuse and coworkers connected the ferrocene moieties to water-soluble polymers and discovered that this ferrocene conjugates exhibit high antitumor activities against the human HeLa cervix epithelia carcinoma [22]. In this section, an outline of dipeptide-induced chirality organization by using ferrocene scaffolds is described.

Conformational enantiomers based on the torsional twist about the Cp(centroid)-Fe-Cp(centroid) axis, *P*- and *M*-helical arrangements, are possible in the case of the 1,1′-disubstituted ferrocene as depicted in Fig. 4.1 [15, 23]. Conformational enantiomers can interconvert with ease due to the low barrier of Cp ring twisting. The introduction of peptides into a ferrocene scaffold is envisaged to induce conformational enantiomerization by restriction of the torsional twist through the formation of intramolecular interchain hydrogen bond. The single-crystal X-ray structure determination of the ferrocene-peptide bioconjugate **1** bearing the -L-Ala-L-Pro-OEt dipeptide chains confirms the "Herrick" pattern of intramolecular interchain antiparallel *β*-sheet-like hydrogen bonding between CO (Ala) and NH (Ala of another chain) of each dipeptide chain to induce the chirality-organized structure (Fig. 4.2a) [24–26]. The ferrocenoyl moiety of **1** adopts the *P*-helical arrangement. The crystal structure of the ferrocene-peptide bioconjugate **2** composed of the corresponding D-dipeptide chains (-D-Ala-D-Pro-OEt) reveals the *M*-helical arrangement of the ferrocenoyl moiety (Fig. 4.2b). The molecular structures of **1** and **2** are in a good mirror image relationship, indicating conformational enantiomers present.
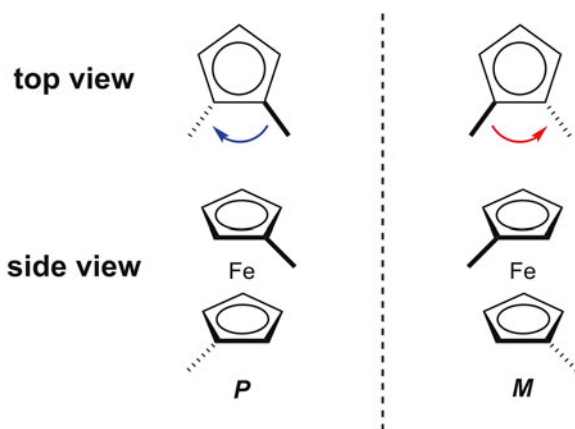
Fig. 4.1 Enantiomorphous conformations of 1,1'-disubstituted ferrocene
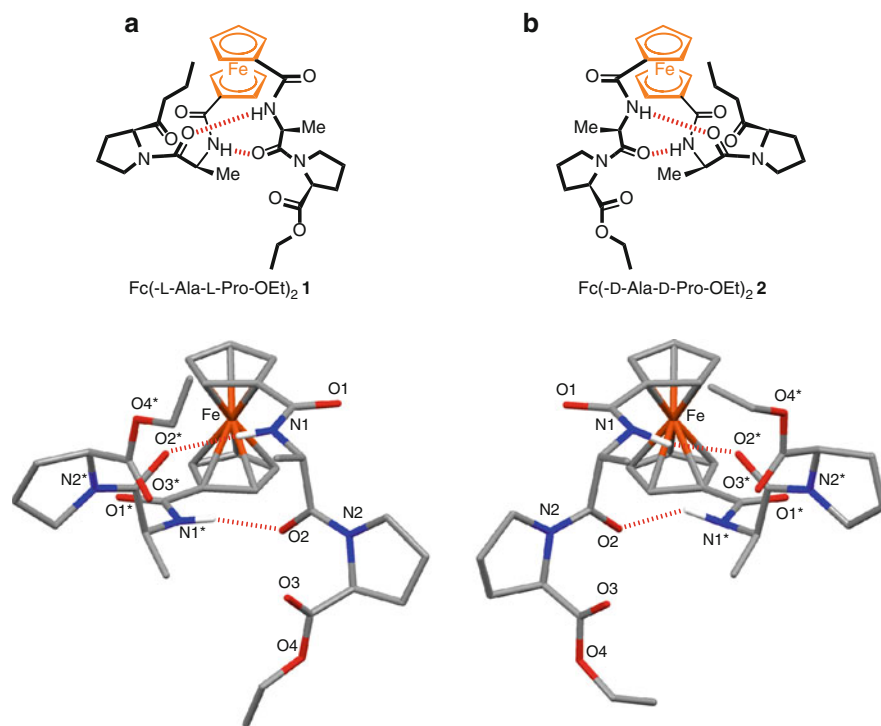
Fig. 4.2 Crystal structures of (**a**) **1** and (**b**) **2**

As a result, the introduction of the chiral dipeptide chains into the ferrocene induces the chirality organization by restriction of the torsional twist through the formation of the intramolecular interchain hydrogen bonds [26].

Circular dichroism (CD) spectrometry is a powerful tool to determine an ordered structure in solution. The ferrocene-dipeptide bioconjugate **1** exhibits a positive Cotton effect at the absorbance region of the ferrocenoyl moiety (Fig. 4.3), which indicates the *P*-helical arrangement of the ferrocenoyl moiety. The mirror image of the signals was obtained in the CD spectrum of **2**, indicating the *M*-helical arrangement of the ferrocenoyl moiety based on the chirality-organized structure through the intramolecular interchain hydrogen bonding [26].

The ferrocene-dipeptide bioconjugate **3** bearing dipeptide chains of the homochiral sequence (-L-Ala-L-Pro-NH-2-Py) is characterized by the formation of the intramolecular interchain antiparallel *β*-sheet-like hydrogen bond between CO (Ala) and NH (Ala of another chain) of each dipeptide chain to induce the chirality-organized structure (Fig. 4.4) [27]. Configuration and sequence of amino acids are key factors for constructing chirality-organized bio-inspired systems. The crystal structure of the ferrocene-dipeptide bioconjugate **4** bearing dipeptide chains of the heterochiral sequence (-L-Ala-D-Pro-NH-2-Py) reveals the formation of the intramolecular interchain antiparallel *β*-sheet-like hydrogen bonds as observed in **1** to induce the chirality-
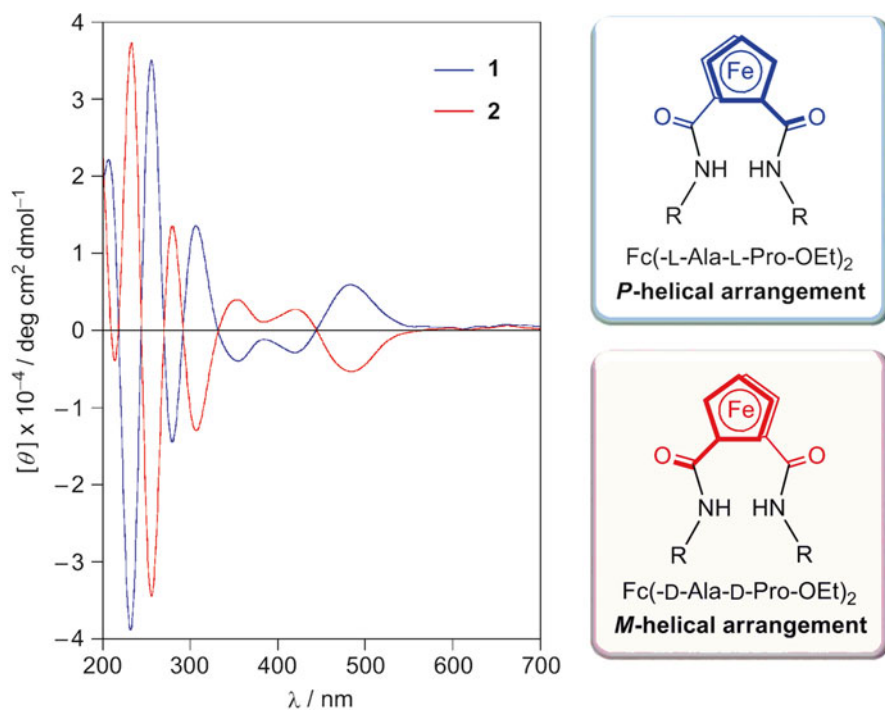
Fig. 4.3 CD spectra of **1** and **2** in MeCN (1.0×10^{-4} M)

Fc(-L-Ala-L-Pro-NH-2-Py)$_2$ **3**
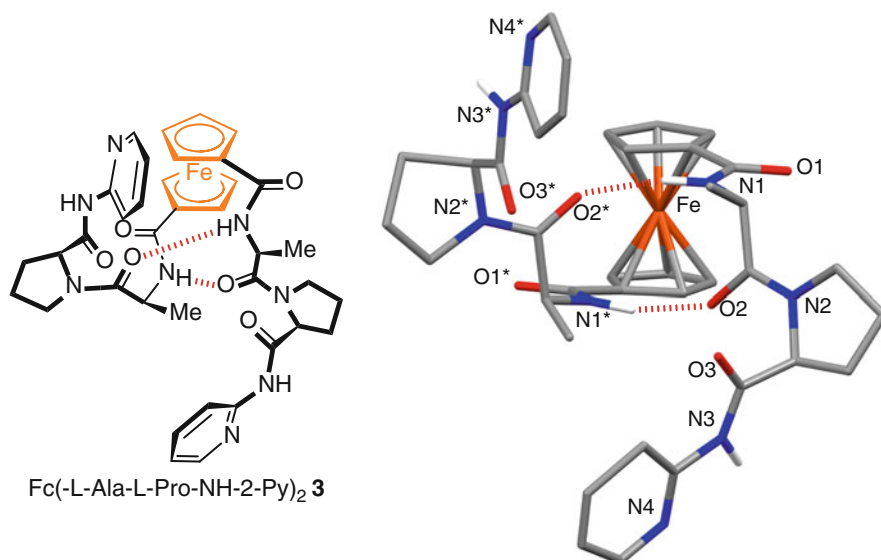
Fig. 4.4 Crystal structure of **3**
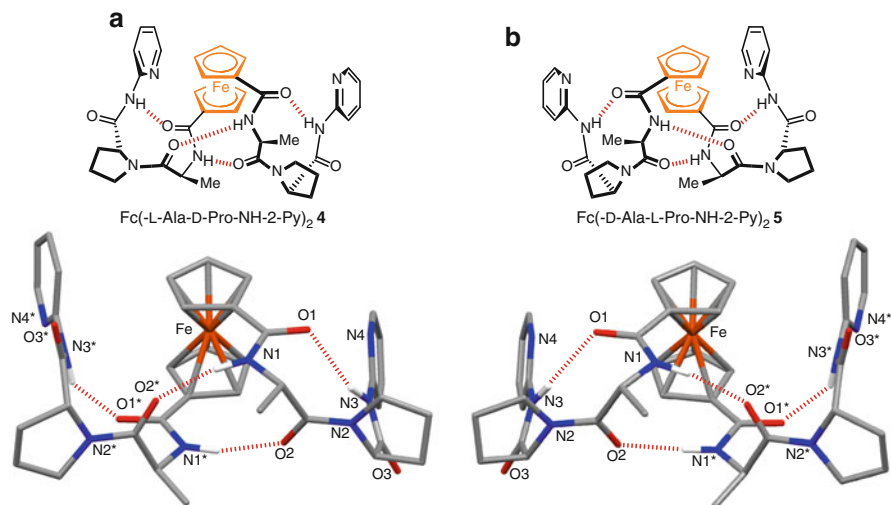
Fig. 4.5 Crystal structures of (**a**) **4** and (**b**) **5**

organized structure (Fig. 4.5a), in which the *P*-helical arrangement of the ferrocenoyl moiety is formed [28, 29]. Also, NH adjacent to the pyridyl moiety participates in the intramolecular hydrogen bonding with CO adjacent to the ferrocene unit of the same dipeptide chain, creating a type II *β*-turn-like structure in each dipeptide chain. The combination of the ferrocene scaffold as a central reverse-turn unit with the L-Ala-D-Pro hetrochiral dipeptide sequence permits the simultaneous formation of the artificially regulated antiparallel *β*-sheet-like and type II *β*-turn-like structures. The crystal structure of the ferrocene-peptide bioconjugate **5** composed of the D-Ala-L-Pro-NH-2-Py dipeptide chains confirms the *M* helical arrangement of the ferrocenoyl moiety as shown in Fig. 4.5b. The *P*-helical arrangement of the ferrocenoyl moiety appears to be controlled by the configuration of the alanyl α-carbon atom [30, 31].

The crystal structure of the ferrocene-peptide bioconjugate **6** bearing dipeptide chains of the homochiral sequence (-L-Pro-L-Ala-NH-2-Py) is characterized by the formation of an inverse *γ*-turn-like structure in each dipeptide chain through intramolecular hydrogen bonding between the NH adjacent to the pyridyl moiety and CO (Pro) of the same dipeptide chain, wherein the intramolecular interchain antiparallel *β*-sheet-like hydrogen bonding between CO adjacent to the ferrocene unit and the NH of the Ala attached to the opposite dipeptide chain are also formed (Fig. 4.6a) [32]. The conjugation of the ferrocene scaffold with the L-Pro-L-Ala homochiral sequence permits the simultaneous formation of the artificial inverse *γ*-turn-like and antiparallel *β*-sheet-like structures. The diastereomeric dipeptide configurations induce different self-assembling properties. The intramolecular interchain antiparallel *β*-sheet-like hydrogen bonds are formed between CO adjacent to the ferrocene unit and the NH of the Ala attached to the opposite dipeptide chain in the crystal structure of the ferrocene **7** bearing L-Pro-D-Ala-NH-2-Py dipeptide chains as shown in Fig. 4.6b [32].
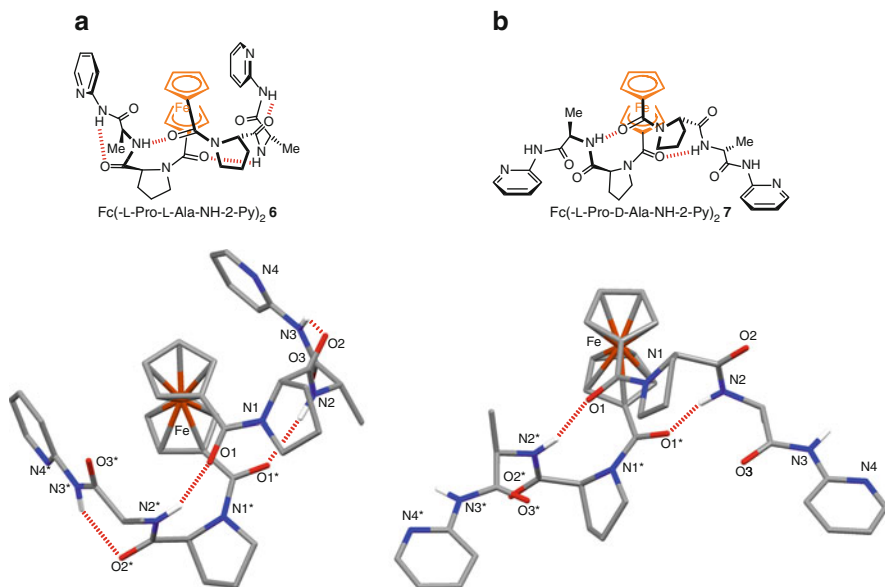
Fig. 4.6 Crystal structures of (**a**) **6** and (**b**) **7**

Utilization of self-assembling properties of amino acids as observed in proteins, which are organized into well-organized three-dimensional structures, is considered to be a useful strategy to the desired receptors for molecular recognition. In the ferrocene-peptide bioconjugate **8** bearing the -L-Ala-L-Pro-NH-2-PyMe dipeptide chains, the two amido pyridyl moieties as hydrogen bonding sites are well regulated for binding of dicarboxylic acids by the chirality organization through two intramolecular hydrogen bonds (Scheme 4.1) [33, 34]. In fact, the ferrocene-peptide bioconjugate **8** forms a 1:1 complex with a series of dicarboxylic acids **9**, wherein a most highest association constant is observed with adipic acid (**9c**, $K_a = 2.1 \times 10^4$ M^{-1}, Scheme 4.1). The binding sites of **8** can discriminate the size of dicarboxylic acids. The chirality-organized binding sites of **8** is also capable of discriminating the chirality of guest molecules. Benzoyl-L-glutamic acid (**9f**, $K_a = 5.5 \times 10^3$ M^{-1}) is bound approximately fifteen times more tightly to **8** than benzoyl-D-glutamic acid (**9g**, $K_a = 3.7 \times 10^2$ M^{-1}).

The chirality-organized ferrocene-peptide bioconjugate **3** bearing dipeptide chains of the homochiral sequence (-L-Ala-L-Pro-NH-2-Py) through two intramolecular interchain hydrogen bonds forms the 1:1 *trans*-palladium complex **10** with PdCl$_2$(MeCN)$_2$ to stabilize the conformational regulation in both solution and solid states (Fig. 4.7) [27]. The single-crystal X-ray structure determination of **10** confirms the pseudo-helical conformation through palladium coordination and chirality organization based on the preservation of the intramolecular interchain hydrogen bonds (Fig. 4.7) [27].
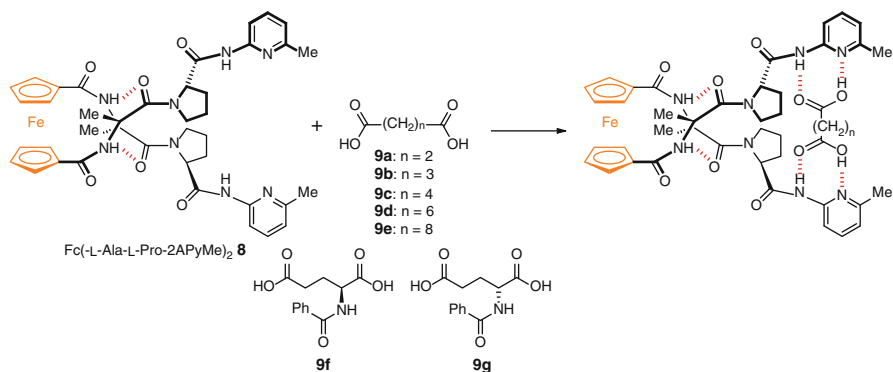
Scheme 4.1 Binding of dicarboxylic acid to the ferrocene-peptide bioconjugate **8**
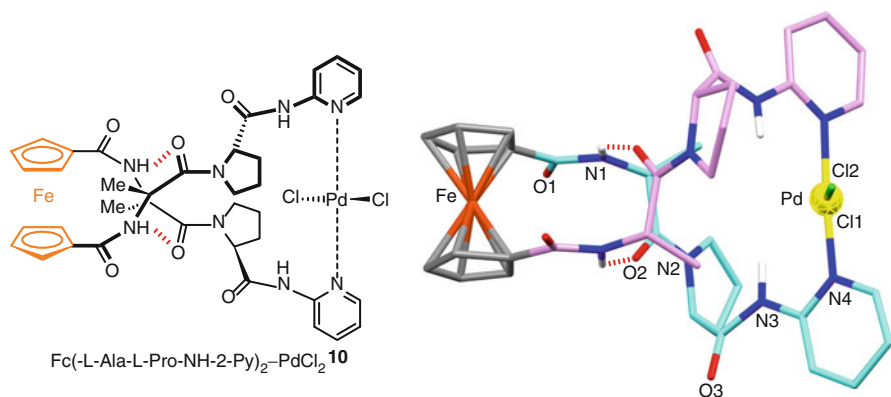
Fig. 4.7 Crystal structure of the 1:1 *trans*-palladium complex **10**

4.2 Monosubstituted Ferrocene-Peptide Bioconjugates

Toshikazu Hirao and Toshiyuki Moriuchi

In the case of ferrocene-peptide bioconjugates bearing only one peptide chain, a network of intermolecular hydrogen bonds is expected to be formed in a solid state. In fact, the ferrocene-peptide bioconjugate **11** bearing one dipeptide chain of the homochiral sequence (-L-Ala-L-Pro-OEt) exhibits intermolecular hydrogen bonding between CO (Ala) and the NH of the Ala attached to another molecule, wherein two independent molecules exist in an asymmetric unit and are connected alternately to form an intermolecular hydrogen bonding network, creating a left-handed helically ordered molecular arrangement (Fig. 4.8a) [25]. An antiparallel hydrogen bonding network is formed in a packing structure of the ferrocene-peptide bioconjugate **12**

a

Fc(-L-Ala-L-Pro-OEt)₁ **11**

b

Fc(-L-Ala-D-Pro-NH-2-Py)₁ **13**

c

Fc(-D-Ala-L-Pro-NH-2-Py)₁ **14**
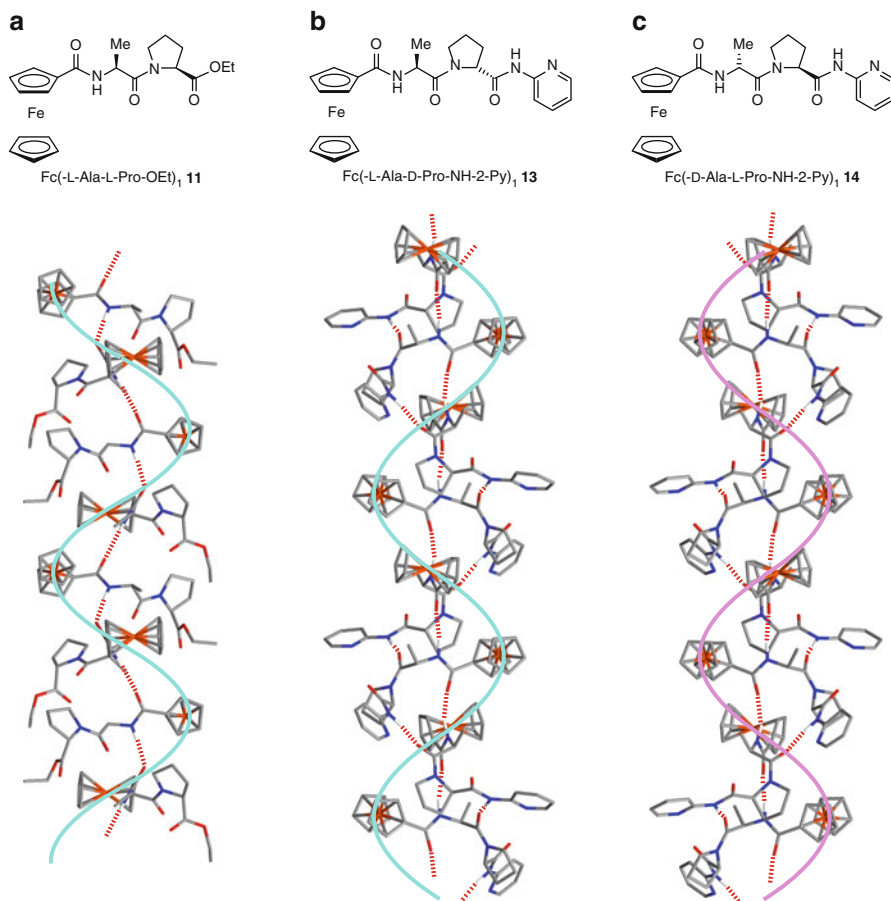
Fig. 4.8 A portion of a layer containing the helical assembly of crystal packing of (**a**) **11**, (**b**) **13**, and (**c**) **14**

bearing one dipeptide chain of the homochiral sequence (-L-Ala-L-Pro-NH-2-Py), wherein each molecule is connected to two neighboring molecules by NH (Ala)/N (pyridine of another molecule) and NH (adjacent to pyridine unit of another molecule)/O (Ala) intermolecular hydrogen bonds (Fig. 4.9) [35]. In contrast, a left-handed helically ordered molecular arrangement through a network of intermolecular hydrogen bonds is created in the ferrocene-peptide bioconjugate **13** bearing one dipeptide chain of the heterochiral sequence (-L-Ala-D-Pro-NH-2-Py), as shown in Fig. 4.8b [28]. An opposite helically ordered molecular assembly, a right-handed helically ordered molecular arrangement, is formed in the crystal packing of the ferrocene-peptide bioconjugate **14** bearing one dipeptide chain of the heterochiral sequence (-D-Ala-L-Pro-NH-2-Py) (Fig. 4.8c) [28].

A type II β-turn-like structure is created by an intramolecular hydrogen bonding between NH adjacent to the pyridyl moiety and CO adjacent to the ferrocene unit of the same dipeptide chain in the ferrocene-peptide bioconjugate **15** bearing one

Fc(-L-Ala-L-Pro-NH-2-Py)$_1$ **12**

Fig. 4.9 A portion of a layer containing the antiparallel arrangement of crystal packing of **12**

dipeptide chain of the heterochiral sequence (-L-Ala-D-Pro-NH-4-Py) as depicted in Fig. 4.10 [36]. This chirality-organized structure is in sharp contrast to the crystal structure of the ferrocene-peptide bioconjugate **13** bearing one dipeptide chain of the heterochiral sequence (-L-Ala-D-Pro-NH-2-Py). The position of the pyridyl nitrogen plays an important role in the self-organization.

The 2:1 *trans*-palladium complex **16** is formed by the complexation of the ferrocene-peptide bioconjugate **12** bearing the one dipeptide chain of the homochiral sequence (-L-Ala-L-Pro-NH-2-Py) with 0.5 equiv. of PdCl$_2$(MeCN)$_2$ [35].

Fc(-L-Ala-D-Pro-NH-4-Py)₁ **15**

Fig. 4.10 Crystal structure of **15**

{Fc(-L-Ala-L-Pro-NH-2-Py)₁}₂–PdCl₂ **16**

E_a = 10.1 kcal mol⁻¹
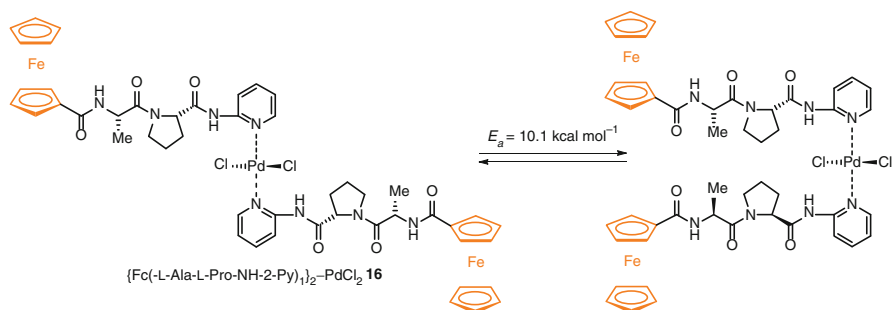
Scheme 4.2 Rotation of the 2:1 *trans*-palladium complex **16** about the palladium center

Two ferrocenoyl dipeptide strands of the palladium complex **16** are able to rotate with respect to each other about the palladium center by the ball-bearing motion of two pyridyl rings as shown in Scheme 4.2. The rotational barrier of the two pyridyl rings in the palladium(II) complex **16** is calculated as 10.1 kcal mol⁻¹.

The ferrocene-peptide bioconjugate **13** bearing one dipeptide chain of the heterochiral sequence (-L-Ala-D-Pro-NH-2-Py) forms the 2:1 *trans*-palladium complex **17** [37]. The crystal structure of **17** reveals a pseudo-helical conformation through coordination to palladium and chirality organization through NH (Ala)/Cl, NH (adjacent to pyridine unit)/O (Ala), and NH (adjacent to pyridine unit of another molecule)/O (Ala) intramolecular hydrogen bonds as shown in Fig. 4.11. The NH adjacent to the pyridyl moiety of one dipeptide chain forms the intramolecular hydrogen bond with CO (Ala) of the same dipeptide chain to nucleate a γ-turn-like structure. This chirality-organized structure is in sharp contrast to the helically ordered molecular arrangement of **13**, in which intermolecular hydrogen bonds are formed instead of the intramolecular hydrogen bonds (Fig. 4.8b) [28].

The ferrocene-peptide bioconjugate ferrocene **14** forms the 4:1 palladium complex **18** with 0.25 equiv. of [Pd(MeCN)₄](BF₄)₂ [36]. The crystal structure of **18** shows that the four chirality-organized ferrocene-dipeptide conjugates are assembled around a palladium center in the same direction to form a chiral pocket surrounded by the dipeptide chains, wherein one BF₄⁻ counter anion is accommodated (Fig. 4.12).

{Fc(-L-Ala-D-Pro-NH-2-Py)$_1$}$_2$–PdCl$_2$ **17**
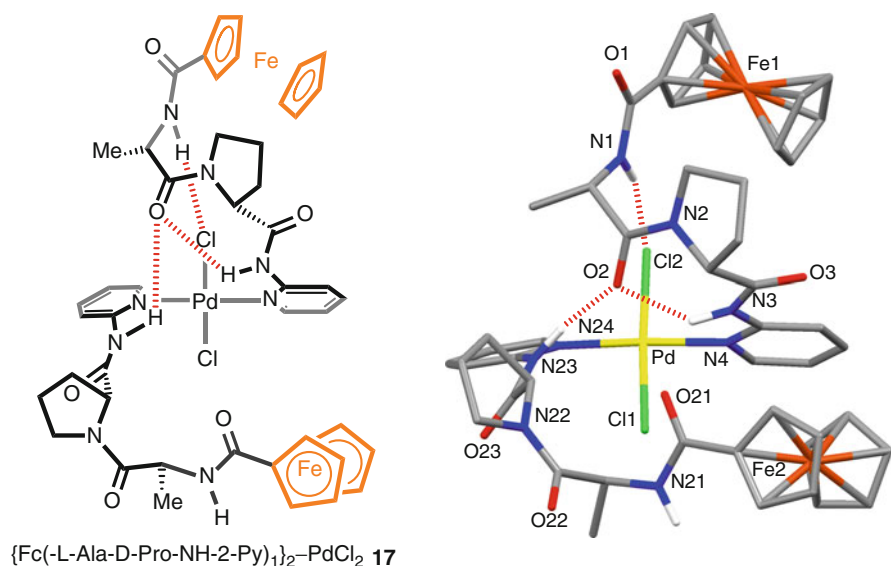
Fig. 4.11 Crystal structure of **17**

{Fc(-L-Ala-D-Pro-NH-4-Py)$_1$}$_4$–Pd(BF$_4$)$_2$ **18**
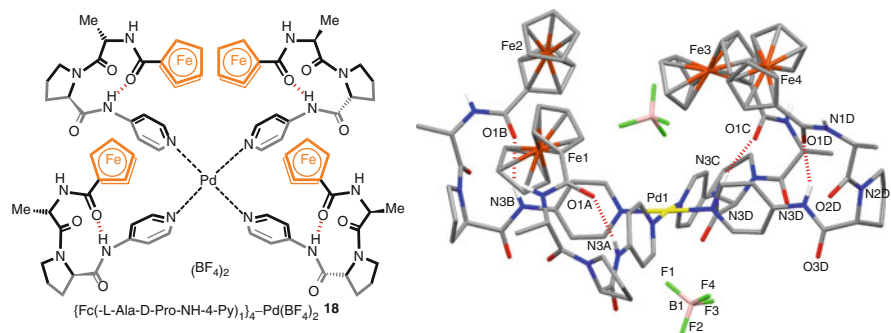
Fig. 4.12 Crystal structure of **18**

4.3 Metal-Free Bioconjugates with Peptide and Amino Acid

Toshikazu Hirao and Toshiyuki Moriuchi

In the Sects. 4.1 and 4.2, the introduction of dipeptide chains into a ferrocene unit as an organometallic scaffold with a central reverse-turn unit is demonstrated to permit chirality organization through the intramolecular interchain hydrogen bonding. The 2,6-pyridinedicarboxamide scaffold has been exploited for a building block to create helices ([38], and references therein). Conjugation of chiral amino acid

with this scaffold can be designed to afford a chiral molecular arrangement [39]. The single-crystal X-ray structure determination of the 2,6-pyridinedicarboxamide **19** bearing the histidyl moieties (-L-His-OMe) shows a left-handed helical conformation through chirality of the histidyl moieties and intramolecular hydrogen bonding between NH (amide) and N (pyridine) to give five-membered hydrogen-bonded rings as depicted in Fig. 4.13a [40, 41]. On the contrary, a right-handed helical conformation is formed in the crystal structure of the 2,6-pyridinedicarboxamide **20** bearing the histidyl moieties (-D-His-OMe) derived from D-histidine methyl ester (Fig. 4.13b) [40]. The chiral helicity appears to be controlled by the configuration of the histidyl α-carbon atoms. Noteworty interesting feature is that each molecule of **19** is connected through continuous intermolecular hydrogen bonds between imidazolyl moieties to give a left-handed helix (*M*-form) as depicted in Fig. 4.13a. An opposite helically ordered molecular assembly, a right-handed helix (*P*-form), is formed in the crystal packing of **20** (Fig. 4.13b). The histidyl moieties of the pyridinedicarboxamide are likely to play an important role in creating the helical arrangement.

Combination of a urea functionality and peptide unit is expected to provide stable hydrogen-bonded molecular assemblies [42–45]. Among the numerous artificial self-assembling systems based on hydrogen bonding, formation of stable hydrogen-bonded molecular duplexes is one of the important targets of current research [46–53]. The crystal structure of the dipeptidyl urea **21** composed of two dipeptide chains (-L-Ala-L-Pro-NH-2-Py) reveals the formation of a hydrogen-bonded duplex through six intermolecular hydrogen bonds (Fig. 4.14a, b) [54]. This hydrogen-bonded duplex adopts a right-handed helical conformation. Each hydrogen-bonded duplex is connected by continuous intermolecular hydrogen bonds to form a double helix-like arrangement as depicted in Fig. 4.14c. This hydrogen-bonded duplex shows a shuttle-like dynamic process based on the recombination of hydrogen bonds in a solution state as shown in Scheme 4.3 [54]. The activation energy of this process is obtained as 9.4 kcal/mol.

Two redox-active π-conjugated units, phenylenediamine as a reduced form and quinonediimine as an oxidized form, are present in polyanilines. The introduction of the amino acid groups into phenylenediamines or quinonediimines is considered to be a convenient strategy to induce chirality into a π-conjugated backbone of polyanilines, affording the hydrogen-bonded chiral polymers wherein redox-active species of polyanilines are expected to be stabilized by hydrogen bonding. The introduction of amino acid moieties, L- or D-Ala-OMe, into aniline oligomers is demonstrated to give chirality-organized aniline oligomers (Fig. 4.15), wherein the formation of intramolecular hydrogen bonds is performed to play an important role to regulate the aniline oligomer moieties conformationally [55]. The aniline oligomer **22-L** shows an induced circular dichroism (ICD) at the absorbance region of the π-conjugated moiety (Fig. 4.16), indicating that the chirality induction of a π-conjugated backbone aniline oligomer is achieved by the chirality organization based on the intramolecular hydrogen bonding. The mirror image of the CD signals observed with **22-L** is obtained in the CD spectrum of **22-D**, supporting a chiral molecular arrangement based on the chirality-organized structures via intramolecular hydrogen bonding.

a

MeO$_2$C, NH   HN CO$_2$Me

Py(-L-His-OMe)$_2$ **19**

O1 O2 N1
O3 N2
N3
N4

b

MeO$_2$C, NH   HN CO$_2$Me

Py(-D-His-OMe)$_2$ **20**

N1 O2 O1
N2 O3
N3
N4
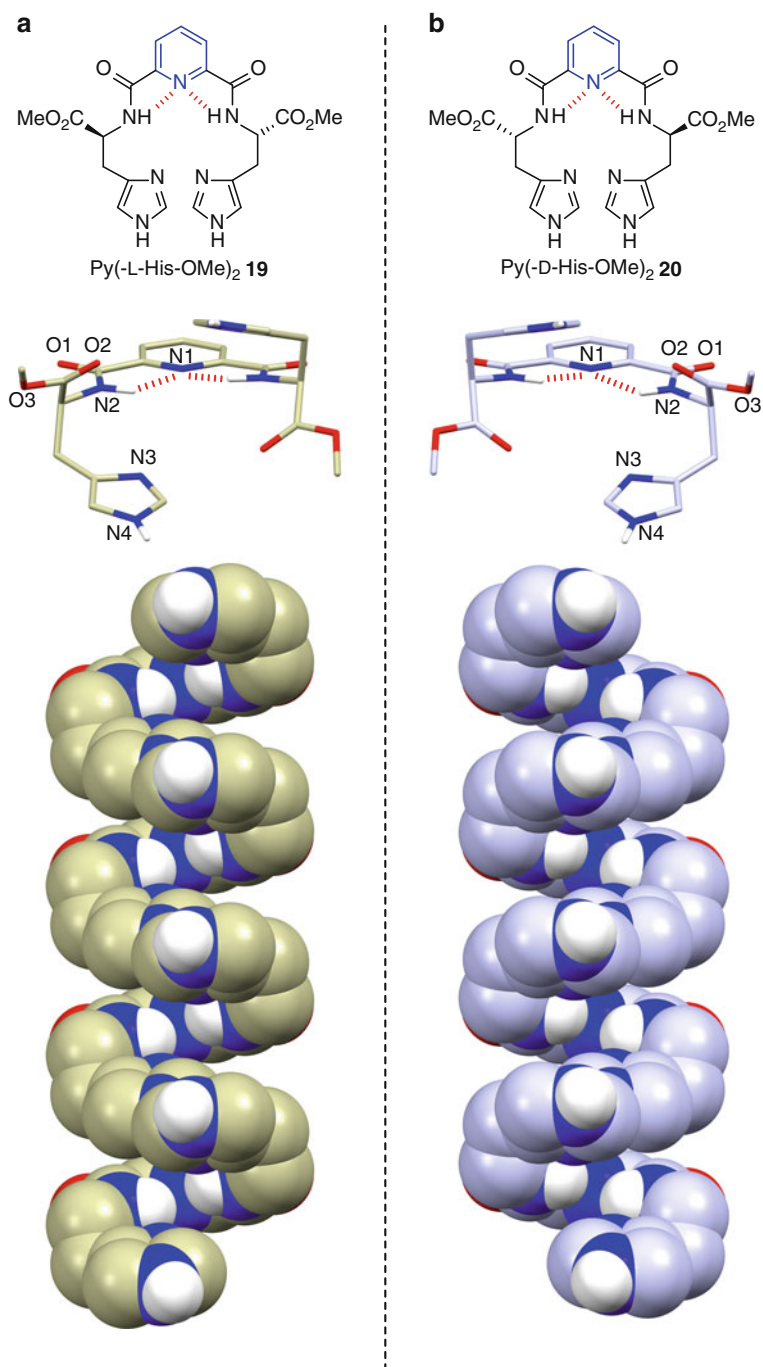
Fig. 4.13 Crystal structures and space-filling representations of a portion of a layer containing the helical assembly of crystal packing of (**a**) **19** and (**b**) **20** (methyl ester moieties are omitted for clarity)

CO(-L-Ala-L-Pro-NH-2-Py)₂ **21**
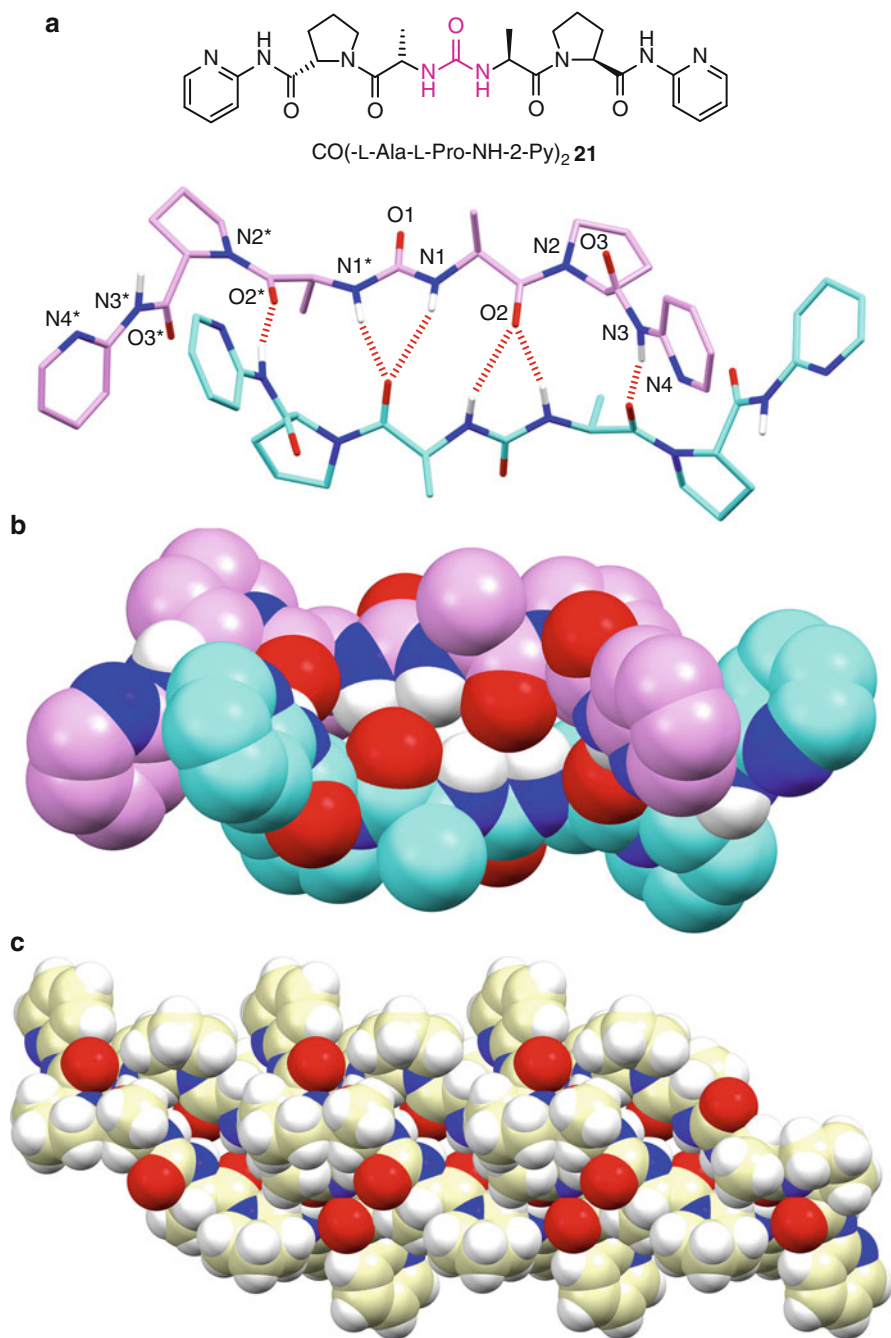
Fig. 4.14 (**a**) Stick, (**b**) space-filling representations of a hydrogen-bonded duplex of **21**, and (**c**) space-filling representation of a portion of a layer containing the double helix-like arrangement of the crystal packing of **21**
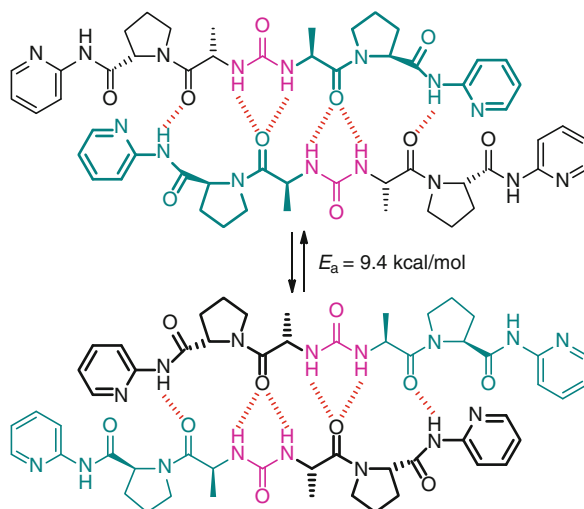
Scheme 4.3 A shuttle-like dynamic process of the dipeptidyl urea **21**
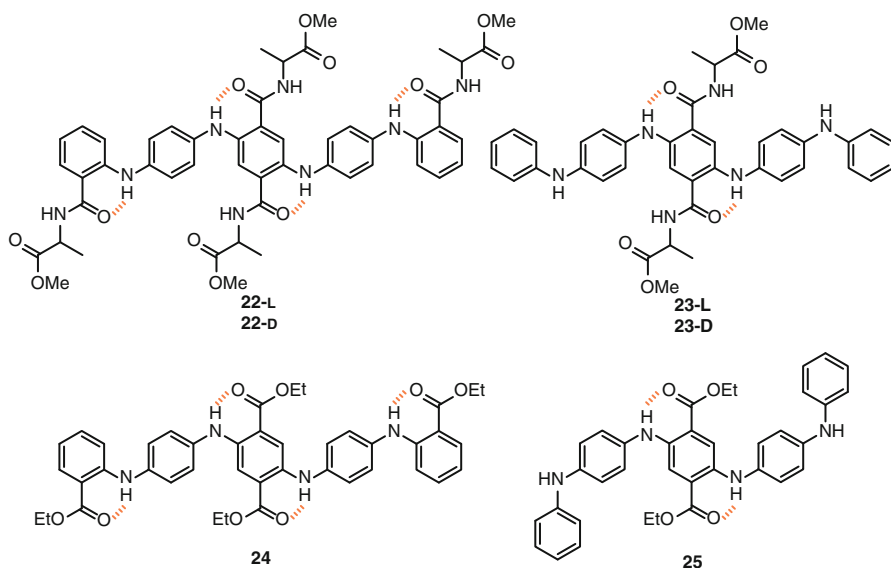
Fig. 4.15 Chemical structures of the aniline oligomers

The aniline oligomers **23-L** and **-D** also exhibit ICD based on the chirality-organized structures. The crystal structure of the aniline oligomer **24** bearing tetraethyl ester confirms the formation of the intramolecular hydrogen bonds between the amino NH and carbonyl oxygen, resulting in an *anti-anti-anti*-conformation of the π-conjugated moieties as shown in Fig. 4.17a. A *syn-anti-syn*-conformation of the
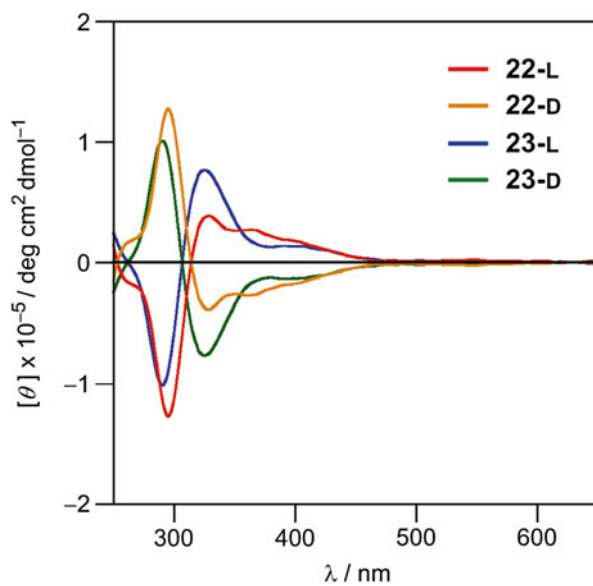
Fig. 4.16 CD spectra of **22** and **23** in CH_2Cl_2 (5.0×10^{-5} M)
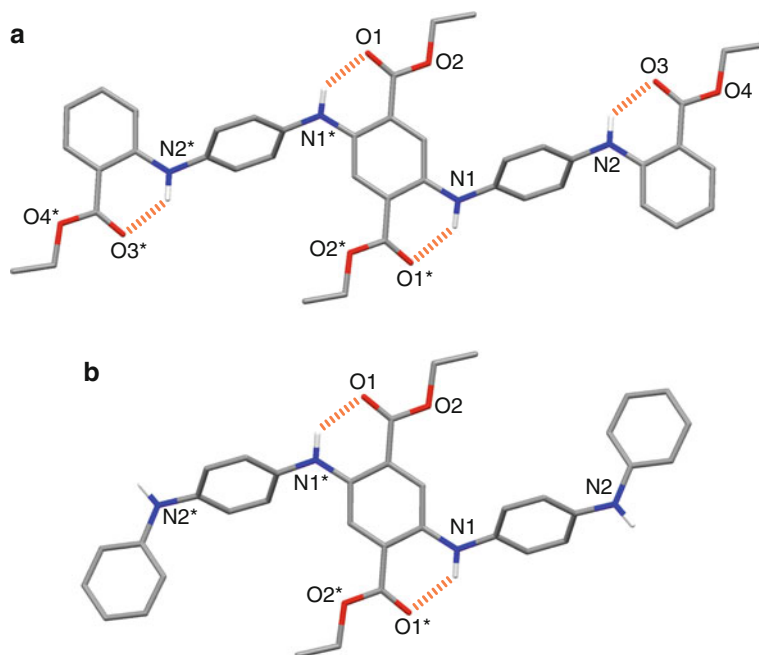
Fig. 4.17 Crystal structures of (**a**) **24** and (**b**) **25**
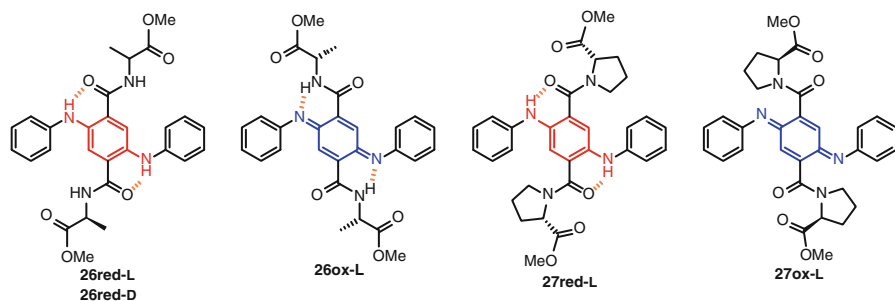
Fig. 4.18 Chemical structures of the phenylenediamine and quinonediimine derivatives bearing amino acids
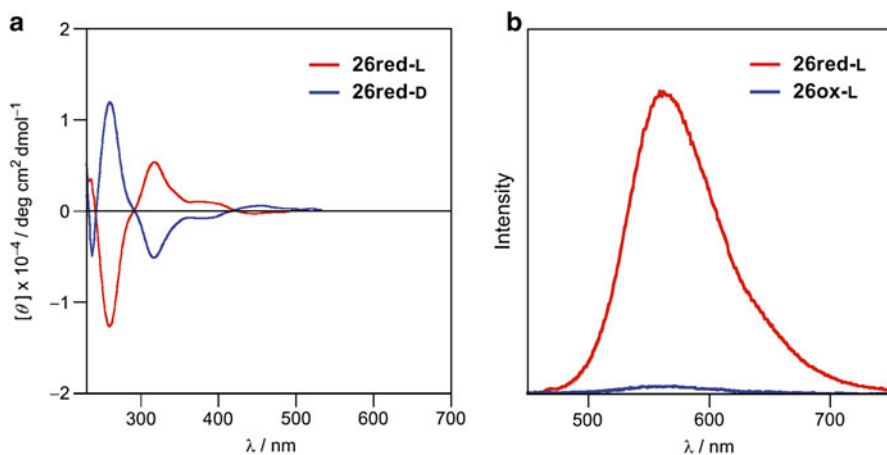
Fig. 4.19 (**a**) The CD spectra of **26red-L** and **26red-D** in dichloromethane (1.0×10^{-4} M) and (**b**) emission spectra of **26red-L** ($\lambda_{ex} = 409$ nm) and **26ox-L** ($\lambda_{ex} = 409$ nm) in dichloromethane (1.0×10^{-4} M) at 298 K under nitrogen atmosphere

π-conjugated moieties based on intramolecular hydrogen bonding is revealed by the single-crystal X-ray structure determination of the diethyl ester **25** (Fig. 4.17b). The terminal π-conjugated moieties of **25** are not regulated because of the absence of the intramolecular hydrogen bonds in the terminal π-conjugated moieties, indicating that the formation of the intramolecular hydrogen bonds play an important role in the structural regulation of the π-conjugated moieties.

The introduction of the amino acid moieties into the phenylenediamine and quinonediimine derivatives is also performed to induce chirality-organized structures and stabilize redox species by the formation of the intramolecular hydrogen bonds (Fig. 4.18) [56]. The phenylenediamine derivative **26red-L** bearing the L-Ala-OMe moieties exhibits an ICD at the absorbance region of the π-conjugated moiety in the CD spectrum (Fig. 4.19a), indicating that the chirality induction of the π-conjugated
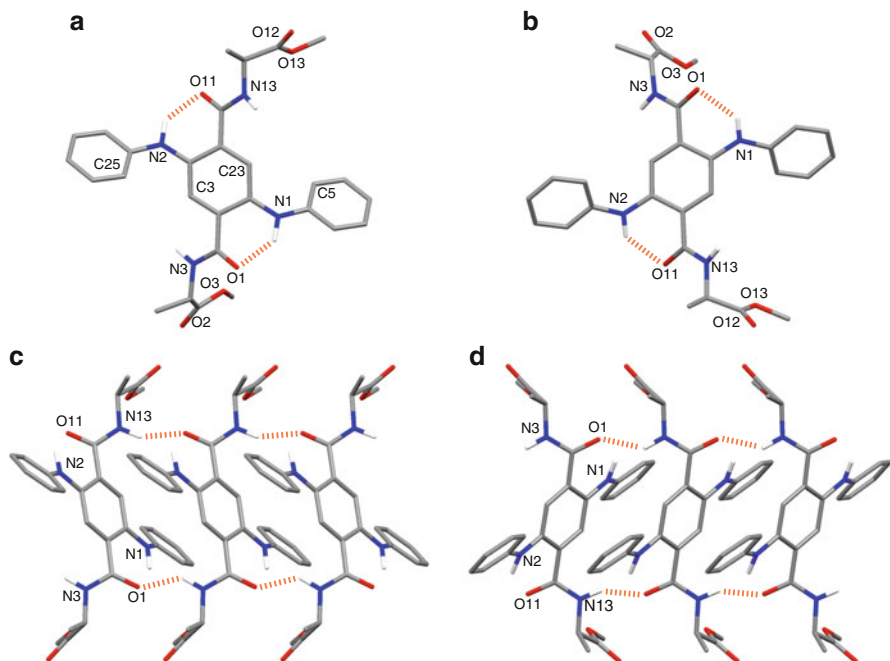
Fig. 4.20 Crystal structures of (**a**) **26red-ʟ** and (**b**) **26red-ᴅ**. A portion of a layer containing a sheet-like molecular arrangement through the intermolecular hydrogen bonding networks in the crystal packing of (**c**) **26red-ʟ** and (**d**) **26red-ᴅ**

backbone is achieved by the chirality organization through the formation of the intramolecular hydrogen bonding. The mirror image of the signals is observed in the CD spectrum of **26red-ᴅ** (Fig. 4.19a). This result indicates that the chirality-organized structure via intramolecular hydrogen bonding is formed even in solution. The phenylenediamine derivative **26red-ʟ** is oxidized into the quinonediimine derivative **26ox-ʟ** by treatment with iodosobenzene as an oxidant. The quinonediimine derivative **26ox-ʟ** also shows an ICD at the absorbance region of the π-conjugated moiety based on the chirality-organized structure through the intramolecular hydrogen bonding. The chirality organization of the phenylenediamine derivative **27red-ʟ** bearing the ʟ-Pro-OMe moieties is supported by the appearance of an ICD at the absorbance region of the π-conjugated moiety. The crystal structure of **26red-ʟ** reveals the formation of the intramolecular hydrogen bonds between the amino NH of the phenylenediamine moiety and the carbonyl oxygen, resulting in an *anti*-conformation of the π-conjugated moiety as shown in Fig. 4.20a. The phenylenediamine derivative **26red-ʟ** exhibits the sheet-like self-assembly through the intermolecular hydrogen bonding networks (Fig. 4.20c). The crystal structure of **26red-ᴅ** composed of the corresponding ᴅ-amino acids (-ᴅ-Ala-OMe) is in a mirror image relationship with **26red-ʟ** (Fig. 4.20b, d).
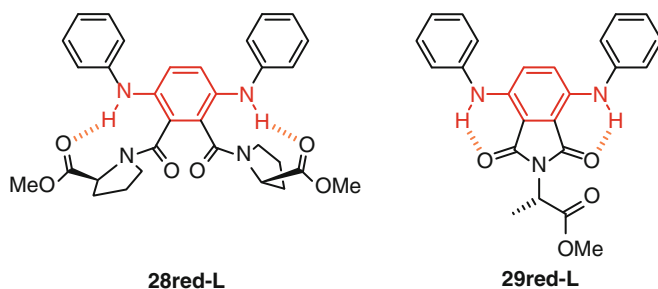
Fig. 4.21 Chemical structures of the phenylenediamine derivatives bearing amino acids

The phenylenediamine derivative **26red-L** exhibits two one-electron redox waves based on the successive one-electron oxidation processes of the phenylenediamine moiety to give the corresponding oxidized species. The quinonediimine derivative **26ox-L** shows two one-electron redox waves assignable to the successive one-electron reduction processes of the quinonediimine moiety to give the corresponding reduced species. The formation of intramolecular hydrogen bonds is considered to stabilize the generated reduced species. The chirality organization and the stabilization of the phenylenediamine radical cation **26red-L** and the semiquinonediimine radical anion **26ox-L** through the formation of intramolecular hydrogen bonds are confirmed by the appearance of an ICD at the absorbance region of the π-conjugated moieties in the CD spectra and the observation of hyperfine coupling in the ESR spectra [56]. The control of luminescent properties is achieved by changing the redox state of the π-conjugated moiety of the phenylenediamine derivatives **26red-L** and **27red-L** [56, 57]. The reduced form **26red-L** shows strong luminescence at 559 nm although weak luminescence is observed with the oxidized form **26ox-L** as shown in Fig. 4.19b.

The introduction of the amino acid groups into the phenylenediamine derivatives at 2,3-positions results in a *syn*-conformation of the π-conjugated moiety of the phenylenediamine derivatives (Fig. 4.21) [58]. The observation of an ICD at the absorbance region of the π-conjugated moiety in the CD spectra of the phenylenediamine derivatives **28red-L** and **29red-L** supports the chirality-organized structure. The crystal structure of **28red-L** reveals the chirality-organized structure based on the formation of the intramolecular hydrogen bonds between the amino NH of the phenylenediamine moiety and the carbonyl oxygen of Pro to form a nonpeptidic reverse-turn 9-membered hydrogen-bonded ring, resulting in a *syn*-conformation of the π-conjugated moiety (Fig. 4.22). Luminescent switching is also observed in the phenylenediamine derivatives **28red-L** and **29red-L**.

Ferrocene-peptide-phenylenediamine conjugate **30red** is designed by the introduction of ferrocene-peptide (Fc-CO-L-Ala-L-Pro-) conjugates into a π-conjugated phenylenediamine spacer [59]. The ferrocene-peptide-phenylenediamine conjugate **30red** is easily oxidized into the ferrocene-peptide-quinonediimine conjugate **30ox** by treatment with lead(IV) acetate as shown in Fig. 4.23. The redox switching of the
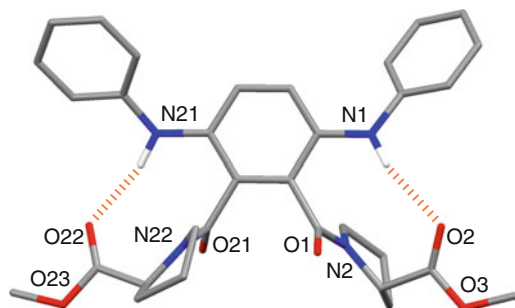
Fig. 4.22 Crystal structure of **28red-**L
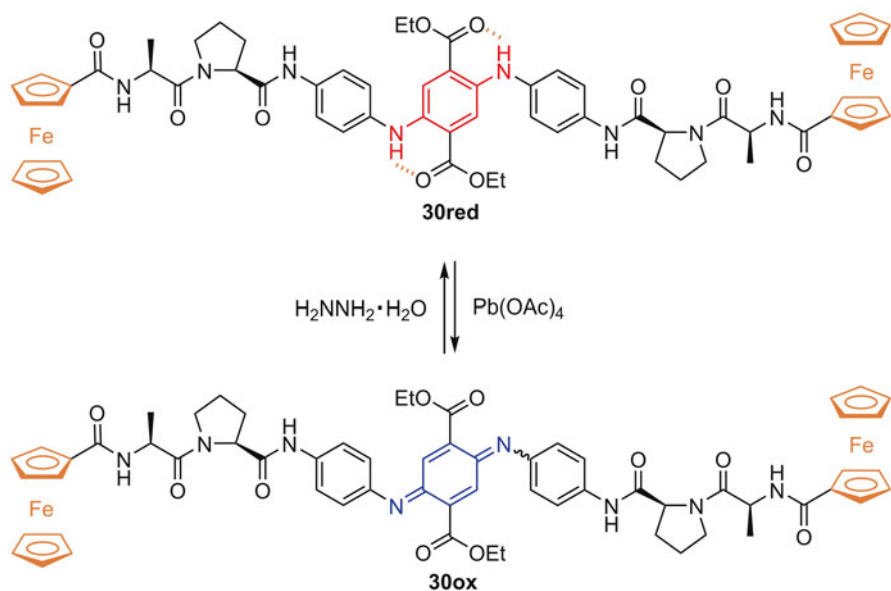
Fig. 4.23 Redox interconversion between **30red** and **30ox**

luminescent properties is performed by changing the redox states of the π-conjugated moiety. The reduced form **30red** exhibits luminescence at 593 nm although weak luminescence is observed with the oxidized form **30ox**. The introduction of ferrocene-peptide conjugates (Fc-CO-L-Ala-L-Pro-) into the π-conjugated phenyl-enediamine spacer is demonstrated to induce the self-aggregation of the π-conjugated moiety in solution, resulting in the chirality organization with a red shift of the maximum emission wavelength.

4.4 Polypeptide or DNA-Induced Aggregates

Toshikazu Hirao and Toshiyuki Moriuchi

The utilization of polyelectrolytes has been recognized to be a convinient strategy for the assembly of opposite-charged functional groups along polyelectrolytes through electrostatic interaction ([60–65], and references therein). Square-planar d^8 transition metal complexes possess the intriguing photophysical and photochemical properties. In particular, luminescent platinum(II) complexes with oligopyridine or cyclometalating ligands have attracted much attention because of their interesting luminescence properties based on metallophilic interaction through $d_z^2 \bullet \bullet \bullet d_z^2$ and/or π–π interactions [66, 67]. The anionic polyelectrolyte-induced aggregation to show metal–metal interaction and concomitant luminescence has been reported with platinum(II) complexes [63–65]. Highly-ordered structures are constructed to fulfill the specific function in biosystems as observed in the double helix of DNA or α-helix and β-sheet of peptides. The introduction of redox-active compounds into such highly-organized biomolecules is envisioned to provide new biomaterials or efficient redox systems.

The redox-active ferrocenes bearing a long alkylene chain are aggregated along the backbone of anionic double helical DNA, providing a redox-active (outer) and hydrophobic (inner) spheres around the double helical core as shown in Fig. 4.24 [68]. In this aggregation, the redox potential of the ferrocenly moiety shifted anodically, compared with the uncomplexed ferrocenes probably due to the hydrophobic interaction between the long alkylene chains.

On the other hand, a design of luminescent gold(I) aggregates [69–72] based on the self-association properties through $d^{10} \bullet \bullet \bullet d^{10}$ closed shell aurophilic bonding interaction [70, 72–76] has gained much attention. Poly(allylamine hydrochloride)
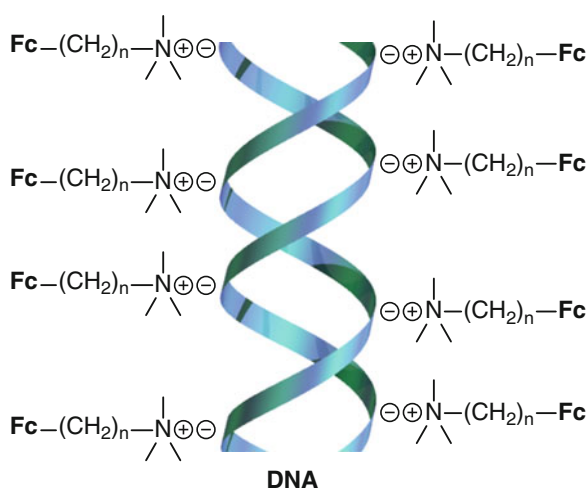
Fig. 4.24 Schematic representation of DNA-induced aggregation of ferrocenes
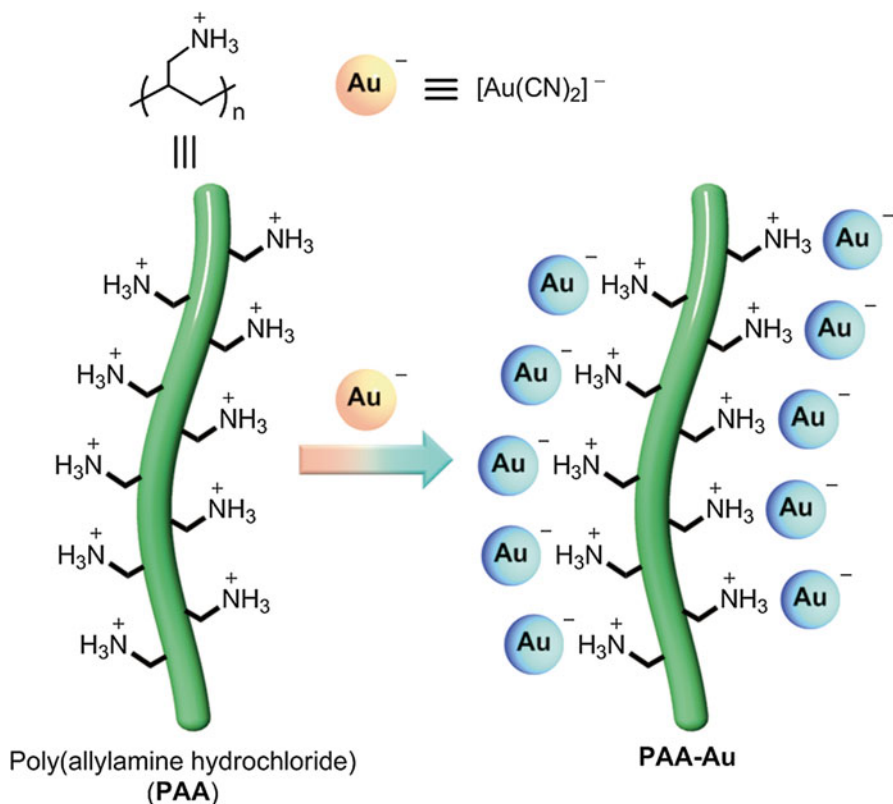
Fig. 4.25 Schematic representation of PAA-induced aggregation and self-association of [Au(CN)$_2$]$^-$

(PAA) having positively charged side chains along the polymer backbone serves as a polymeric spatially aligned scaffold for the aggregation and self-association of negatively charged [Au(CN)$_2$]$^-$ through the electrostatic interaction as shown in Fig. 4.25 [77]. The aggregation and self-association of [Au(CN)$_2$]$^-$ around the backbone of positively charged PAA exhibits the unique luminescent properties (Fig. 4.26). The addition of 0.5 molar equivalents of PAA (based on the PAA unit) to an ultra-pure water 1.0×10^{-3} M solution of K[Au(CN)$_2$] causes the appearance of the emission band at 484 nm. Such luminescence is not detected in the absence of PAA. Further addition of PAA (1–5 molar equivalents of PAA unit) results in a decrease of the emission intensity with a continuous blue shift of the emission band. Oligomerization of [Au(CN)$_2$]$^-$ by increased concentration is known to cause the red-shift of the emission band [78, 79]. High loading of PAA is likely to induce the arrangement of [Au(CN)$_2$]$^-$ separately along the backbone of positively charged PAA, which prevents the aggregation, and thus causes the blue shift of the emission band with decrease of the emission intensity. When PAA loading is lowered, the ratio of [Au(CN)$_2$]$^-$ aggregates around the backbone of positively charged PAA is increased, resulting in a red shift of the emission band. A gradual blue shift of the
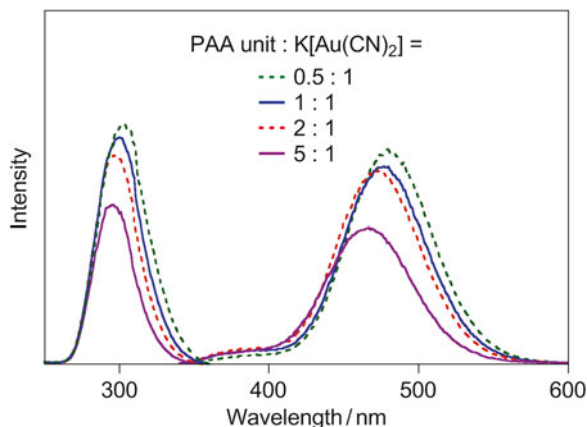
Fig. 4.26 Emission (*right*, $\lambda_{ex} = 290$ nm) and excitation (*left*) of K[Au(CN)$_2$] (1.0×10^{-3} M) in ultra-pure water solution containing various amounts of PAA (0.5, 1.0, 2.0, and 5.0×10^{-3} M PAA unit, respectively) at 298 K

excitation band by the continuous addition of PAA supports the PAA-induced self-association and luminescence of [Au(CN)$_2$]$^-$.

Poly-L-lysine (**P(Lys)**) exists in an α-helical conformation at above pH 10.6 due to the reduced charge on the side chains at a pH above the pKa (10.5), and a random coil conformation at neutral pH due to repulsion between positively charged side chains. Above pH 10.6, increasing temperature leads to the transformation of an α-helical conformation into a β-sheet structure, which is stabilized by hydrophobic interaction between the side chains. The assembling and self-association of anionic [Au(CN)$_2$]$^-$ spatially along cationic β-sheeted **P(Lys)** through electrostatic interaction is also demonstrated to form luminescent [Au(CN)$_2$]$^-$ aggregates, wherein negatively charged [Au(CN)$_2$]$^-$ stabilizes the β-sheet structure by suppressing repulsion between the positively charged side chains (Fig. 4.27) [80]. The excitation and emission spectra of K[Au(CN)$_2$] in the presence of **P(Lys)** are shown in Fig. 4.28. The control of luminescence properties of [Au(CN)$_2$]$^-$ aggregates is performed by changing the ratio of the Lys unit of **P(Lys)**. Addition of 0.5–1 molar equivalents of the Lys unit of **P(Lys)** to the ultra-pure water solution of K[Au(CN)$_2$] results in a gradual increase of the emission intensity and a slightly blue shift of the emission band. Further addition of **P(Lys)** (1–5 molar equivalents of the Lys unit) leads to a decrease in the emission intensity with a continuous blue shift of the emission band.

Poly-L-glutamic acid (**P(Glu)**) is known to form an α-helical structure at around pH 4.3 and a random coil conformation at a neutral pH due to repulsion between negatively charged side chains. **P(Glu)** bearing multiple negatively charged side chains is demonstrated to serve as a polymeric spatially aligned scaffold for the aggregation of positively charged platinum(II) complexes [Pt(tpy)C≡CR](OTf) (tpy = 2,2′,6′,2″-terpyridine; R=Ph (**PtH**), PhC$_{12}$H$_{25}$-p (**PtC$_{12}$**)) through electrostatic interaction, resulting in tunable emission properties (Fig. 4.29) [81]. The addition of **P(Glu)** to a tris/HCl buffer (pH 7.6)/MeOH (v/v = 1/14) solution of the platinum(II) complex **PtH** causes the enhancement of the emission intensity based on the triplet metal-to-ligand charge transfer (^{3}MLCT)/the triplet ligand-to-ligand charge transfer
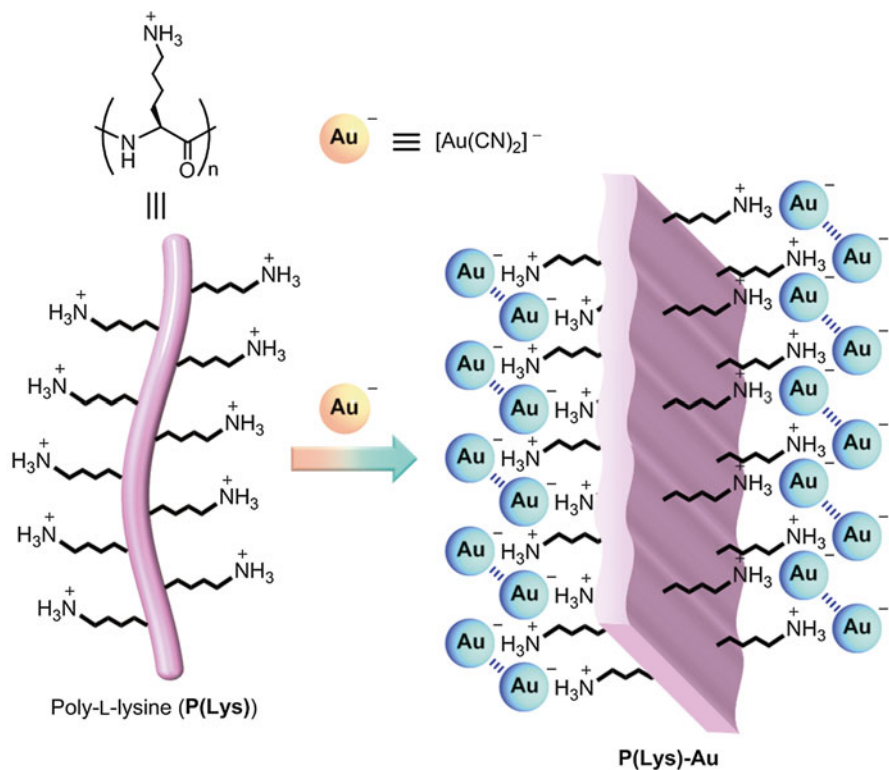
Fig. 4.27 Schematic representation of **P(Lys)**-induced aggregation and self-association of [Au(CN)$_2$]$^-$

Fig. 4.28 Excitation (*left*) and emission (*right*) ($\lambda_{ex} = 280$ nm) of K[Au(CN)$_2$] (5.0×10^{-3} M) in an ultra-pure water solution containing various amounts of P(Lys) (2.5, 5.0, 10.0, and 25.0×10^{-3} M Lys unit, respectively) at 298 K
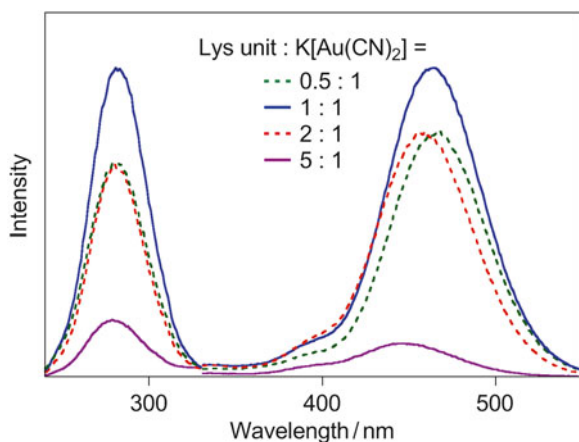
PtH : R = H
PtC$_{12}$: R = C$_{12}$H$_{25}$
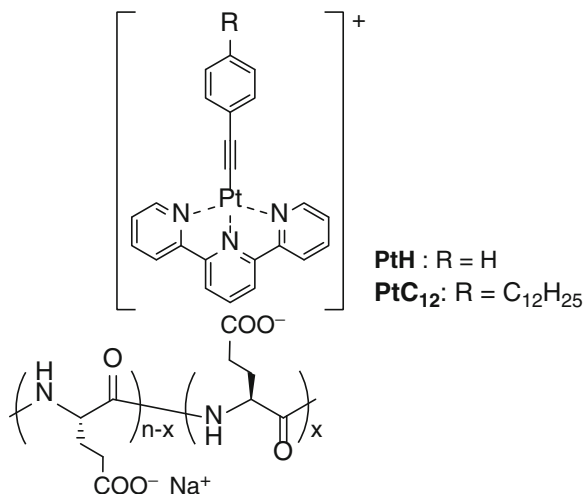
Fig. 4.29 Schematic representation of the platinum(II) terpyridyl complexes with **P(Glu)**
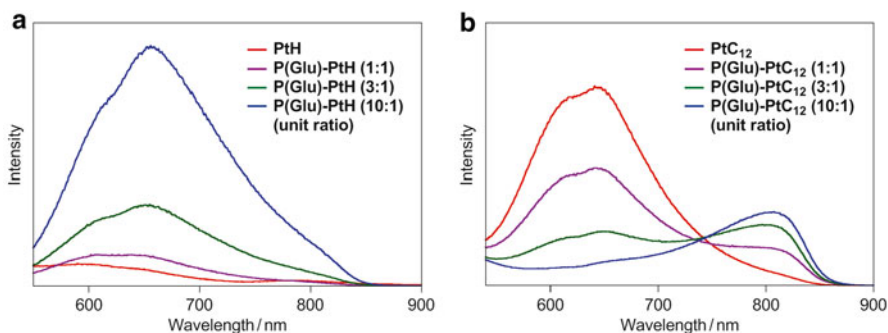
Fig. 4.30 (**a**) Emission spectra (λ_{ex} = 350 nm) of **PtH** (5.0×10^{-5} M) in a tris/HCl buffer (pH 7.6)/MeOH (v/v = 1/14) containing various amounts of **P(Glu)** (0.0, 0.5, 1.5, and 5.0×10^{-4} M Glu unit, respectively) at 298 K and (**b**) Emission spectra (λ_{ex} = 350 nm) of **PtC$_{12}$** (5.0×10^{-5} M) in a tris/HCl buffer (pH 7.6)/MeOH (v/v = 1/14) containing various amounts of **P(Glu)** (0.0, 0.5, 1.5, and 5.0×10^{-4} M Glu unit, respectively) at 298 K

(^{3}LLCT) as shown in Fig. 4.30a. Increasing the ratio of the Glu unit to **PtH** leads to gradual increase of the emission intensity. **PtH** is considered to be accommodated in a hydrophobic sphere of **P(Glu)** to avoid the solvent effect, wherein the α-helical structure of **P(Glu)** is stabilized by suppressing repulsion between negatively charged side chains through the electrostatic interaction between the cationic platinum(II) complexes and negatively charged side chains of **P(Glu)**. In the case of the platinum(II) complex **PtC$_{12}$**, gradual increase of the emission intensity based on the triplet metal-metal-to-ligand charge transfer (^{3}MMLCT) with concomitant decrease of the emission intensity based on the triplet metal-to-ligand charge transfer (^{3}MLCT)/the triplet ligand-to-ligand charge transfer (^{3}LLCT) is observed as the
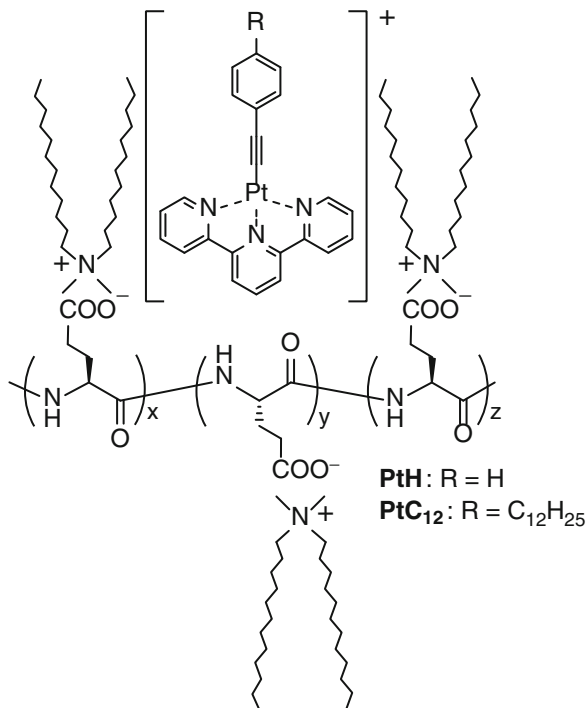
Fig. 4.31 Schematic representation of the platinum(II) terpyridyl complexes with **P(Glu)-DDA**

amount of **P(Glu)** is increased (Fig. 4.30b). This result indicates that the alkyl long chain of **PtC$_{12}$** is considered to play an important role in the aggregation of the platinum(II) terpyridyl moieties to exhibit Pt(II)-Pt(II) and π–π interactions.

The reaction of the sodium salt of **P(Glu)** with didodecyldimethylammonium (DDA) bromide affords **P(Glu)-DDA**, which is indicated to form the α-helical structure even in methanol [82]. **P(Glu)-DDA** decorating hydrophobic sphere along the backbone of anionic helical **P(Glu)** is performed to serve as a polymeric spatially aligned scaffold for the accommodation and aggregation of **PtC$_{12}$** (Fig. 4.31) [82]. The introduction of 0.2 molar equivalents of the platinum(II) complex **PtC$_{12}$** into **P(Glu)-DDA** in methanol induces the aggregation of **PtC$_{12}$** to exhibit ^{3}MMLCT emission (Fig. 4.32a), wherein the dodecyl moiety of the platinum(II) complex plays an important role in the aggregation of the platinum(II) terpyridyl moieties to induce Pt(II)-Pt(II) and π–π interactions. Such synergistic effect is not observed in the case of the platinum(II) complex **PtH**, wherein the emission intensity based on ^{3}MLCT/^{3}LLCT is increased (Fig. 4.32b).

Photo active iridium complexes are of potential in the organic EL device, which was also studied [83–86]. The introduction of the cationic luminescent iridium(III) complexes into negatively charged **P(Glu)** as a polymeric scaffold is allowed to perform the tuning of the emission properties in an aqueous media (Fig. 4.33) [87]. Increasing the ratio of the Glu unit of **P(Glu)** to the cationic cyclometalated
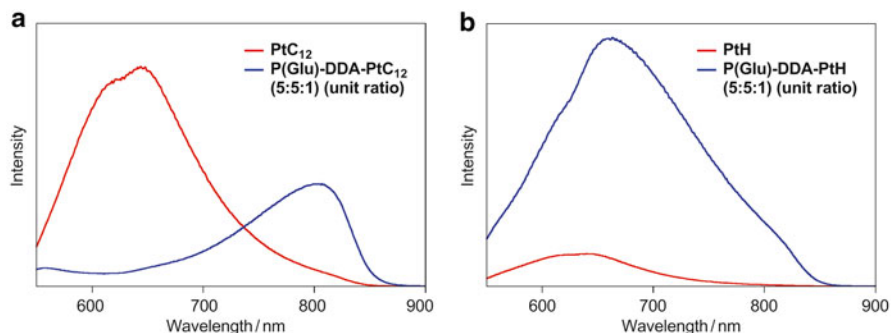
Fig. 4.32 (**a**) Emission spectra of **PtH**, **DDA-PtC₁₂** (5:1), and **P(Glu)-DDA-PtC₁₂** (5:5:1) in methanol (**PtC₁₂** unit: 5.0×10^{-5} M) at 298 K and (**b**) Emission spectra of **PtH**, **DDA-PtH** (5:1), and **P(Glu)-DDA-PtH** (5:5:1) in methanol (**PtH** unit: 5.0×10^{-5} M) at 298 K
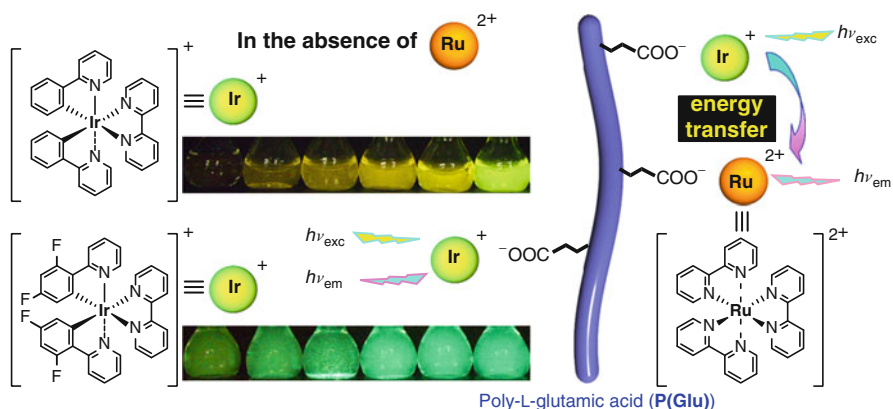
Fig. 4.33 Schematic representation of the introduction of the cationic iridium(III) complex **Ir** or **Ir(F)** with/without ruthenium(II) complex **Ru** into negatively charged **P(Glu)**

iridium(III) complex [Ir(ppy)₂(bpy)]Cl (**Ir**) (where ppy = 2-phenylpyridine, bpy = 2,2′-bipyridine) or [Ir(ppyFF)₂(bpy)]Cl (**Ir(F)**)) (where ppyFF = 2-(2,4-difluorophenyl)pyridine) causes a gradual increase of the emission intensity and a slightly blue shift of the emission band as shown in Fig. 4.34a, b [87]. The cyclometalated iridium(III) complexes are known to show the emission maximum with the lower energy and weaker emission in the more polar solvent than in the less polar water [88, 89]. High loading of **P(Glu)** might lead to the accommodation of the iridium(III) complex in a hydrophobic sphere of **P(Glu)**, resulting in the increase of the emission intensity. The controlled conformational change (random coil–α-helical structure–random coil) of **P(Glu)** is also observed by changing the raitio of **P(Glu)** and the iridium(III) complex. The introduction of the iridium(III) complex **Ir(F)** as an energy donor and the ruthenium(II) complex [Ru(bpy)₃]Cl₂ (**Ru**) as an energy acceptor
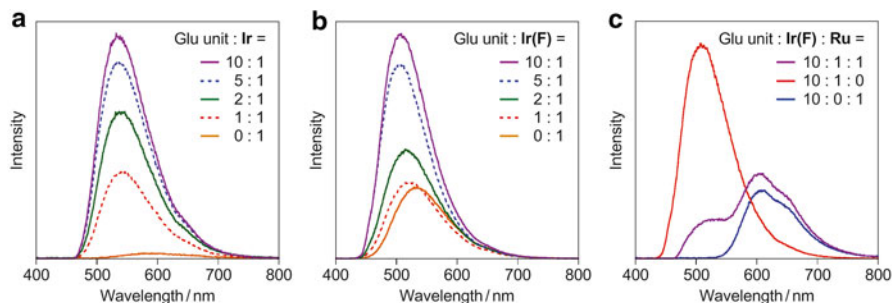
Fig. 4.34 (**a**) Emission spectra ($\lambda_{ex}=310$ nm) of [Ir(ppy)$_2$(bpy)]Cl (**Ir**) (5.0×10^{-5} M) in water solution containing various amounts of **P(Glu)** (0, 0.5, 1.0, 2.5, and 5.0×10^{-4} M Glu unit, respectively) at 298 K, (**b**) Emission spectra ($\lambda_{ex}=310$ nm) of [Ir(ppyFF)$_2$(bpy)]Cl (**Ir(F)**) (5.0×10^{-5} M) in water solution containing various amounts of **P(Glu)** (0, 0.5, 1.0, 2.5, and 5.0×10^{-4} M Glu unit, respectively) at 298 K, and (**c**) Emission spectra ($\lambda_{ex}=290$ nm) of a mixture of **P(Glu)**, [Ir(ppyFF)$_2$(bpy)] Cl (**Ir(F)**), and [Ru(bpy)$_3$]Cl$_2$ (**Ru**) (2.0×10^{-5} M **Ir(F)** and **Ru** unit) in water solution at 298 K

into a hydrophobic sphere of **P(Glu)** is performed to induce an efficient energy transfer (ET). In the emission spectrum of a 10:1:1 mixture of **P(Glu)**, **Ir(F)**, and **Ru**, the decrease of the characteristic emission at around at 500 nm from the excited state of **Ir(F)** is observed with concomitant increase of the emission intensity of **Ru** at around 625 nm (Fig. 4.34c) [87], indicating that an efficient ET process from the excited state of **Ir(F)** to **Ru** is likely to occur in a hydrophobic sphere of **P(Glu)**.

Highly-oraganized molecular arrangement of π-conjugated molecules has attracted much attention because of their potential applications as advanced molecular materials based on defined functional properties [1–3]. Construction of structurally defined molecular aggregates is of importance for the development of functional materials based on aggregation-induced properties. The introduction of pyrene derivatives into polypeptides through electrostatic interaction is performed to control the fluorescence properties of pyrene derivatives (Fig. 4.35) [90]. **P(Lys)**-induced fluorescence arising from aggregated pyrenyl moieties is observed by the addition of **P(Lys)** to ultrapure water solution of 1-pyreneacetic acid sodium salt (**Pyr(CH$_2$COONa)**) although **Pyr(CH$_2$COONa)** shows monomer fluorescence (Fig. 4.36a) [90]. A gradual increase of the fluorescence intensity of the aggregates is induced by increasing the ratio of **P(Lys)** probably due to the aggregation of the pyrenyl moieties in a hydrophobic sphere of **P(Lys)**. The tuning of the fluorescence properties of 1-pyrenemethylamine hydrochloride (**Pyr(CH$_2$NH$_3$Cl)**) is also demonstrated by using **P(Glu)** bearing multiple negatively charged side chains as a polymeric scaffold as shown in Fig. 4.36b [90]. The architectural control of molecular aggregates using pre-organized biomolecules is considered to be a reliable strategy to artificial highly-organized systems without complicated chemical synthesis. Also, the aggregation of opposite-charged pyrene derivatives around the backbone of polypeptides stabilizes the α-helical structure by suppressing repulsive forces between the electrically charged side chains.
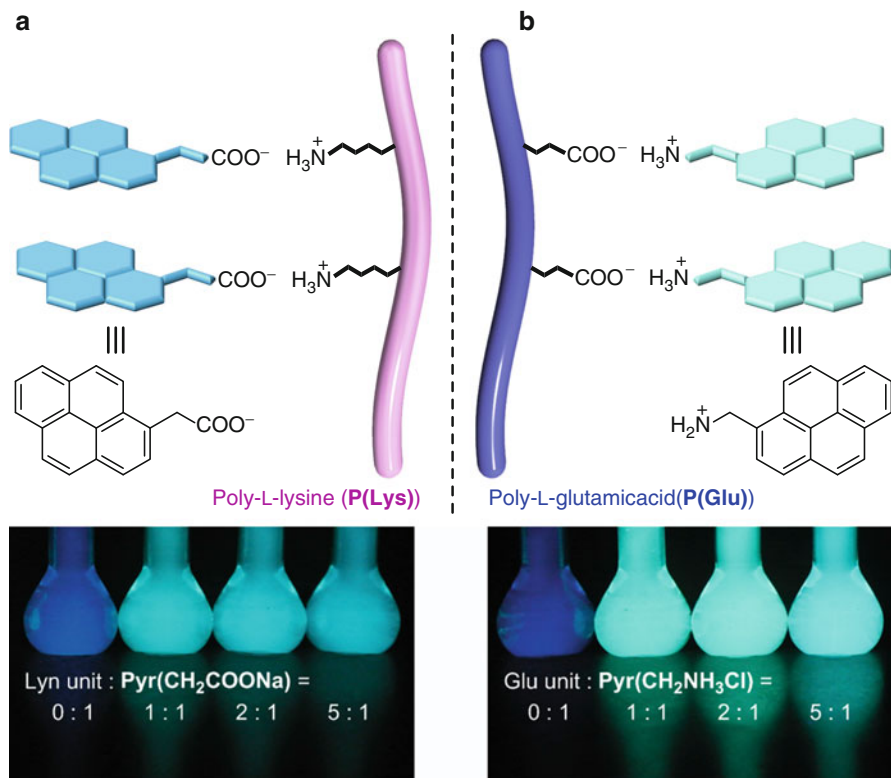
Fig. 4.35 Schematic representation of (**a**) the introduction of negatively charged 1-pyreneacetate anion into **P(Lys)** and (**b**) the introduction of positively charged 1-pyrenemethylammonium cation into **P(Glu)**
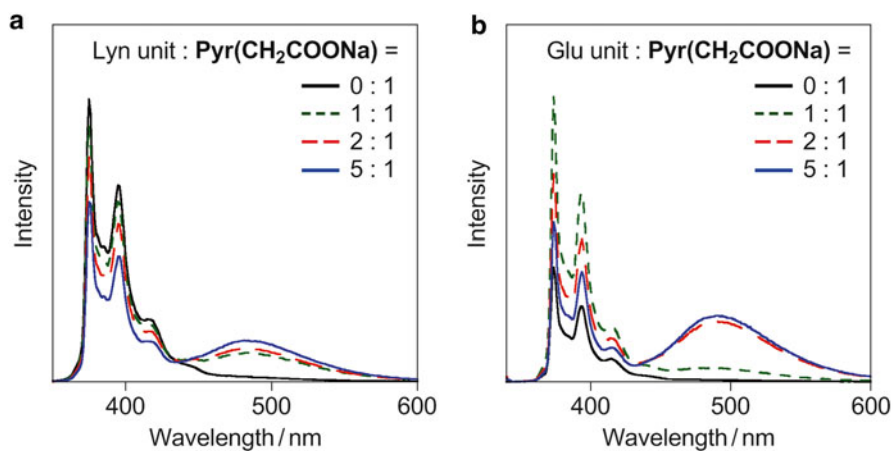
Fig. 4.36 (**a**) Emission spectra ($\lambda_{ex} = 310$ nm) of [Ir(ppy)$_2$(bpy)]Cl (**Ir**) (5.0×10^{-5} M) in water solution containing various amounts of **P(Glu)** (0, 0.5, 1.0, 2.5, and 5.0×10^{-4} M Glu unit, respectively) at 298 K and (**b**) Emission spectra ($\lambda_{ex} = 310$ nm) of [Ir(ppyFF)$_2$(bpy)]Cl (**Ir(F)**) (5.0×10^{-5} M) in water solution containing various amounts of **P(Glu)** (0, 0.5, 1.0, 2.5, and 5.0×10^{-4} M Glu unit, respectively) at 298 K

4.5 Organometallic Bioconjugates Bearing Nucleobase Moieties

Toshikazu Hirao and Toshiyuki Moriuchi

Highly-organized molecular assemblies are created in bio-systems to exhibit unique functions. The double helical DNA is created by A-T and G-C base pairs, which are controlled mainly by complementary hydrogen bonding, π-stacking interaction, and hydrophobic interaction [91, 92]. The utilization of self-assembling properties of nucleobases is considered to be a convenient approach to design well-defined molecular assemblies [93–99]. A variety of metal-modified nucleobases have been designed to demonstrate the formation of highly-organized molecular assemblies through hydrogen bonds [95, 100, 101]. A combination of nucleobases with functional organometallic compounds is envisioned to provide novel bioconjugates depending on both properties. The transition metal complexes with pincer ligands, which involve a direct metal-carbon σ bond, have been investigated and utilized as materials and catalysts [102, 103]. The NCN-pincer ligand **U6P** bearing the uracil moiety, which is easily synthesized by the reaction of 6-ethynyl-1-octyluracil with 4-bromo-3,5-bis(dimethylaminomethyl)iodobenzene (Fig. 4.37) [104]. The crystal structure of **U6P** reveals the formation of a hydrogen-bonded dimer through intermolecular hydrogen bonds between the uracil moieties in the crystal packing, wherein each hydrogen-bonded dimer is connected through π–π interaction between the benzene moiety of the NCN-pincer ligand and the uracil moiety (Fig. 4.38a).
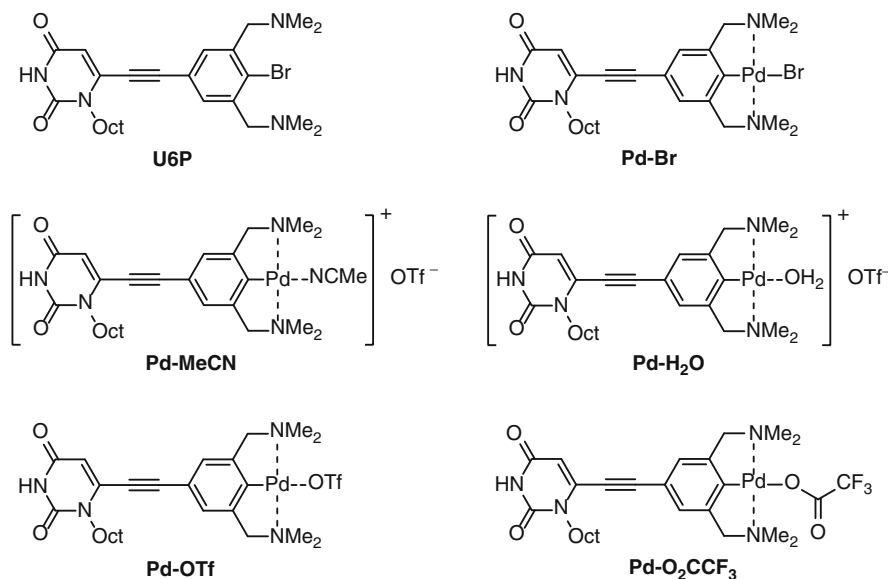
Fig. 4.37 Chemical structures of the NCN-pincer ligand **U6P** and the NCN-pincer palladium(II) complexes **Pd-Br**, **Pd-MeCN**, **Pd-H₂O**, **Pd-OTf**, and **Pd-O₂CCF₃**

Fig. 4.38 A portion of a layer containing the hydrogen-bonded assemblies of (**a**) **U6P**, (**b**) **Pd-MeCN**, (**c**) **Pd-H₂O**, (**d**) **Pd-OTf**, and (**e**) **Pd-O₂CCF₃**

The reaction of the NCN-pincer ligand **U6P** with Pd(dba)$_2$ affords the NCN-pincer palladium(II) complex **Pd-Br** bearing the 6-ethynyl-1-octyluracil moiety (Fig. 4.37) [105]. The cationic complex **Pd-MeCN** can be obtained by the treatment of **Pd-Br** with AgOTf in acetonitrile (Fig. 4.37). The hydrogen-bonded dimer through intermolecular hydrogen bonds between the uracil moieties of two independent molecules as observed in a wobble base pair is formed in the crystal packing. Each hydrogen-bonded dimer shows π–π interaction between the uracil moieties to form π-stacks in a crystal packing 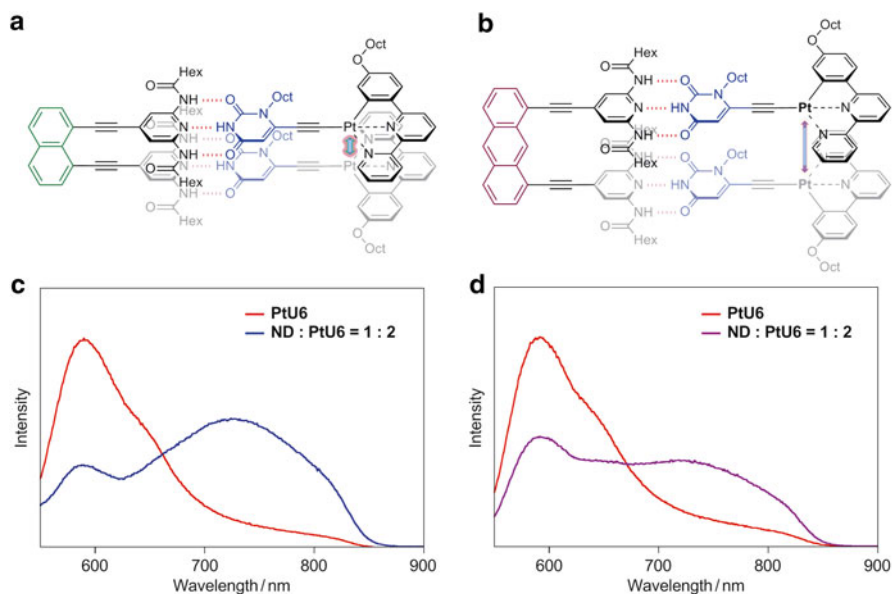as shown in Fig. 4.38b. Recrystallization of **Pd-MeCN** from chloroform/hexane/diethyl ether (not dried solvents) is allowed to form of the NCN-pincer palladium(II) complex **Pd-H₂O**, in which the ancillary acetonitrile of **Pd-MeCN** is displaced by water molecule (Fig. 4.37). In the case of **Pd-H₂O**, each hydrogen-bonded dimer is connected through intermolecular hydrogen bonding bridge between the coordinated water molecule and triflate anion. Furthermore, each hydrogen-bonded assemlies is stacked through π–π interaction (Fig. 4.38c). On the contrary, the NCN-pincer palladium(II) complex **Pd-OTf** can be obtained by recrystallization of **Pd-MeCN** from dichloromethane/hexane/diethyl ether through removal of a labile acetonitrile ligand (Fig. 4.37). The intermolecular hydrogen bond between the uracil moiety and the triflate anion bound to the palladium center is formed in the crystal structure of **Pd-OTf** as drawn in Fig. 4.38d. The NCN-pincer palladium(II) complex **Pd-O₂CCF₃**, which is obtained by the abstraction of the bromide ion from **Pd-Br** with AgO₂CCF₃ (Fig. 4.37), shows the dimeric structure based on the formation of intermolecular hydrogen bonds between the uracil moieties (Fig. 4.38e).

The bioorganometallic platinum(II) compounds **PtU6** and **PtU5** are prepared by the conjugation of the corresponding uracil derivative and the organoplatinum(II) compound [4-octyloxy-(C^N^N)PtCl] (Fig. 4.39) [106]. The crystal structure of **PtU6** reveals the formation of the dimeric structure through intermolecular hydrogen bonds between the uracil moieties of two independent molecules, wherein each hydrogen-bonded dimer is connected through Pt(II)-Pt(II) and π–π interactions as shown in Fig. 4.40. The platinum(II) complex **PtU6** exhibits the emission band at around 720 nm, derived from the ^{3}MMLCT excited state resulting from Pt(II)-Pt(II) and π–π interactions. Synergistic effects of emission properties depend on the aggregation properties of the platinum(II) complexes. The platinum(II) complex **PtU5**, wherein the direction of hydrogen bonding sites of the uracil moieties is different from **PtU6**, shows the ^{3}MLCT and/or ^{3}LLCT emission.

The molecular scaffolds **ND** and **AD** composed of aromatic rigid frameworks, naphthalene and anthracene, respectively, having two 2,6-dihexamidopyridine moieties as a complementary hydrogen bonding site for the uracil moiety are synthesized to control the aggregate of the organoplatinum(II) complexes having uracil moieties as shown in Fig. 4.39. The tuning of the emission properties of the organoplatinum(II) compounds is performed by changing the molecular scaffold, which depends on the regulation of the aggregated structures to induce the Pt(II)-Pt(II) and π–π interactions [106].The platinum(II) complex **PtU6** exhibits a new emission band based on the ^{3}MMLCT excited state resulting from Pt(II)-Pt(II) and π–π interactions at around 730 nm with concomitant decrease of the ^{3}MLCT/^{3}LLCT

Fig. 4.39 Design of the bioorganometallic platinum(II) compound with uracils and molecular scaffolds

Fig. 4.40 (**a**) A hydrogen-bonded dimer through intermolecular hydrogen bonds between the uracil moieties and (**b**) a portion of a layer containing the π-stack molecular assembly in a crystal packing of **PtU6**

Fig. 4.41 Schematic representation of the controlled aggregation of the bioorganometallic platinum(II) compound **PtU6** by using the molecular scaffold (**a**) **ND** and (**b**) **AD**. (**c**) Emission spectra (λ_{ex} = 530 nm) of **PtU6** and **ND-PtU6** (1:2) in dichloromethane ([**ND**] = 0.5×10^{-3} M, [**PtU6**] = 1.0×10^{-3} M) at 298 K and (**d**) emission spectra (λ_{ex} = 530 nm) of **PtU6** and **AD-PtU6** (1:2) in dichloromethane ([**AD**] = 0.5×10^{-3} M, [**PtU6**] = 1.0×10^{-3} M) at 298 K

emission in the presence of the molecular scaffold **ND** as shown in Fig. 4.41c. The molecular scaffold **ND** is likely to induce the aggregation of **PtU6** through the complementary hydrogen bonding and π–π interaction between the ligands in a solution state (Fig. 4.41a). An interbase distance affects the Pt(II)-Pt(II) and π–π interactions in aggregated complexes. In comparison to the emission of the aggregation of **PtU6** with **ND**, the use of the molecular scaffold **AD** composed of anthracene causes the low intensity of the ^{3}MMLCT emission and the high intensity of the ^{3}MLCT emission (Fig. 4.41d) probably due to the weak Pt(II)-Pt(II) and π–π interactions based on the longer interbase distance (Fig. 4.41b).

Among natural nucleobases, the utilization of guanine (G) derivatives is a reliable strategy for the construction of highly-ordered molecular assemblis because they self-assemble into dimers, ribbons, G-octamers, G-hexadecamers and helices [94, 107]. A variety of guanosine derivatives have been reported to investigate the assembling properties [108–112]. The G-octamer is recognized as an attractive scaffold, in which π-functional molecules can be covalently attached and stacked in a well-defined arrangement. A bioorganometallic guanosine-based Au(I) isonitrile complex **GAu(I)** is performed to serve as the reliable G-octamer scaffold via self-assembly, wherein the octamer is formed in the presence of KPF$_6$, exhibiting a switchable emission based on Au(I)-Au(I) interaction as depicted in Fig. 4.42 [113].
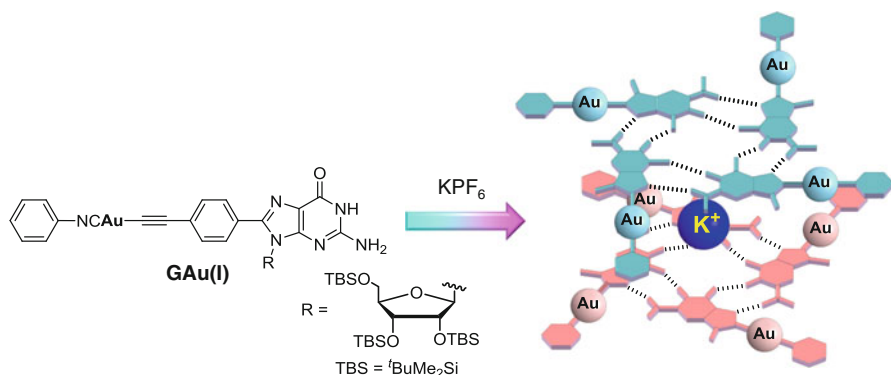
Fig. 4.42 Formation of G-octamer of **GAu(I)** to induce Au(I)-Au(I) interaction upon addition of KPF$_6$
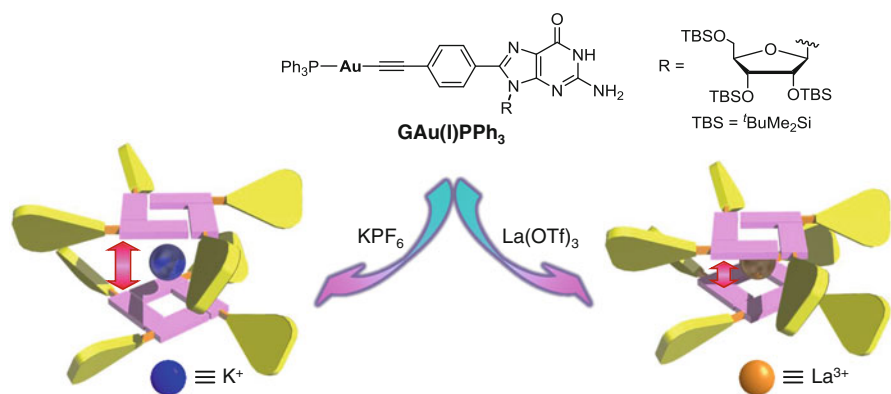
Fig. 4.43 Formation of G-octamer of **GAu(I)PPh$_3$** upon addition of KPF$_6$ or La(OTf)$_3$

A bioorganometallic conjugate **GPhAuPPh$_3$** composed of the guanosine and alkynyl-Au(I)PPh$_3$ moiety is demonstrated to form the expected octamer in the presence of KPF$_6$ (Fig. 4.43) [114]. Thus-obtained G-octamer, however, shows no Au(I)-Au(I) interaction probably due to the bulky phosphine moiety to arrange the Au(I) moiety far away each other. On the contrary, a more closely stacked octamer is obtained in the presence of trivalent La(OTf)$_3$ than those in the presence of KPF$_6$, leading to Au(I)-Au(I) interaction as depicted in Fig. 4.43 [114].

A bioorganometallic conjugate **GAu(III)** composed of the guanosine and cyclo-metalated gold(III) moiety is performed to form the empty quartet, octamer, and poly-meric columnar aggregate depending on the amount of KPF$_6$, wherein the formation of the G-quarteruplex via self-assembly induces a π–π interaction (Fig. 4.44) [115].
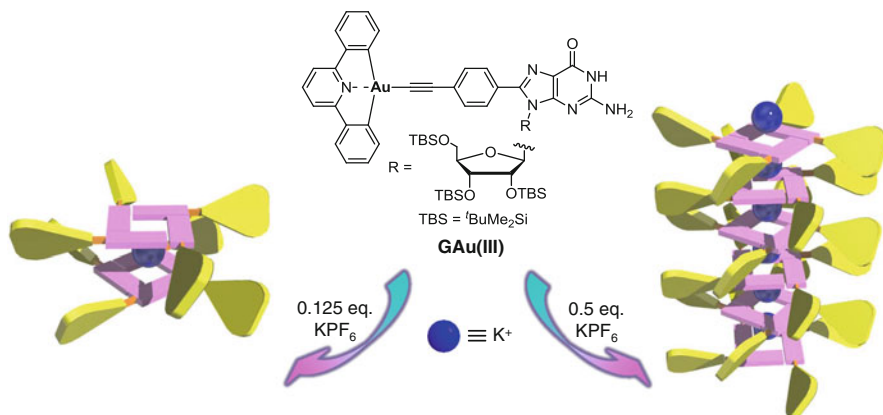
Fig. 4.44 Formation of G-octamer or polymeric columnar aggregate of **GAu(III)** depending on the amount of KPF$_6$

References

1. D. Braga, F. Grepioni, G.R. Desiraju, Chem. Rev. **98**, 1375 (1998)
2. V. Balzani, A. Credi, F.M. Raymo, J.F. Stoddart, Angew. Chem. Int. Ed. **39**, 3348 (2000)
3. G.F. Swiegers, T.J. Malefetse, Chem. Rev. **100**, 3483 (2000)
4. J. Kyte, *Structure in Protein Chemistry* (Garland, New York, 1995)
5. C. Branden, J. Tooze, *Introduction to Protein Structure*, 2nd edn. (Garland, New York, 1998)
6. G.A. Jeffrey, *An Introduction to Hydrogen Bonding*, 1st edn. (Oxford University Press, New York, 1997)
7. M.M. Conn, J. Rebek Jr., Chem. Rev. **97**, 1647 (1997)
8. E.A. Archer, H. Gong, M.J. Krische, Tetrahedron **57**, 1139 (2001)
9. L.J. Prins, D.N. Reinhoudt, P. Timmerman, Angew. Chem. Int. Ed. **40**, 2382 (2001)
10. G. Jaouen, A. Vessiéres, I.S. Butler, Acc. Chem. Res. **26**, 361 (1993)
11. R. Severin, R. Bergs, W. Beck, Angew. Chem. Int. Ed. **37**, 1634 (1998)
12. G. Jaouen (ed.), Bioorganometallic chemistry (special issue). J. Organomet. Chem. **589**, 1–126 (1999)
13. R.H. Fish, G. Jaouen, Organometallics **22**, 2166 (2003)
14. G. Jaouen (ed.), *Bioorganometallics; Biomolecules, Labeling, Medicine* (Wiley-VCH, Weinheim, 2006)
15. A. Togni, T. Hayashi, *Ferrocenes* (Wiley-VCH, Weinheim, 1995)
16. S. Top, A. Vessieres, G. Leclercq, J. Quivy, J. Tang, J. Vaissermann, M. Huche, G. Jaouen, Chem. Eur. J. **9**, 5223 (2003)
17. C. Biot, D. Taramelli, I. Forfar-Bares, L.A. Maciejewski, M. Boyce, G. Nowogrocki, J.S. Brocard, N. Basilico, P. Olliaro, T.J. Egan, Mol. Pharm. **2**, 185 (2005)
18. M. Patra, G. Gasser, M. Wenzel, K. Merz, J.E. Bandow, N. Metzler-Nolte, Organometallics **31**, 5760 (2012)
19. B. Fraenzel, C. Frese, M. Penkova, N. Metzler-Nolte, J.E. Bandow, D.A. Wolters, J. Biol. Inorg. Chem. **15**, 1293 (2010)
20. J.T. Chantson, M.V.V. Falzacappa, S. Crovella, N. Metzler-Nolte, ChemMedChem **1**, 1268 (2006)
21. P. Koepf-Maier, H. Koepf, Chem. Rev. **87**, 1137 (1987)
22. G. Caldwell, M.G. Meirim, E.W. Neuse, C.E.J. Van Rensburg, Appl. Organomet. Chem. **12**, 793 (1998)
23. G. Cerichelli, B. Floris, G. Ortaggi, J. Organomet. Chem. **76**, 73 (1974)

24. A. Nomoto, T. Moriuchi, S. Yamazaki, A. Ogawa, T. Hirao, Chem. Commun. 1963 (1998)
25. T. Moriuchi, A. Nomoto, K. Yoshida, T. Hirao, J. Organomet. Chem. **589**, 50 (1999)
26. T. Moriuchi, A. Nomoto, K. Yoshida, A. Ogawa, T. Hirao, J. Am. Chem. Soc. **123**, 68 (2001)
27. T. Moriuchi, K. Yoshida, T. Hirao, Organometallics **20**, 3101 (2001)
28. T. Moriuchi, T. Nagai, T. Hirao, Org. Lett. **7**, 5265 (2005)
29. T. Moriuchi, T. Nagai, T. Fujiwara, N. Honda, T. Hirao, Heterocycles **76**, 595 (2008)
30. S.I. Kirin, D. Wissenbach, N. Metzler-Nolte, New J. Chem. **29**, 1168 (2005)
31. K. Heinze, M. Beckmann, Eur. J. Inorg. Chem. **3450** (2005)
32. T. Moriuchi, T. Nagai, T. Hirao, Org. Lett. **8**, 31 (2006)
33. T. Moriuchi, K. Yoshida, T. Hirao, Org. Lett. **5**, 4285 (2003)
34. T. Moriuchi, K. Yoshida, T. Hirao, J. Organomet. Chem. **668**, 31 (2003)
35. T. Moriuchi, K. Yoshida, T. Hirao, J. Organomet. Chem. **637–639**, 75 (2001)
36. T. Moriuchi, T. Fujiwara, T. Hirao, Dalton Trans., 4286 (2009)
37. T. Moriuchi, T. Fujiwara, T. Hirao, J. Organomet. Chem. **692**, 1353 (2007)
38. I. Huc, Eur. J. Org. Chem., 17 (2004)
39. Q. Yu, T.E. Baroni, L. Liable-Sands, G.P.A. Yap, A.L. Rheingold, A.S. Borovik, Chem. Commun. 1467 (1999)
40. T. Moriuchi, M. Nishiyama, K. Yoshida, T. Ishikawa, T. Hirao, Org. Lett. **3**, 1459 (2001)
41. T. Moriuchi, M. Nishiyama, K. Yoshida, T. Hirao, Heterocycles **67**, 375 (2006)
42. J.S. Nowick, E.M. Smith, G. Noronha, J. Org. Chem. **60**, 7386 (1995)
43. R.K. Castellano, B.H. Kim, J. Rebek Jr., J. Am. Chem. Soc. **119**, 12671 (1997)
44. D. Ranganathan, C. Lakshmi, I.L. Karle, J. Am. Chem. Soc. **121**, 6103 (1999)
45. A.M. Rincón, P. Prados, J. de Mendoza, J. Am. Chem. Soc. **123**, 3493 (2001)
46. A.P. Bisson, C.A. Hunter, Chem. Commun. **1723** (1996)
47. B. Gong, Y. Yan, H. Zeng, E. Skrzypczak-Jankunn, Y.W. Kim, J. Zhu, H. Ickes, J. Am. Chem. Soc. **121**, 5607 (1999)
48. J.S. Nowick, J.H. Tsai, Q.-C.D. Bui, S. Maitra, J. Am. Chem. Soc. **121**, 8409 (1999)
49. B.J.B. Folmer, R.P. Sijbesma, H. Kooijman, A.L. Spek, E.W. Meijer, J. Am. Chem. Soc. **121**, 9001 (1999)
50. H. Zeng, R.S. Miller, R.A. Flowers II, B. Gong, J. Am. Chem. Soc. **122**, 2635 (2000)
51. P.S. Corbin, S.C. Zimmerman, J. Am. Chem. Soc. **122**, 3779 (2000)
52. V. Berl, I. Huc, R.G. Khoury, M.J. Krische, J.-M. Lehn, Nature **407**, 720 (2000)
53. P.S. Corbin, S.C. Zimmerman, P.A. Thiessen, N.A. Hawryluk, T.J. Murray, J. Am. Chem. Soc. **123**, 10475 (2001)
54. T. Moriuchi, T. Tamura, T. Hirao, J. Am. Chem. Soc. **124**, 9356 (2002)
55. S.D. Ohmura, T. Moriuchi, T. Hirao, J. Org. Chem. **75**, 7909 (2010)
56. T. Moriuchi, S.D. Ohmura, K. Morita, T. Hirao, Chem. Asian. J. **6**, 3206 (2011)
57. S.D. Ohmura, T. Moriuchi, T. Hirao, Tetrahedron Lett. **51**, 3190 (2010)
58. T. Moriuchi, S.D. Ohmura, K. Morita, T. Hirao, Asian J. Org. Chem. **1**, 52 (2012)
59. T. Moriuchi, N. Kikushima-Honda, S.D. Ohmura, T. Hirao, Tetrahedron Lett. **51**, 4530 (2010)
60. K. Ariga, Y. Lvov, T. Kunitake, J. Am. Chem. Soc. **119**, 2224 (1997)
61. N. Kimizuka, Adv. Mater. **12**, 1461 (2000)
62. P.G.V. Patten, A.P. Shreve, R.J. Donohoe, J. Phys. Chem. B **104**, 5986 (2000)
63. C. Yu, K.M.-C. Wong, K.H.-Y. Chan, V.W.-W. Yam, Angew. Chem. Int. Ed. **44**, 791 (2005)
64. C. Yu, K.H.-Y. Chan, K.M.-C. Wong, V.W.-W. Yam, Proc. Natl. Acad. Sci. U. S. A. **103**, 19652 (2006)
65. C. Yu, K.H.-Y. Chan, K.M.-C. Wong, V.W.-W. Yam, Chem. Eur. J. **14**, 4577 (2008)
66. L. Mao, T. Moriuchi, H. Sakurai, H. Fujii, T. Hirao, Tetrahedron Lett. **46**, 8419 (2005)
67. A. Gross, T. Moriuchi, T. Hirao, Chem. Commun. **49**, 1163 (2013)
68. T. Hirao, A. Nomoto, S. Yamazaki, A. Ogawa, T. Moriuchi, Tetrahedron Lett. **39**, 4295 (1998)
69. V.W.-W. Yam, K.K.-W. Lo, Chem. Soc. Rev. **28**, 323 (1999)
70. P. Pyykkö, Angew. Chem. Int. Ed. **43**, 4412 (2004)
71. V.W.-W. Yam, E.C.-C. Cheng, Chem. Soc. Rev. **37**, 1806 (2008)
72. A. Laguna, *Modern Supramolecular Gold Chemistry: Gold-Metal Interactions and Applications* (Wiley-VCH, Weinheim, 2008)
73. H. Schmidbaur, Chem. Soc. Rev. **24**, 391 (1995)

74. P. Pyykkö, Chem. Rev. **97**, 597 (1997)
75. M.J. Katz, K. Sakai, D.B. Leznoff, Chem. Soc. Rev. **37**, 1884 (2008)
76. H. Schmidbaur, A. Schier, Chem. Soc. Rev. **37**, 1931 (2008)
77. T. Moriuchi, K. Yoshii, C. Katano, T. Hirao, Tetrahedron Lett. **51**, 4030 (2010)
78. M.A. Rawashdeh-Omary, M.A. Omary, H.H. Patterson, J. Am. Chem. Soc. **122**, 10371 (2000)
79. M. Stender, R.L. White-Morris, M.M. Olmstead, A.L. Balch, Inorg. Chem. **42**, 4504 (2003)
80. T. Moriuchi, K. Yoshii, C. Katano, T. Hirao, Chem. Lett. **39**, 841 (2010)
81. T. Moriuchi, M. Yamada, K. Yoshii, T. Hirao, J. Organomet. Chem. **695**, 2562 (2010)
82. T. Moriuchi, M. Yamada, K. Yoshii, S.D. Ohmura, T. Hirao, Supramol. Chem. **23**, 113 (2011)
83. H. Fujii, H. Sakurai, K. Tani, L. Mao, K. Wakisaka, T. Hirao, IEICE Trans. Electron. **E87-C**, 2119 (2004)
84. H. Fujii, H. Sakurai, K. Tani, K. Wakisaka, T. Hirao, IEICE Electron. Express **2**, 260 (2005)
85. K. Tani, H. Fujii, L. Mao, H. Sakurai, T. Hirao, Bull. Chem. Soc. Jpn. **80**, 783 (2007)
86. T. Moriuchi, L. Mao, H.-L. Wu, S.D. Ohmura, M. Watanabe, T. Hirao, Dalton Trans. **41**, 9519 (2012)
87. T. Moriuchi, C. Katano, T. Hirao, Chem. Lett. **41**, 310 (2012)
88. A.P. Wilde, R.J. Watts, J. Phys. Chem. **95**, 622 (1991)
89. Q. Zhao, F. Li, S. Liu, M. Yu, Z. Liu, T. Yi, C. Huang, Inorg. Chem. **47**, 9256 (2008)
90. T. Moriuchi, K. Ebisu, C. Katano, T. Hirao, Chem. Lett. **43**, 1101 (2014)
91. W. Saenger, *Principles of Nucleic Acid Structure* (Springer, New York, 1984)
92. V.A. Bloomfield, D.M. Crothers, I. Tinoco Jr., *Nucleic Acids: Structures, Properties, and Functions* (University Science Books, Sausalito, 2000)
93. S. Sivakova, S.J. Rowan, Chem. Soc. Rev. **34**, 9 (2005)
94. J.T. Davis, G.P. Spada, Chem. Soc. Rev. **36**, 296 (2007)
95. J.L. Sessler, C.M. Lawrence, J. Jayawickramarajah, Chem. Soc. Rev. **36**, 314 (2007)
96. K. Tanaka, M. Shionoya, Coord. Chem. Rev. **251**, 2732 (2007)
97. J. Müller, Eur. J. Inorg. Chem. 3749 (2008)
98. S. Lena, S. Masiero, S. Pieraccini, G.P. Spada, Chem. Eur. J. **15**, 7792 (2009)
99. G.H. Clever, M. Shionoya, Coord. Chem. Rev. **254**, 2391 (2010)
100. J.A.R. Navarro, B. Lippert, Coord. Chem. Rev. **185–186**, 653 (1999)
101. M.D. Ward, F. Barigelletti, Coord. Chem. Rev. **216–217**, 127 (2001)
102. B. Wieczorek, H.P. Dijkstra, M.R. Egmond, R.J.M. Klein Gebbink, G. van Koten, J. Organomet. Chem. **694**, 812 (2009)
103. M. Albrecht, G. van Koten, Angew. Chem. Int. Ed. **40**, 3750 (2001)
104. T. Moriuchi, S. Noguchi, Y. Sakamoto, T. Hirao, J. Organomet. Chem. **696**, 1089 (2011)
105. T. Moriuchi, R. Ohata, Y. Sakamoto, T. Hirao, Eur. J. Inorg. Chem. 4626 (2014)
106. T. Moriuchi, Y. Sakamoto, S. Noguchi, T. Fujiwara, S. Akine, T. Nabeshima, T. Hirao, Dalton Trans. **41**, 8524 (2012)
107. J.T. Davis, Angew. Chem. Int. Ed. **43**, 668 (2004)
108. S. Masiero, G. Gottarelli, S. Pieraccini, Chem. Commun. **1995** (2000)
109. S. Martic, X. Liu, S. Wang, G. Wu, Chem. Eur. J. **14**, 1196 (2008)
110. S. Pieraccini, S. Bonacchi, S. Lena, S. Masiero, M. Montalti, N. Zaccheroni, G.P. Spada, Org. Biomol. Chem. **8**, 774 (2010)
111. G.P. Spada, S. Lena, S. Masiero, S. Pieraccini, M. Surin, S. Samori, Adv. Mater. **20**, 2433 (2008)
112. D. González-Rodríguez, P.G.A. Janssen, R. Martín-Rapún, I. De Cat, S. De Feyter, A.P.H.J. Schenning, E.W. Meijer, J. Am. Chem. Soc. **123**, 4710 (2010)
113. X. Meng, T. Moriuchi, M. Kawahata, K. Yamaguchi, T. Hirao, Chem. Commun. **47**, 4682 (2011)
114. X. Meng, T. Moriuchi, Y. Sakamoto, M. Kawahata, K. Yamaguchi, T. Hirao, RSC Adv. **2**, 4359 (2012)
115. X. Meng, T. Moriuchi, N. Tohnai, M. Miyata, M. Kawahata, K. Yamaguchi, T. Hirao, Org. Biomol. Chem. **9**, 5633 (2011)

Chapter 5
Conclusions

Toshikazu Hirao

Abstract The summary and outlook of this book is described in the conclusion. Reduction and phosphonation with dialkyl phosphonate, vanadium-catalyzed or -induced dehalogenation, pinacol coupling, oxidative transformations of carbonyl compounds, ligand coupling, and oxidative halogenation are developed. For π, d, π-redox systems, coenzyme PQQ, polyanilines, and quinonediimines are used to achieve efficient catalysts and materials. The redox-active ligands are demonstrated to be useful in organic synthesis. Sumanene is synthesized for the first time, which is allowed to construct nonplanar π-conjugated systems and d, nonplanar π-conjugated ones. Chirality-organized spaces are developed by hybridization of organmetallic compounds and biomolecules like dipeptide, peptide, nucleobase, and DNA, which contributes to one of key researches in bioorganometallic chemistry. A combination of these fields will permit conceptionally new chemistry.

Redox reactions with synthetic potential have been developed by use of dialkyl phosphonate, early transition metals, and lanthanides. The Lewis acidic nature of metallic compounds is another key factor in their reactivities in addition to the redox properties. Controlling the metal-based redox systems leads to greater selectivities in their electron transfer reactions. Likewise, fine-tuning the ligands coordinated to metals results in more efficient redox systems. These approaches yield a variety of fruitful redox reactions for organic synthesis as observed in the ligand coupling and haloperoxidase-inspired reactions.

The tautomerism of dialkyl phosphonate permits new synthetic protocols in dehalogenation and/or C–P bond formation. The multi-component system consisting of a catalyst, a co-reductant, and an additive promoter cooperates with each other to achieve the catalytic reactions through efficient one-electron reduction. In this system, the active catalyst is smoothly regenerated by redox interaction with the co-reductant. The selection of the co-reductant is important from this point of view. Furthermore, the oxidized form of the co-reductant should not interfere with, but assist the reduction reaction or at least, be tolerant under the conditions. Additive promoters, which are considered to contribute to the redox cycle, possibly facilitate the electron transfer and/or liberate the catalyst from the reaction adduct.

T. Hirao (✉)

Department of Applied Chemistry, Graduate School of Engineering, Osaka University, Yamada-oka, Suita, Osaka 565-0871, Japan
e-mail: hirao@chem.eng.osaka-u.ac.jp

Oxovanadium(V) compounds are potential Lewis acids with oxidation ability to induce one-electron oxidation reactions based on their characteristics. Oxidation capability and redox potential are effectively controlled by the substituent of oxovanadium(V) compounds. A catalytic system is allowed to be realized by the redox interaction with molecular oxygen. The oxidative ligand coupling proceeds via the intermetallic interaction between vanadium species and main-group organometallics.

These synthetic methods are expected to be promising as versatile synthetic tools. The reactions are complementary and useful to generate radical intermediates with the higher selectivity. The higher stereoselectivity is attained [1–2].

Next, the efficient redox systems are to be constructed to realize electron-transfer reactions as observed in biological systems. Based on the redox properties of π-conjugated systems, coenzyme PQQ and polyanilines are found to serve as a coenzyme catalyst and synthetic metal catalyst, respectively, that are organocatalysts for dehydrogenation reaction through proton-coupled electron transfer. Both compounds are able to be used as redox-active ligands, which contribute to the efficient redox processes of transition metals or metal nanoparticles [3]. A variety of d,π-conjugated systems have been developed by using polyanilines and quinonediimines [4]. Such systems are likely to be of potential in organic synthesis and materials synthesis.

Another π-conjugated system depends on nonplanar π bowl, sumanene, which is a partial C_{3v} structure of C_{60}. The π-bowl chemistry of sumanene has been developed together with derivatization of sumanene through use of the benzylic positions. Complexation with nonplanar π-conjugated plane leads to various coordination modes including selective concave and convex complexation. Thus-obtained complexes are envisioned to exhibit unique reactivities due to coordination to nonplanar π surface [5].

The last challenging issue is how to construct the sterically regulated chiral space using biomolecules. Organometallic compounds are introduced to dipeptide, peptide, nucleobase, and DNA to achieve steric regulation and self-assembly to afford the corresponding chiral spaces [6]. These systems are evaluated as potential catalysis and materials from the viewpoint of bioorganometallic chemistry.

In the future, a combination of the efficient redox reactions, π-conjugated redox systems, and sterically regulated spaces will permit the more efficient and selective redox catalysts and materials in artificial systems as observed in nature.

References

1. T. Hirao, Chem. Rev. **97**, 2707 (1997)
2. T. Hirao, in *Vanadium: The Versatile Metal*, ed. by K. Kustin, J.C. Pessoa, D.C. Crans. ACS Symposium Series, vol 974 (American Chemical Society, Washington, DC, 2007), pp. 2–27
3. T. Amaya, T. Hirao, Synlett, 435 (2011)
4. T. Moriuchi, T. Hirao, Acc. Chem. Res. **45**, 347 (2012)
5. T. Amaya, T. Hirao, Chem. Commun. **47**, 10524 (2011)
6. T. Moriuchi, T. Hirao, Acc. Chem. Res. **43**, 1040 (2010)